GEOLOGY AND HYDROCARBON POTENTIAL

ATRATO AND SAN JUAN BASINS

Chocó (Panamá) Arc, Colombia

TUMACO BASIN

(Pacific Realm)

FONDO EDITORIAL UNIVERSIDAD EAFIT

ANH
AGENCIA NACIONAL DE HIDROCARBUROS

GEOLOGY AND HYDROCARBON POTENTIAL

ATRATO AND SAN JUAN BASINS

Chocó (Panamá) Arc, Colombia

TUMACO BASIN

(Pacific Realm)

GEOLOGY AND HYDROCARBON POTENTIAL
ATRATO AND SAN JUAN BASINS
Chocó (Panamá) Arc, Colombia

TUMACO BASIN
(Pacific Realm)

First Edition: January 2010

UNIVERSITY EAFIT
Department of Geology
Medellin, Colombia

Executive Director: Geovany Bedoya, Msc.

Authors:
Fabio Cediel, Ph.D
Isabel Restrepo, Msc.
María I. Marín-Cerón, Ph.D
Hermman Duque-Caro, PhD
Carlos Cuartas, MSc.
Cesar Mora, MSc.
Gustavo Montenegro
Edgar García
Diego Tovar
Guillermo Muñoz

Scientific Advisors:
Iván Dario Correa, Ph.D.
Michel Hermelin, MSc.
José Ignacio Martínez, Ph.D.
Gloria Sierra, MSc.
Gloria Elena Toro, Ph.D.
Juan Dario Restrepo, Ph.D.

Please cite as: Cediel F., Restrepo I., Marín-Cerón M.I., Duque-Caro H., Cuartas C., Mora C., Montenegro G., García E., Tovar D., Muñoz G., (2009), Geology and Hydrocarbon Potential, Atrato and San Juan Basins, Chocó (Panamá) Arc. Tumaco Basin (Pacific Realm), Colombia.

Designed by: María Elena Uribe Alzate

ISBN: 978-958-720-052-2

Printed in Medellín - Colombia

Fondo Editorial Universidad EAFIT. Medellín, Colombia 172 pp.

President of the Republic of Colombia
ÁLVARO URIBE VÉLEZ

Minister of Mines and Energy
HERNÁN MARTÍNEZ TORRES

ANH
AGENCIA NACIONAL DE HIDROCARBUROS

General Director ANH
JOSÉ ARMANDO ZAMORA REYES

Technical Sub-director
CAROLYNNA ARCE HERNÁNDEZ

Chief Geologist
CLEMENCIA GÓMEZ GONZÁLEZ

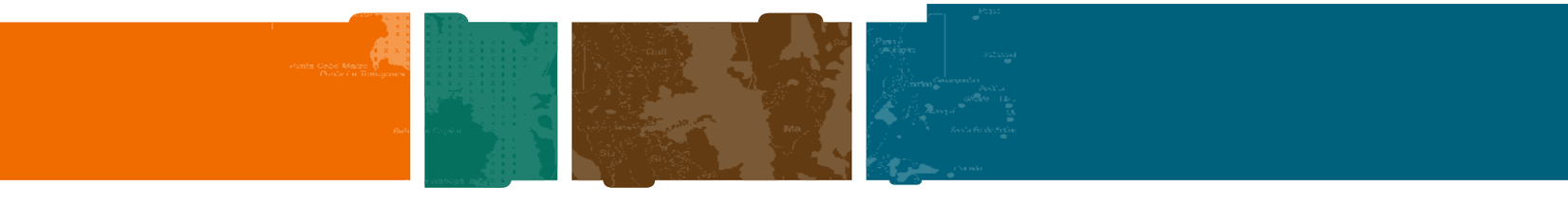

FOREWORD

Regional geology and basin analysis constitutes an important tool in the search for hydrocarbons. Our geological knowledge of the pacific basins of Colombia is still in a preliminary stage; notwithstanding, significant field data and local geophysical and geochemical data collected over the last five decades allows a new tecto-sedimentary evaluation. The results of this exercise are encouraging, open new questions and challenges our exploration capabilities.

The Atrato and San Juan Basins within the Chocó-Panamá Arc and the Tumaco Basin in the Pacific geological realm are frontier exploration basins, where oil and gas shows recorded in eight exploration wells and numerous oil seeps attest to active petroleum systems.

The Agencia Nacional de Hidrocarburos is commited to improve the geological knowledge in frontier basins. Nowadays, we are shooting new seismic programs and drilling stratigraphic wells. I invite you to enjoy this travel through new promising areas in Colombia.

José Armando Zamora Reyes
GENERAL DIRECTOR ANH

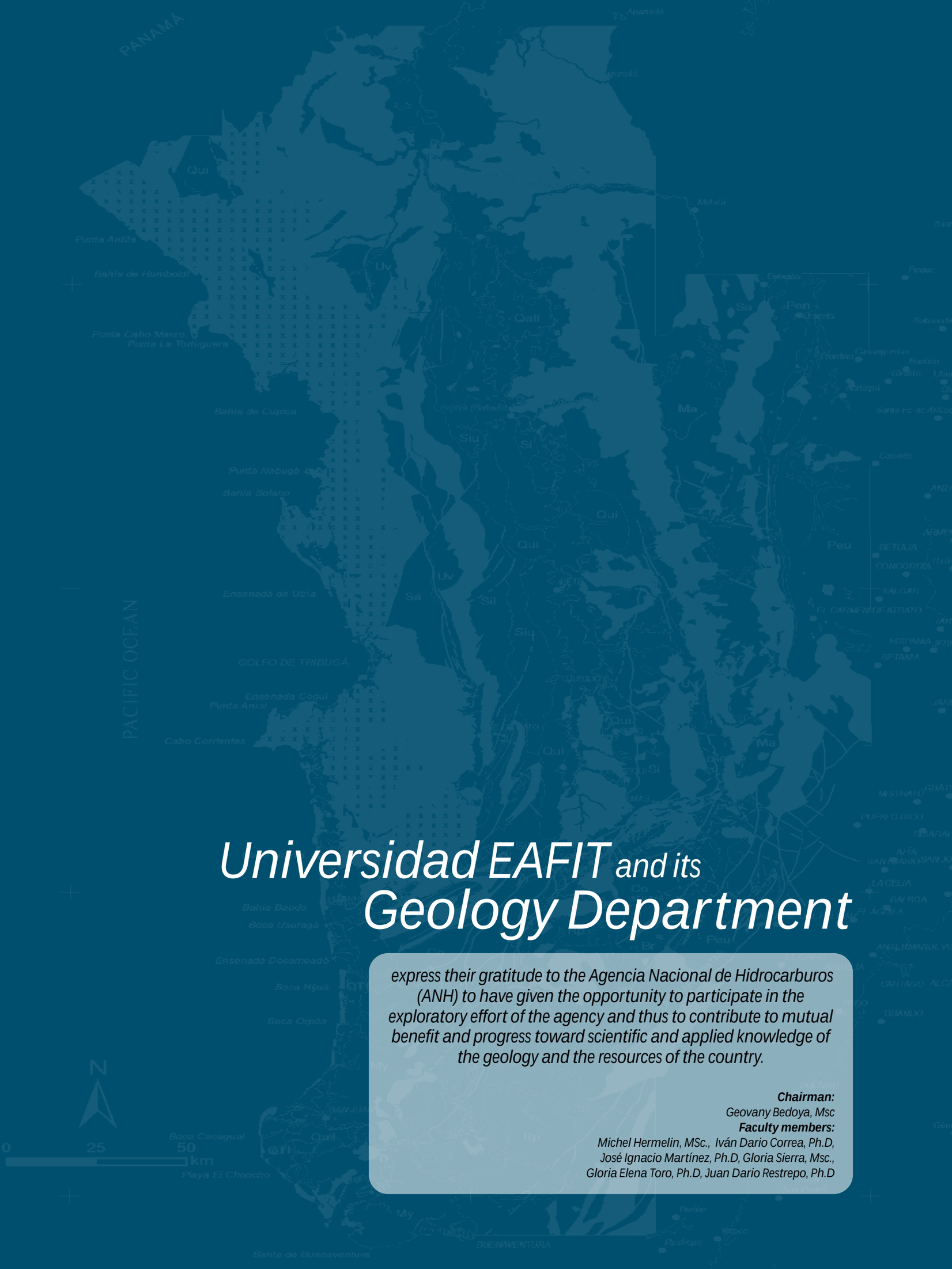

Universidad EAFIT and its Geology Department

express their gratitude to the Agencia Nacional de Hidrocarburos (ANH) to have given the opportunity to participate in the exploratory effort of the agency and thus to contribute to mutual benefit and progress toward scientific and applied knowledge of the geology and the resources of the country.

Chairman:
Geovany Bedoya, Msc
Faculty members:
Michel Hermelin, MSc., Iván Dario Correa, Ph.D, José Ignacio Martínez, Ph.D, Gloria Sierra, Msc., Gloria Elena Toro, Ph.D, Juan Dario Restrepo, Ph.D

PANAMA
PACIFIC OCEAN
Punta Ardita
Bahía de Humboldt
Punta Cabo Marzo
Punta La Tortuguera
Bahía de Cupica
Punta Nabugá
Bahía Solano
Ensenada de Utría
GOLFO DE TRIBUGÁ
Ensenada Coqui
Punta Arusí
Cabo Corrientes
Playa Nueva
Bahía Baudo
Boca Usuragá
Ensenada Docampadó
Boca Hijuá
Boca Orpúa
Boca Cacagual
Playa El Choncho
Bahía de Buenaventura
SAN JUAN
Qui
Uv
Qall
Siu
Si
Sa
Ma
Pen
Peu
Co
Rp
Br
Is
My
QTT
Cl
N
0
25
50
km

GEOLOGY AND HYDROCARBON POTENTIAL
ATRATO AND SAN JUAN BASINS
Chocó (Panamá) Arc, Colombia

TUMACO BASIN
(Pacific Realm)

Technical Presentation

The inventory, compilation, interpretation and integral evaluation of the geological, geophysical and geochemical data of Atrato, San Juan and Tumaco Basins, aimed to improve and update the knowledge of the basins in terms of their exploratory potential, was carried out according to the technical proposal agreed upon by the Agencia Nacional de Hidrocarburos (ANH) and the Universidad EAFIT.

The technical data used, was generated by early-phase exploration campaigns undertaken by various petroleum and mineral exploration companies since the 1940's. Many of the documents produced during these programs are lost; only a fraction is preserved, sometimes in poor physical condition. Regardless, we feel that efforts to recover the most relevant information and results have been successful, and that these data augment and support the conclusions presented herein.

The evaluation and interpretation of available information were completed using present-day techniques, such as aero-gravity and –magnetometry, radar and DEM images. We were particularly careful to review geological concepts and interpretations frequently repeated in technical reports in order attain an adequate regional evaluation according to the (very low) density of available information for the three basins.

The result of this new regional geological and geophysical analysis clearly outlines the presence of three sedimentary basins, each one with particular characteristics, presented here as follows:

PART ONE

1. **Atrato Basin**: Cenozoic Fore-Arc Basin
2. **San Juan Basin**: Cenozoic Paleodelta

PART TWO

Tumaco Basin: Cenozoic Fore-Arc Basin

The Atrato and San Juán Basins are located within the Chocó-Panamá Arc, whereas the Tumaco Basin (onshore and offshore) belongs to the Pacific realm.

The ocurrence of hydrocarbon-source rocks in the San Juan Basin is deduced upon the basis of the geochemical analysis of the Iró Formation (Paleocene), outcroping in the Istmina-Condoto High. Time-stratigraphic equivalents of Iró Formation in the Atrato Basin such as the Salaquí and Clavo Formations, were subjected to important hydrocarbon generation and expulsion processes during late Miocene-Pliocene. The presence of oil and gas seeps attests to bedrock permeability, which allows the migration of hydrocarbons. In the Tumaco Basin the Oligocene rock units are probably the most significant hydrocarbon sources.

Resources to be discovered

It can now be asserted that Atrato, San Juán and Tumaco basins are sub-explored. However, this does not mean that their exploration merit is negative. On the contrary, the balance is positive; we have identified important exploration opportunities which deserve further investigation.

Based on geological and geochemical modeling, there are expectations for the presence of 600 MBPE (P50) in the San Juan basin and of 850 MBPE (P50) in the Atrato basin. In the Tumaco Basin due to the poor available information, it was not possible to estimate the resources to be discovered.

Suggested future exploration activities

The present document contains bases and guidelines necessary for the design of an exploration program according to the level of knowledge available for the Atrato, San Juan and Tumaco basins. It is necessary to obtain primary field data (geology, geophysics and geochemistry). The following steps are essential:

- Define the stratigraphy, and petrographically and geochemically characterize the potential hydrocarbon source rock units, on the basis of a sampling with a proper density.
- Carry out 2D modeling for hydrocarbon generation and migration in order to evaluate the load risk of the principal plays identified in the basins.
- Produce geological maps at scales greater than 1:500,000 in selected areas, according to exploration criteria defined by structural geology.
- Design new seismic exploration programs, integrating parameters established via previous programs and the present state of geological knowledge for each of the basins.
- Carry out a spectral GR program on outcrops, in order to standardize the sparse existing records and to improve the possibility to characterize future drilling projects.
- Vectorize seismic information, which has not been classified in SEGY files.
- Re-process the existing seismic programs in order to improve their resolution.
- Obtain petrological information and isotopic dates from the rock units which define the eastern and western limits of the Atrato Basin (Mandé Magmatic Arc and Baudó Range) in order to establish geological and geochronological evolution models for the Atrato and San Juán basins.
- Include the Urabá basin in the regional geological analysis. This basin is an important tectonic element and an exploratory goal within the Chocó Arc.

PART ONE

***1. Atrato Basin**: Cenozoic Fore-Arc Basin*
***2. San Juan Basin**: Cenozoic Paleodelta*

PANAMA
PACIFIC OCEAN
Punta Ardita
Bahia de Humboldt
Punta Cabo Marzo
Punta La Tortuguera
Bahia de Cupica
Punta Nabugá
Bahía Solano
Ensenada de Utría
GOLFO DE TRIBUGÁ
Ensenada Coquí
Punta Arusí
Cabo Corrientes
Playa Nueva
Bahía Baudó
Boca Usuraga
Ensenada Docampadó
Boca Hijuá
Boca Orpúa
Boca Cacagual
Playa El Choncho
Bahía de Buenaventura
BUENAVENTURA
SISTEMA DE FALLAS GARRAPATAS
Qui
Uv
Qall
Siu
Sil
Sa
Ma
Peu
Pen
Co
Rp
Br
Is
My
Ci
QTt
BETULIA
CONCORDIA
SALGAR
EL CARMEN DE ATRATO
HISPANIA
BETANIA
MISTRATO
PUEBLO RICO
APIA
SANTUARIO
LA CELIA
BALBOA
EL AGUILA
SAN JOSE DEL PALMAR
ANSERMANUEVO
EL CAIRO
ARGELIA
CARTAGO
TORO
VERSALLES
OBANDO
EL DOVIO
BOLIVAR
N
0
25
50
km

1 2 3 4 5 6 7

GEOLOGY AND HYDROCARBON POTENTIAL
ATRATO AND SAN JUAN BASINS

Chocó (Panamá) Arc, Colombia

CONTENTS

CONTENTS

LIST OF ILLUSTRATIONS

LIST OF ILLUSTRATIONS

TABLES

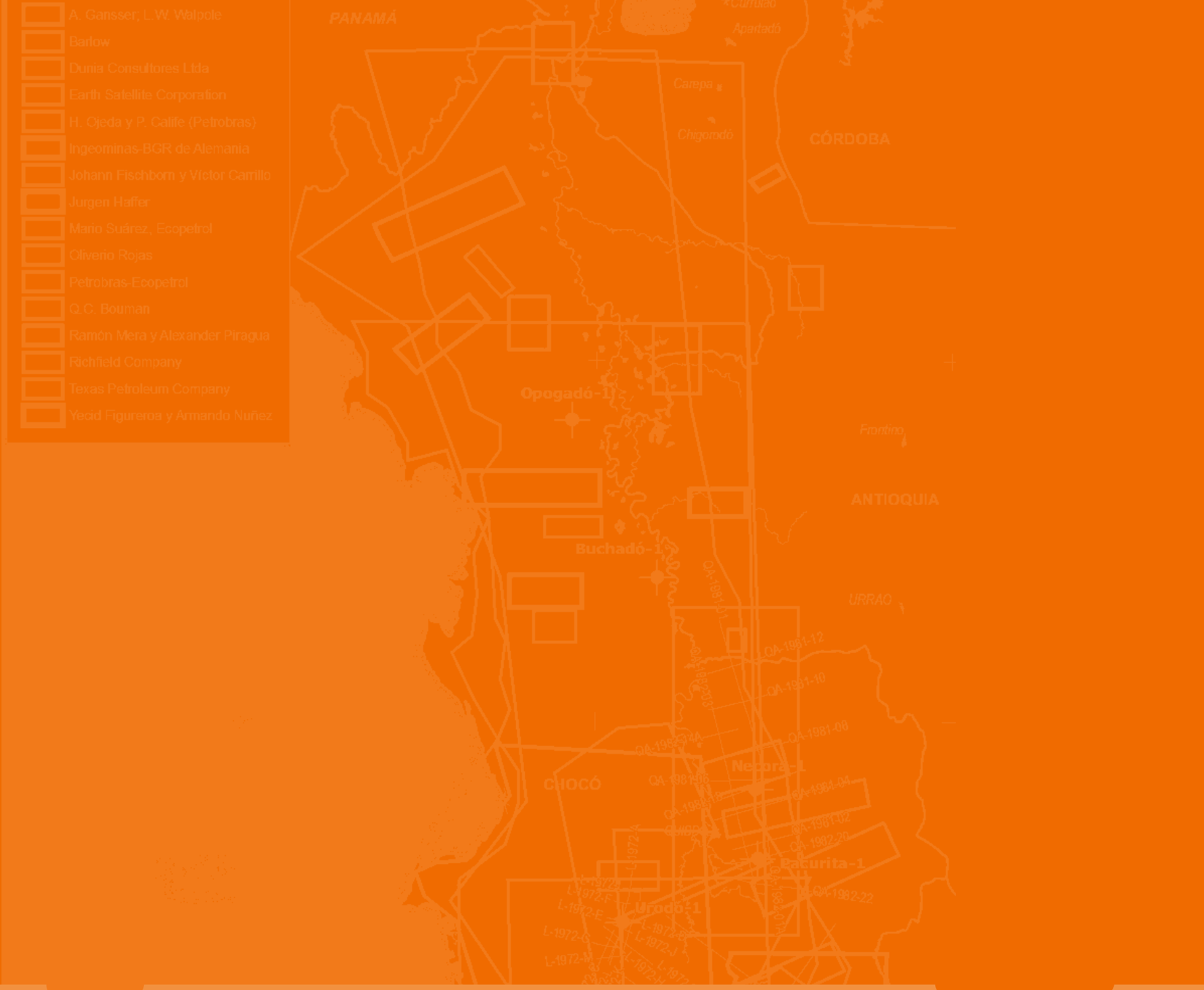

1. INTRODUCTION

1. INTRODUCTION

1.1. Definition and Location

The Atrato and San Juan Basins are essentially sub-basins contained within what was historically referred to as the Chocó Basin. They are physiographically bound to the west by the Baudó Range, to the east by the Western Cordillera, and to the south-south west along the Pacific Ocean coastline. To the north they are geographically limited along the border with Panamá. The Chocó Basin can be divided in the Atrato River Basin to the north, and the San Juan River Basin to the south, separated by the Istmina-Condoto Highland. The Atrato Basin covers approximately 25,000 km^2 whilst the San Juan Basin covers approximately 10,500 km^2. In geological terms and as a result of the present study, the basins are redefined as two separate exploration plays *(Fig. 1)*

1.2. Exploration History

Principle field exploration to date, including seismic programs and wildcats wells are shown in *Fig. 2* Taking into account the surface extension of each of the basins, the results obtained in the present study, and the identified exploratory potential, it can be concluded that both basins are in an incipient exploration stage or, in other words, are sub-explored. For instance, only five wildcat wells have been drilled in the Atrato Basin.

- Buchadó-1, Richmond 1953, T.D. 15.539'
- Opogadó-1, Continental 1973, T.D. 11.372'
- Urodó-1, Superior 1973, T.D. 15.000'
- Pacurita-1, Asamera 1981, T.D. 9.489'
- Nécora-1, Asamera 1983, T.D. 6503'

Amongst the mentioned wells, Opogadó - 1 and Urodó - 1 were drilled, at least partially, into "structural highs" now identified as mud diapirs.

Pacurita-1 and Nécora-1 stopped near the top of the Oligocene, and did not reach their exploration objective which included higher potential rock units, at lower stratigraphic levels.

Buchadó-1 totaled 15,539 feet in depth, reaching the top of the Upper Eocene. These rocks are chronostratigraphic equivalents to the Iró Formation, recorded in the Istmina-Condoto High, known for it's capacity to generate hydrocarbons. Buchadó-1 seems to have been drilled out-of-structure. Regardless, it presented important hydrocarbon showings between 5,800' (gas) and 11,500' (oil).

In the San Juan Basin, only one well, Tambora-1, was drilled. It is located off-shore and partially crossed a mud diapir.

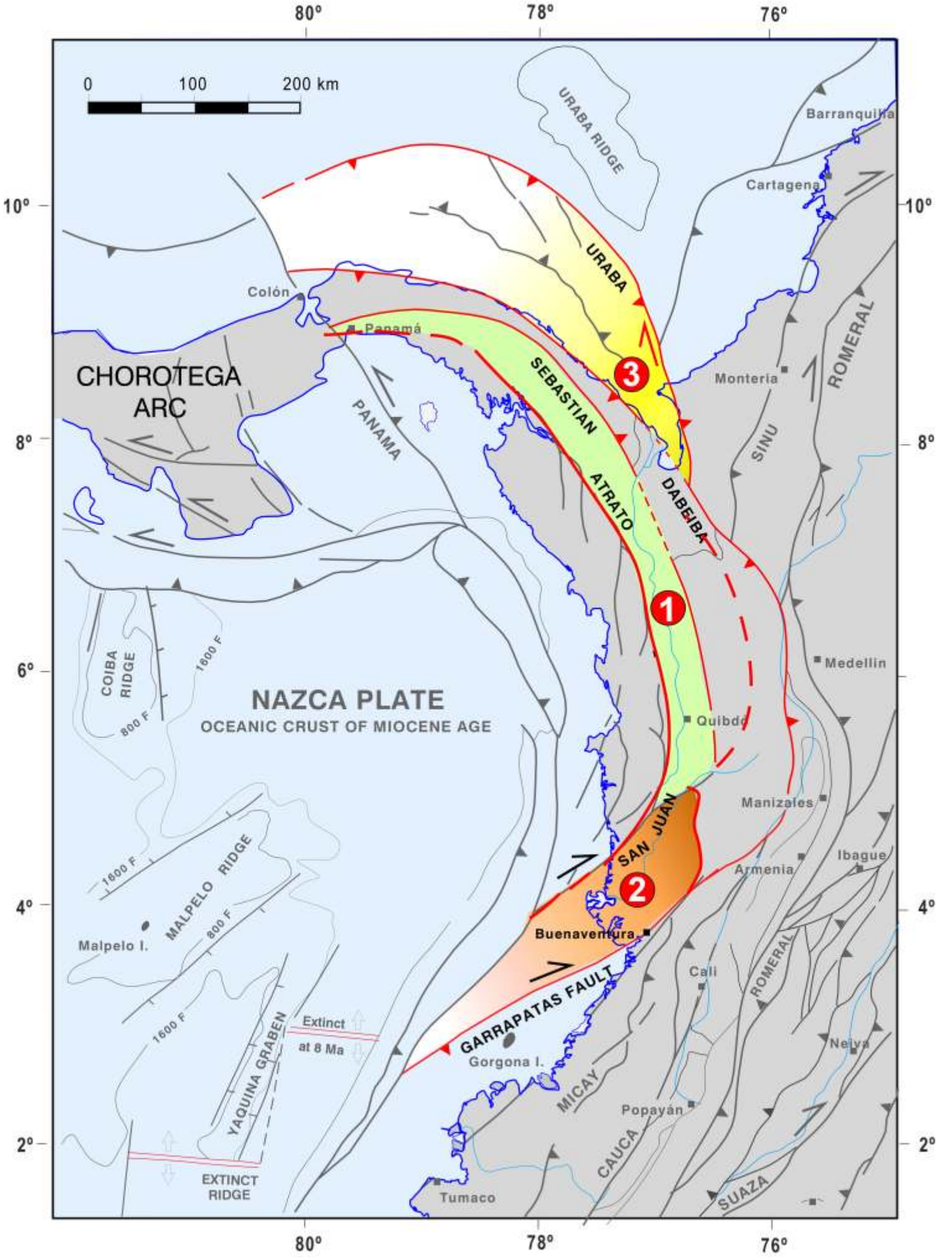

1 **Atrato** Basin

2 **San Juan** Basin

3 **Urabá** Basin

Figure 1. *Geological situation of the Atrato and San Juan Basins. Modified after Cediel, et al, 2003*

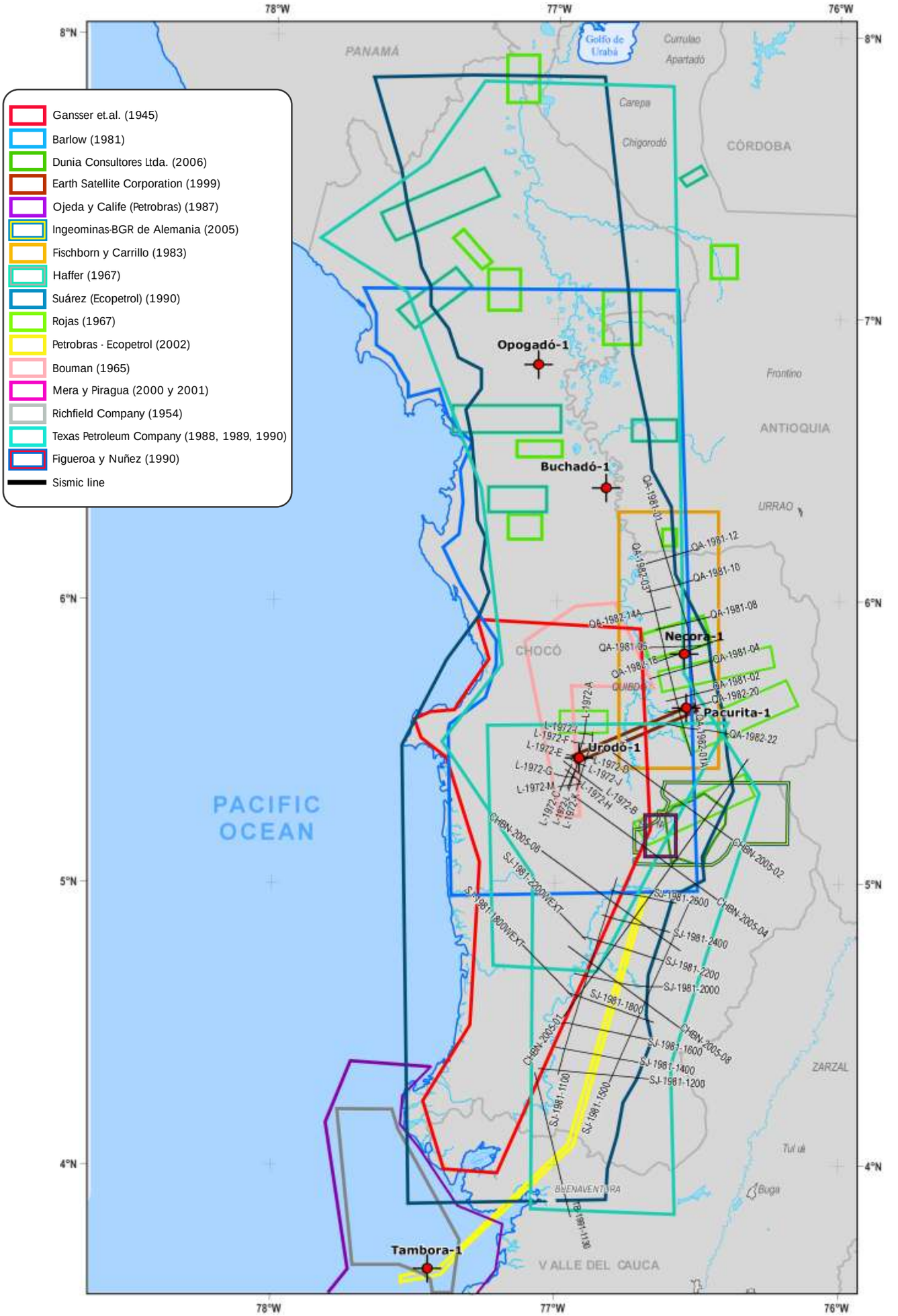

Figure 2. Location of source data used in this study

2. GEOLOGICAL FRAMEWORK

2. GEOLOGICAL FRAMEWORK

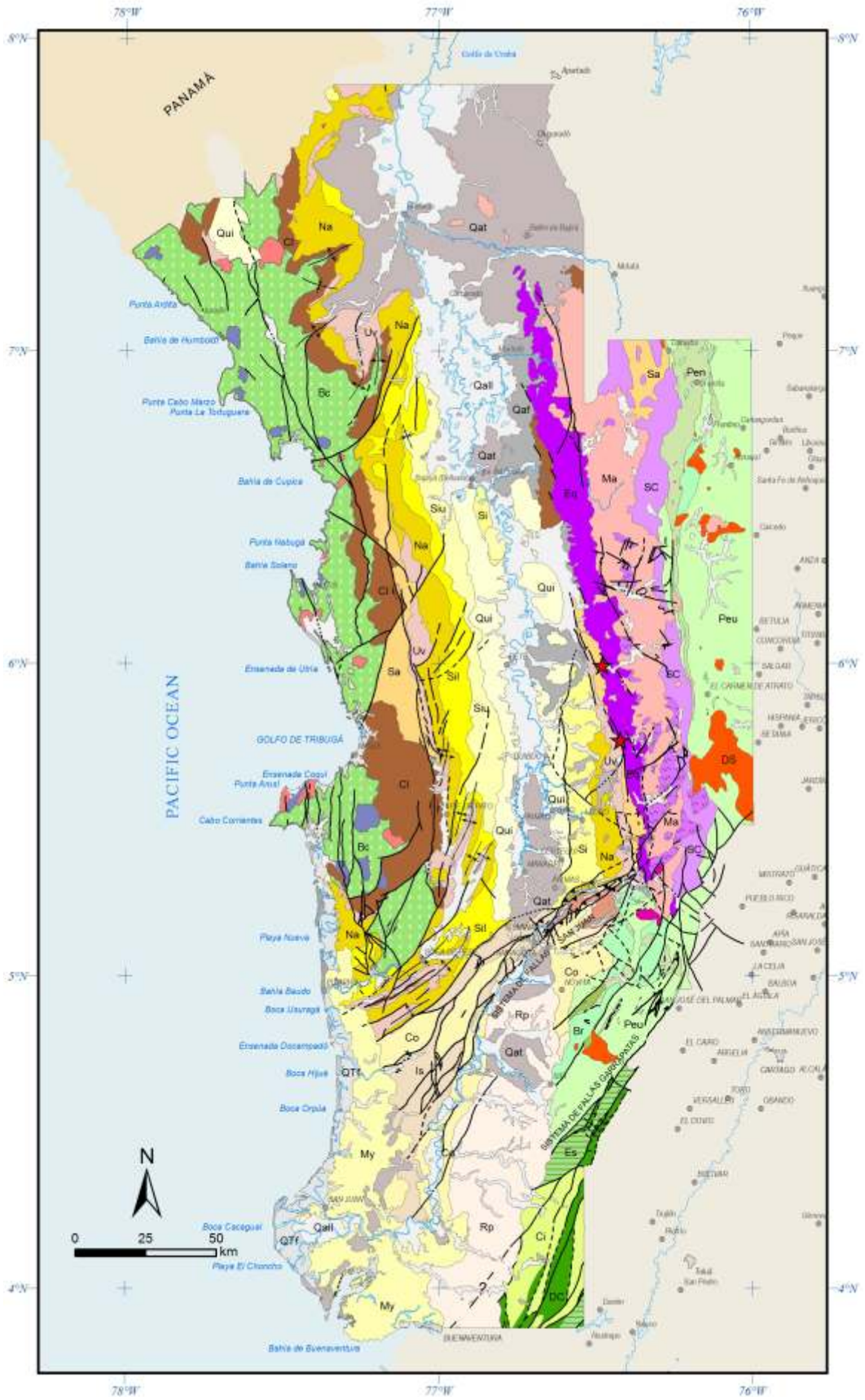

Figure 3.
Geological Map, Chocó Arc; Atrato and San Juan Basins

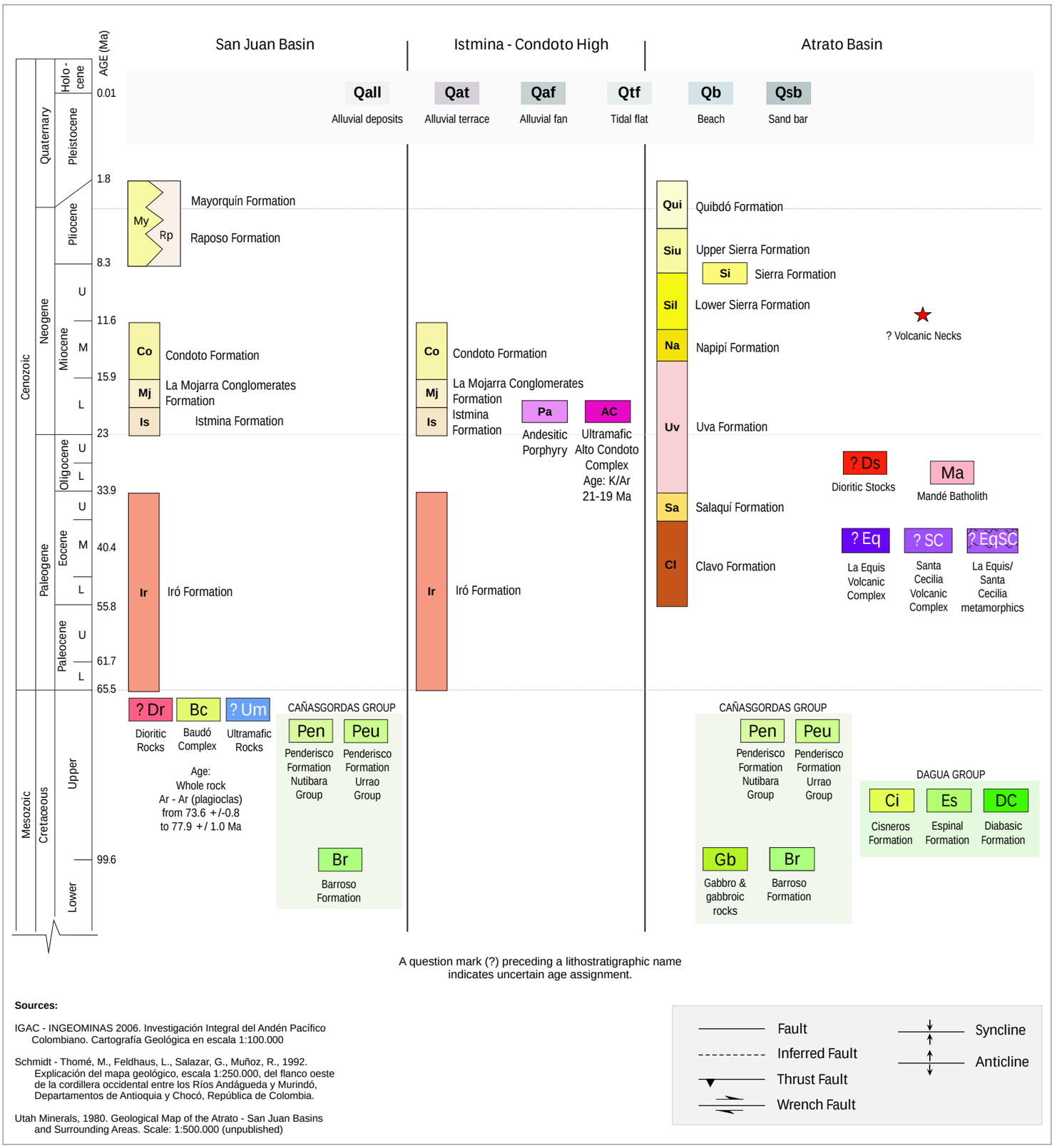

Sources:

IGAC - INGEOMINAS 2006. Investigación Integral del Andén Pacífico Colombiano. Cartografía Geológica en escala 1:100.000

Schmidt - Thomé, M., Feldhaus, L., Salazar, G., Muñoz, R., 1992. Explicación del mapa geológico, escala 1:250.000, del flanco oeste de la cordillera occidental entre los Ríos Andágueda y Murindó, Departamentos de Antioquia y Chocó, República de Colombia.

Utah Minerals, 1980. Geological Map of the Atrato - San Juan Basins and Surrounding Areas. Scale: 1:500.000 (unpublished)

Figure 3. continuation
Geological Map, Chocó Arc; Atrato and San Juan Basins

2.1. Tectonic Setting

The formation and development of the Atrato and San Juan Basins took place within a sequence of events which are schematically outlined in Fig. 4

The geological characterization of these events remains incomplete due to lack of geological and geophysical data. Regardless, evaluation of the available information within a regional context, permits recognition of the principle tectonic elements and tectono-stratigraphic events for the region. These include:

a. The Garrapatas-Dabeiba Suture (Late Cretaceous)

The youngest age recorded in the Cañasgordas Group (the principle component of the Cañasgordas Terrane), is Late Cretaceous (Maastrichtian). Accretion of the Cañasgordas Terrane to the continental margin took place along the Garrapatas-Dabeiba Suture during the Maastrichtian and possibly continued into the Paleocene. This event generated discrete (calc-alkaline subduction-related) magmatism which is not yet fully understood.

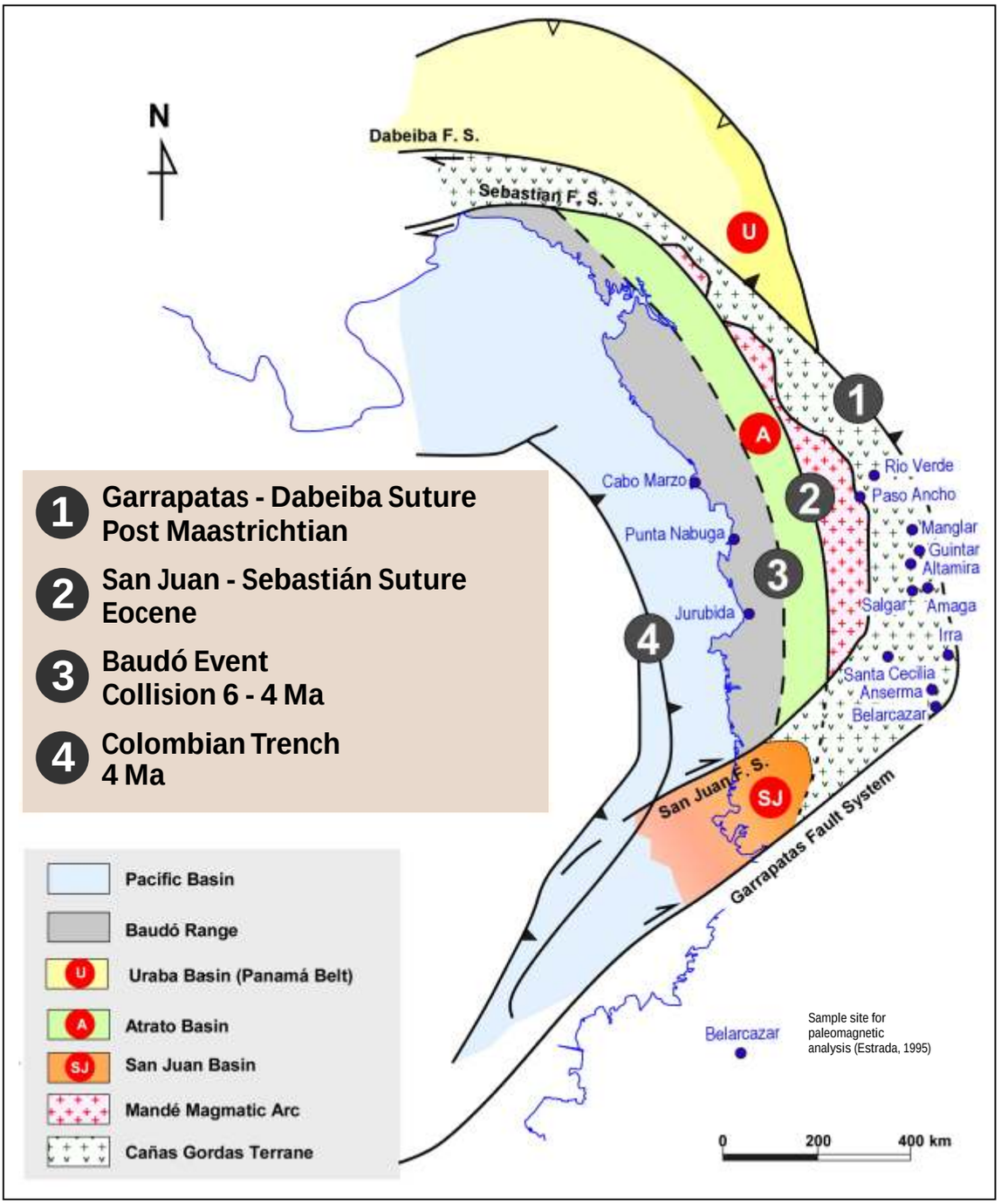

Figure 4. *Sequence of major tectonic events in the Chocó Arc*

b. The San Juan-Sebastián Suture (Eocene)

The second tectonic event of regional importance involves the collision and accretion of the El Paso Terrane along the San Juan-Sebastian Suture. The Mandé Magmatic Arc, dated between 54 and 49 Ma, was generated via Chilean-type subduction processes. At the same time as the San Juan-Sebastián Suture was formed, the Atrato Forearc Basin developed, open to a western sea, the Pacific Ocean.

c. The Baudó Event (? 8-4 Ma)

The third event, of poorly defined age, involves the appearence of the Baudó Range. The mechanisms responsible for this appearance remain uncertain, however, they led to the formation of the western margin and closure of the Atrato Basin. Presently available data are insufficient to fully explain the kinematics of Baudó Range emplacement. The following possible explanation for the geological evolution of the Baudó Range is offered:

Baudó is without doubt an assemblage of allochtonous oceanic rocks emplaced along the continental margin by the continuous interaction of an oceanic plate with the NW corner of the South American continent. The subduction of the oceanic plate (El Paso?) and related Mandé magmatism developed until the relationship between density and buoyancy of the various plates curbed the process, substantially diminishing the rate of subduction. Continued compression produced a positive flexure in the oceanic plate, leading to the uplift of today's Baudó Range. This mechanism was enhanced by a rapid increase in sedimentary / lithostatic load in the forearc basin.

The following facts, support the postulated sequence of tectonic event s (see figure 4):

1. San Juan Basin basement is formed by the Cañasgordas Terrane, or alternatively by the Gorgona Terrane (in the case that paleogeographic interpretations by Estrada (1995), are correct), as it shows a distinct gravimetric and magnetometric texture with respect to the one observed in the basement of the Atrato Basin.

2. The Atrato Basin basement is formed by the El Paso Terrane (Baudó Complex?), which outcrops in a tectonic window in the Istmina-Condoto High (along the San Juan Suture).

3. The San Juan Basin is limited by two important sutures / subparallel transcurrent fault systems (the Garrapatas-Dabeiba Suture and the San Juan- Sebastián Suture). These structures controlled sedimentation since the Oligocene (?), and gave rise to a deltaic system which prograded in a NE to SW direction.

4. It is evident that the initial approach and collision of both the Cañasgordas Terrane and the El Paso Terrane were orthogonal. During subsequent tectonic migration a NW rotation occurred, liberating part of the collisional energy and leading to the morpho-structural development of the present-day Panamá-Chocó Arc. This rotation is inferred from the existence of tear faults and E-W trending lineaments, and from the progressive SW-NE to SE-NW orientation of fold axes mapped along the western flank of the Atrato Basin and in it's extensions into Panamá *(Figure 5)*

5. The allochtonous character of the Cañasgordas Terrane and of the Baudó Range has been demonstrated using paleomagnetic evidence by Estrada (1995). Paleomagnetic data have significantly improved knowledge of the paleogeography and paleotectonics of the Chocó Arc. Some of the important conclusions of Estradas's work are summarized below:

- There are at least three distinct latitudinal provinces and ages for the rock assemblages in this region, including the Baudó Arc, Cañasgordas Terrane and Gorgona Terrane (the Chocó Terrane, Western Cordillera Terrane and Gorgona Terrane, respectively, Estrada, 1995). The paleolatitudinal origins of these assemblages are directly associated with the tectonic evolution of the eastern Pacific plates. In this sense, it is known that since the Late Cretaceous, plate interactions along NW South America have been dominated by subduction of the Farallón Plate (Pardo-Casas and Molnar, 1987, in Estrada 1995). In these and others reconstructions the Farallón plate moved along a north-directed vector up to the Paleogene, when motion shifted to mainly SW to NE. The relative motion of the Farallón plate suggests that terranes accreted against the western edge of South America were transported from southern latitudes.

- The Gorgona terrane is composed of a sequence of Mesozoic mafic and ultramafic rocks, including komatiitic flows. Paleomagnetic data indicates that the El Horno basalt (86 +/- 3 Ma) was located at about 25 S relative to South America in Late Cretaceous time. The longitude cannot be precisely fixed by paleomagnetic methods. However Estrada (1995) presented some reconstructions and possible trajectories that suggest a longitude of origin of 135º W. The accretion of the

Gorgona Terrane is considered to be pre-Miocene (McGeary and Ben-Abraham, 1989 in Estrada, 1995), and was possibly followed by strike-slip faulting along the Buenaventura fault zone, resulting in the break up of the original terrane. Paleomagnetic data from the Gorgona Terrane doesn´t have any clear correlation with data from the Caribbean Plate.

- The Cañasgordas Terrane and the Baudó Arc, present two groups of paleomagnetic data with the main group having a mean of about 10, suggesting equatorial paleolatitudes of origin.

- Based upon preliminary geological mapping, the Baudó Arc, is comprised of oceanic basalts with interbedded sediments of late Mesozoic-early Cenozoic age. Samples recorded two sets of data, one compatible with a 15 paleolatitude origin, and a second with 5 to 10 equatorial paleolatitudes. The nature of the paleomagnetic data is not conclusive but the geological framework favors a southern provenance.

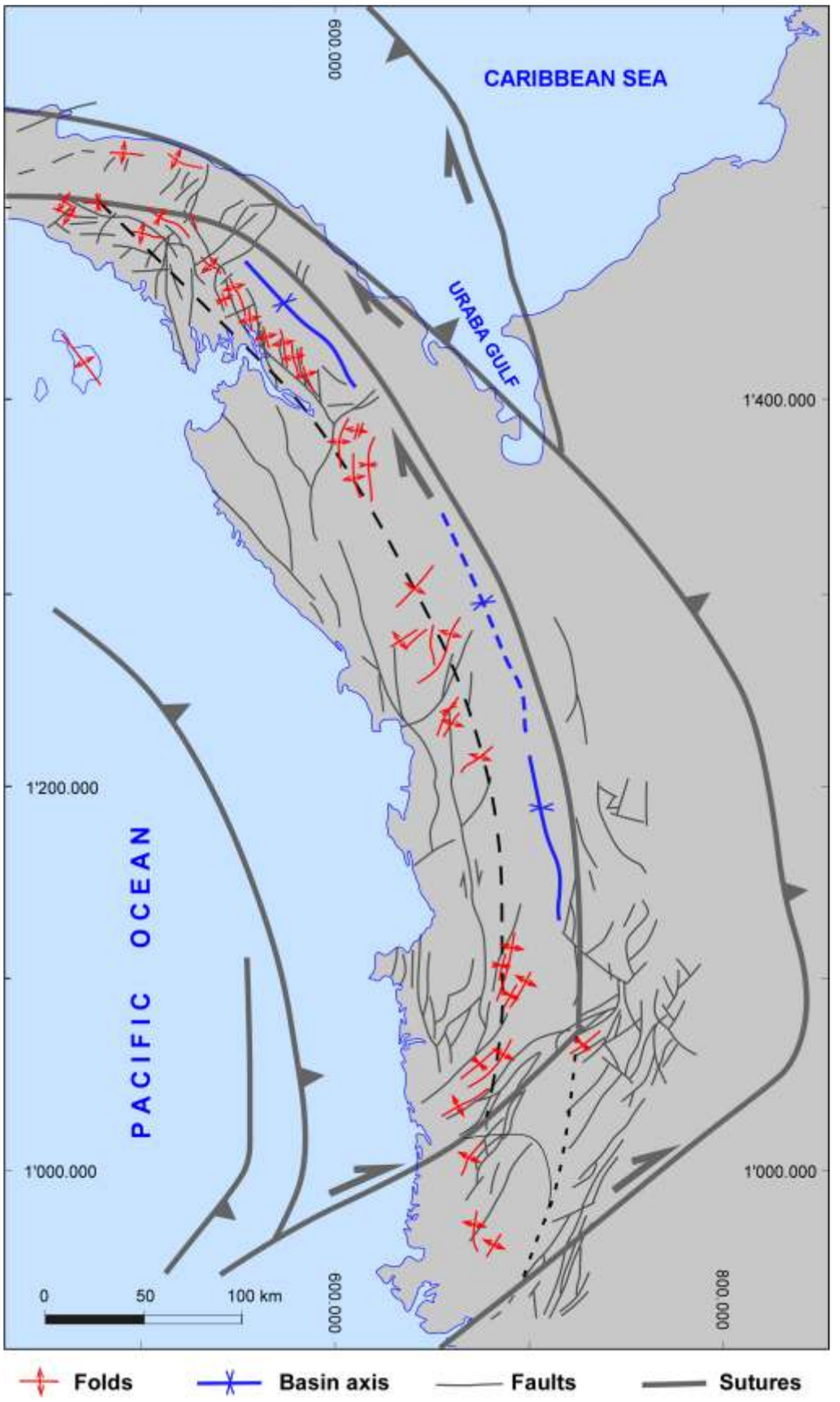

Figure 5. SW-NE to SE-NW rotation of fold axes in the Choco Arc

2. 2. Surface Structural Expression

Faults and folds shown in the surface structural map *(Figure 6)* were compiled from data recorded during various field campaigns as well as from air photo interpretation. All of the available information was compiled at 1:500,000, and reinterpreted and corrected using a Digital Terrain Model (DTM) and radar images.

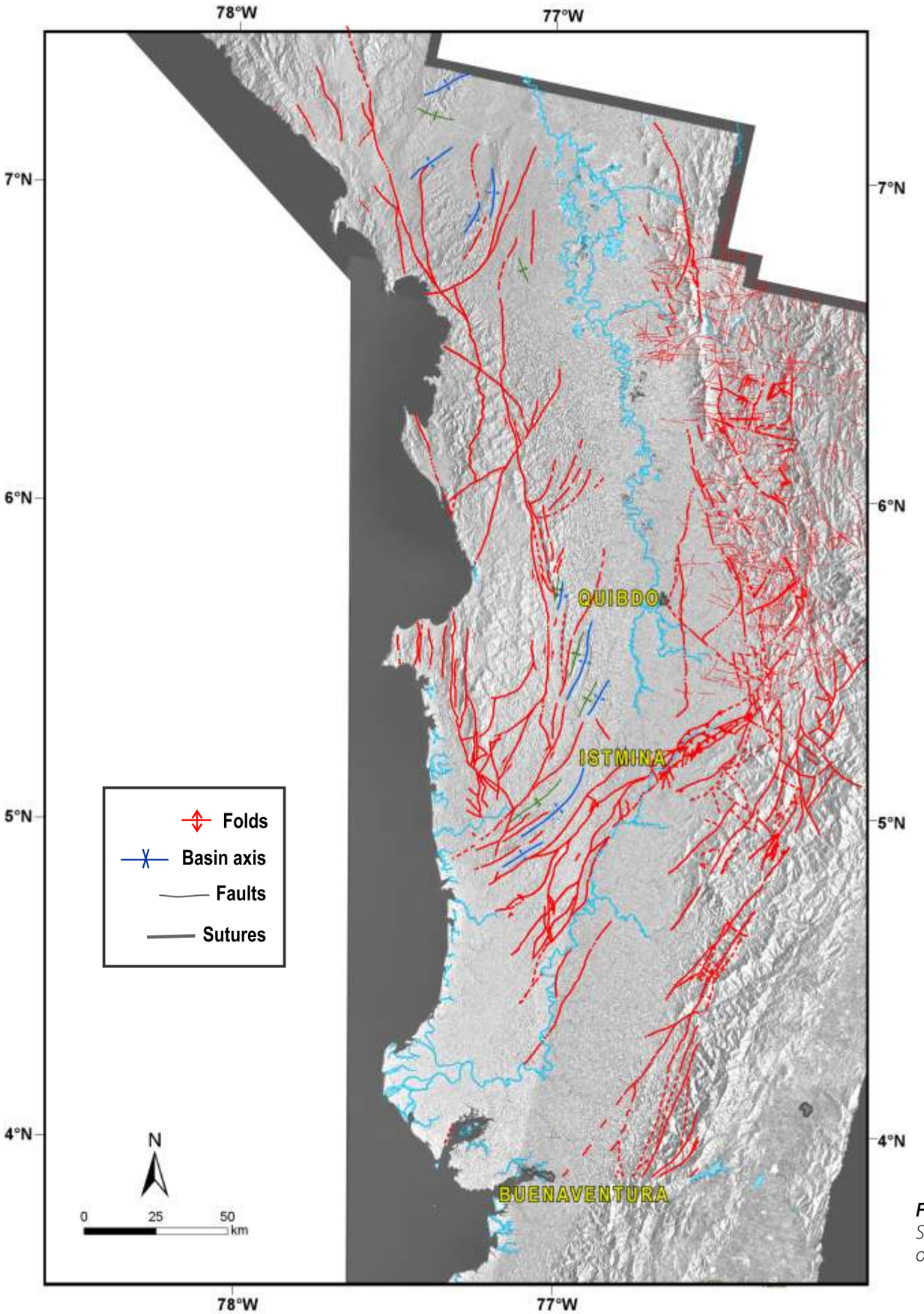

Figure 6.
Surface structural map of the study area.

Subsurface structural control is limited to the interpretation of gravity and magnetic-based geophysical studies. Faults, interpreted in various seismic campaigns, apparently don't reach the youngest strata. It appears that this recent cover is very thick and contemporaneous with deformation.

• Atrato Basin

The Atrato Basin is limited to the west by faults which put the "Baudó Complex" in contact with several sedimentary units. Some of these "faults" or lineaments could correspond to stratigraphic unconformities. The general impression is that the entire fault system is formed by a series of growth faults of varying ages. Absence of field and subsurface data precludes a better understanding of the type of deformation which controls the basins western flank.

It is important to stress that the orientation of fold axes developed in the western flank of the basin shift progressively from SW-NE to SE-NW. This observation attests to stress field rotation, compatible with the geometry of the Chocó-Panamá Arc.

The eastern flank of the Atrato Basin coincides with an almost rectilinear fault system with a preferential N-S orientation, which places part of the sedimentary sequence in contact with igneous rocks of the Mandé Magmatic Arc**.** Data from outcrop favors the interpretation of these faults as normal faults or as high-angle reverse faults. The geometric pattern of this fault system, and it's location along the eastern boundary of the basin however, suggests that it records right lateral displacement during most of the Neogene.

To the north, the Atrato Basin continues into Panamá, recorded as the Chucunaque-Tuira Basin. The southern limit of the Atrato Basin is formed by the Istmina-Condoto High, which is also the N-NW limit of the San Juan Basin.

With respect to the San Juan Basin, at surface, no important structures are presently discernable, as more that 90% of it's surface area is masked by recent sedimentary deposits. A distinct geomorphological architechture is apparent; however, and given sufficient thought; it could potentially be interpreted from a structural standpoint. Such a study deserves future consideration.

2.3. Structural Cross Sections

Balanced structural sections were developed in order to interpret fault and fold complexes, both in compressional (thrust-dominated) settings as well as in tensional and transcurrent environments (Mitra and Namson, 1991). Structural concepts applied to the interpretation of folds and faults vary as a function of the availability of new and improved data, and also with respect to the understanding of fold geometries and fold mechanisms. In order to prepare cross sections for the present work, we used the interpreted seismic lines SJ-81-1200, SJ-81-2600, SJ-81-2200, QA-81-10 and QA-81-04 as presented in the Seismic Atlas of Colombia (Cediel et al., 1998). Mapped reflectors correspond to unconformities to which we assigned ages derived from regional stratigraphic analysis, as follows:

Reflector 10, Sub-Oligocene
Reflector 11, Sub-Lower Miocene
Reflector 14, Sub-Upper Miocene
Reflector 16, Sub-Pliocene

The construction of sections was carried out manually, taking into account theories and guidelines developed by Suppe, Connors and Zhang, 2004. In 2D vision, most sections show high angle faults; some are considered to be reverse faults (SJ-81-200, SJ-81-2200) whilst others are considered to be normal faults (SJ-81-1200). Furthermore, strata are observed to be displaced along fault planes without generating associated folds. This suggests a transcurrent regional tectonic regime, a hypothesis that will be discussed later.

Restoration of structural sections

According to McClay's (1997) definition, a balanced structural cross section is a section in a deformed state which is both admissible and feasible. With respect to folds and faults, it represents a realistic geometry and structural style that can be restored in such a manner that the length and thus the area of individual layers is preserved.

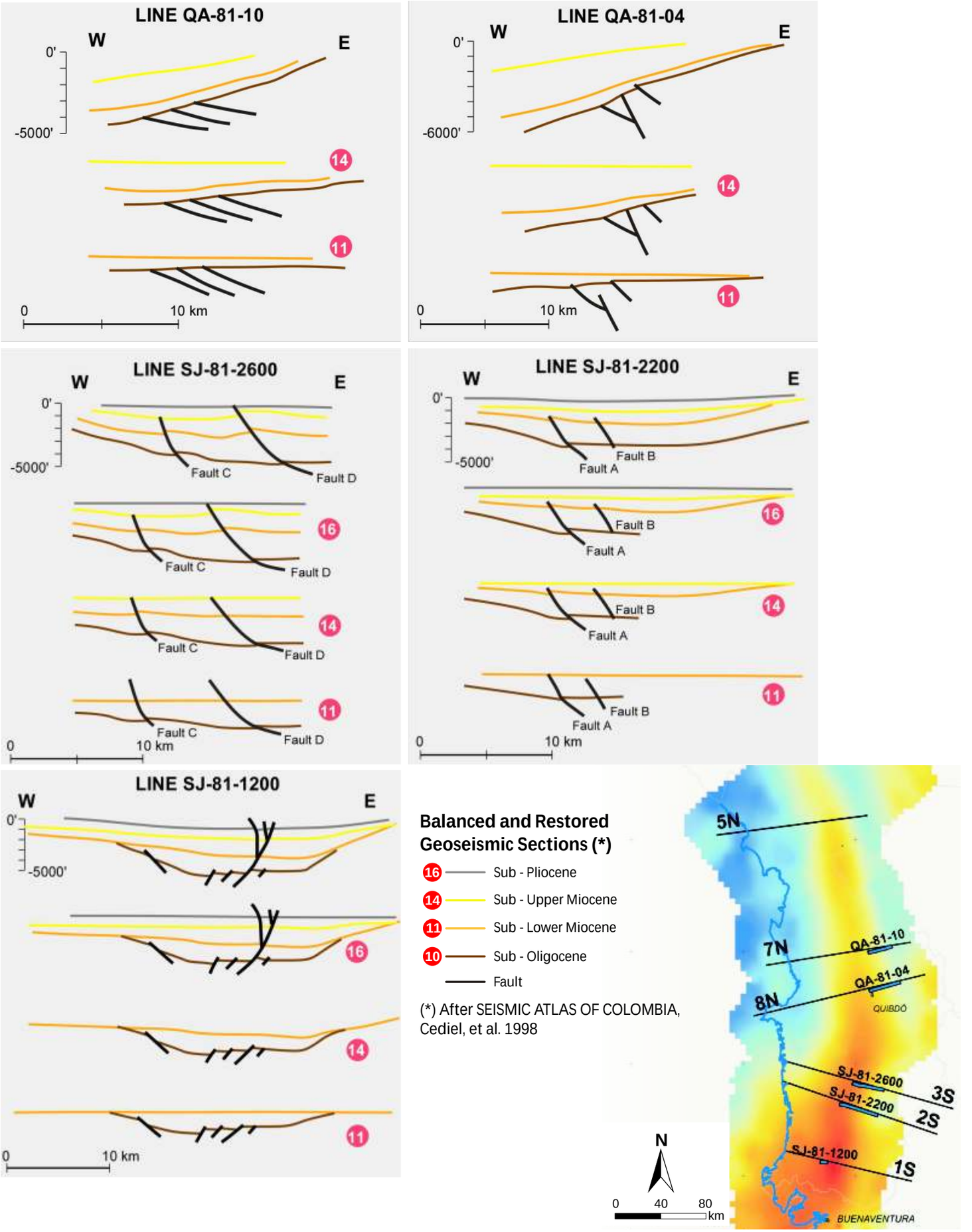

Figure 7. Restored structural cross-sections

The results of the above mentioned exercises are summarized in Figure 7 Based upon these results we conclude that:

- The formation of conjugate high angle faults with short vertical displacements and the absence of fault-related folds, as well as the simultaneous presence of normal and reverse faults, together with faults forming negative flower structures (see seismic line SJ-81-1200) has been interpreted to represent a regional tectonic regime dominated by transcurrent movements.

- Toward the eastern flank of the basin, faults observed in seismic lines QA-81-10 and QA-81-04 affect only reflector 10 (Sub-Oligocene). Progressive restoration shows that the inclination of reflector 10 has increased from the flattening of reflector 11 to the present deformed state. It is concluded that at the same time as sediments were deposited, the basin tilted westwards.

- The western slope observed in seismic line SJ-81-2600 shows a lesser inclination to that observed on the eastern slope, with reverse faults verging westward; these faults controlled the deposition of lithological units underlying unconformity 11 (Sub-Lower Miocene) and unconformity 14 (Sub-Upper Miocene).

- Normal faults seen in seismic line SJ-81-1200 affect all the units from the basement to reflector 16 (Sub-Pliocene unconformity), and even affect some overlying strata. On the other hand, reverse faults found in lines SJ-81-2200 and SJ-81-2600 affect reflectors 10, 11 and 14 but don't reach reflector 16. We therefore infer that normal faulting is more recent that reverse faulting (despite the fact than transcurrent regime is still active).

2.4 Gravimetric and Magnetometric Interpretation

Through the interpretation of aerial gravimetric and magnetic data, a geophysical model of the basin was built. The characterization of the basement proved to be critical to the understanding of basin evolution. The basement map shows that the two basins -Atrato and San Juan- have significant different gravimetric and magnetometric textures.

Data Sources

Aeromagnetic and aerogravimetric data were provided by the *Agencia Nacional de Hidrocarburos* (ANH) and by *Ecopetrol* (at ANH's request). ANH data were collected in 2005 by Carson Helicopters Ltd., and cover the Atrato basin area. Survey lines were flown at two altitudes, 1,280 m and 3,300 m, with a flight pattern covering 7.5 km by 10 km. Ecopetrol data were collected by the same company in 1999, with a flight altitude at 2,257 m and cover the San Juan Basin *(Fig. 8)*. Digital files were received in ASCII format with Magna coordinates for the Atrato Basin and with Bogota-West coordinates for the San Juan Basin.

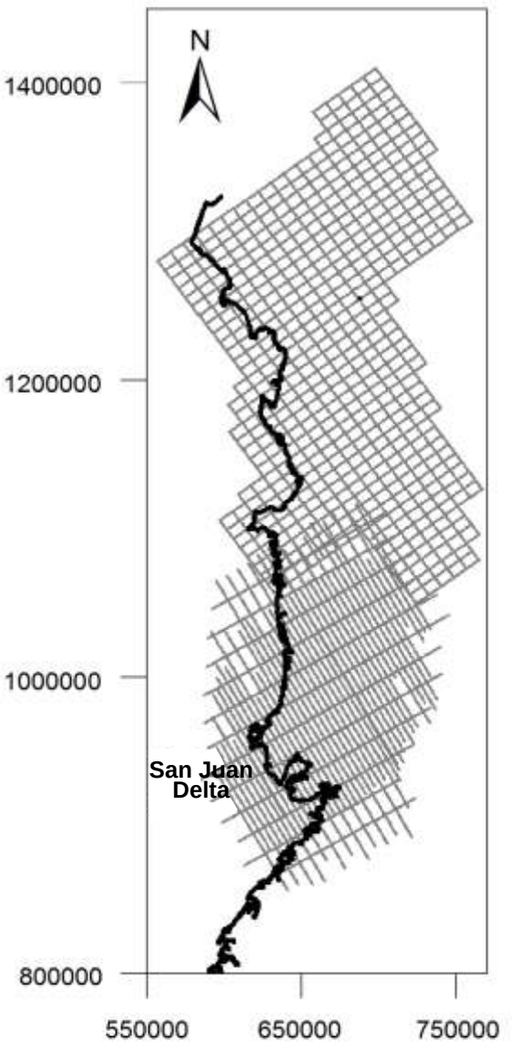

Figure 8 Location of two aerogravimetric and aeromagnetometric data sets, used for geophysical modeling.

Total Magnetic Intensity (TMI) values and Bouguer Gravimetric Anomaly (BGA) values found in the data bases were used for the generation of Bouguer anomaly, gravimetric basement and total magnetic intensity maps presented in this report. No altitudinal correction was made before merging the data.

Methodology

Bouguer anomalies map (BGA) *(Fig. 9)*

BGA data (P = 2.67 gr/cm^3) from both databases were integrated. Two BGA maps were elaborated, one with the Krigging interpolation method and the other one with minimum curvature. The first was selected for interpretation, with a cell size of 5 km.

The interpretation of the BGA data was complemented with gravimetric profiles to which an inverse modeling was applied, in order to determine the gravimetric basement profiles which fit better the observed values. Inverse modeling was carried using a non-commercial program. This program is based on the determination of the Fourier Transform for a set of (x,z) data following the equation proposed by Parker (1973) and improved by Oldenburg (1974), in order to make it more iterative. This equation enables the calculation of the shape of a body based upon it's anomaly. The program builds a relief function which is best adjusted to the BGA profile, based upon the previous determination of parameters including density contrast, input data separation and topographic level of inversion (z_o).

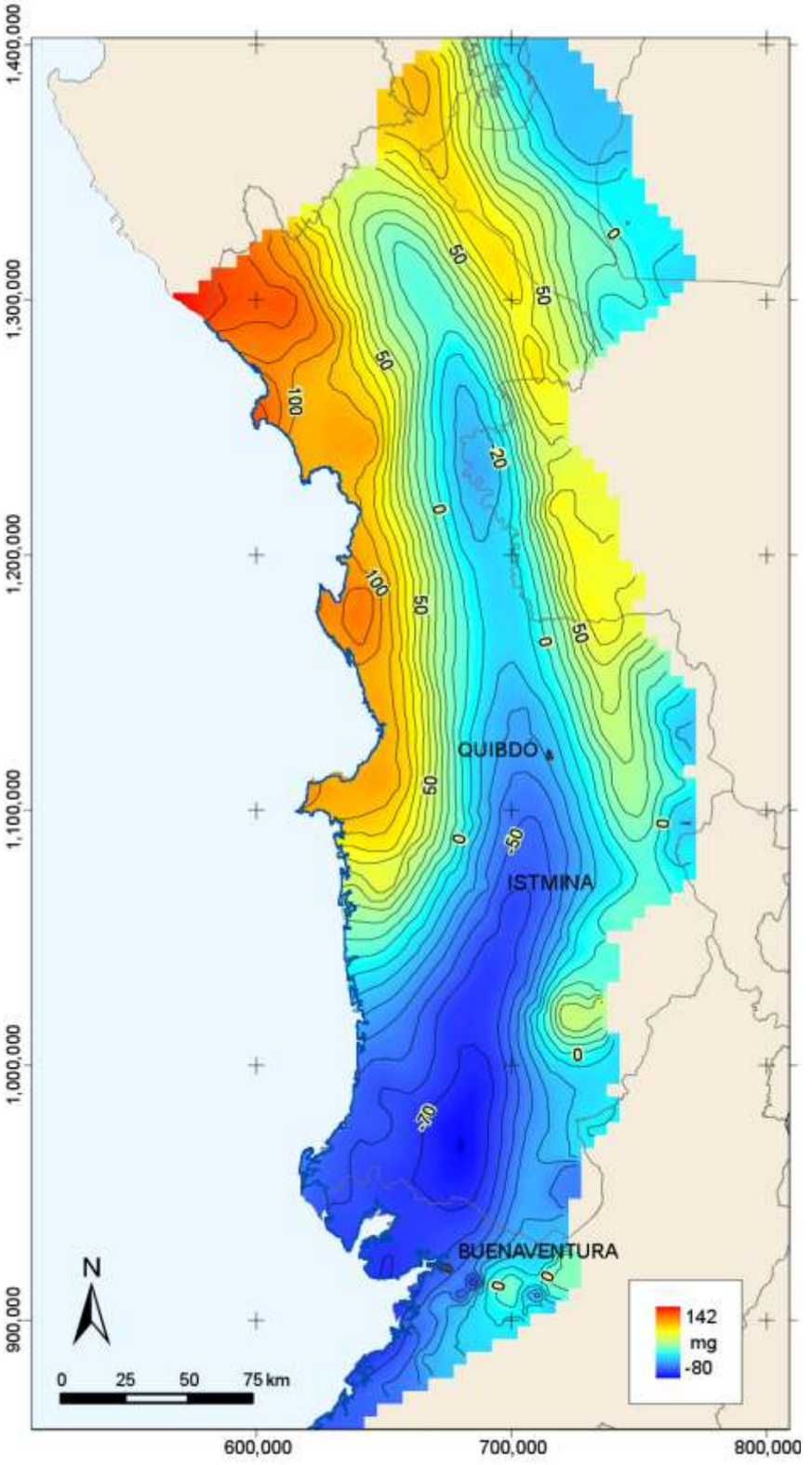

Figure 9. Bouguer Anomaly map. This map suggests the presence of only one basin; it is necessary to remove the topographic influence (Graterol and Gummert, 1998) to see a better configuration like the on shown in Figure 10

2.4.1. Basement Map

It is possible to draw a basement map through gravimetric inversion of the BGA data applying analytical continuation to 2 km depth and using surface and subsurface basement control points *(Table 1)*. As a preliminary step, the signal produced by the regional trend should be separated in the BGA map from the signal produced by residual affects. This separation was made in a quantitative way, following the methodology proposed by Graterol and Gumert (1998). Once the signals are separated, the residual map is inverted using proper software (Bhaskara Rao & Rameshu Babu, 1991). This inversion produces a controlled gravimetric basement map (figure 10)with depths expressed in kilometers.

Basin geometry is interpreted from the Basement map. Low-density values reflected through negatives anomalies in the Figure 9, correspond to the sedimentary sequence. West to the coastline, off-shore, the modeled map shows a pseudo "positive" relief which means that The Serranía del Baudó has a strong gravimetric anomaly and the model used was insufficient to filter this signal. The methodology used in this model applies control over the sedimentary sequence, only. Additional geophysical treatment is necessary to model the crystalline bodies.

t	X	Y	Z
sup6	654812	1076322	179
sup2	619627	1326335	1000
sup0	635514	1259938	378
qa-81-10-400	726795	1162894	36
qa-81-10-250	719516	1161036	2790.5
qa-81-10-150	714689.9	1159805.8	4194
qa-81-04-550	734448.3	1131329.5	180
qa-81-04-385	726889.4	1129194.5	2440
qa-81-04-180	716907.3	1126318	6013
bv9	719384.4	1000166	0
bv7	707538.3	1038255	5060
bv6	704431.3	1014744	2942
bv3	679056.4	927491.9	4193
bv26	607403.2	1040711	2000
bv25	607228.3	1000637	2400
bv24	686704.9	1024833	2880
bv23	685131.5	1008319	1820
bv22	685095.5	999809.1	2016
bv21	684800	989047.1	2657
bv 20	682757.4	979042.9	3334
bv18	708790.7	1038500	5199
bv17	706242.3	1028251	3570
bv15	700386.3	1005251	3598
bv14	697483.6	995751.1	4449
bv13	694299.4	986004.6	3932
bv12	692258.7	976501.8	4484
bv11	687220	968261.9	4757

Table 1. Control points used to obtain the basement map Z values are depths expressed in meters. Negative values represent values above sea level where the basement crops out . Control point prefixes were obtained from Carson's (2006) report and were corroborated with the seismic lines.

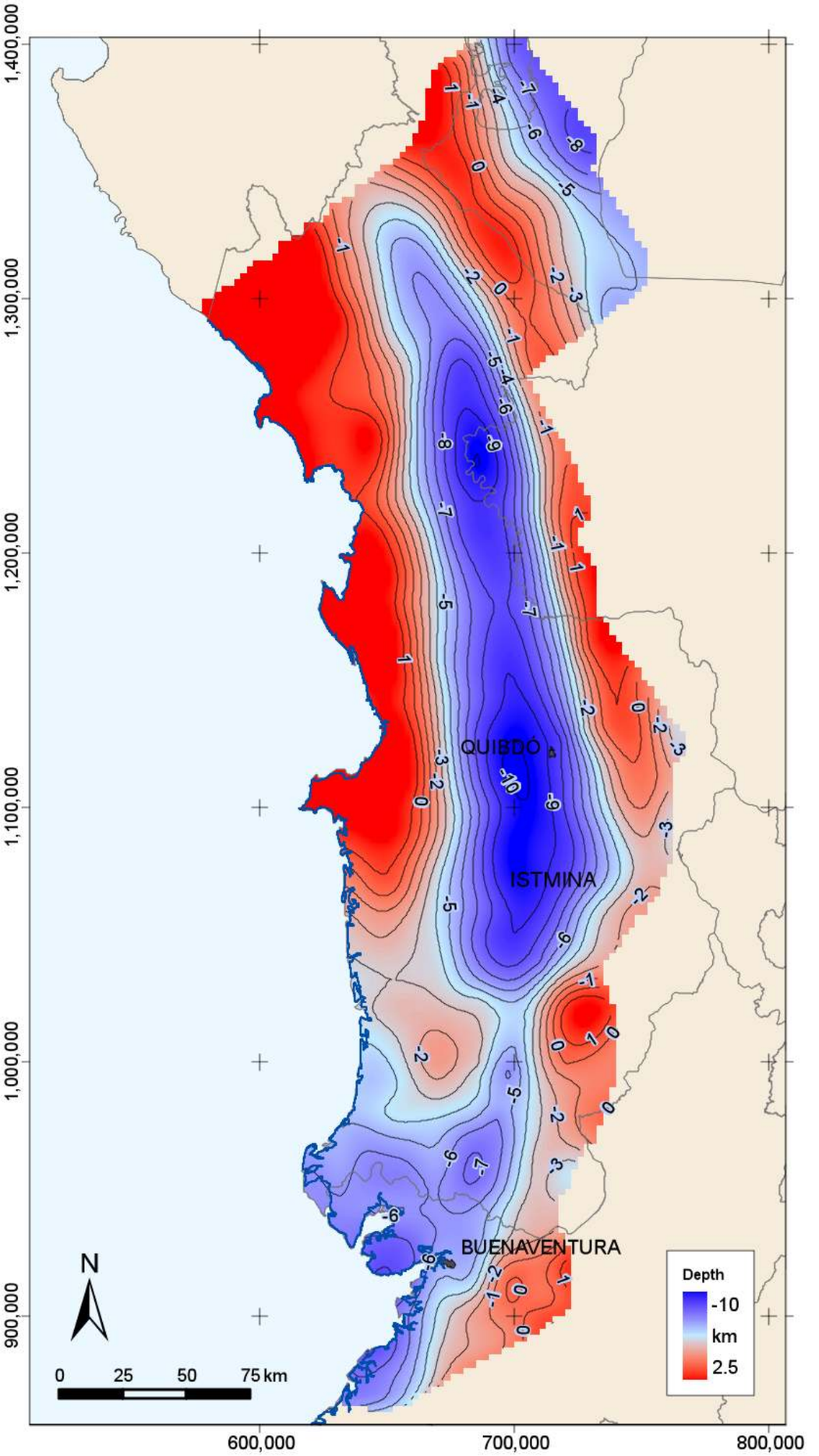

Figure 10. Gravimetric Basement map of the San Juan and Atrato Basins. Two distinct gravimetric patterns clearly distinguish show two different basins.

• *Total magnetic intensity map (TMI)*

The integration of TMI values required a previous procedure known as "demeaning", used when it is clear that values are calibrated on the basis of two different data sets. Once the datum was standardized, interpolation was carried out with both Krigging and the minimum curvature methods. The best model was obtained by using Krigging, with a cell size of 5 km. The TMI map shows a very high magnetometric anomaly between the San Juan Basin and the Atrato Basin (close to or in the Istmina-Condoto High). This anomaly was masked in the grid, so a new map was generated to allow more contrast in the magnetic response in the rest of the study area. This procedure permits us to distinguish six magnetic provinces *(see Fig. 11)*

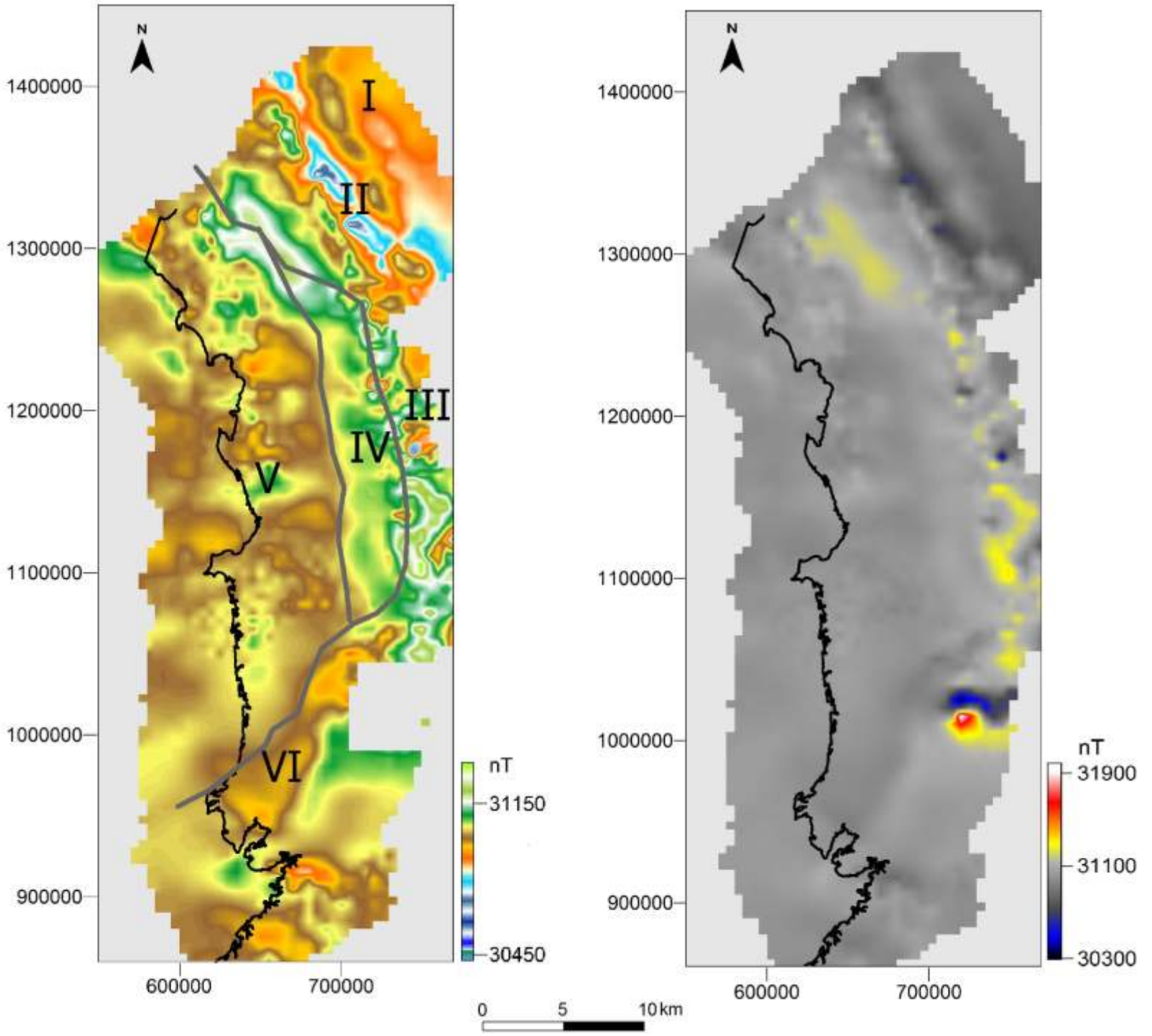

Figure 11. Total Magnetic Intensity maps. At right TMI shows a high anomaly whilst at left the anomaly is masked. At left, Roman numerals show six magnetometric provinces:(I) Uraba Basin, (II,III) Western flank of the Western Cordillera, (IV) magnetometric basement of the Atrato Basin, (V) Baudó Range, and (VI) magnetometric basement of the San Juan Basin. Gray lines depict two principal lineaments named the Baudó Structure (left) and the San Juan-San Sebastián Suture (right curved line). More structures are suggested between provinces, but aren't drawn.

• *TMI first directional derivate map (TMIFD)*

In this TMI map (figure 12) it is possible to see conspicuous limits between different areas with specific magnetic patterns, which suggests the presence of basement faults. Two first derivative maps (E-W and N-S) were created in order to reveal the principal structures in two directions.

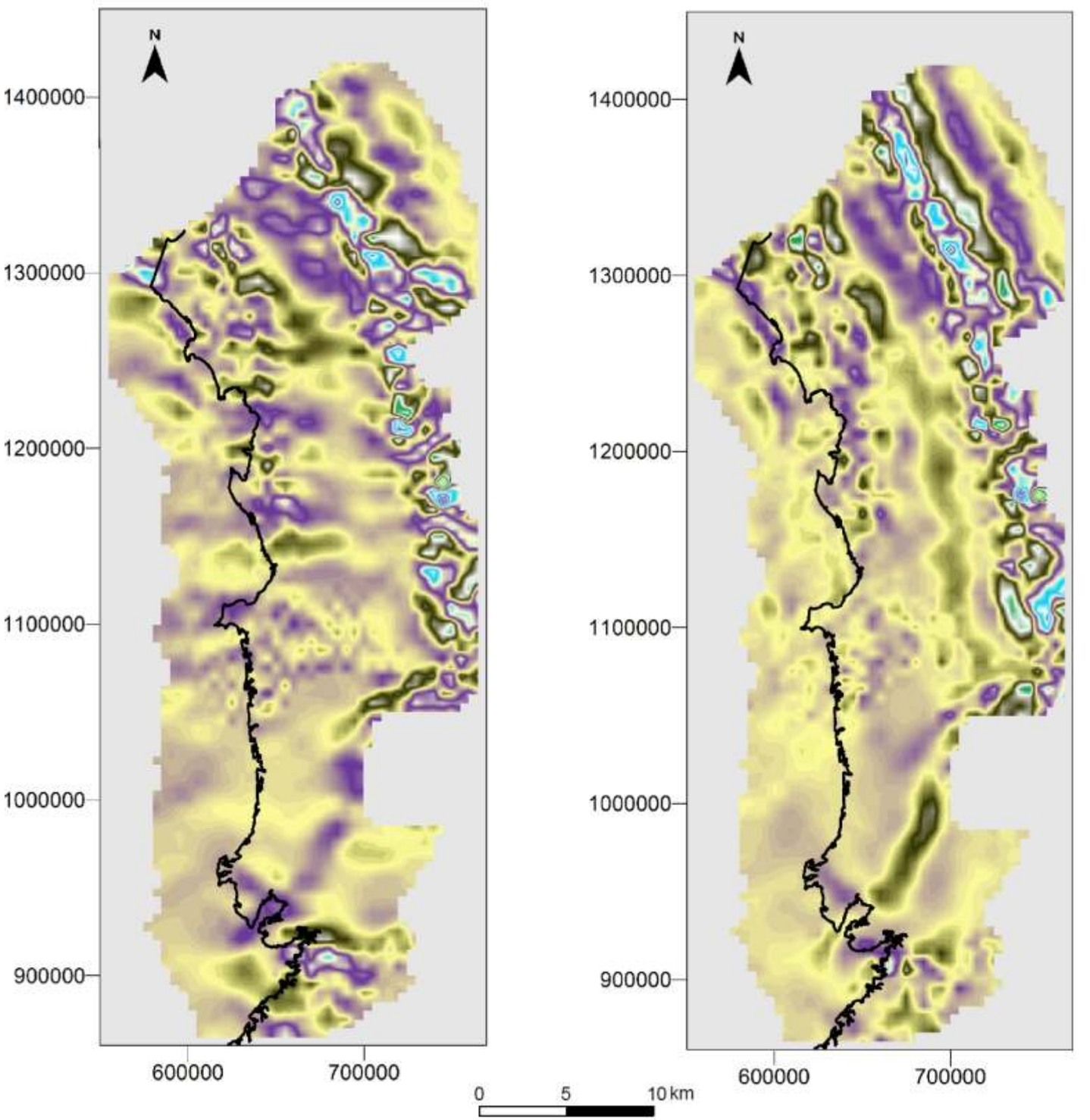

Figure 12. TMI first directional derivate map (TMIFD). The N-S directional derivative at left clearly shows the normal inverse magnetometric pattern in Baudó Range (detailed in Figure 13). At right, the E-W directional derivative highlights N-S-oriented structures and lithological contacts.

• Magnetometric profiles along the Baudó Range *(Figure 13 and 14)*. TMI map of the Baudó Range generated by masking the rest of the study area. Next, four N-S profiles were obtained removing the geometric mean (31,000 nT) in order to analyze local magnetometric variations *(Fig. 14)*.

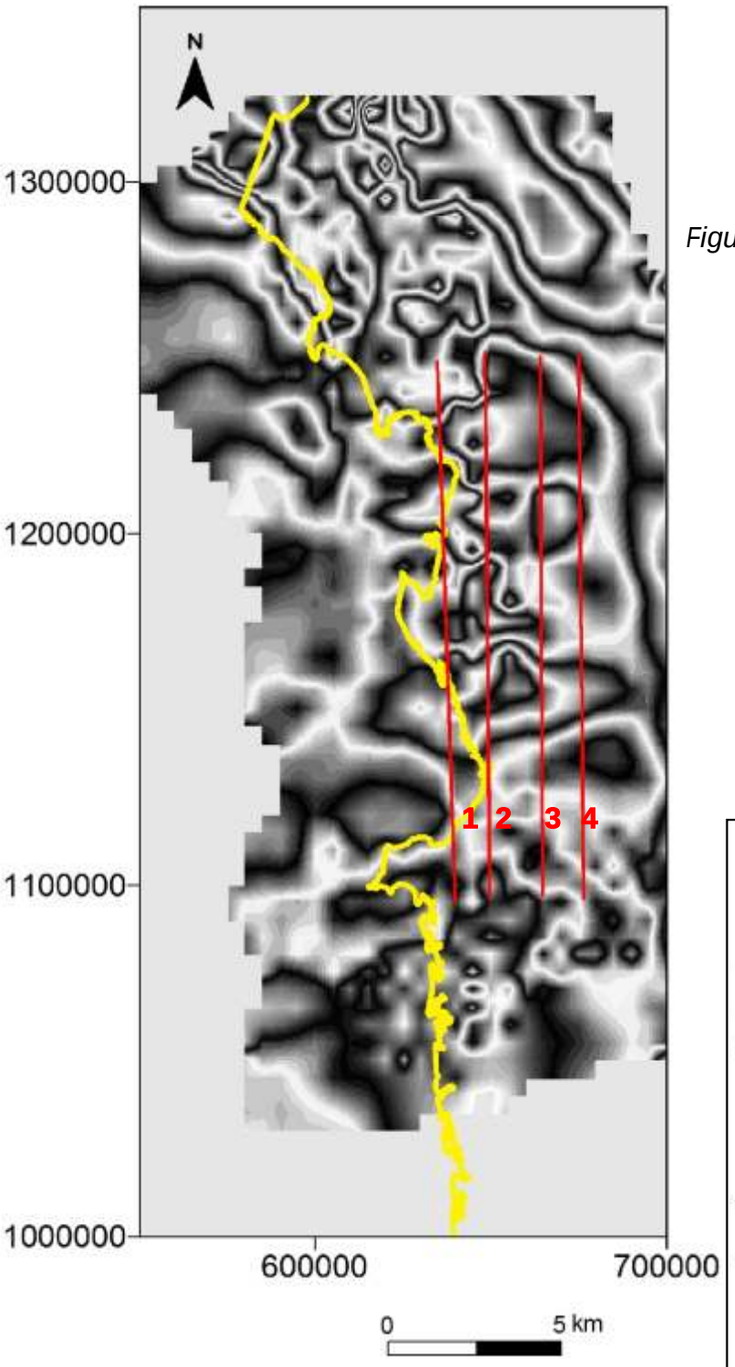

Figure 13. Detailed TMI along the Baudó Range. The red lines show the four profiles shown in Figure 14.

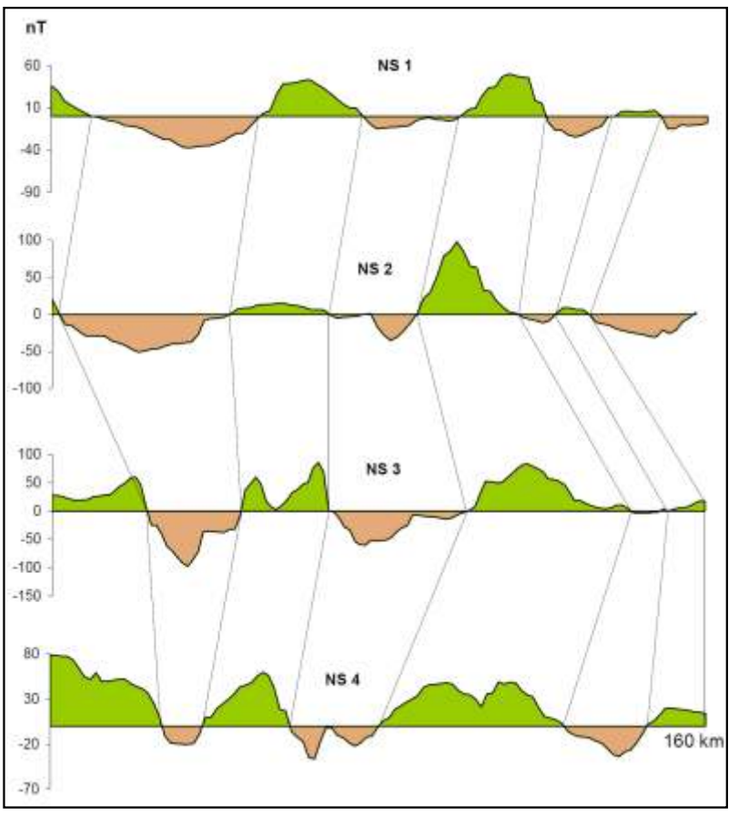

Figure 14. North-south magnetic profiles along the Baudó Range.

Results

Once the above outlined maps were completed, geophysical modeling was carried out for each basin, including the Atrato *(Fig.15)*, and the San Juan *(Fig. 16)*. Profiles used for geophysical basin modeling are located perpendicular to the basin axis. Some of them coincide with seismic lines.

Atrato Basin

This elongated, asymmetric basin, has a general N1OW orientation. The gentle slope of it's west flank dominates the geometry of the basin. The Atrato basin has depths which reach 10 km. The BGA map outlines lower anomaly values and the TMI map reveals relatively homogeneous characteristics in the central part of the basin. Toward the flanks, TMI values are irregular due to the presence of faults and the contacts with lithologies of higher magnetic susceptibility *(Fig. 15)*

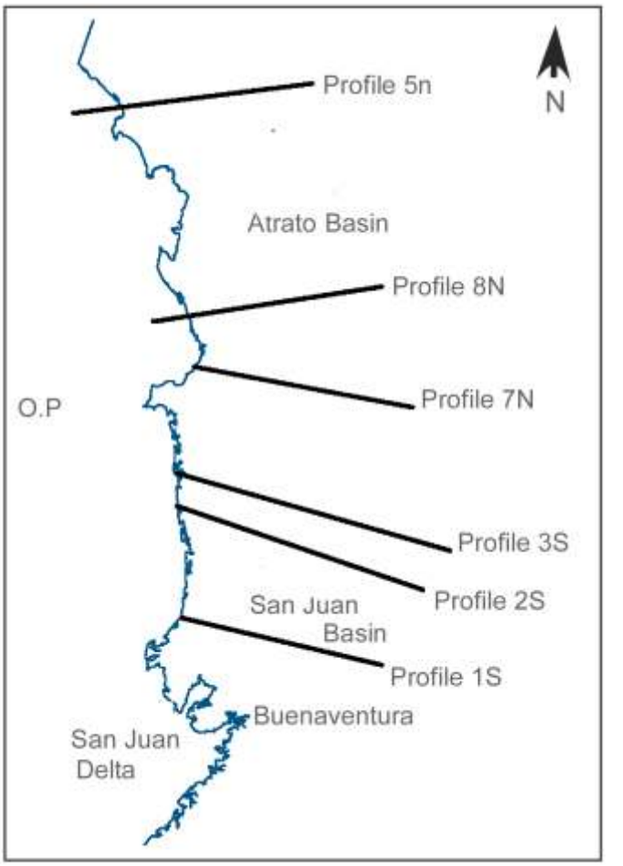

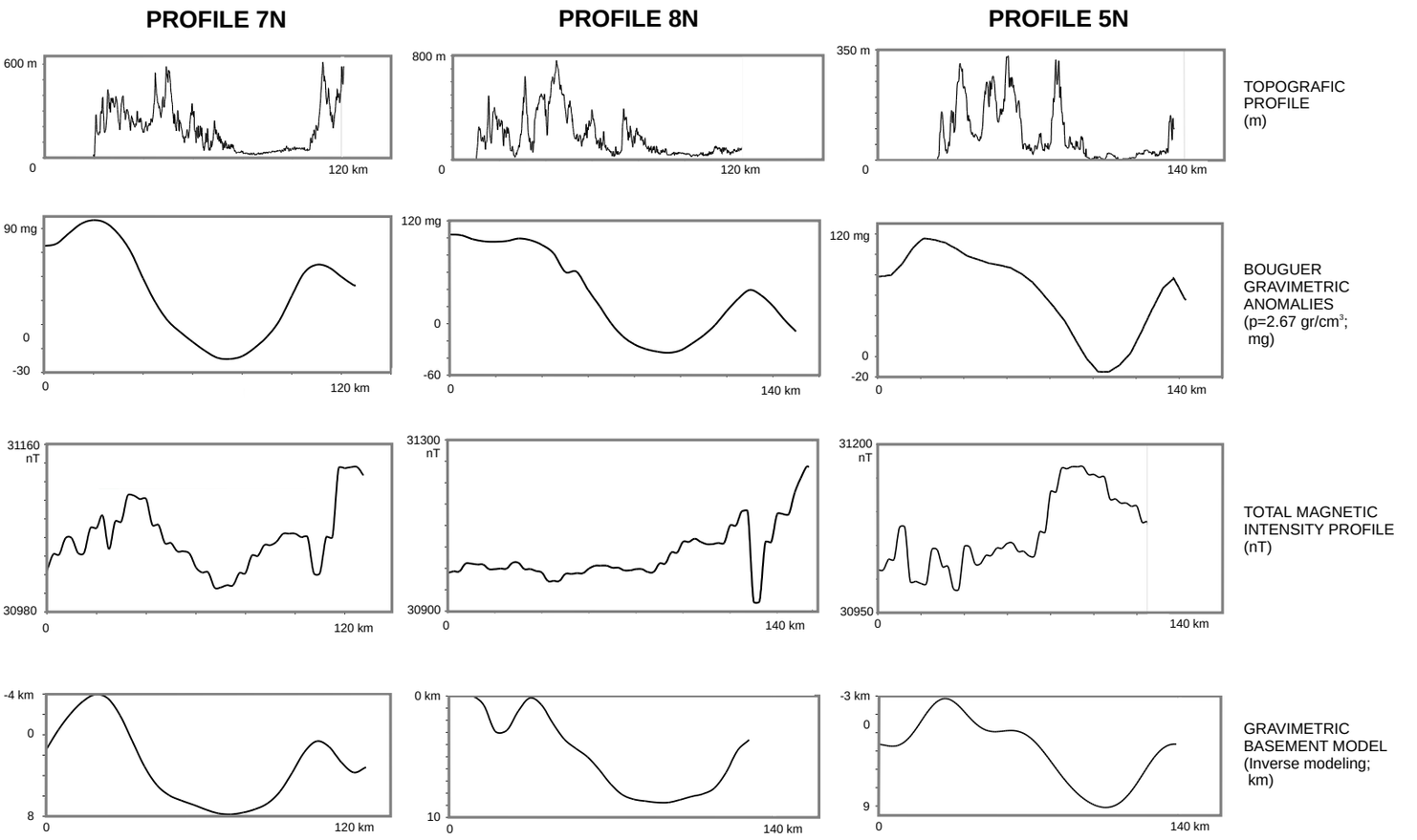

Figure 15 Geophysical modeling in the Atrato Basin. Note the corresponding normal-reverse magnetometric pattern along each line and between lines.

San Juan Basin

The San Juan basin is clearly separate from the Atrato Basin. As revealed by the basement map, each basin presents a very distinct geometry. The San Juan Fault/Suture system forms the northern and north western boundary of the San Juan basin whilst the southern limit is defined by the Garrapatas Fault and suture system. Both of these structurally defined boundaries are clearly seen on the TMI map. The strongest TMI anomaly is on the NE part of the basin and corresponds to a mafic to ultramafic body (high anomaly in TMI map, *Fig. 11*) which controls the shape of the basin and makes it narrower in this direction. On the TMI map this area has a distinct magnetic pattern (Province IV in *Fig. 11)*. The magnetometric response is similar to the one south of Buenaventura.

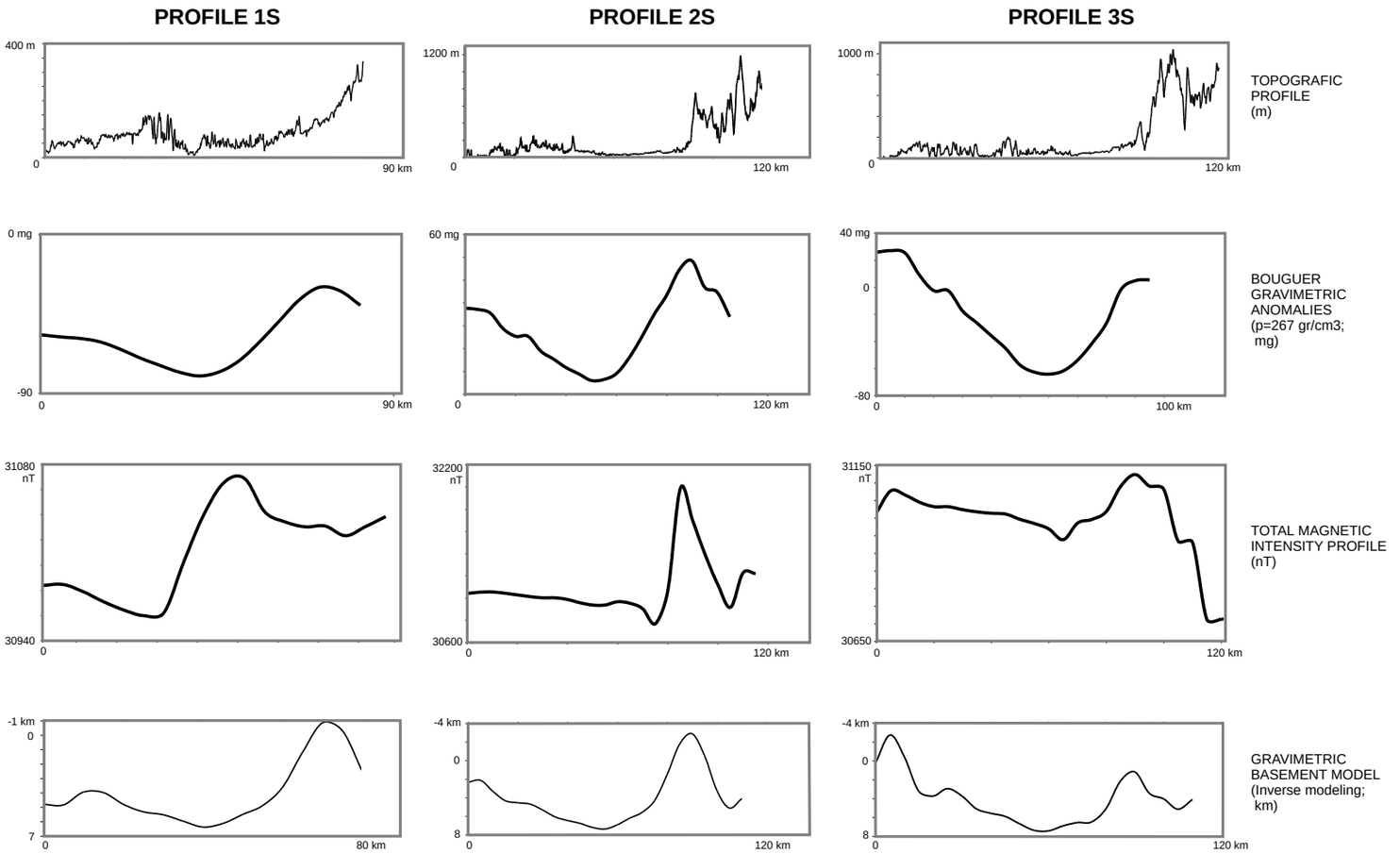

Figure 16. *Geophysical modeling in San Juan Basin*

Baudó Arc

The Baudó Arc is very well defined in the seven modeled maps. The BGA map indicates the highest gravity anomaly values for this body in the entire area, even higher than those found in the western margin of Western Cordillera, which has a much higher relief. Inverse gravity modeling suggests 4 km of hypothetical relief versus the observed 1.2 km of topography.

This contradiction was explained by Vargas (2007) who applied tomographic inversion techniques along Profile 03 N. At 77°W and at a 40 km depth, a Low Velocity Zone is encountered, suggesting the presence of a shallow anticline in the Moho. Similar structure appears again on the 6.0°N profile *(see Fig. 17)*

As outlined previously, the geomorphology of the Baudó Arc is the result of flexural processes involving the up-warping of oceanic crust. Vargas (2007) suggested that the MOHO below the Baudó displaced upwards and high density material migrated to higher levels. We concur with this conclusion which explains the anomalously high BGA beneath the Baudó Arc.

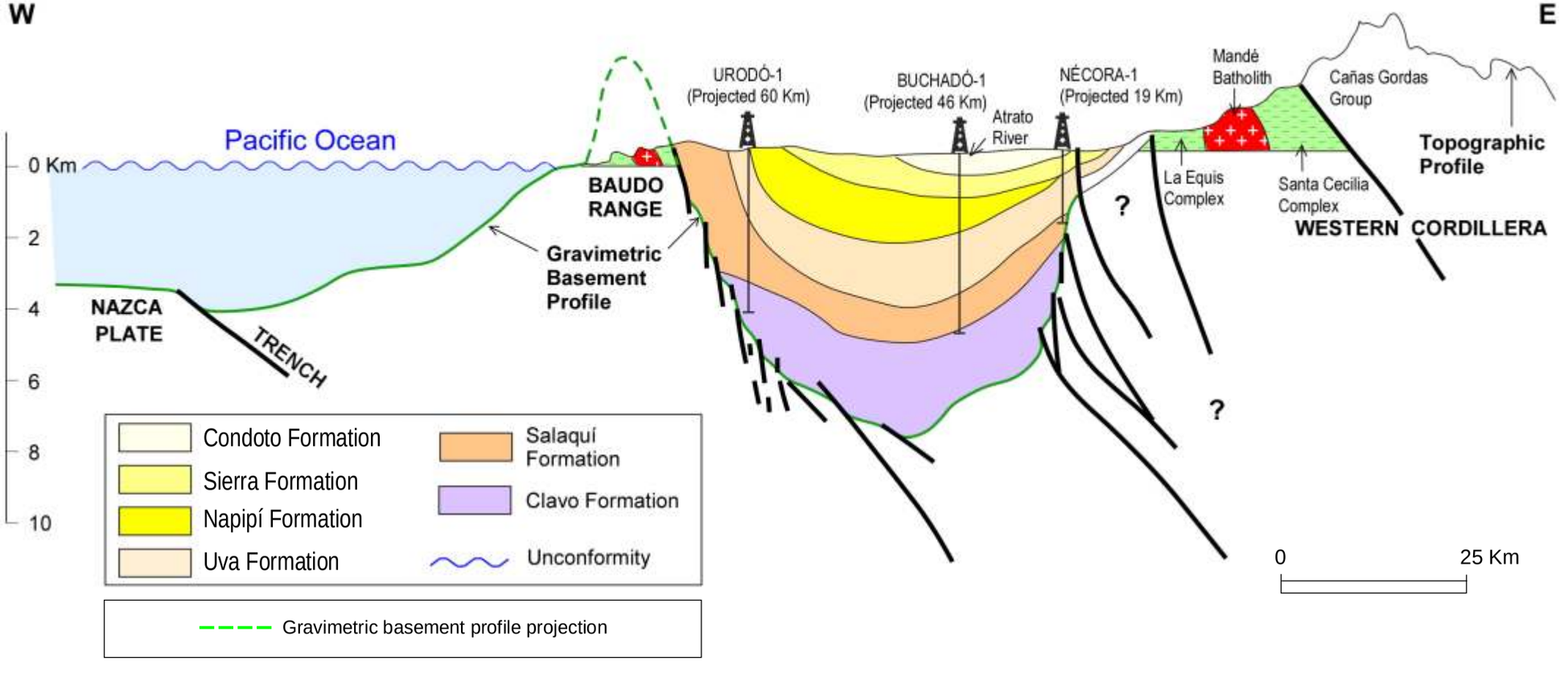

Figure 17. Schematic profile along parallel 6.0°N

• The TMI texture also was evaluated. Magnetic profiling was undertaken to evaluate the different geological configurations capable of generating such geophysical response *(Figs. 13 and 14)*. *Fig. 14* shows a magnetic alternation between normal and reversal picks, inside a north to south profile. Similar alternation patterns repeat along the four profiles. Although no synthetic profiles to determine age were generated, a comparison with magnetometric patterns along the Colombian Pacific coast, as shown by Hardy (1995) is possible. Correlation with an extinct spreading centre is suggested, thus the Baudó magnetic pattern could be associated with a fossil ridge *(Fig. 14)*

Further geological mapping, geophysical and geochemical research is needed to better support an appropriate model for the Baudó Range including it's relation with the Atrato basin.[1]

2. 5. The Istmina-Condoto High

The BGR-INGEOMINAS (1990) study provides the most comprehensive geological knowledge of this area.

The (ICH) *(Fig. 18)* is a SW-NE elongate composite structure, approximately 130 km long and up to 30 km wide, which plunges to the SW beneath a thick cover of Cenozoic sediments and into the Pacific Ocean. This structural assemblage contains thrust, high-angle reverse, and normal faults and associated folds, all of which define a transpressive shear zone with right lateral displacement. With the exception of the Pleistocene deposits, all rock units present angular base-and-top unconformities and a high degree of deformation. Based upon a close association with typical upper mantle ultramafic rocks, it is inferred that the composite Istmina-Condoto structure evolved within an intra-oceanic suture, beginning in the late Cretaceous followed by exhumation in the Cenozoic.

The last phase of uplift took place along SW-NE striking faults, causing flow reversal of the regional drainage system into the present San Juan basin, especially along the Mondo, Bochoroma and Iró rivers.

The following is a brief description of the most significant igneous rocks associated with the Istmina-Condoto High:

1. El Paso Complex

El Paso Complex is the oldest lithological unit in the Chocó Arc. It is a strongly fractured sequence of high Mg-tholeiitic basalts and ophiolitic diabases with interbeds of chert, claystone and mudstone. Cr/Y and Ti/Zr ratios suggest an oceanic (MORB) origin. No radiometric dates are available, however regional geologic analysis indicates that the El Paso Complex is likely late Cretaceous to Paleocene in age.

2. Viravira Complex

This complex includes a sequence of basalt, basaltic breccia, peridotite, harzburgite and serpentinizied dunite, along with mudstone, black claystone, fine grained sandstone, some calcareous sediments and chert. The marine deposits attain 500 m to 1,000 m in thickness. Radiolaria and globorotaloid fossils represent the Upper Eocene to Lower Miocene. Ultramafic rocks (Alto Condoto) dated at 17.8 and 21.5 Ma are known to intrude sedimentary interbeds which belong to the Viravira Complex, producing a metamorphic contact zone up to 1.5 km wide. Geochemical data from basalt and serpentinite samples suggest magmas originated in the upper mantle, generating the komatiitic facies and high Mg contents.

3. Alto Condoto Ultramafic Complex

The mapped out crops of this complex occupy an area of approximately 3 km^2 by 6 km^2. It appears to be a zoned intrusive with a dunite core, grading in composition outwards to wherlite and clinopyroxenite. In the outer rim small out crops of hornblendite, diorite and dioritic dykes are observed. Potassium-Argon radiometric dates range from 21.5 Ma, to 17.8 (Lower to Middle Miocene). Ultramafic intrusive assemblages of similar age and/or composition have not been documented elsewhere in northwestern South America.

(1) We acknowledge the advice given by geophysicist G.Y. Ojeda during aeromagnetic and aero-gravimetric data processing. We also thank geophysicist J. Ceron for facilitating the acquisition of the data. Geophysicist C. Vargas kindly provided a pre-print his paper entitled "Seismic structure of the South-Central Andes of Colombia by tomographic Inversion" (in press).

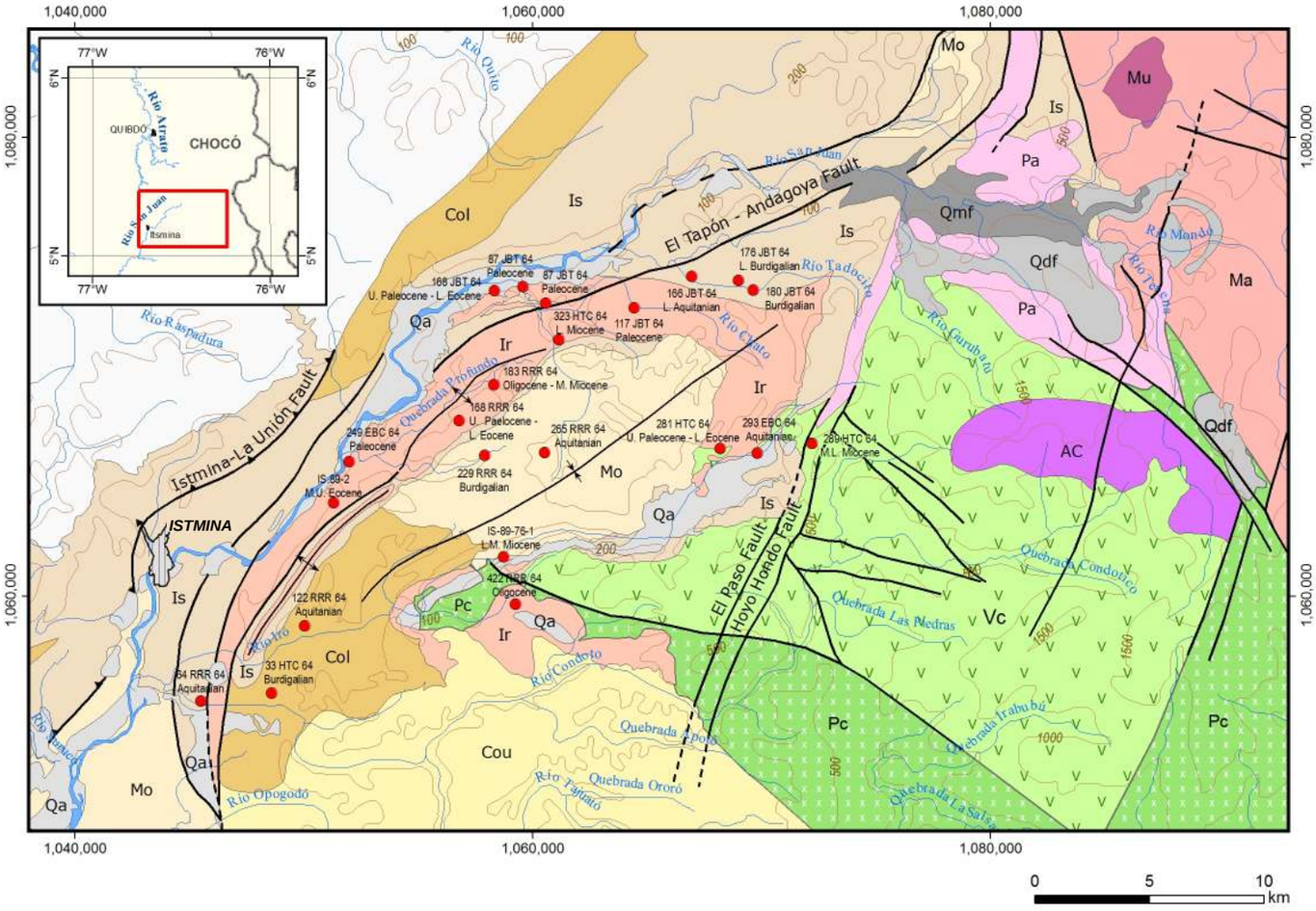

Qdf **Debris flood**

Qmf **Mudflows**

Qa Alluvial deposits

Mo **La Mojarra Conglomerates Formation:** Polygenetic conglomerates. ? Lower Miocene

Multiple Dejection Cone. ? Lower Miocene

Cou **Upper Condoto Formation:** Sandstone and conglomerates

Col **Lower Condoto Formation:** Claystone rich in organic detritus

Is **Istmina Formation:** Siltstone, claystone, sandstone and conglomerates. Lower Miocene

Ir **Iró Formation:** Fossiliferous limestone, shale and chert. ? Paleocene - Eocene

Vc **Viravira Complex:** Komatiitic basalts and breccia. Sedimentary rock interbeds. ? Upper Eocene - Oligocene

Pc **El Paso Complex:** Mafic rock assemblage. (Tectonic window of the ? Baudó Complex / Oceanic crust). Late Cretaceous

AC Mu **Ultramafic bodies(Alto Condoto and Mumbú)** 21.5 - 17.8 Ma

Pa **Andesitic porphyry**

Ma **Mandé Batholith:** Tonalite - granodiorite. 54.7 - 34 Ma

Burdigalian **Sample site, biostratigraphic date (Texas)** Note that some sample ages disagree with ages ascribed to lithologic units.

Fault

Inferred Fault

Thrust Fault

Syncline

Anticline

Sources:

Dunia Consultores, 2006. Informe de integración e interpretación de la información geológica de campo. ANH, Bogotá.

BGR – Instituto Federal de Geociencias y Recursos Naturales de Alemania & Ingeominas, 1990. Mineralizaciones Primarias de Minerales del Grupo de Platino y Oro en la Cuenca de los Ríos Condoto e Iró, Chocó, Colombia.

Texas Petroleum Company, 1989. Informe geológico área de asociación Istmina. EPIS

Figure 18. The Istmina-Condoto High (geological map)

Qui
Punta Ardita
Bahía de Humboldt
Uv
Qall
Punta Cabo Marzo
Punta La Tortuguera
Bahía de Cupica
Sa
Pen
Ma
Siu
Si
Punta Nabugá
Bahía Solano
Qui
Peu
BETULIA
CONCORDIA
SALGAR
EL CARMEN DE ATRATO
Uv
Sa
Sil
Ensenada de Utría
PACIFIC OCEAN
Siu
BETANIA
GOLFO DE TRIBUGÁ
Ensenada Coquí
Punta Arusí
Cabo Corrientes
Qui
Ma
Si
MISTRATO
PUEBLO RICO
Playa Nueva
Sil
SANTUARIO
LA CELIA
BALBOA
Co
Bahía Baudó
Boca Usuragá
SAN JOSE DEL PALMAR
Rp
Br
Peu
EL CAIRO
ARGELIA
Ensenada Docampadó
Co
Is
QTf
Boca Hijua
CARTAGO
SISTEMA DE FALLAS GARRAPATAS
TORO
VERSALLES
OBANDO
Boca Orpúa
EL DOVIO
My
N
BOLIVAR
SAN JUAN
Boca Cacagual
Qall
Rp
Ci
25
50
km
QTf
Playa El Choncho

3. STRATIGRAPHY AND FACIES

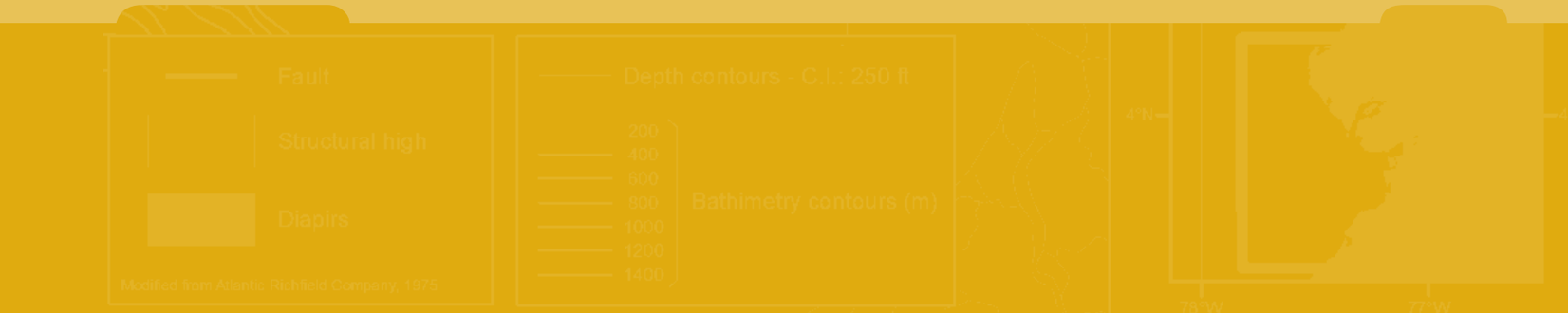

3. STRATIGRAPHY AND FACIES

3.1. General Statement

The so called Chocó Pacific Basin (ANH - 2007) is characterized by marine to continental deposits resting on an igneous sedimentary basement. However, stratigraphic characteristics recognized during the present revision, and the evaluation of available information, allow the differentiation of two distinct sedimentary basins: Atrato and San Juan. *(Fig. 19)*

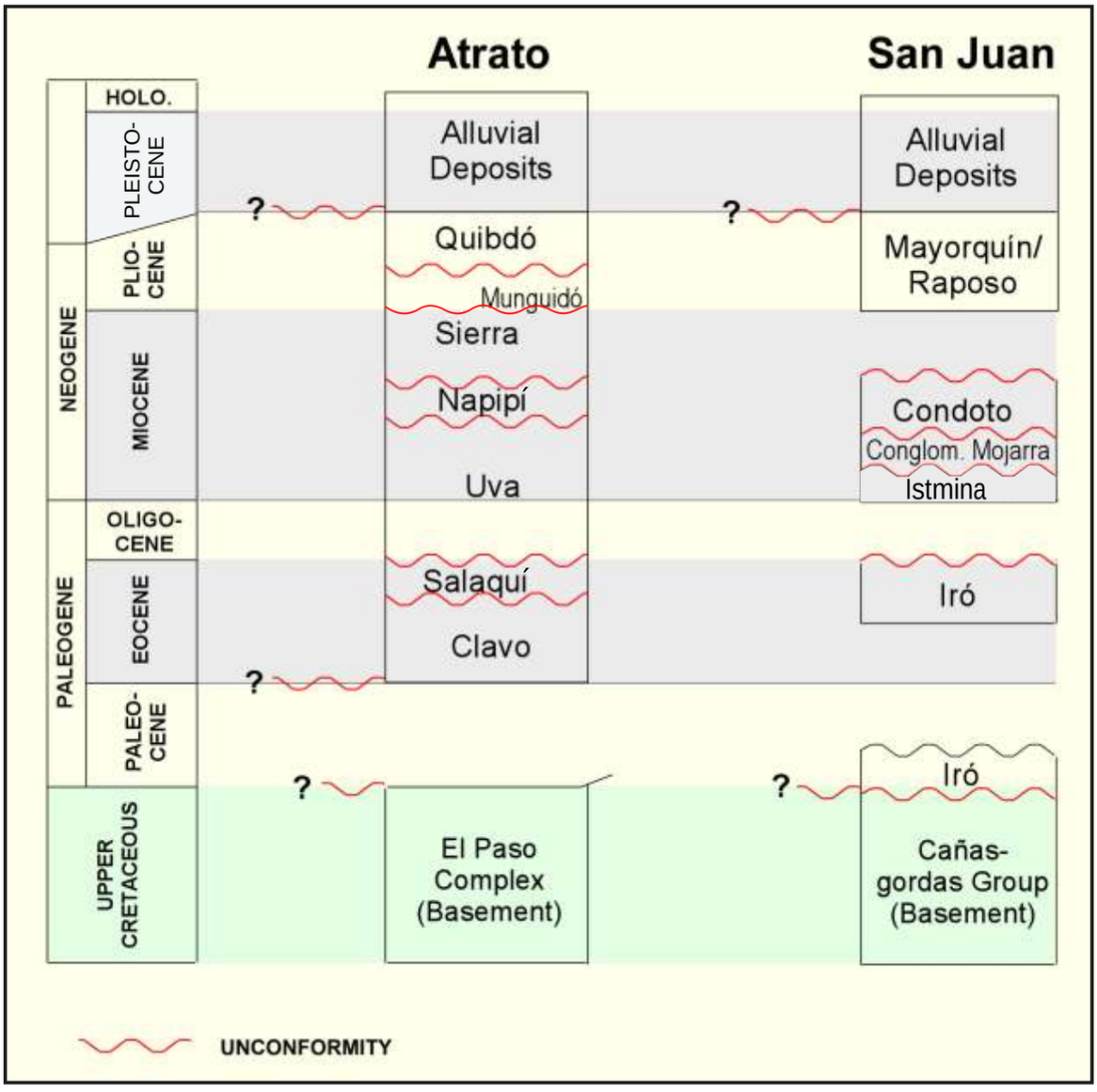

Figure 19. General lithostratigraphic sequence in the Atrato and San Juan Basins

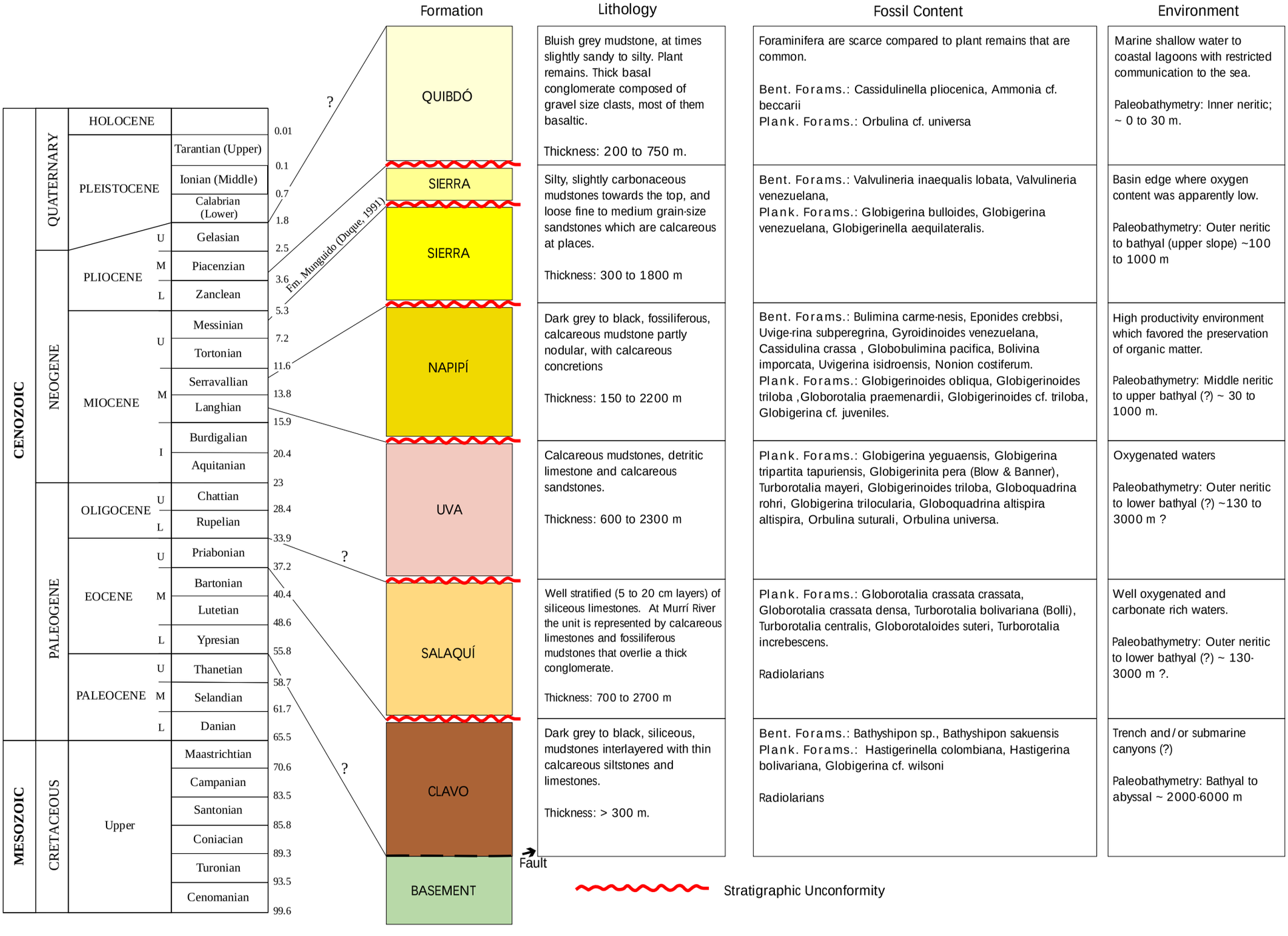

Figure 20. Chronostratigraphic chart and depositional environment of the Atrato Basin.

3.2. Atrato Basin

Geologically, few cartographic studies have been undertaken in the Atrato Basin. The most comprehensive was completed by Haffer (1967), who also provided various biostratigraphic analyses. Haffer's 1967 lithostratigraphic descriptions are utilized in the present report.

The Atrato sedimentary sequence is composed of six lithostratigraphic units ranging from the Lower Eocene to the Pliocene *(Fig. 20)*. Ages were determined utilizing the abundant planktonic and benthic foraminifera. Limits between lithostratigraphic units are similar to those recognized previously (Haffer, 1967; Duque, 1991), but have been updated to recent time scales (Gradstein et al., 2004).

The Atrato Basin contains a thick sedimentary sequence, deposited over an igneous sedimentary basement. The total thickness reaches 10 km and was deposited in marine environments with minor transitional and continental influences towards the Pliocene.

The Uva, Napipí, Sierra, and Quibdó Formations outcrop extensively and are widely distributed over the western margin of the basin, and to a lesser extent, over the eastern margin of the upper Atrato River region. By contrast, the Clavo Formation is restricted to a single sector of the western margin of the basin.The Salaquí Formation outcrops along both margins.

Each of these Formations purports unique lithologic characteristics, including internal facies variations, that represent differences in depositional conditions, as derived from field descriptions.

The available information shows that there are sandier facies over the eastern margin of the basin. At present however, available data does not allow the definition of source and provenance directions.

Correlation of these units clearly shows the degree of stratigraphic continuity, and relations at depth, according to the biostratigraphic interpretation of some wells *(Fig. 21)*. Similarly, variations in thickness of each unit are evident, indicating sedimentary processes controlled by differential tectonic activity. In general terms, stratigraphic units tend to become thicker towards the south. This is most conspicuous for the Uva Formation whose thickness varies from approximately 1,200 m in the north to approximately 2,300 m in the south.

It is also worth noting that the Salaquí Formation, in the Rio Murrí section, outcrops in fault contact with the Quibdó Formation. In this section, the Salaquí Formation is composed of 1,700 m of conglomerates with two interbedded lava flows.

3.2.1 Exploratory wells in the Atrato Basin

Between 1953 and 1983, various oil companies drilled five wells in the Atrato Basin. The stratigraphic and biostratigraphic information of each well has been re-evaluated by various authors, looking to define more precisely the limits between each lithologic unit. The comparison of lithostratigraphic boundaries demonstrates incongruency in the definition of the tops and bases of each unit. With respect to the present study, only those biostratigraphic schemes considered most consistent were utilized in stratigraphic correlation between wells.

Buchadó-1 was the first well drilled in the basin and the one that provides the most significant data (Table 2). Studies are mainly biostratigraphic, based on foraminifera.

	BUCHADÓ-1 (T.D. 15539') (Richmond Petroleum Company, 1953)					
FORMATION	Richmond, 1954	Robertson, 1985	Robertson, 1988	Suárez, 1990	Duque-Caro, 1991	Muñoz y Cogollo, 2000
Quibdó	1320'	5000'	No samples above 6090'	1305'		
Munguidó Sierra	5805'	7000'	6300' (?)	8650'	~8659'	6750'
Napipí	6490'	11000'	8700' (?)	10140'	~10345'	No samples below 6750'
Uva	10160'	12740'	13400' (?)	13160'	~10120'	
Salaquí	13170'			15539'	Unknow sedimentary sequence 15539'	
Clavo	15539' (?)	15539' (?)	15424' (?)			

Table 2. Tops of the lithostratigraphic units as defined in the Buchadó-1

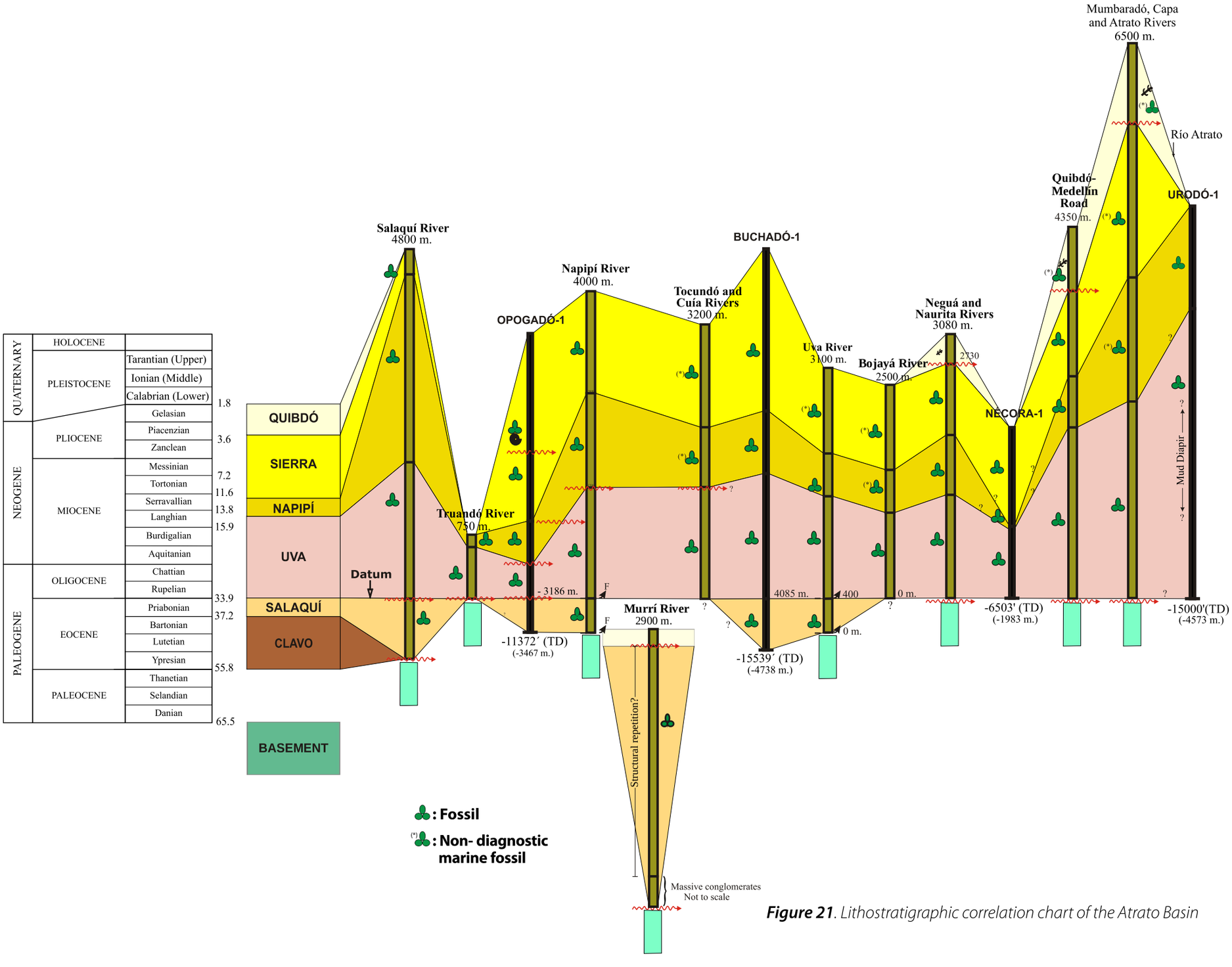

***Figure 21**. Lithostratigraphic correlation chart of the Atrato Basin*

Table 3 shows the stratigraphic schemes for the Urodó-1 and Opogadó-1 wells. For the Urodó-1 the tops of each lithostratigraphic unit, as defined by Muñoz and Cogollo (2001) are based on biostratigraphic information. For the same well, Suárez (1990) and Duque-Caro (1991) defined each top according to seismic horizons tied to the Buchadó-1 and Opogadó-1 wells.

	URODÓ-1 (T.D. 15000') (Superior Oil Co., 1953)			OPOGADÓ-1 (T.D. 11372') (Continental de Col. & Oil Gulf Co. , 1974)			
FORMATION	Suárez, 1990	Duque-Caro, 1991	Muñoz y Cogollo, 2000	Cont. y Gulf, 1974	Robertson, 1985	Suarez, 1990	Duque-Caro, 1991
Quibdó				4650' (?)			
Munguidó Sierra				7350'	5600' (?)	7300'	7300'
Napipí	1000'	~1057'	3850'	9700'	9719' (?)	9050'	9050'
Uva	6400'	~6400'	13850' (?)	10050'	10382' (?)	9950'	10450'
Salaquí	11200' (?)	Unknow sedimentary sequence 15000'	No samples below 13850'			10450'	Unknow sedimentary sequence 11372'
Clavo	15000' (?)			11372' (?)	11372' (?)	11372'	

Table 3. Tops of lithostratigraphic units as defined in the Urodó-1 and Opogadó-1

Table 4 presents stratigraphic schemes for the Pacurita-1 and Nécora-1 wells. Muñoz and Cogollo (2001) presented schemes are based on biostratigraphy, whereas others are based on seismic reflectors tied to the Opogadó-1 well.

	PACURITA-1 (T.D. 9489') (Asamera Inc., 1981)			NÉCORA-1 (T.D. 6503') (Asamera Inc. , 1983)	
FORMATION	Suárez, 1990	Duque-Caro, 1991	Muñoz y Cogollo, 2000	Suárez, 1990	Muñoz y Cogollo, 2000
Quibdó					No samples above 3170'
Munguidó Sierra	1605'	~1312'	2210' (?)	660'	3890'
Napipí	4550'	~3490'	6530' (?)	2860'	3980'
Uva	5405'		No samples below 6530'	4630'	6503'
Salaquí	9489'	Unknow sedimentary sequence 9489'		5600'	
Clavo				6503'	

Table 4. Tops of lithostratigraphic units as defined in the Pacurita-1 and Nécora-1

3.3. San Juan Basin

A large percentage of stratigraphic studies on the San Juan Basin are of local character and are concentrated in the Istmina Condoto High, in the upper San Juan River. From this point information has been extrapolated southward into the entire basin.

The sedimentary succession consists of five lithostratigraphic units that range in age from Paleocene to Pliocene. Temporal limits that were taken from the available biostratigraphic data are shown in *Fig. 22*. According to its faunal content, most of the succession was deposited in marine environments with a strong continental influence. The possible absence of the Paleocene Eocene and Oligocene Upper Miocene, as evidenced in the Istmina Condoto high, suggests intense and long lasting erosive periods. The Pliocene Raposo and Mayorquín Formations outcrop widely. The Iró and Mojarra Conglomerates outcrop exclusively in the Istmina - Condoto High, *(Fig. 22)*.

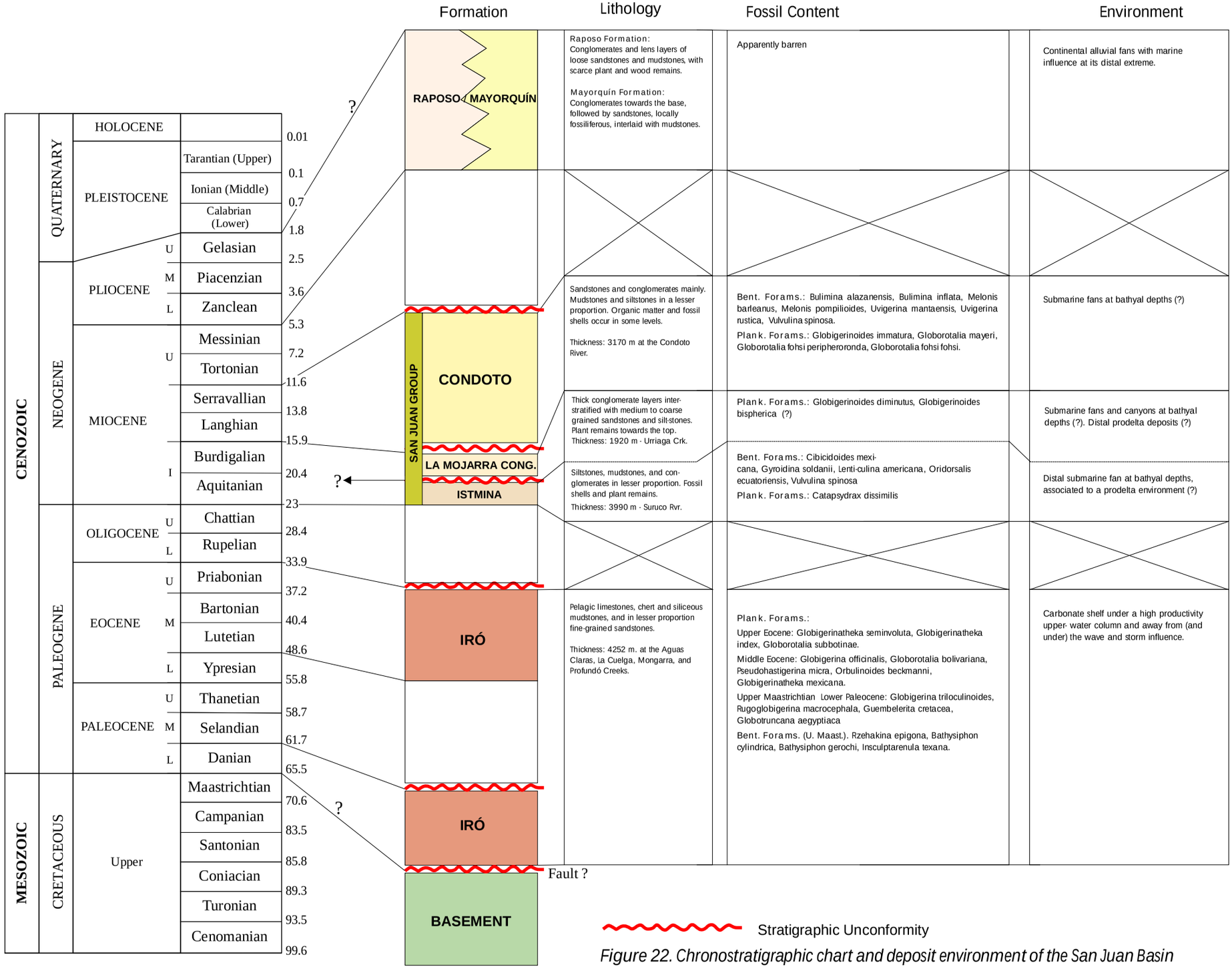

Figure 22. Chronostratigraphic chart and deposit environment of the San Juan Basin

The available information does not allow the construction of stratigraphic correlation models similar to those proposed for the Atrato Basin. However, the seismic profile and facies interpretation presented by Petrobras (1990, *Fig. 23*) offers an excellent overview for the San Juan Basin.

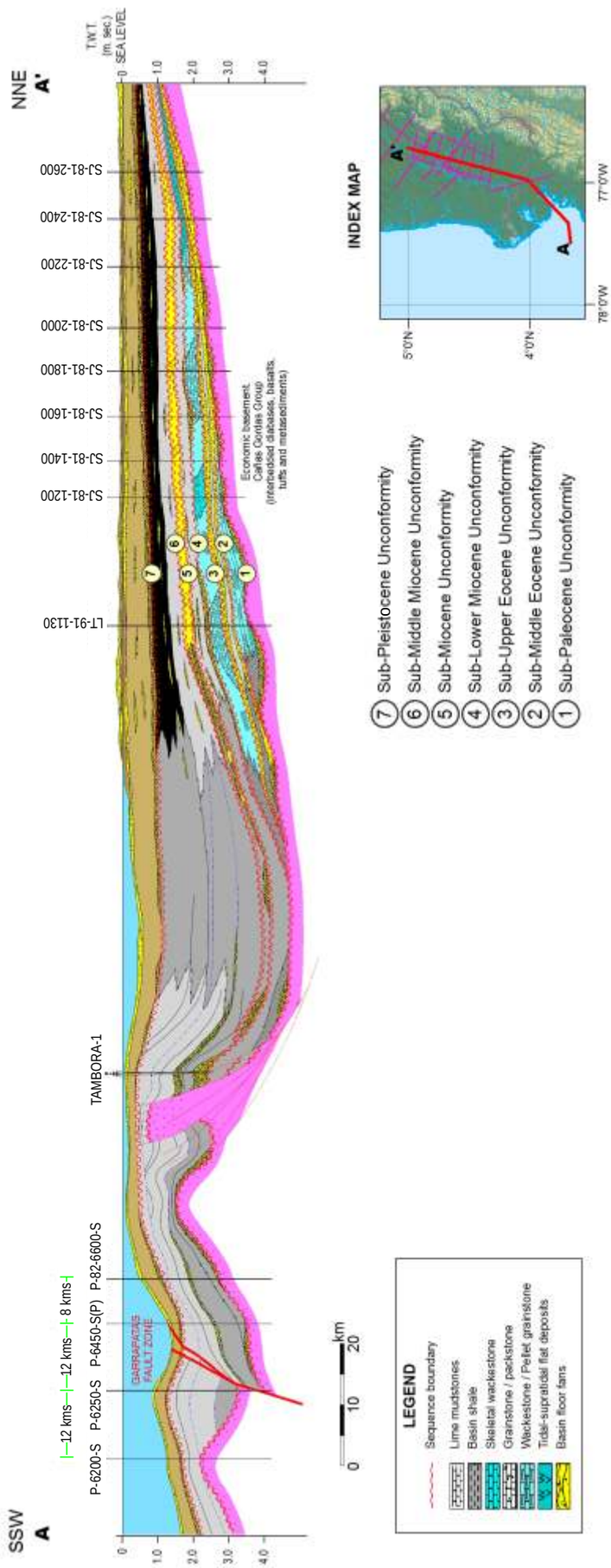

Figure 23. Schematic cross-section along the San Juan Basin modified after Petrobras, 1990.

3.3.1 Exploratory wells in the San Juan Basin

The onshore portion of the San Juan Basin has not been drilled. Offshore, the Tambora 1 well (southwest of Buenaventura) has been used to tie-in seismic information from the San Juan Basin. According to biostratigraphic reports, most of Tambora-1 well material was barren. However, it is thought that the well did not reach the lower Miocene *(Table 5)*.

	TAMBORA-1 (T.D. 11365') (Intercol, 1967)	
FORMATION	Robertson 1988	Muñoz y Cogollo, 2000
Raposo/Mayorquín	No samples above 2666'	?
Condoto	2696'	No samples above 8501'
Mojarra Cong.	4727'	8501' (?)
Istmina		
Iró	(6848' - 11252') barren interval	No samples below 8501'

Table 5. Lithostratigraphic units as defined in the Tambora-1

3.3.2. The San Juan Delta. A geological model for the Cenozoic San Juan Basin

The present San Juan River delta covers a rectangular area of approximately 800 km^2, limited by latitudes 4º 20' N and 3º 40' N and longitudes 77º 20' W and 77º 40' W. Including the continental platform, maximum depths are around 1,000 m.

Progressive widening of the continental platform and the extensive San Juan submarine lobe (defined to a depth of 1,000 m) confirms the presence of an accretionary prism, resulting from the accumulation and consolidation of sediments deposited under deltaic and marine transitional conditions, with a high sediment input due to important tectonic controls.

Furthermore, preliminary evidence of the presence of submarine canyons in the area, suggests turbiditic events were involved in prism development and modeling. Available geophysical data from the Golfo de Tortugas and Bahía Málaga identify major diapiric structures and additional structural anomalies ("structural highs") which have not yet been characterized (see Fig. 24 and Fig. 25).

The Plio-Quaternary evolution of the region provides a good model for marine and transitional marine conditions under which abundant organic matter may accumulate. North of the area, the San Juan River has developed a Holocene delta of approximately 800 km^2, which accommodates extensive fresh water and intertidal-brackish swamps containing luxuriant mangroves and humid tropical forests, developed under temperatures of 27º C and 10,000 mm average annual rainfall. This environment permits the production and accumulation of volumenous quantities of organic matter. Co-seismic subsidence related to large magnitude earthquakes frequently increases the capacity of the basin to accommodate additional sediments. A 4 m tidal range and strong coastal currents promote the formation of fine- and medium-grained sand bodies with kilometric dimensions, represented by longitudinal fluvial tidal bars, extended tidal flats and at least four sequences of beach and barrier island-beach complexes, which indicate the overlapping of successive deltaic events.

With an average discharge of about 6000 $m^3 s^{-1}$, the San Juan River alone supplies about $16x10^6$ tonne/year of suspended sediment. This material is distributed and deposited within the present prodelta and additionally contributes to the formation of the vast shallow platform which characterizes the Golfo de Tortugas, recipient of important amounts of organic muds supplied by the Raposo, Dagua and Anchicaya Rivers. Sedimentary coverage is varied and includes muds and calcareous muds with sandy patches.

Geological data from the San Juan River delta (Correa and Restrepo, 2002; Restrepo et al., 2002) and a first approximation of understanding of the San Juan Basin, as derived from stratigraphy and sedimentary facies, enables us to conclude that during the Cenozoic the region provided a depocentre for calcareous, muddy and sandy sediments sourced from the north northeast. The sediments accumulated in a southwest-prograding delta whose migration was influenced by recurring seismic (tectonic) activity.

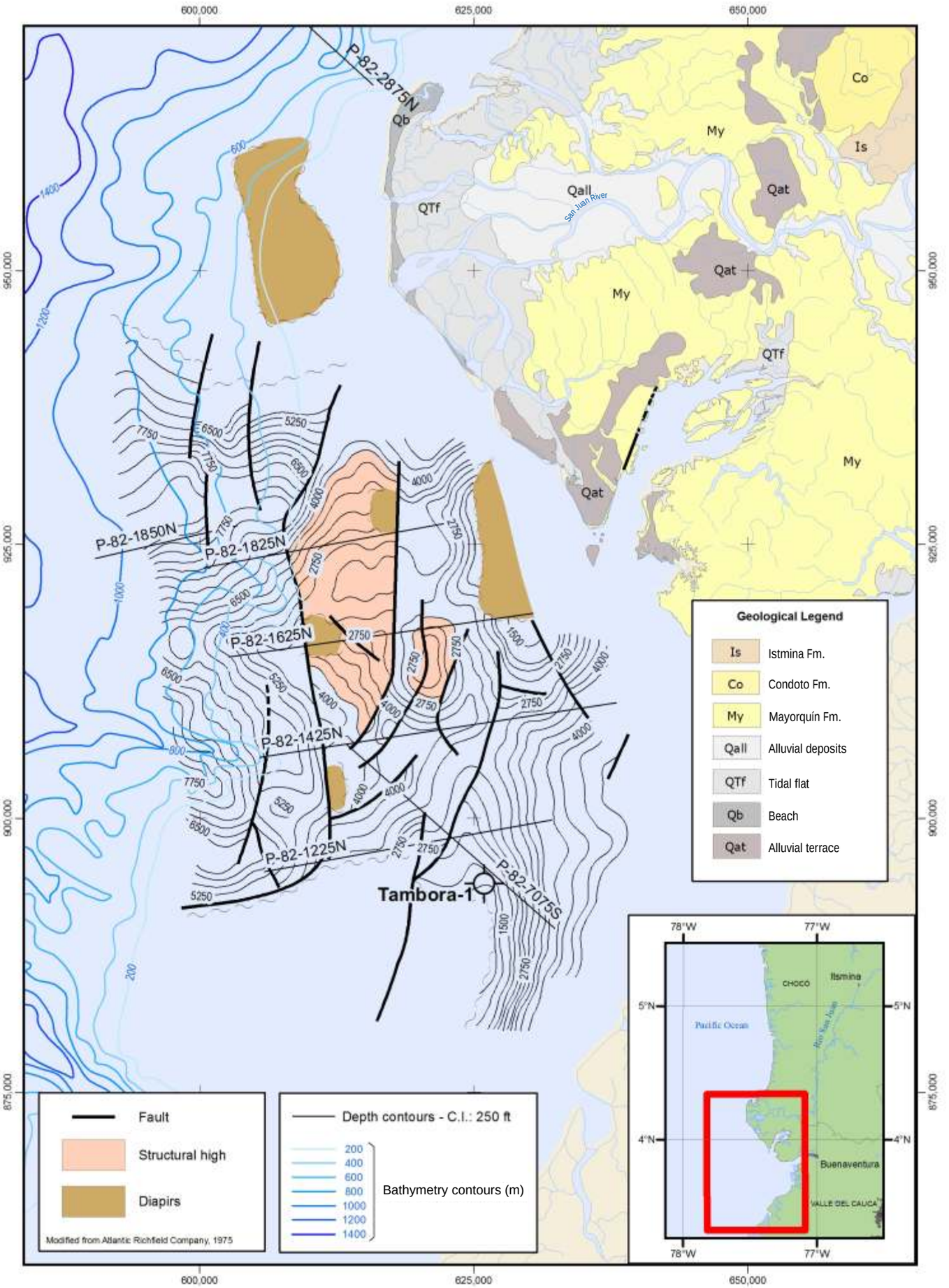

Figure 24. Structural map of the off-shore San Juan Basin

Line P82_2875_N

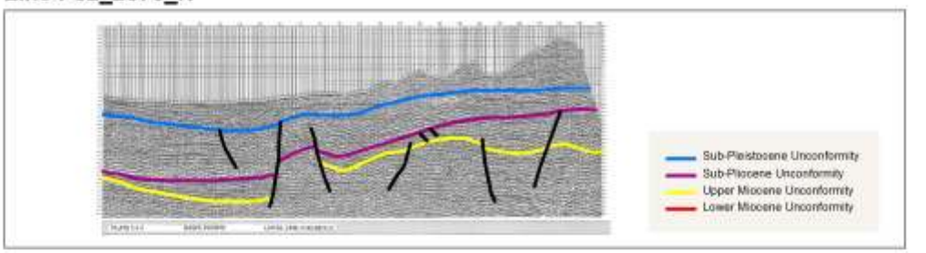

Lines P82_1850 and P82_1825_N

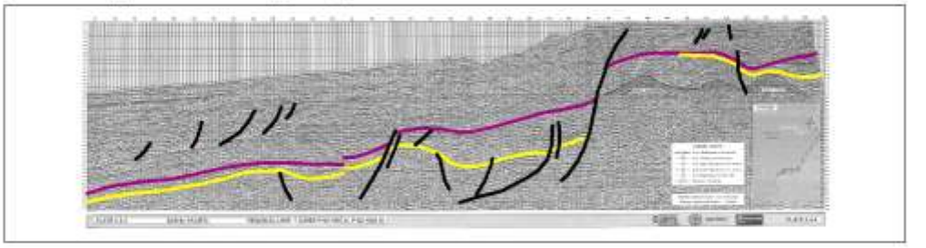

Line P82_1625_N

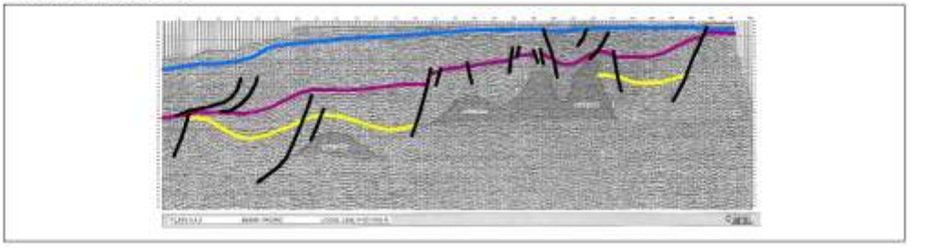

Line P82_1425_N

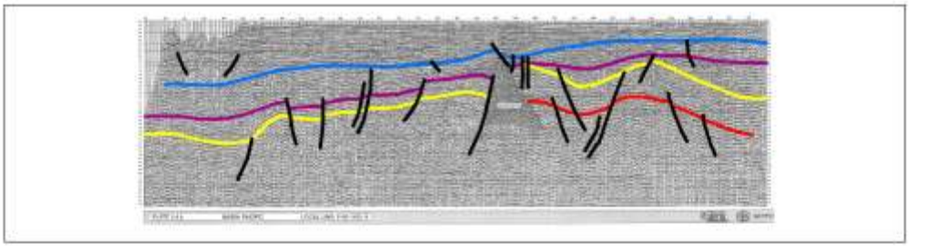

Line P82_1225_N

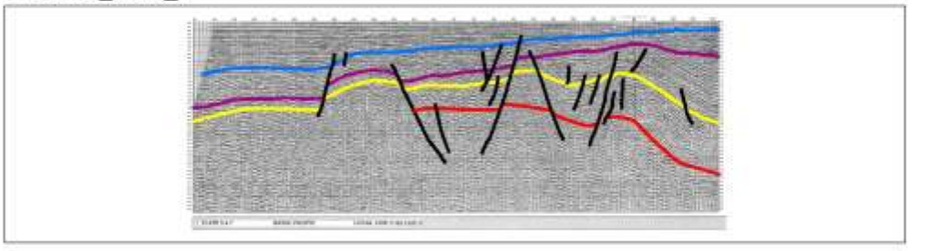

Line P82_7075_N

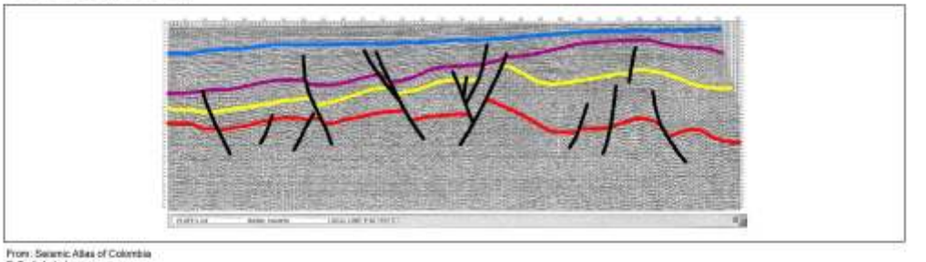

From: Seismic Atlas of Colombia
F. Cediel et al
Geotec. Robertson, Ecopetrol. 1999

Figure 25. Geoseismic profiles across the off-shore San Juan Basin

PACIFIC OCEAN
Punta Ardita
Bahia de Humboldt
Punta Cabo Marzo
Punta La Tortuguera
Bahia de Cupica
Punta Nabugá
Bahia Solano
Ensenada de Utria
GOLFO DE TRIBUGÁ
Ensenada Coquí
Punta Arusí
Cabo Corrientes
Playa Nueva
Bahia Baudo
Boca Usuragá
Ensenada Docampado
Boca Hijua
Boca Orpúa
Boca Cacaguai
Playa El Choncho
SAN JUAN
Qui
Uv
Qall
Siu
Si
Sa
Sil
Ma
Pen
Peu
Co
Is
QTf
My
Rp
Br
Ci
SISTEMA DE FALLAS GARRAPATAS
Dabeiba
BETULIA
CONCORDIA
SALGAR
EL CARMEN DE ATRATO
HISPANIA
BETANIA
MISTRATO
PUEBLO RICO
SANTUARIO
LA CELIA
BALBOA
SAN JOSE DEL PALMAR
EL CAIRO
ARGELIA
CARTAGO
TORO
VERSALLES
EL DOVIO
OBANDO
BOLIVAR
N
25
50
km

4. SEISMIC INTERPRETATION

4. SEISMIC INTERPRETATION

4.1. Introduction

Seismic data available to analyze the subsurface geology of the Atrato and San Juan Basins is scarce, sparsely distributed and incomplete. The principle of "conceptual uncertainty" inherent to seismic interpretation, as discussed by Bond et al. 2007 should prevent the propagation of uncertainties into the future modeling and/or risk assessments for these basins. Likewise, this statement applies to the petrophysical analysis of the exploratory wells drilled in the Atrato Basin *(Chapter 5)*.

The present seismic study and interpretation was executed in three phases: 1. Compilation, quality control and digital input of the available data, 2. Interpretation of tectono stratigraphic units and, 3. Subsurface cartography, *(see Fig. 26 and Table 6)*.

The seismic data was read and loaded in GEOGRAPHIX TM, a specialized software of LANDMARK. The Rio Atrato-82 and Tutunendo-81 programs lack SEGY information. Elaboration and interpretation of maps for these programs was done manually.

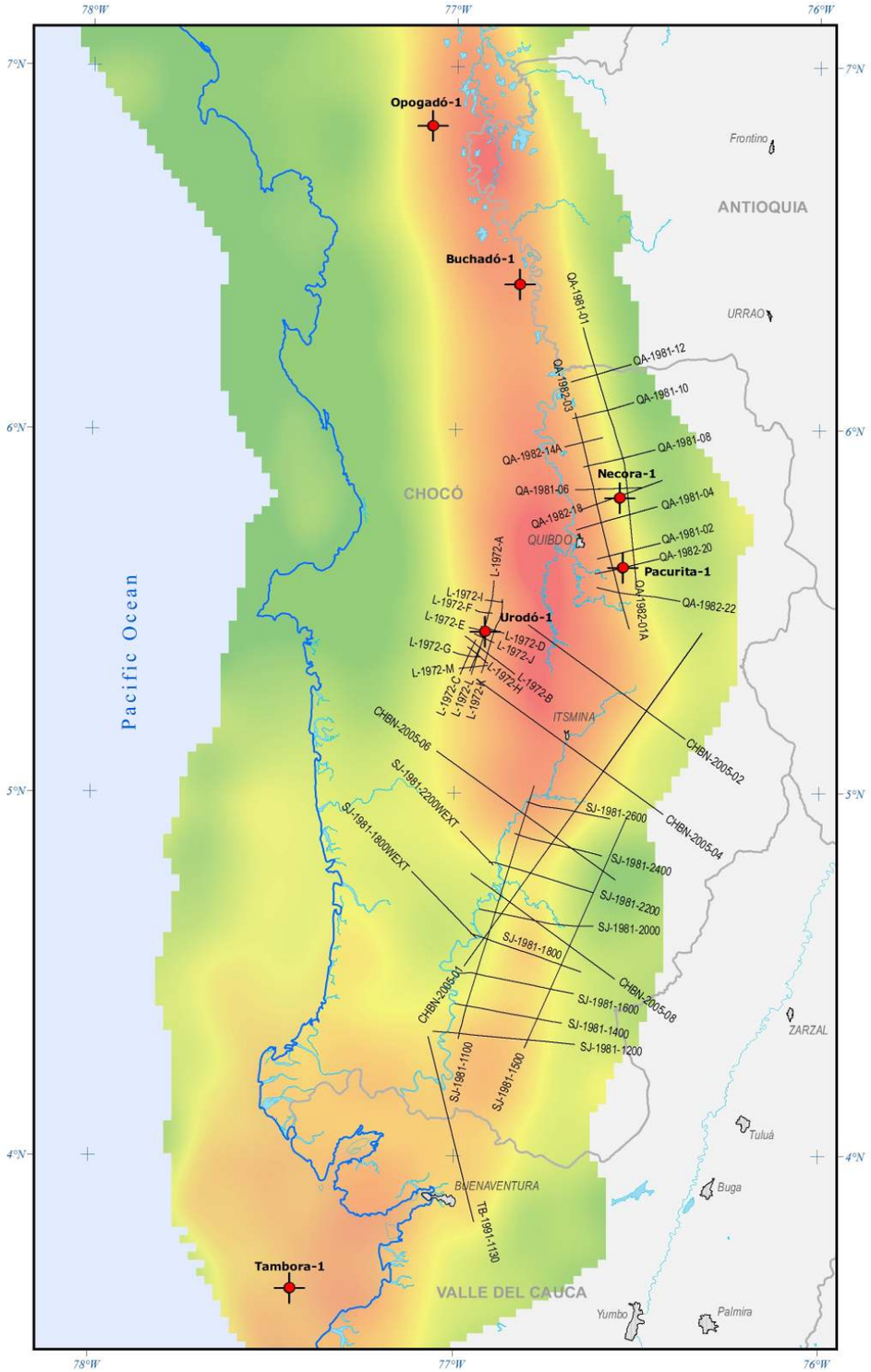

Figure 26. Distribution of seismic data in the study area.

PROGRAM	LINE	Interpreted Version
ANH-2005	A01	MIG_in_in
ANH-2005	A02	MIG_in_in
ANH-2005	A04	MIG_in_in
ANH-2005	A06	MIG_in_in
ANH-2005	A08	MIG_in_in
SAN JUAN-81	SJ-1981-1100	GEOSOURCE_1981_MIG_IN
SAN JUAN-81	SJ-1981-1200	GEOSOURCE_1981_MIG_IN
SAN JUAN-81	SJ-1981-1400	GAPS_2000_MIG_IN
SAN JUAN-81	SJ-1981-1500	SISMOCOL_1995_MIG_IN
SAN JUAN-81	SJ-1981-1600	Not loaded
SAN JUAN-81	SJ-1981-1800	GEOSOURCE_1981_MIG_IN
SAN JUAN-81	SJ-1981-1800West	GAPS_2000_MIG_IN
SAN JUAN-81	SJ-1981-2000	GEOSOURCE_1981_MIG_IN
SAN JUAN-81	SJ-1981-2200	GEOSOURCE_1981_MIG_IN
SAN JUAN-81	SJ-1981-2200West	GAPS_2000_MIG_IN
SAN JUAN-81	SJ-1981-2400	GEOSOURCE_1981_STACK_I
SAN JUAN-81	SJ-1981-2600	SISMOCOL_1995_MIG_IN
TUMACO_91	T-91-1130	GAPS_2000_MIG_IN
URODO-72	L-1972-A	1991-CGG-MIG-O-O
URODO-72	L-1972-B	1991-CGG-MIG-O-O
URODO-72	L-1972-C	1991-CGG-MIG-O-O
URODO-72	L-1972-D	1991-CGG-MIG-O-O
URODO-72	L-1972-E	1991-CGG-MIG-O-O
URODO-72	L-1972-F	1991-CGG-MIG-O-O
URODO-72	L-1972-G	1991-CGG-MIG-O-O
URODO-72	L-1972-H	1991-CGG-MIG-O-O
URODO-72	L-1972-I	1991-CGG-MIG-O-O
URODO-72	L-1972-J	1991-CGG-MIG-O-O
URODO-72	L-1972-K	1991-CGG-MIG-O-O
URODO-72	L-1972-L	1991-CGG-MIG-O-O
URODO-72	L-1972-M	1991-CGG-MIG-O-O
TUTUNENDO-81	QA-1981-01	MIG_in_in
TUTUNENDO-81	QA-1981-02	MIG_in_in
TUTUNENDO-81	QA-1981-04	MIG_in_in
TUTUNENDO-81	QA-1981-06	MIG_in_in
TUTUNENDO-81	QA-1981-08	MIG_in_in
TUTUNENDO-81	QA-1981-10	MIG_in_in
TUTUNENDO-81	QA-1981-12	MIG_in_in
RIO ATRATO-82	QA-1982-03	MIG_in_in
RIO ATRATO-82	QA-1982-06A	MIG_in_in
RIO ATRATO-82	QA-1982-14A	MIG_in_in
RIO ATRATO-82	QA-1982-18	MIG_in_in
RIO ATRATO-82	QA-1982-20	MIG_in_in
RIO ATRATO-82	QA-1982-22	MIG_in_in
RIO ATRATO-82	QA-1982-01A	MIG_in_in

Table 6. Inventory of Seismic data.

The results of the seismic interpretation for both the Atrato and San Juan basins are summarized in the following pages, using the most relevant geoseismic profiles and structural maps. For lithostratigraphic and facies interpretations the reader is referred to descriptions in Chapter 3.

4.2. Tectonic - Stratigraphic Interpretation of the Atrato Basin

The units defined and drilled in the basin, including the Clavo, Salaquí, Uva, Napipí, Sierra and Quibdó Formations, are described in Chapter 3.

Some important general observations deserve particular attention here:

- None of the wells drilled in the basin reached the basal Clavo Formation. A seismic sequence appears beneath sediments mapped as the Clavo sedimentary sequence.
- In the Atrato-82 program, along the eastern flank of the basin the Pre-Clavo sequence becomes thicker towards the east. This is an exceptional case within the Cenozoic deposits, given that all other mapped lithostratigraphic units indicate basin development towards the west.

4.2.1. Tectonic - Statigraphic Units 1 *(Clavo Formation)*

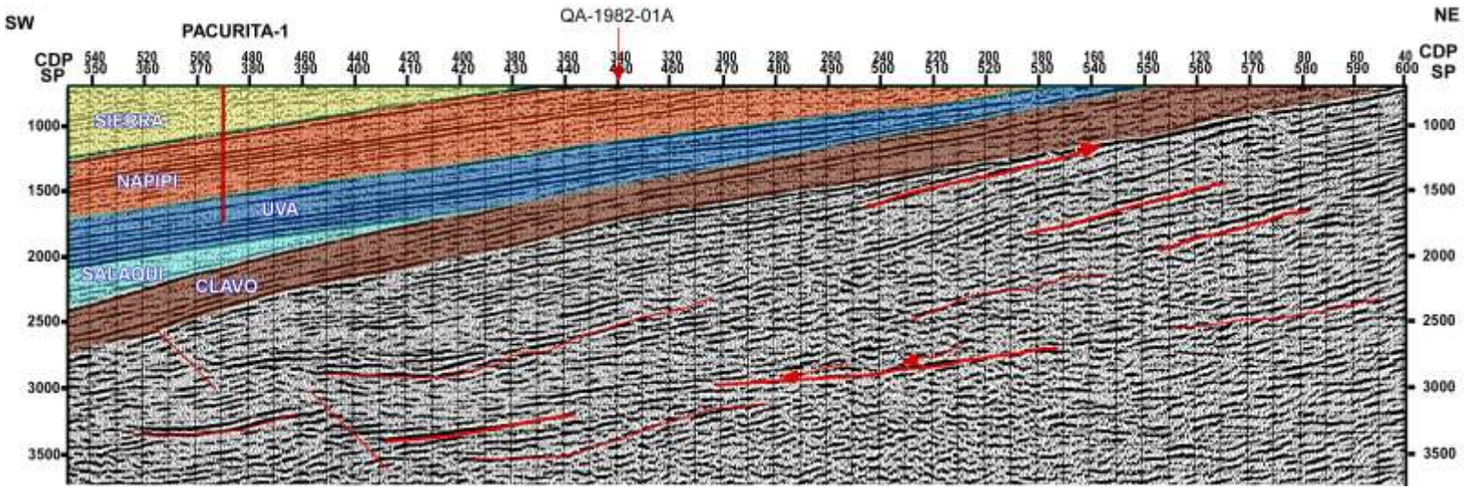

Figure 27. Seismic sequence underneath the Clavo Formation. The figure corresponds to the seismic line QA-82-20

4.2.2. Tectonic Stratigraphic Unit 2 *(Salaquí-Uva-Napipí Formation)*

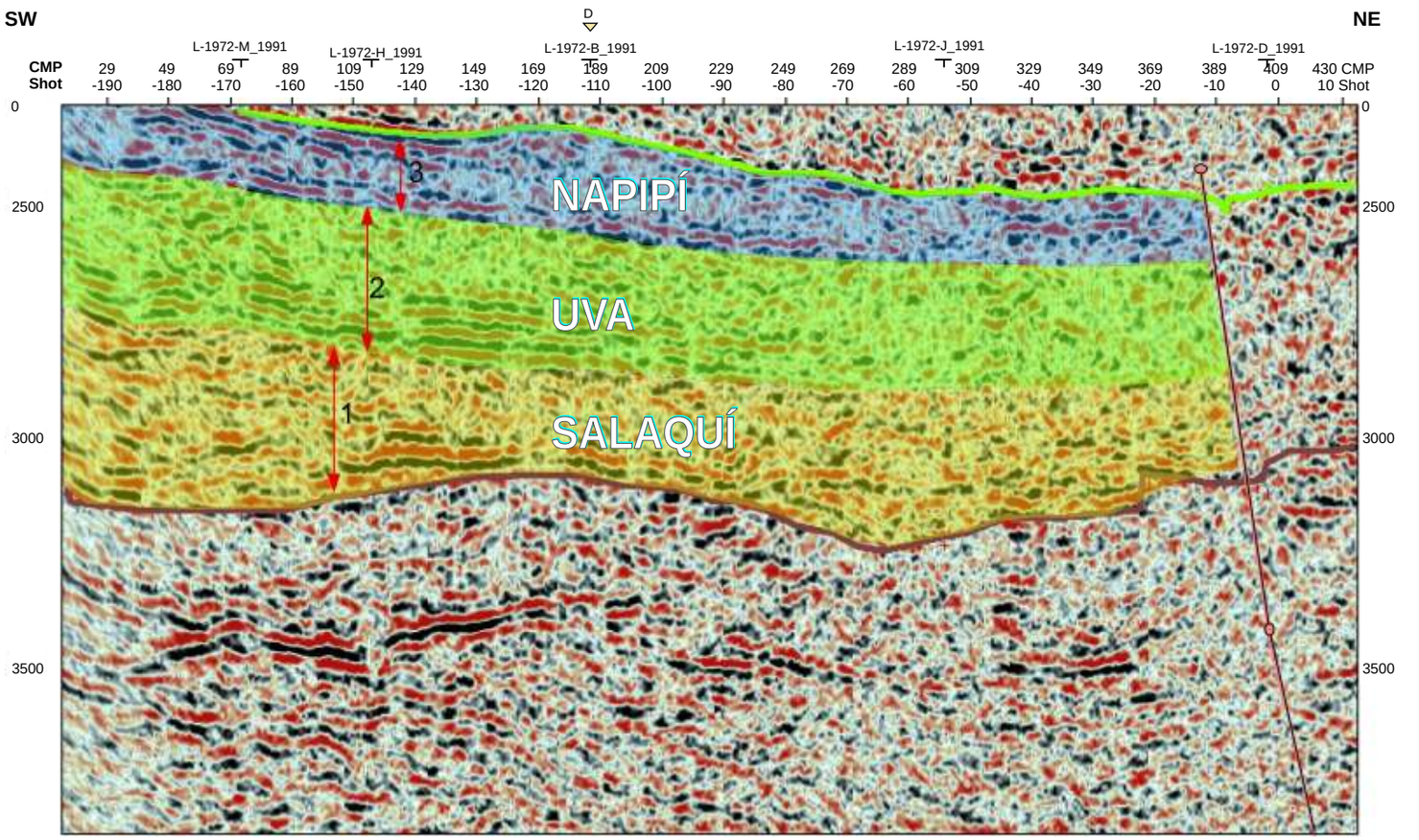

Figure 28. Seismic configuration of the Salaquí Formation within which two cycles are observed.

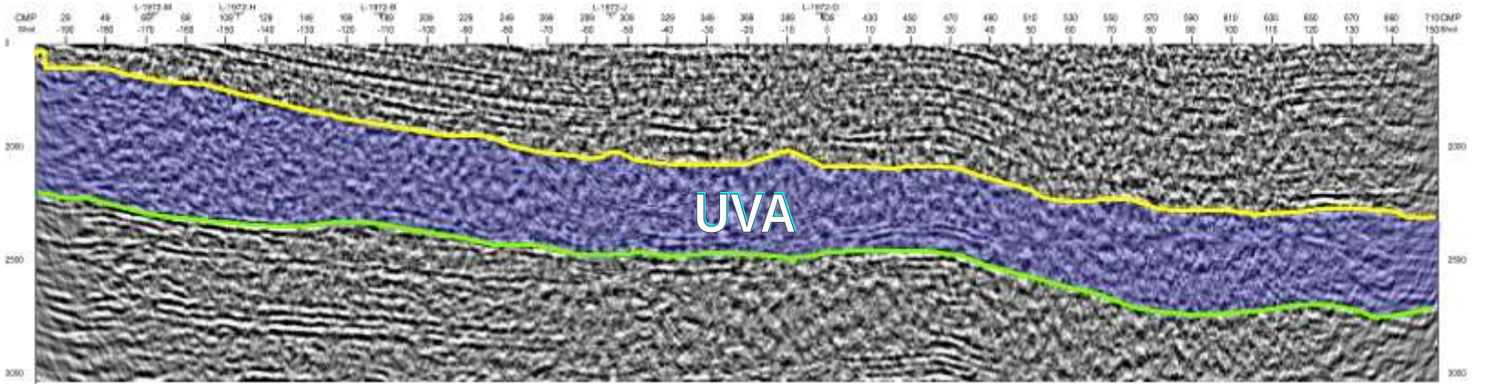

Figure 29. *Seismic configuration of the Uva Formation (blue) along seismic line L-72-B.*

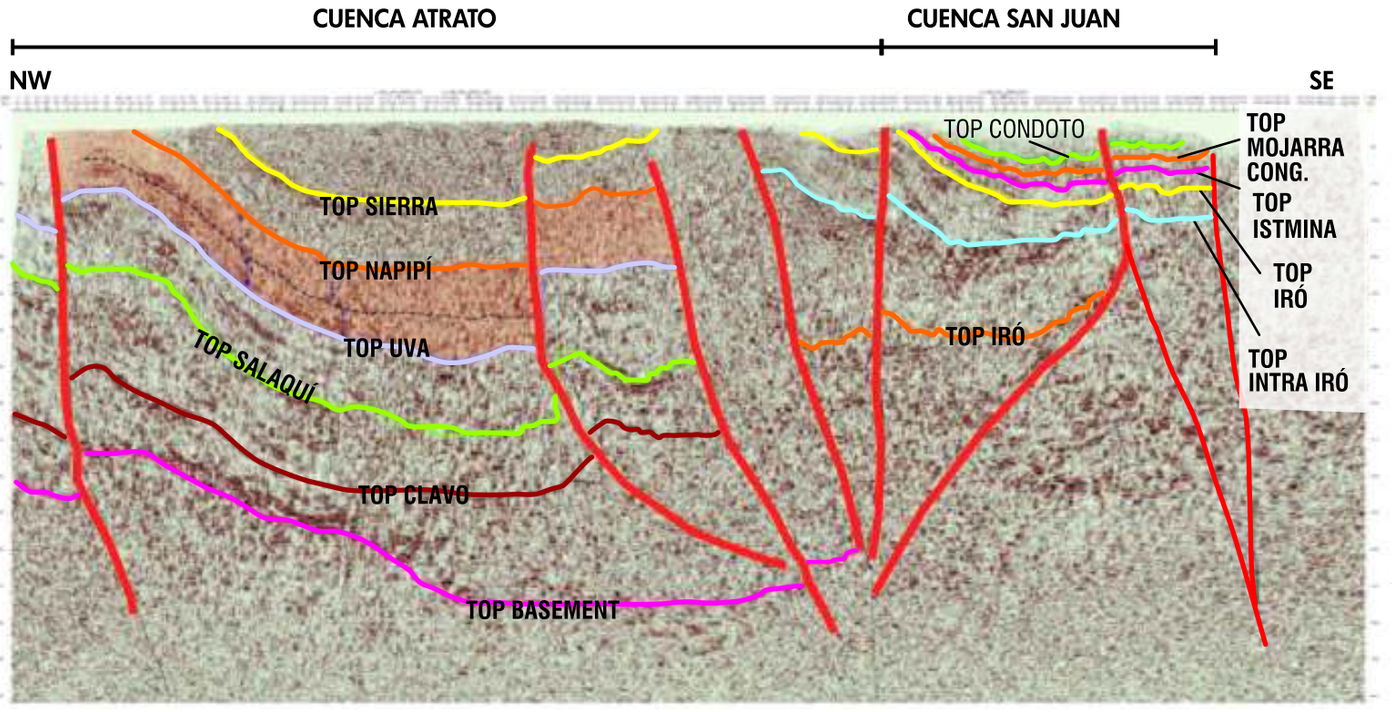

Figure 30. *Interpretation of seismic line ANH-2005-04. Flower structure separete Atrato and San Juan Basins*

4.2.3. Tectonic - Stratigraphic Unit 3 *(Sierra Formation)*

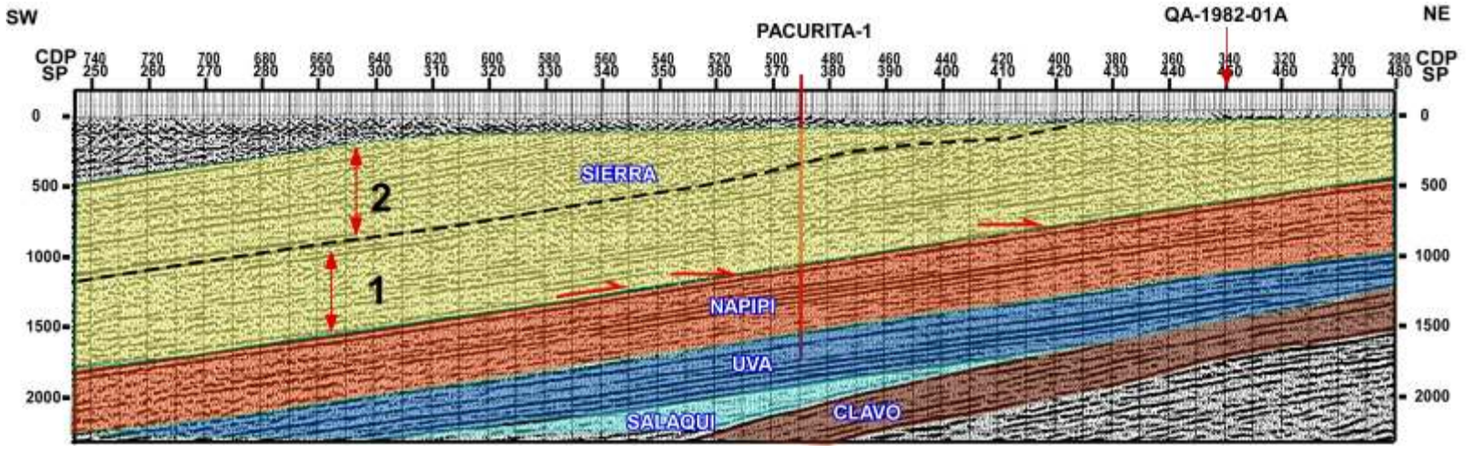

Figure 31. *Seismic configuration of the Sierra Formation along seismic line QA-82-20.*

4.2.4. Tectonic - Stratigraphic Unit 4 *(Quibdó Formation)*

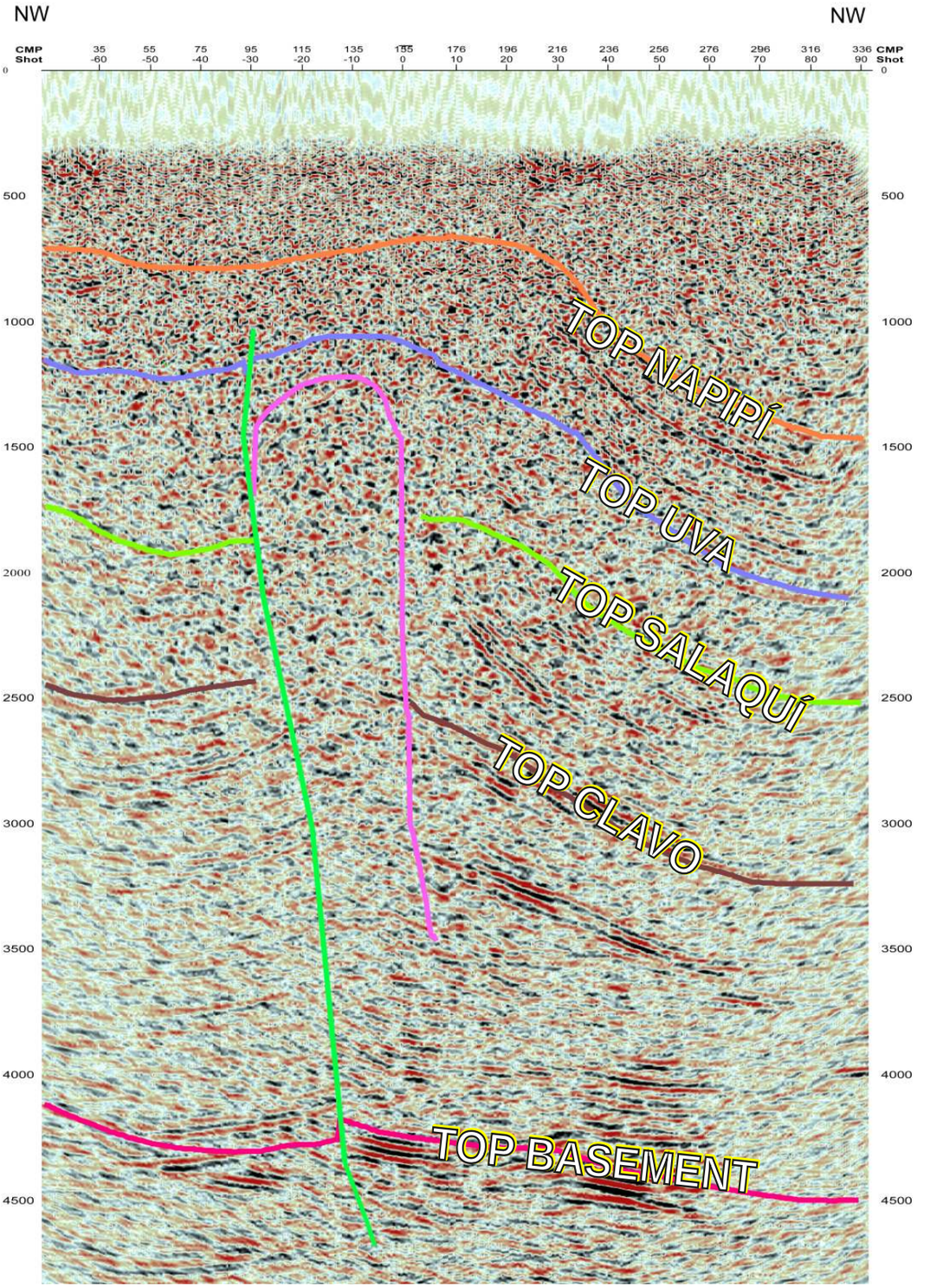

Figure 32. Mud diapirism is associated with tectonic events in Quibdó Formation time. Seismic line L-72-J.

4.3. Tectonic - Stratigraphic Interpretation of the San Juan Basin

Note that the seismic pattern and features recorded in this basin are quite different from those defined in the Atrato basin.

4.3.1. Tectonic-Stratigraphic Unit 1 *(Iró, Istmina Formations)*

Tectono-stratigraphic unit 1 represents the development of the Iró and Istmina Formations, deposited on a rapidly subsiding platform limited along the flanks by submarine canyons. The basement can be inferred as the oldest reflector, which outlines some of the paleomorphology.

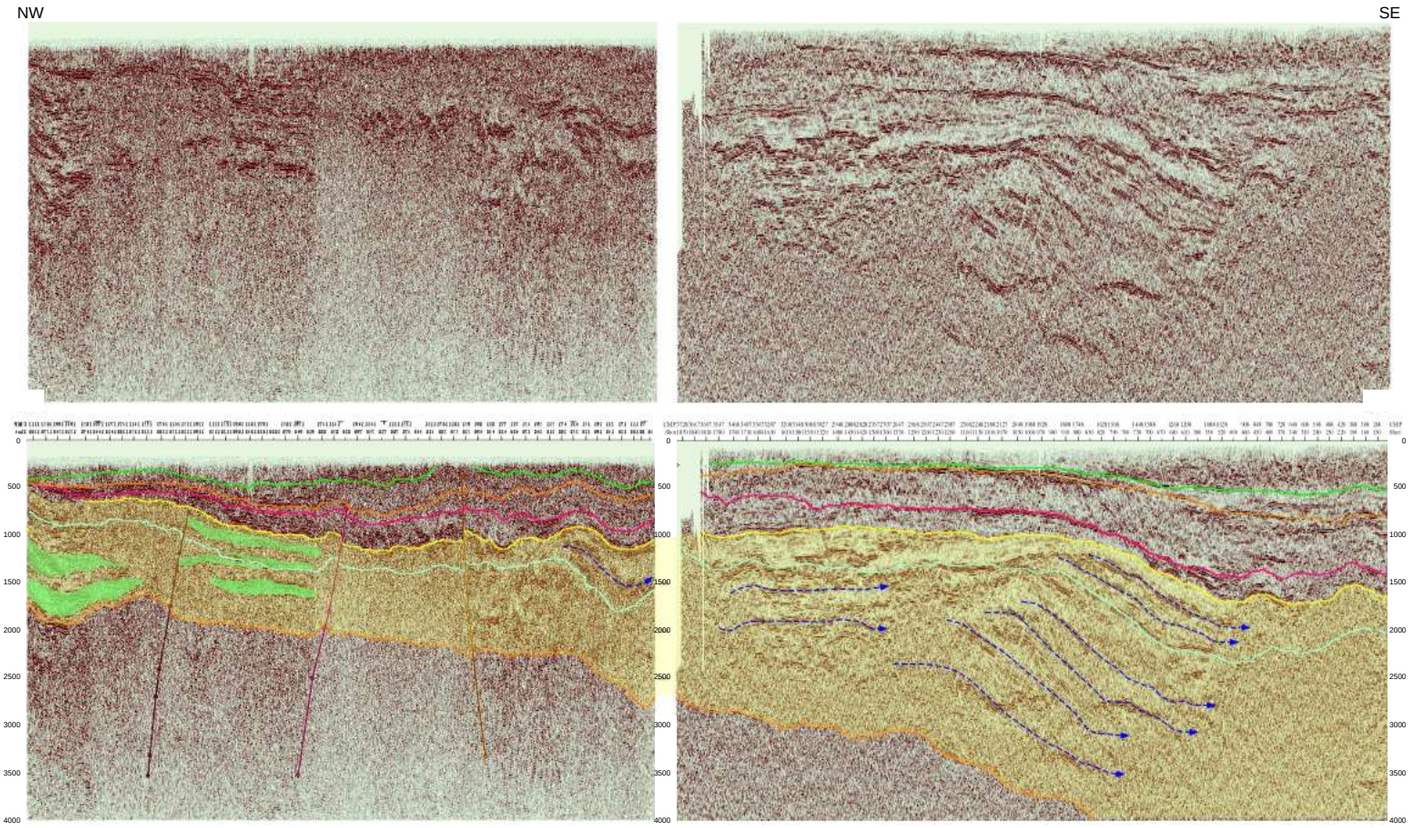

Figure 33. Seismic configuration of Tectono-Stratigraphic Unit 1 along seismic lines SJ-81-1100 and TB-91-1130. The Iró Formation, which forms the basal part of this unit, is highlighted in yellow. Carbonate sequences are highlighted in green. A S-SW prograding sequence (composite submarine fans?) appears at right, following basement paleo-relief. This configuration is interpreted as part of a NE-SW oriented paleo-delta.

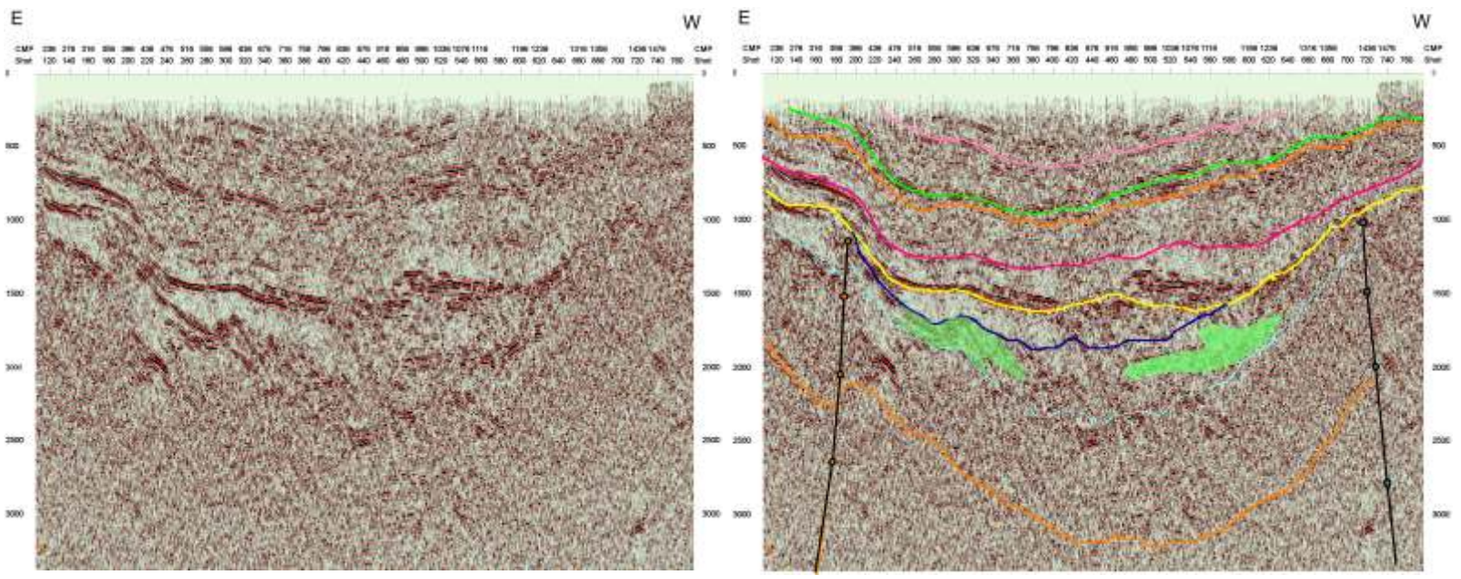

Figure 34. Carbonate patch reefs in Tectono-Stratigraphic Unit 1. Line SJ-81-1400.

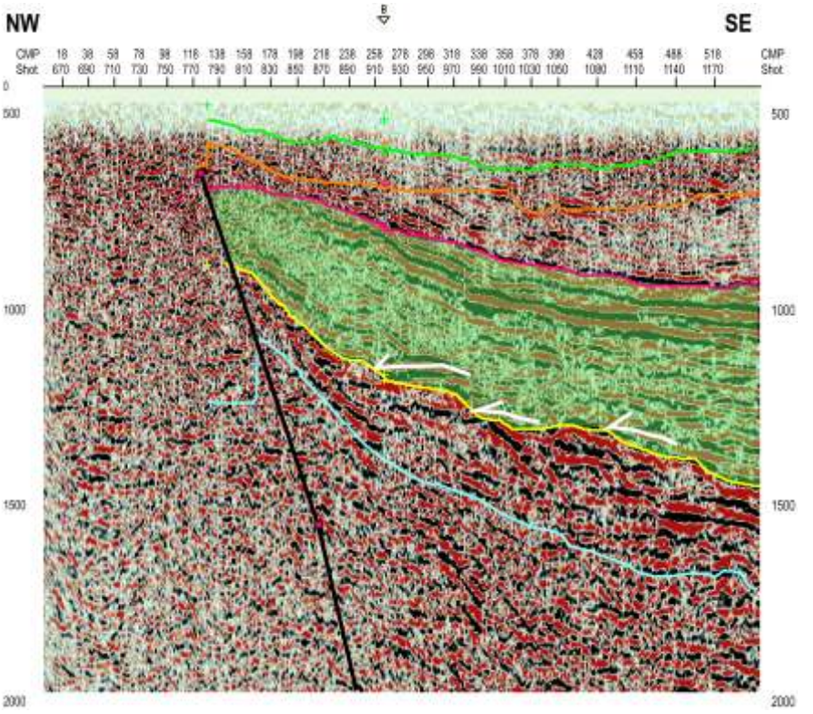

Figure 35. Seismic configuration of the Istmina Formation (green) along seismic line SJ-81-2200.

4.3.2. Tectono - Stratigraphic Unit 2 *(La Mojarra Conglomerates - Condoto Formation)*

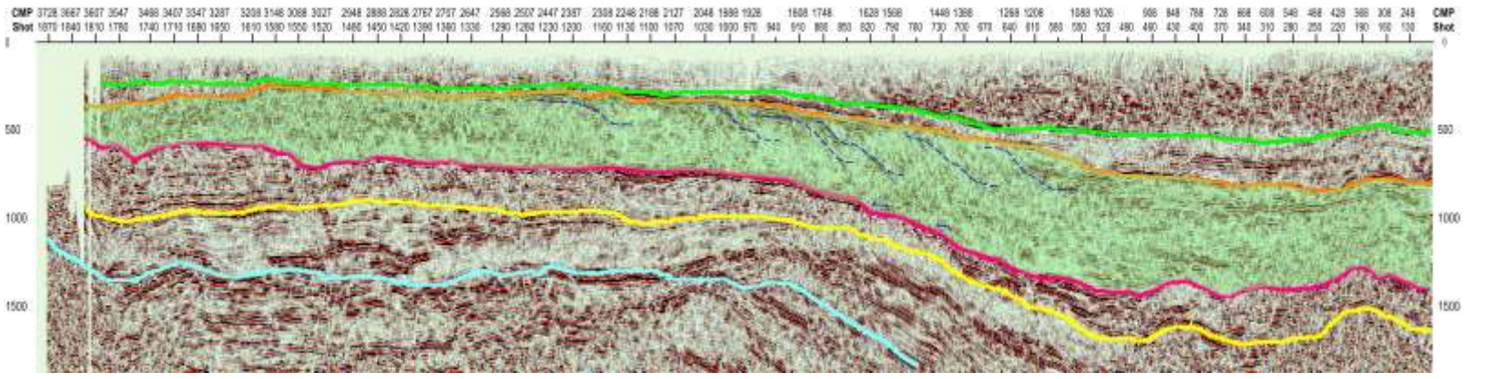

Figure 36. Seismic configuration of La Mojarra Conglomerates (green) along seismic line TB-91-1130.

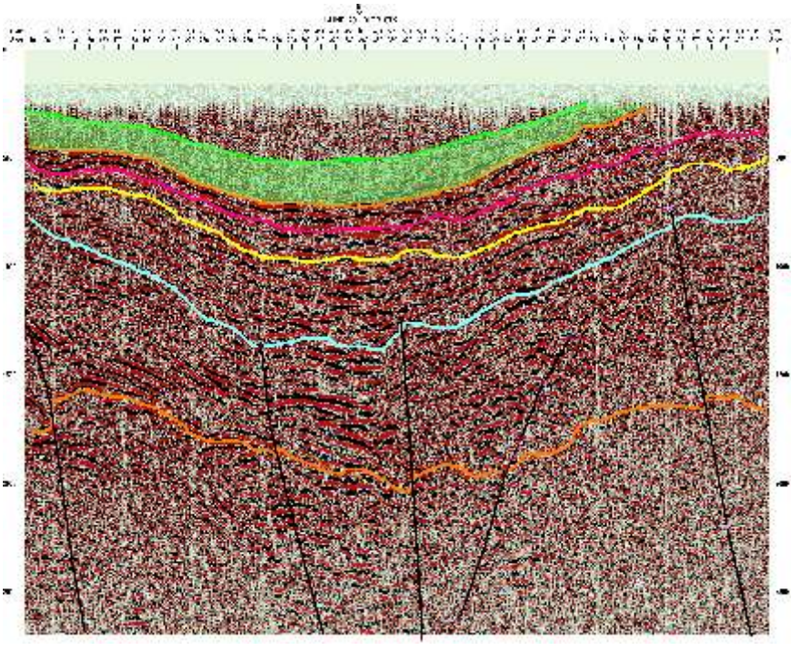

Figure 36. Seismic configuration of the Condoto Formation (green) along seismic line SJ-81-2400

4.4. Sub-Surface Structural Maps

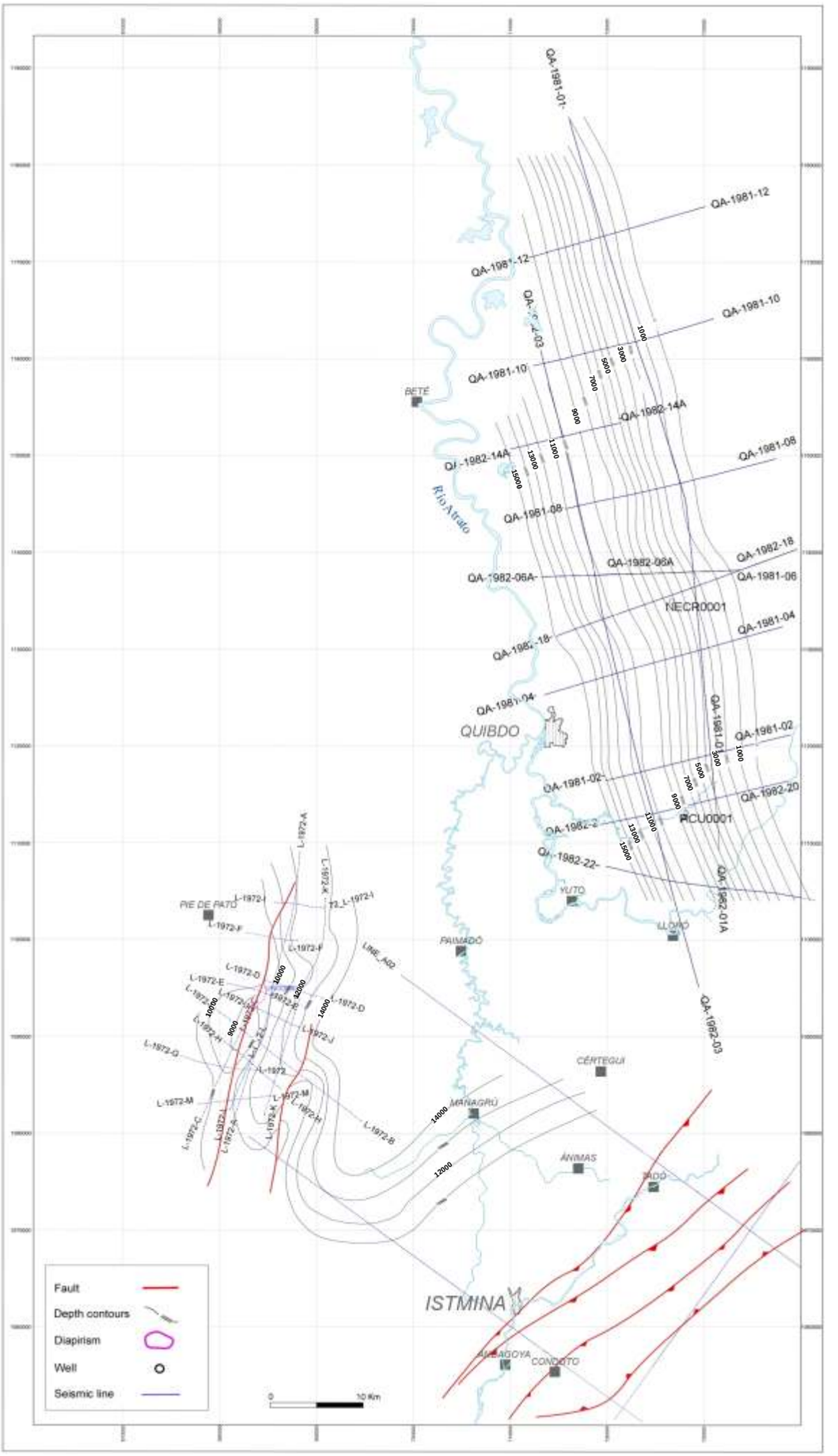

Figure 38. Structural Map Top El Clavo Formation

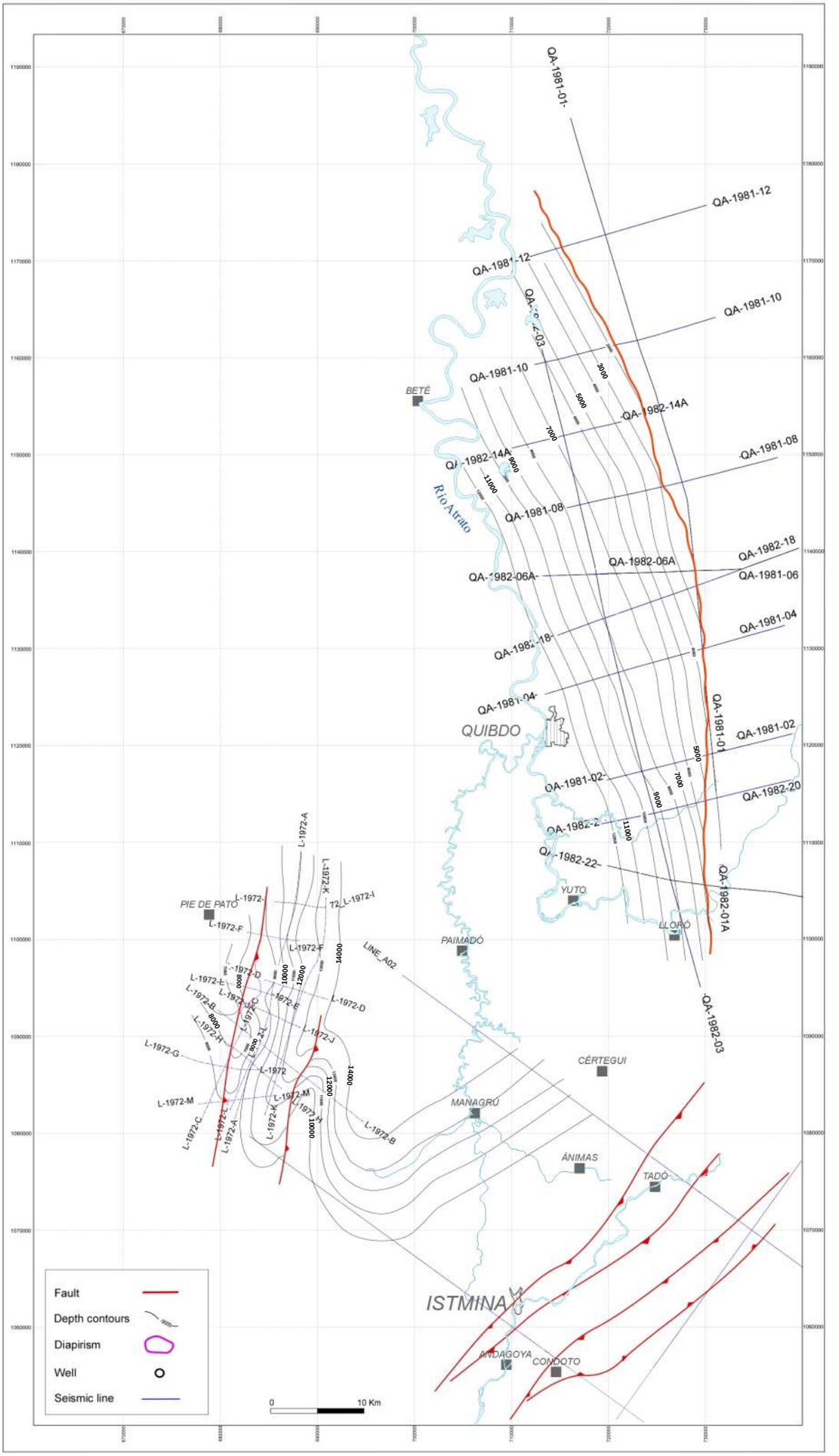

Figure 39. Structural Map Top Salaquí Formation

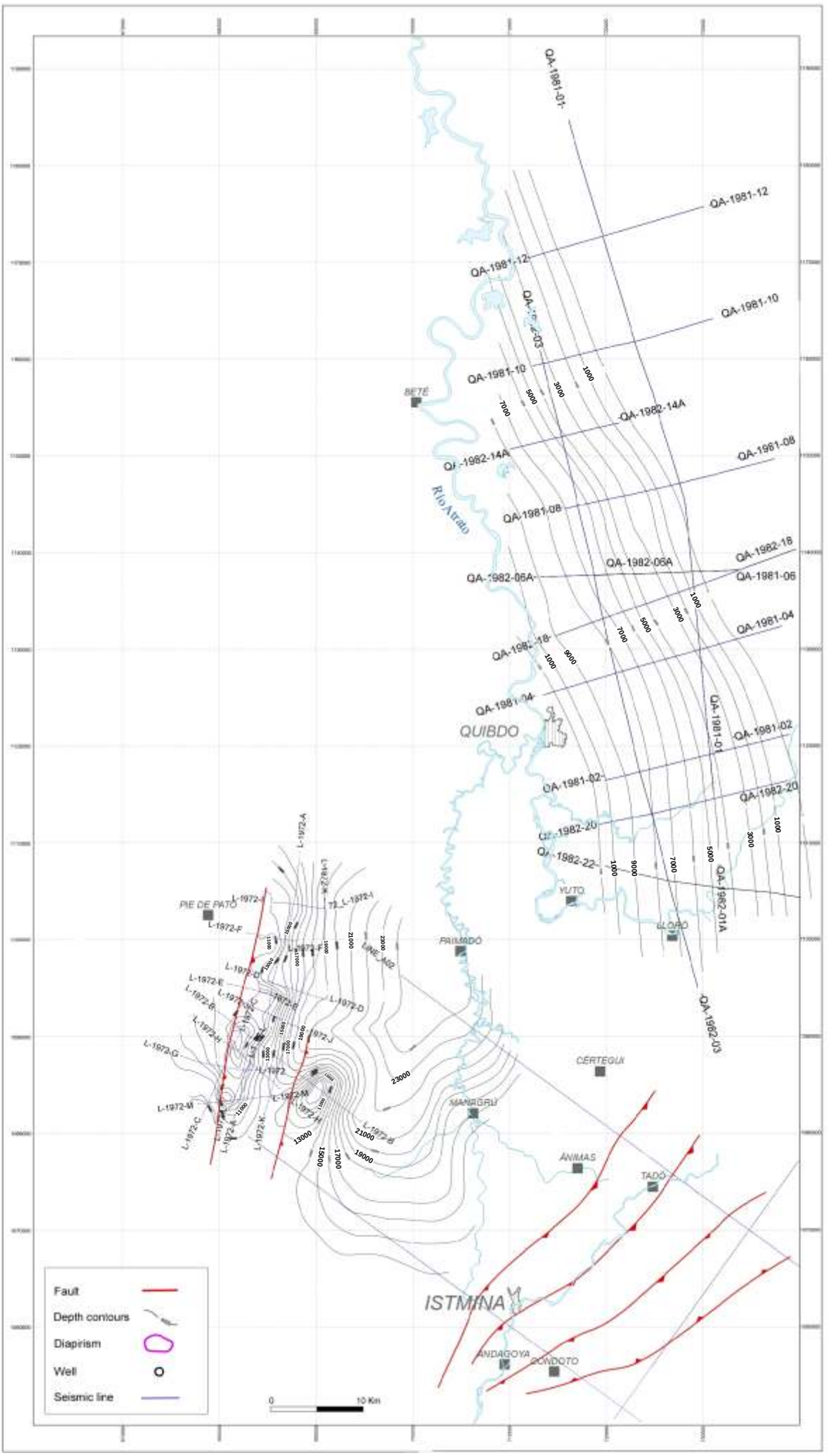

Figure 40. Structural Map Top Uva Formation

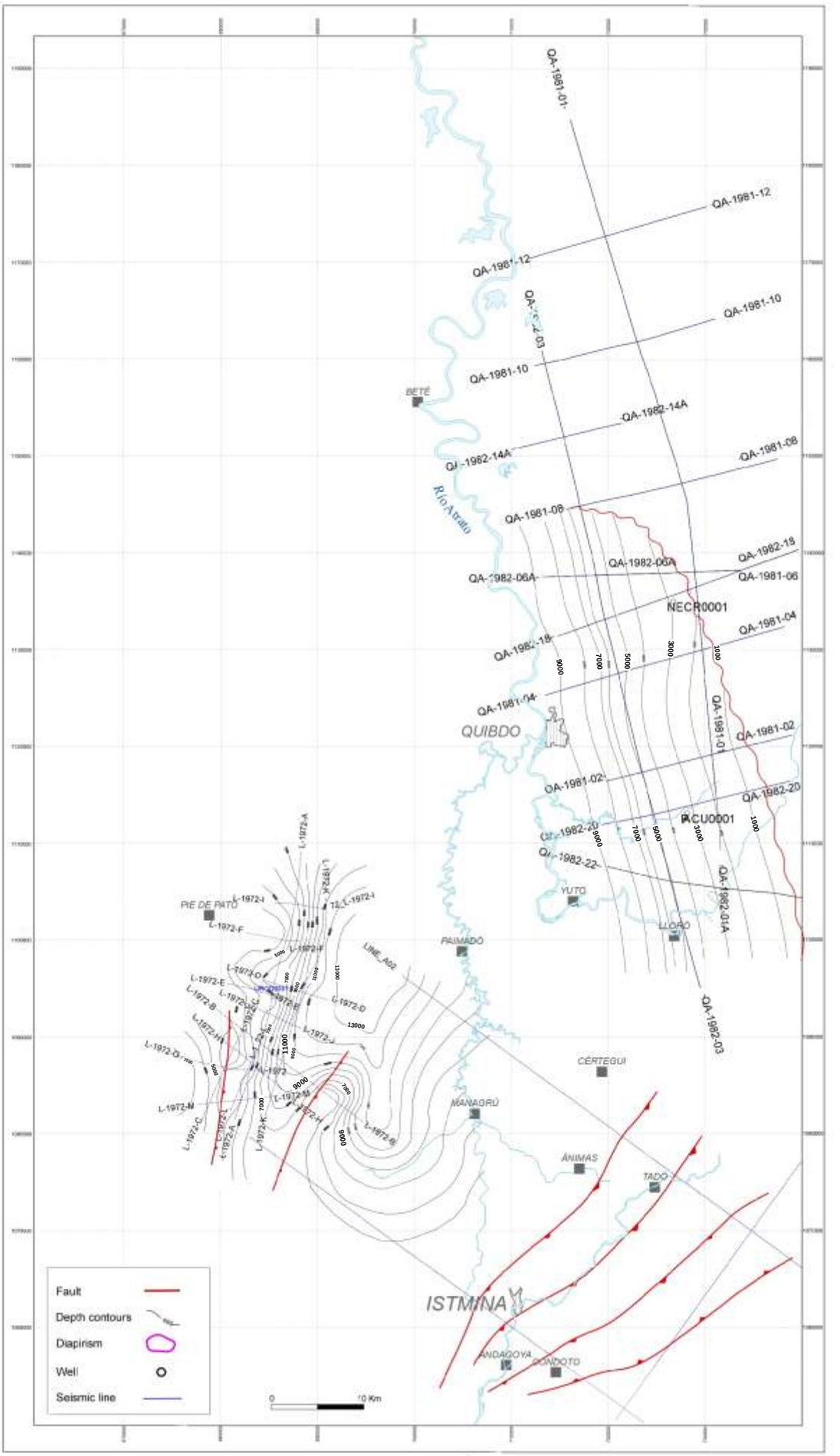

Figure 41. Structural Map Top Napipi Formation

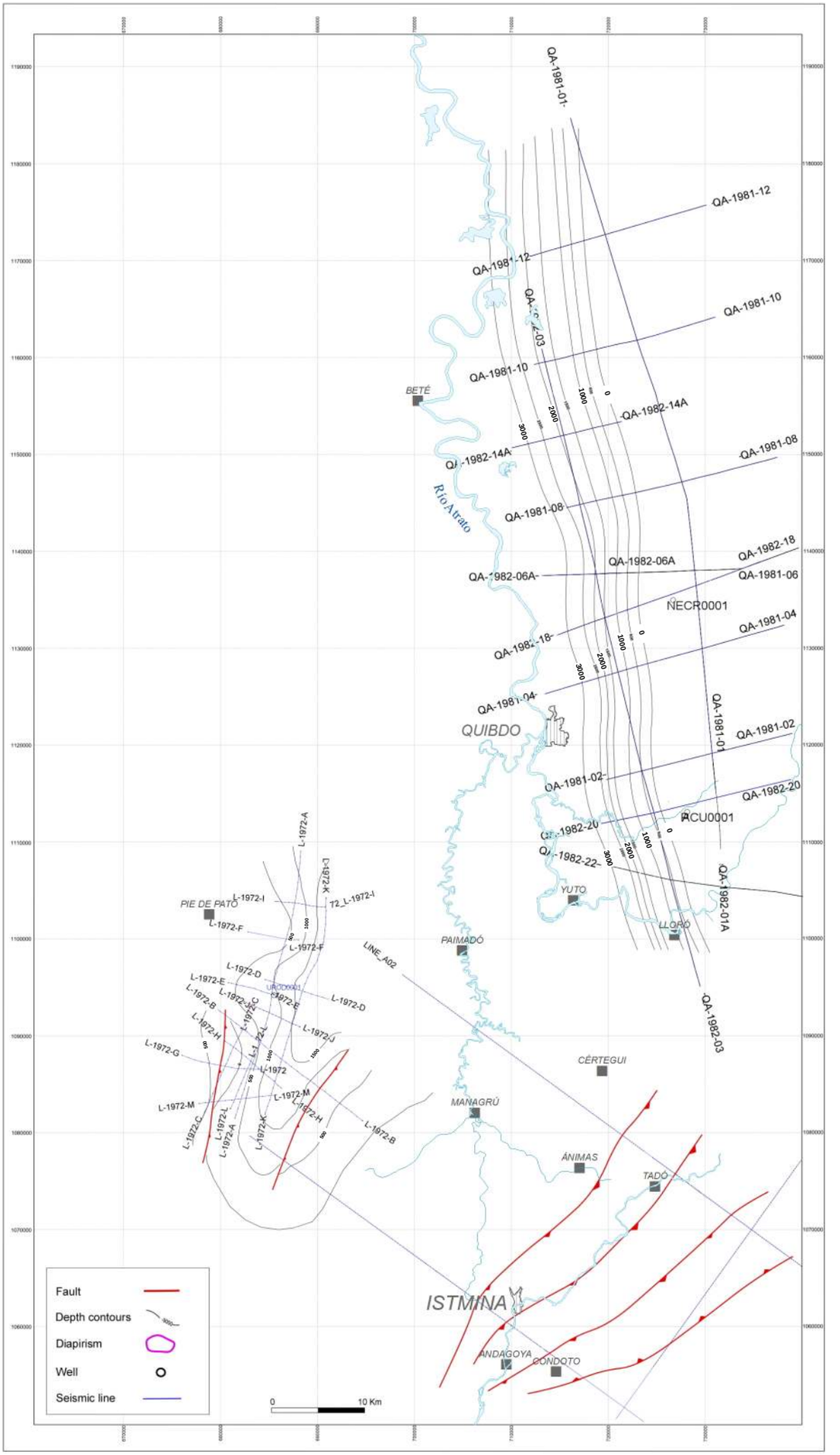

Figure 42. Structural Map Top Sierra Formation

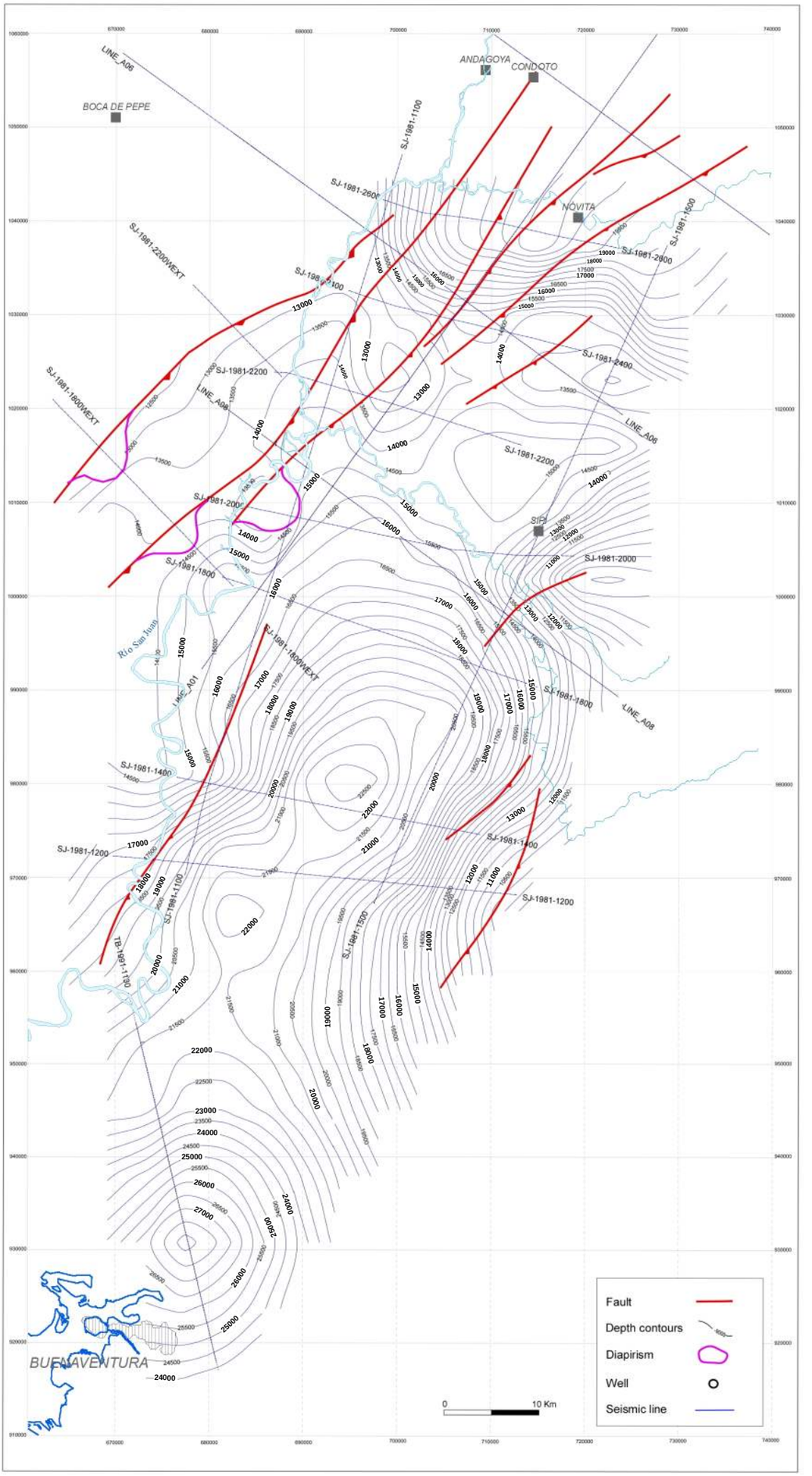

Figure 43. Structural Map Top Basement

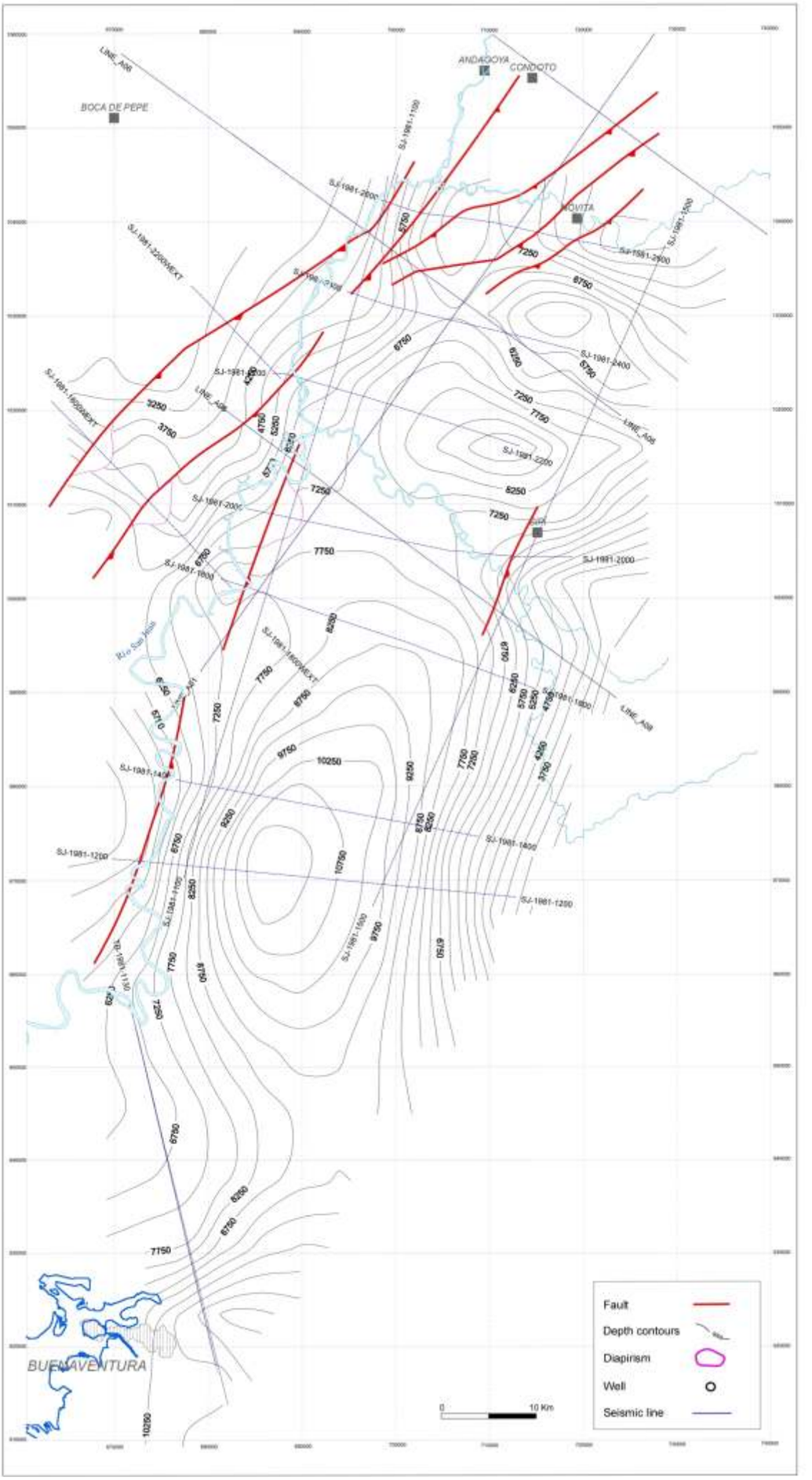

Figure 44. Structural Map Top Iró Formation

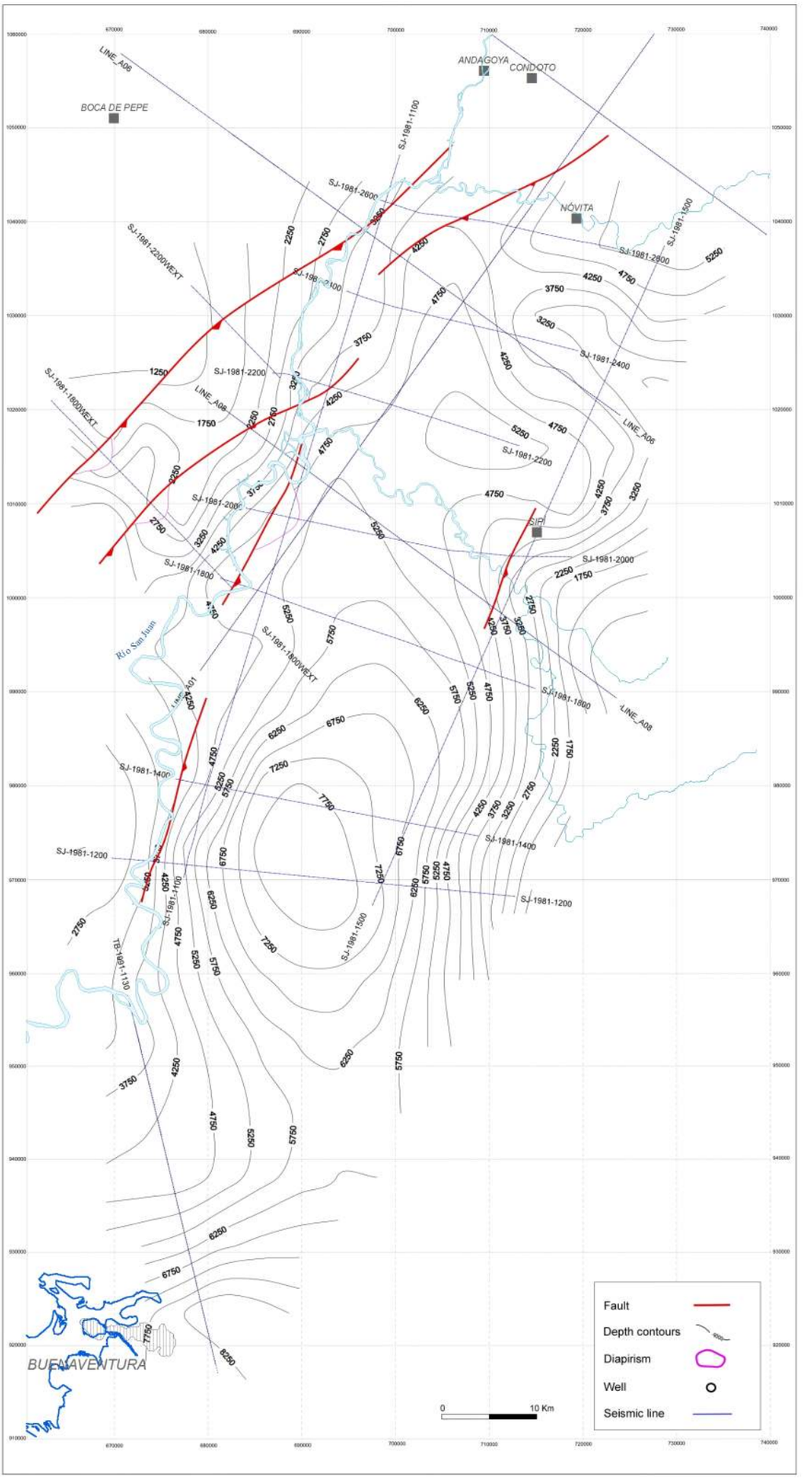

Figure 45. Structural Map Top Istmina Formation

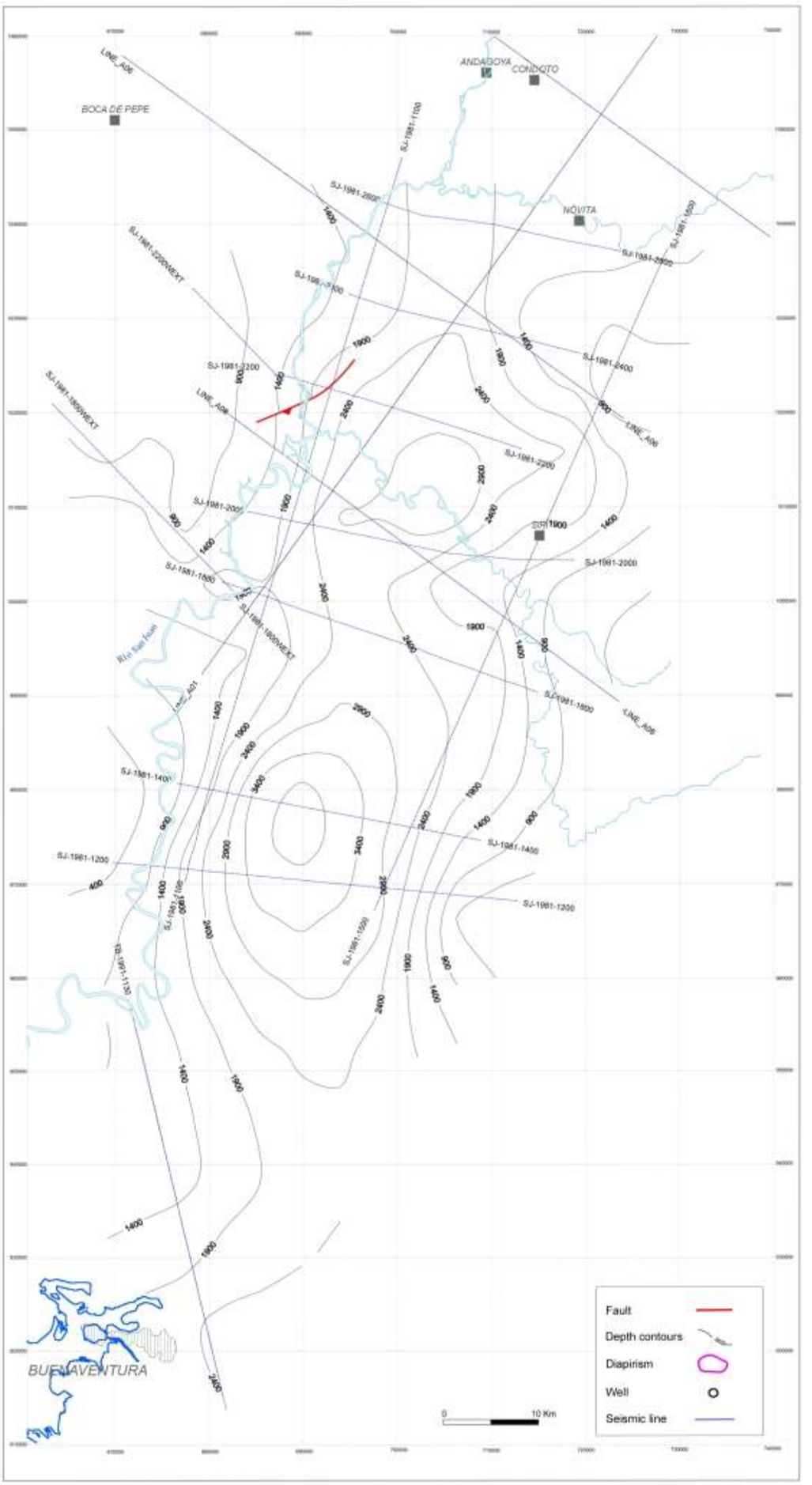

Figure 46. Structural Map Top Condoto Formation

PACIFIC OCEAN
Punta Ardita
Bahía de Humboldt
Punta Cabo Marzo
Punta La Tortuguera
Bahía de Cupica
Punta Nabugá
Bahía Solano
Ensenada de Utría
GOLFO DE TRIBUGÁ
Ensenada Coquí
Punta Arusí
Cabo Corrientes
Playa Nueva
Bahía Baudó
Boca Usuragá
Ensenada Docampado
Boca Hijua
Boca Orpúa
Boca Cacagual
Playa El Choncho
Mutatá
Dabeiba
Cañasgordas
Frontino
Abriaquí
Caicedo
BETULIA
CONCORDIA
SALGAR
EL CARMEN DE ATRATO
HISPANIA
BETANIA
MISTRATÓ
PUEBLO RICO
SANTUARIO
LA CELIA
BALBOA
SAN JOSÉ DEL PALMAR
EL ÁGUILA
ANSERMANUEVO
EL CAIRO
ARGELIA
CARTAGO
TORO
VERSALLES
OBANDO
EL DOVIO
BOLÍVAR
SAN JUAN
Tuluá
San Pedro
SISTEMA DE FALLAS GARRAPATAS
Qui
Qall
Uv
Sa
Pen
Ma
Siu
Si
Sil
Peu
Co
Rp
Br
Is
QTt
My
Ci
N
25
50
km

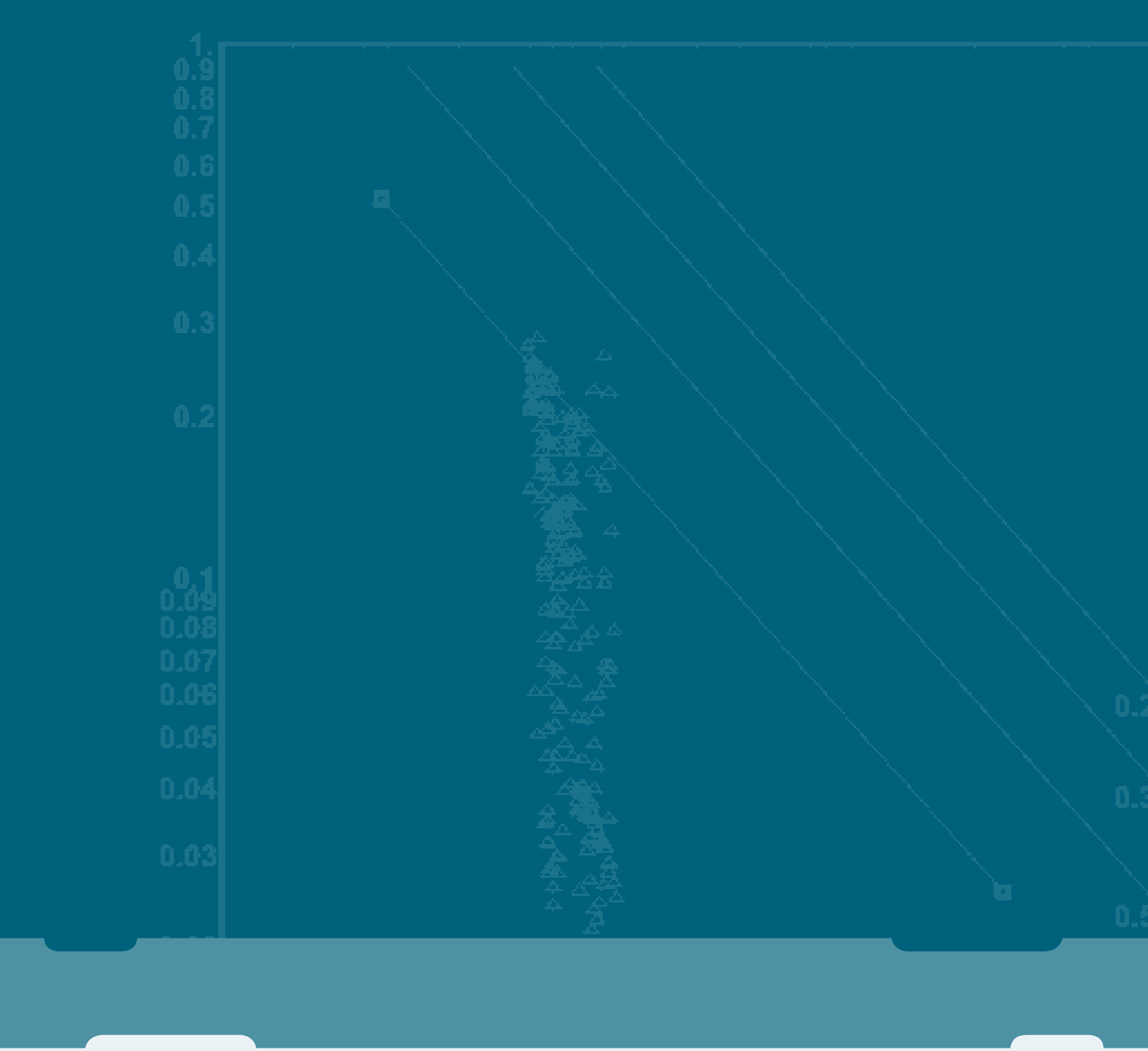

5. PETROPHYSICAL EVALUATION

Parameter : m exponent : 2.

Parameter : n exponent : 2.

Parameter : a factor : 1.

	Zone	Depths
△	(1) Zone 1	62.F - 15002.F

5. PETROPHYSICAL EVALUATION

5.1. Introduction

This study includes the petrophysical evaluation of the sedimentary sequence drilled by five wells in the Atrato basin.

The main lithological units that were characterized are Sierra, Napipí, Uva, Salaquí and Clavo Formations.

5.2. Objectives

- To carry out petrophysical analysis in five wells drilled in the Atrato basin, in order to determining clay volume, lithology, porosity, and fluid saturation in the different reservoirs identified.
- To obtain an internally consistent compilation of petrophysical properties and results for the evaluated wells. To present validated standardized data of original curves, and petrophysical calculations that allow a more precise evaluation of potential hydrocarbon reservoirs.

5.3. Available Data and Quality Control

As noted, evaluations were based upon information from five wells drilled by different operators between 1953 and 1983. Well logs were obtained in consistent LAS format. Graphic images of some of the field logs and various well reports were also used.

Table 7 presents an inventory of the wells and the available logs. The sampling frequency of the input files for the evaluations was two (2) data points per foot. The applied neutron porosity (NPHI) was acquired in a sandstone matrix (2.65 gr/cc).

5.3.1. Core Data

No conventional core analysis data is available for any of the wells, in order to complete a core-log calibration. For this reason the present evaluation is based upon typical log responses in open holes.

5.4. Shale Content

Due to the absence of GR logs for most of the intervals, the "average clay volume" (VCLAV) method was used. This consists of the calculation of an arithmetic average of the clay volume, as obtained from the curves GR, SP and Resistivity (VclGR, VclSP and VclR).

When applicable, the GR log was used to generate a normalized gamma ray curve, assuming a linear relationship, as supplied by the following equation:

$$VclGR\ (clay\ volume) = (GR_{log}\ \ GR_{clean}) / (GR_{shale}\ \ Gr_{clean})$$

For the SP curve the following lineal method was used:

$$VclSP\ (clay\ volume) = (SP_{log}\ \ SP_{clean}) / (SP_{shale}\ \ Sp_{clean})$$

WELL LOG INVENTORY

Well	Interval	Well Log											
	(ft)	GR	SP	ILD	LN	SN	LAT	SFLA	DT	NPHI	RHOB	MNOR	MINV
Buchadó-1	15 - 3510		X		X	X	X						
1953	3510 - 7350		X		X	X	X					X	X
	7350 - 9700		X		X	X	X						
	9700 - 9850		X		X	X	X					X	X
	9850 - 10700		X		X	X	X						
	10700 - 12585		X		X	X	X					X	X
	12585 - 13040		X		X	X	X						
	13040 - 13250		X		X	X	X					X	X
	14600 - 14520		X		X	X	X						
	14520 - 15492		X		X	X	X					X	X
Urodó-1	60 - 995		X	X		X							
1973	1008 - 3490		X	X		X			X				
	3510 - 9430	X	X	X		X			X				
	9525 - 11995		X	X		X			X				
	12030 - 15000		X	X		X							
Opogadó-1	100 - 990		X	X		X							
1974	1015 - 3640	X								X			
	3680 - 5050	X	X	X		X			X				
	5200 - 7700		X	X		X							
	7700 - 10020	X	X	X		X			X				
	10020 - 10515		X	X		X							
	10515 - 11358	X	X	X		X			X				
Pacurita-1	40 - 1220		X	X				X					
1981	1220 - 4000		X	X				X	X				
	4000 - 6790	X	X	X				X	X	X	X		
	6800 - 9445	X	X	X				X	X	X	X	X	X
Nécora-1	60 - 640		X	X				X					
1983	690 - 2370		X	X				X					
	2460 - 6300	X	X	X				X	X	X	X	X	X
	6300 - 6380		X	X				X	X			X	X
	6380 - 6470	X	X	X				X	X	X	X	X	X

Table 7. Well log inventory, Atrato Basin

In the case of the resistivity logs, the shale indicator was obtained in the following way:

$$Z = \frac{Rshale}{Rt} + \frac{(Rclean - Rt)}{(Rclean - Rshale)}$$

When Rt is greater than $2 * R_{shale}$:

Whilst for all other cases VclR = Z

$$VclR\ (clay\ volume) = 0.5 * (2*Z)^{0.67*(Z+1)}$$

The SP log was corrected for drift using a "base line clay" value of zero (0). The obtained curve (SP_shift) indicates the presence of permeable rock in the cases that there exists enough salinity contrast between the mud filtrate and the formation water. VclSP generally indicates a larger quantity of reservoir rock than VclGR.

In general VclSP> VclGR> VclR, however, the curve VclGR approximately corresponds to VclAV. As such, when using this finished curve, an appropriate shale indicator may be obtained.

5.5. Porosity Determination

In the case of the wells Nécora-1 and Pacurita-1, porosity was estimated using the Cross density (RHOB) and neutron (NPHI) Plot, applying a grain density of 2.65 gr/cc and a fluid density of 0.8 gr/cc (well perforated with water based mud). Values for wet clay density were between 2.67-2.70 gr/cc and for dry clay density 2.80 gr/cc. The neutron value for wet clay was between 0.53-0.57.

When the density (RHOB) and neutron (NPHI) logs were not available, the total porosity was obtained from the sonic log (DT) using the Wyllie's equation:

$$PHIT = \Phi S = \frac{DT - Dtma}{Dtf - DTma}$$

The maximum limit of settled porosity was 30%, with a matrix travel time of 55.5 sec/ft, water travel time of 189 sec/ft and a compaction factor of 1.

In the case of wells Opogadó-1 and Buchadó-1, for which curves to calculate porosity were unavailable, the empirical relationship of Faust was used. This consists of making petrophysical correlations between velocity (travel time) and Resistivity, and in turn between the Resistivity and porosity.

$$\text{SVEL\_Faust (ft/sec)} = 1948 * (\text{Resistivity})^{0.167} * (\text{Depth})^{0.167}$$

$$\text{DT\_Faust (msec)} = 1{,}000{,}000 / \text{SVEL\_Faust}$$

For the evaluated units, the total porosity was obtained using the curve DT_Faust (pseudo sonic), contained within Wyllie's equation for average time, as follows:

$$\Phi = \frac{Dt - \text{Dtma} - \text{Vcl} * (\text{Dtcl} - \text{Dtma})}{(Dtfl * Sxo + Dthy * (1 - Sxo) - Dtma) * Cp}$$

Where:

Dt = Sonic input curve (DT_Faust)
Dtma = Sonic matrix value (55.5 uSec/ft)
Dtcl = Sonic clay value (98 uSec/ft)
Dtfl = Sonic filtrate value (189 uSec/ft)
Dthy = Sonic hydrocarbon (220 uSec/ft)
Vcl = Wet clay volume (VCLRes)
Sxo = Flushed zone water saturation (0.8 1.0)
Cp = Compaction factor (1,0)

The effective porosity (PHIE) was obtained in order to correct the apparent total porosity value (PHIT), with respect to the clay volume (VCL).

5.6. Hydrocarbon Saturation

5.6.1. Temperature

The calculated temperature was derived from the calculated linear gradient based upon the maximum temperature registered at the bottom of the well and the temperature measured on the surface at the moment of log's acquisition (80 °F).

5.7. Salinity and Rw

The values of formation water resistivity (Rw) were obtained using the crossplot method of Pickett, where, for a water bearing zone, the relationship of Total Porosity (PHIT) to True Resistivity (RT) and Index of Clay Volume (VCLAV) in the axis Z, can be plotted.

Different Rw's were obtained for each of the wells. It was not possible to differentiate them based upon individual drilled units due to the low quality of information from the wells. The obtained values of Rw and their corresponding salinity with respect to reference temperature (60 F°) are presented below:

Well	Rw (Ohm-m)	Salinity ppm [NaCl]	Salinity ppm [Cl^-]
Nécora-1	0.045 @ 60 F°	102,115	62,075
Pacurita-1	0.320 @ 60 F°	18,170	11,045
Opogadó-1	0.650 @ 60 F°	9,740	5,920
Urodó-1	0.750 @ 60 F°	8,585	5,220
Buchadó-1	0.620 @ 60 F°	10,150	6,170

Using the above Rw values an evaluation of water saturation (Sw) for each of the wells was carried out.

5.8. Sw from Resistivity

For the calculation of water saturation (Sw) the modified method of Simandoux was used, in order to correct for the argillaceous nature of some of the lithological units of interest. The appropriate is:

$$\frac{1}{Rt} = \frac{\phi^m \times Sw^n}{a \times Rw \times (1 - Vcl)} + \frac{Vcl \times Sw}{Rclay}$$

The obtained curve appears like SWF (Final Water Saturation). As values required in the model, the theoretical values of tortuosity factor were assumed "a" = 1, cementation factor of Archie "m" = 2 and saturation exponent of Archie n = 2.

5.9. Permeability

There is no available core data which permits calculation of a permeability relationship, however in order to present a qualitative value, the empirical relationships between Tixier and Timur may be applied. Timur represents the most conservative value and was used herein to represent permeability relationship averages.

5.10. Results

5.10.1. Sums and Averages

For the intervals of interest, average petrophysical properties were obtained using the following parameters \cutoffs:

Maximum clay volume for a Net Reservoir Rock	*65%*
Minimum Porosity for a Net Reservoir Rock	*1%*
Maximum Sw for a Net pay cutoff	*50%*

The Net Reservoir Rock summary is as follows:

Well	Top MD (ft)	Base MD (ft)	Gross Thickness (ft)	Net Thickness (ft)	N/G Ratio	PHIE (%)	Sw (%)	Vcl (%)
Nécora-1	43	6490	6447	32	0.005	10.5	77.5	62.6
Pacurita-1	3957	8984	5028	106	0.021	15.4	81.0	46.5
Opogadó-1	94	11357	11263	395	0.035	12.0	90.4	58.6
Urodó-1	62	15002	14940	1154	0.077	7.8	99.1	34.6
Buchadó-1	2399	15539	13141	911	0.069	14.5	100	45.6

The units do not present areas saturated in hydrocarbons. None of the analyzed wells is a producer.

5.11. Graphics

Composite logs of the evaluations completed for each of the wells are contained in Figs. 47-51. The 1:2,500 vertical graphic scale shows the original completed logs and petrophysical evaluations.

The composite logs each contain nine tracks with the following information:

Track	Curves
1	GR, Caliper, Bit Size and tops
2	Depth in feet (MD)
3	Resistivity curves (deep and shallow)
4	Density (RHOB), neutron (NPHI), acoustic (DT)
5	Effective porosity (PHIE), oil and water
6	Final Water Saturation (SWF)
7	Volume evaluation (clay, porosity, grains)
8	Net Reservoir Rock flag (green) and Net Pay flag (red)
9	Empirical Permeability KTI (Timur) and Ktx (Tixier)

5.12. Digital Data

Files were generated in LAS format with a sampling frequency of 2 values per foot. Mnemonics of the curves generated and exported in this evaluation are:

BVW *Volume of water in the porous space.*
LIT *Interpreted Lithology.*
KTI *Permeability Timur.*
PHIE *Effective porosity.*
PHIT *Total porosity.*
SWF *Final Water Saturation.*
VWCL *Volume of Wet Clay.*
VCLGR *Index of Clay Volume.*

5.13. Conclusions

- Only the wells Nécora-1 and Pacurita-1 present logs data that lead to a quantitative petrophysical interpretation.
- In general the drilled units are shale-rich and a well developed reservoir was not recorded. Regardless, it is possible to identify small sandy packages of reservoir quality, with porosities in the range of 8 to 15% and water saturations exceeding 80%. No commercial accumulations of hydrocarbons have been drilled in the Atrato and San Juan Basins, but during drilling, significant showings of oil and gas were recorded.

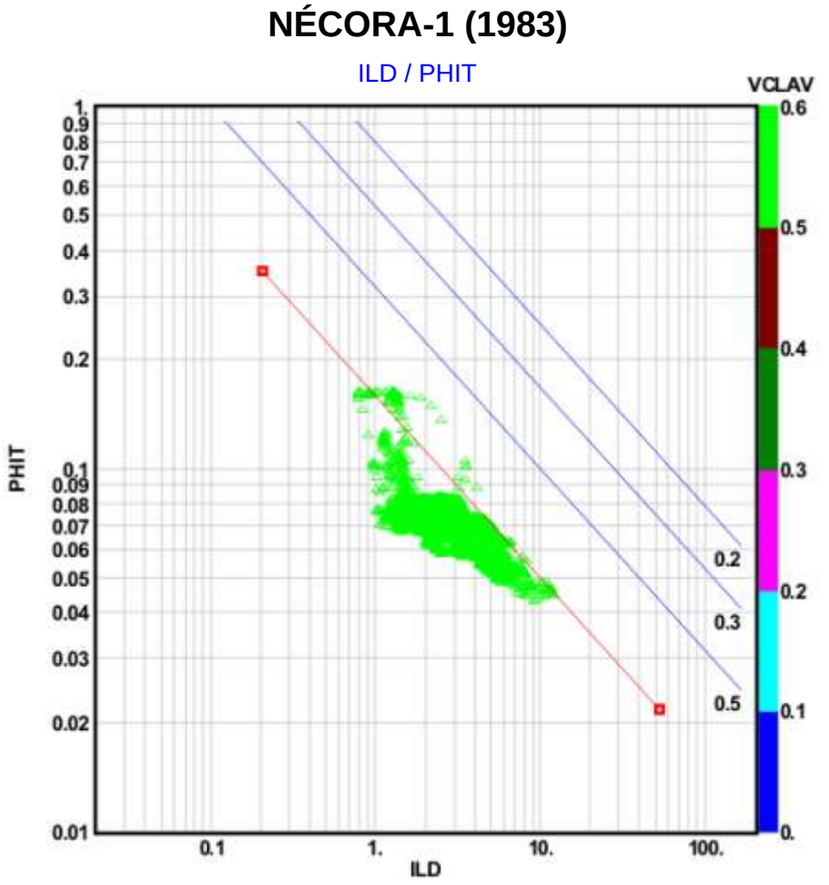

7795 points plotted out of 12895

Parameter : Rw : 0.045
Parameter : Rw Form Temp : 0.0251
Parameter : m exponent : 2.
Parameter : n exponent : 2.
Parameter : a factor : 1.

Depths
43.F - 6490.F

Figure 47. Pickett crossplot Nécora-1

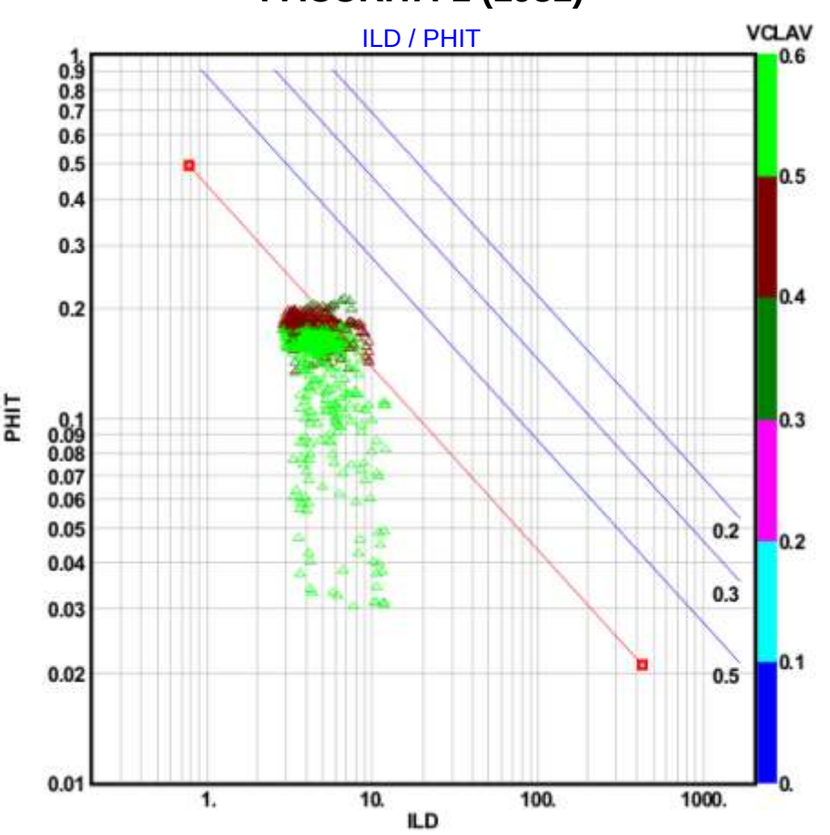

825 points plotted out of 16472

Parameter : Rw : 0.32
Parameter : Rw Form Temp : 0.189
Parameter : m exponent : 2.
Parameter : n exponent : 2.
Parameter : a factor : 1.

Depths
1223.5F - 3999.5F
3999.5F - 9458.5F

Figure 48. Pickett crossplot Pacurita-1

OPOGADÓ-1 (1974)

ILD / PHIT

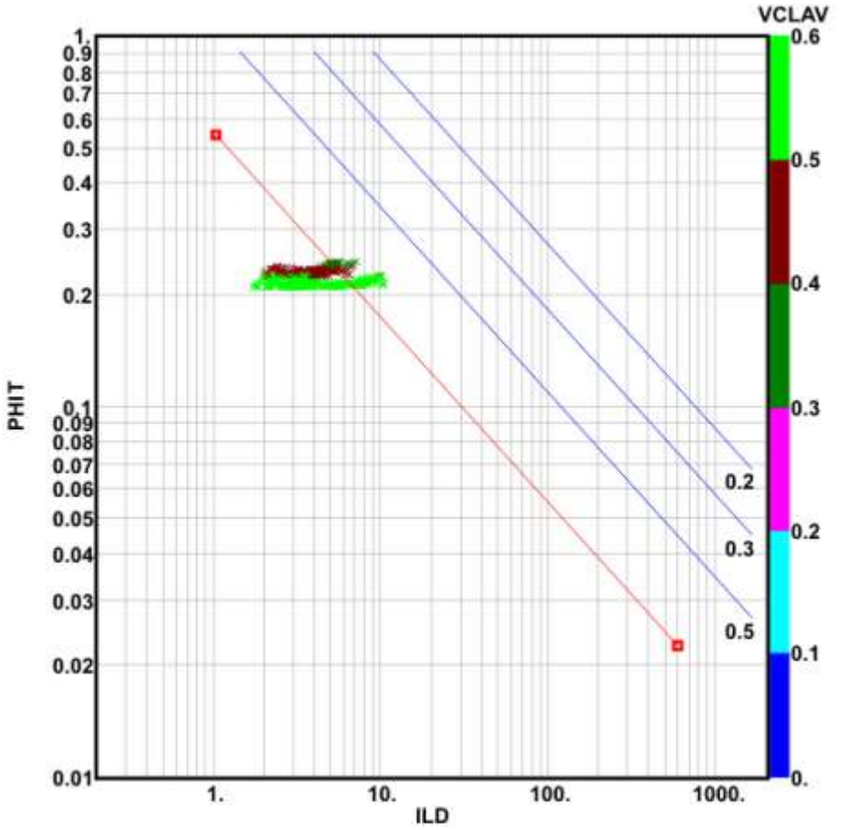

703 points plotted out of 22527

Parameter : Rw : 0.65
Parameter : Rw Form Temp : 0.301
Parameter : m exponent : 2.
Parameter : n exponent : 2.
Parameter : a factor : 1.

Depths
94.F - 11357.F

Figure 49. Pickett crossplot Opogadó-1

URODÓ-1 (1973)

ILD / PHIT

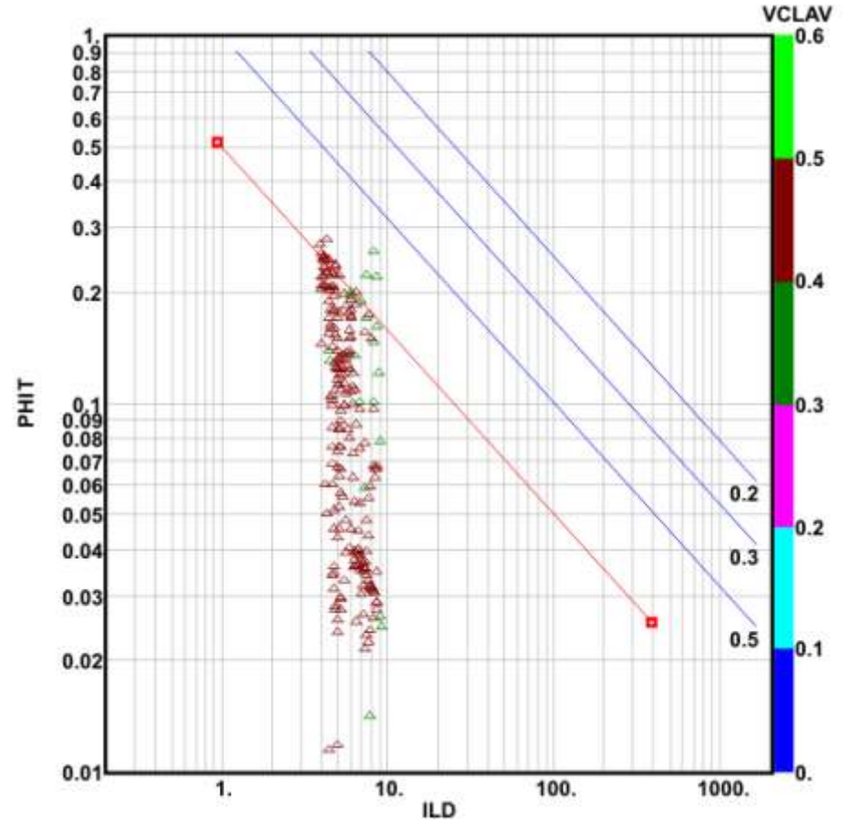

224 points plotted out of 29881

Parameter : Rw : 0.75
Parameter : Rw Form Temp : 0.252
Parameter : m exponent : 2.
Parameter : n exponent : 2.
Parameter : a factor : 1.

Depths
62.F - 15002.F

Figure 50. Pickett crossplot Urodó-1

BUCHADÓ-1 (1953)

ILD / PHIT

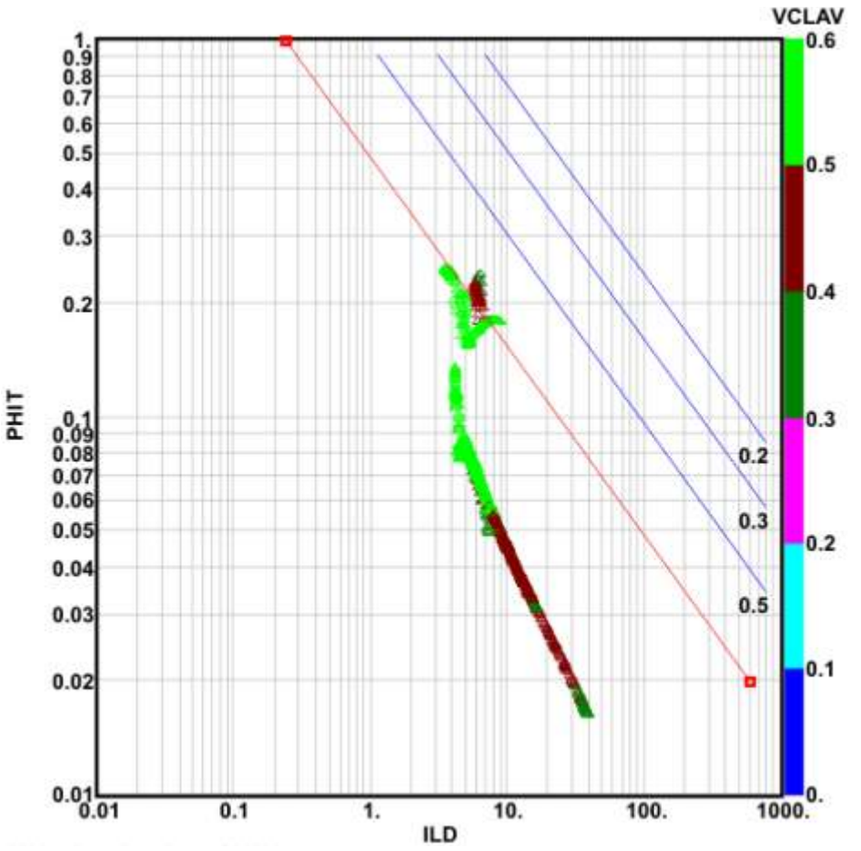

2600 points plotted out of 26282

Parameter : Rw : 0.62
Parameter : Rw Form Temp : 0.234
Parameter : m exponent : 2.
Parameter : n exponent : 2.
Parameter : a factor : 1.

Depths
2398.F - 15539.F

Figure 51. Pickett crossplot Buchadó-1

PACIFIC OCEAN
Punta Ardita
Bahía de Humboldt
Punta Cabo Marzo
Punta La Tortuguera
Bahía de Cupica
Punta Nabugá
Bahía Solano
Ensenada de Utría
GOLFO DE TRIBUGÁ
Ensenada Coquí
Punta Arusí
Cabo Corrientes
Playa Nueva
Bahía Baudó
Boca Usuragá
Ensenada Docampado
Boca Hijua
Boca Orpúa
Boca Cacagual
Playa El Choncho
Mutatá
Dabeiba
Frontino
Cañasgordas
Abriaquí
Santa Fe de A
Caicedo
BETULIA
CONCORDIA
SALGAR
EL CARMEN DE ATRATO
HISPANIA
BETANIA
MISTRATÓ
PUEBLO RICO
APIA
SANTUARIO
LA CELIA
BALBOA
SAN JOSÉ DEL PALMAR
EL CAIRO
ARGELIA
ANSERMANUEVO
CARTAGO
TORO
VERSALLES
OBANDO
EL DOVIO
BOLÍVAR
Trujillo
Riofrío
Tuluá
San Pedro
SAN JUAN
NÓVITA
SISTEMA DE FALLAS GARRAPATAS
Qui
Uv
Qall
Siu
Si
Sil
Sa
Ma
Pen
Peu
Co
Rp
Br
Is
QTf
My
Ci
N
25
50
km

6. GEOCHEMICAL EVALUATION AND MODELING

6. GEOCHEMICAL EVALUATION AND MODELING

6.1. INTRODUCTION

The presence of active hydrocarbon seeps in the both San Juan and Atrato basins evidences the present-day generation and migration of crude oil, and thus, the existence of at least two as yet untested oil systems. In order to clarify these observations, a geochemical reinterpretation of all available information was initiated. This information permitted the geochemical characterization of potential source rocks, their correlation to the hydrocarbon found in seeps, and simulation of hydrocarbon generation and expulsion mechanisms in both basins.

Although results of the generation and expulsion modeling in the two basins suggest very favorable generation conditions, there is no doubt that the most significant obstacle preventing a better understanding of the geochemistry of these two basins is the lack of field data.

Approximately 60 PDF Format documents were gathered, 19 of which contain geochemical information. However, most of these documents reiterate information from previous studies. The compilation of geochemical source data is presented in *Fig. 52*

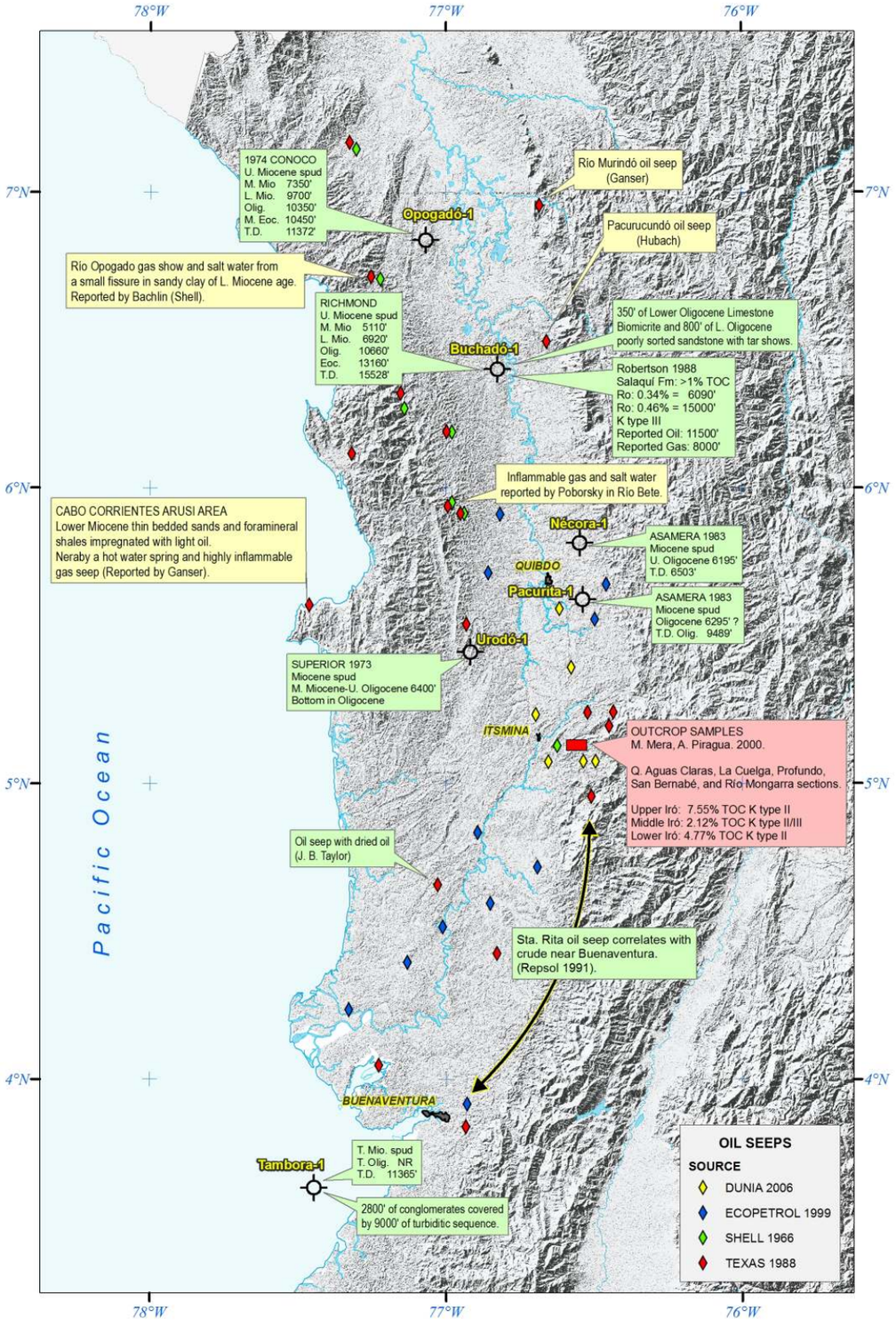

Figure 52. Geochemical source data available for the evaluation and modeling of the Atrato and San Juan Basins.

6.2. Objectives

6.2.1. Atrato Basin

- Gather and assess existing geochemical information for the Atrato basin.
- Identify potential generating rock(s) within the context of the sedimentary environment.
- Characterize in a generalized manner the potential generating rocks, based upon data from wells drilled in the basin.
- Simulate the basin's hydrocarbon generation and expulsion processes, based upon a feasible hypothetical model.

6.2.2. San Juan Basin

- Gather and assess existing geochemical information for the basin.
- Assess generation potential of the Iró Formation based upon litho-geochemical analysis.
- Correlate crude oil from seeps found in the basin with out crop samples (Iró Formation).
- Simulate the Basin's hydrocarbon generation and expulsion processes.

6.3. Atrato Basin

(See Fig. 53)

6.3.1. Clavo Formation

Some sedimentological characteristics suggest the Clavo Formation may hypothetically be a source rock in the Atrato basin; however, geochemical characterization of this formation and correlations to oil seeps are lacking.

6.3.2. Geochemical Characterization

The Clavo Formation consists of very compact, black claystone, with thin interbeds of calcareous limonite and limestone. Sedimentation of this sequence may have taken place during a low stand system tract, under low energy conditions (Suárez 1990).

It must be highlighted that no quantitative, geochemical data exist for Clavo Formation. Evidence of oil and gas generation and expulsion, as seen in Buchadó-1, remains a qualitative record.

6.3.3 Thermal Maturity

In Buchadó-1, the section analyzed records low maturity, as confirmed by low Tmax values, ranging from 417 °C to 435 °C, and vitrinite reflectance values (Ro) ranging from 0.34 at 6,090 feet up to 0.46 from 15,300 to 15,400 feet. According to a Robertson Research (1988) report, a BHT of 198 °F at 11,501 feet was recorded.

The Eocene-Miocene section, records immaturity with respect to the oil generation window, with spore coloration index values between 3.0 and 5.5, vitrinite reflectance values (Ro) between 0.23 and 0.61. Additionally, Tmax Pyrolysis values range from 417 to 439, reflecting the low maturity of potential generating rocks (Compañía Petrolera Latina, 1998).

In general, low thermal maturity is reported for the rocks studied, but it must be highlighted that the research level of the Atrato Basin in geochemical terms is quite low. Not withstanding, generation sites in areas where the Clavo Formation attained an appropriate depth cannot be discarded.

6.3.4 Organic Content

According to Robertson Research (1988), the organic content in Buchadó-1 is low, but intervals with "average" organic richness have been reported at 8,600, 10,100, 12,500, 13,300 and 14,000 feet. Additionally, the Salaquí Formation, also present in Buchadó-1 containes TOC values exceeding 1%.

Compañía Petrolera Latina (1998) reported TOC values for the Atrato Basin ranging from 0.23% to 0.94%, which are too low and would definitely not match the source rocks reported for this basin. Rocks with higher organic content remain to be located.

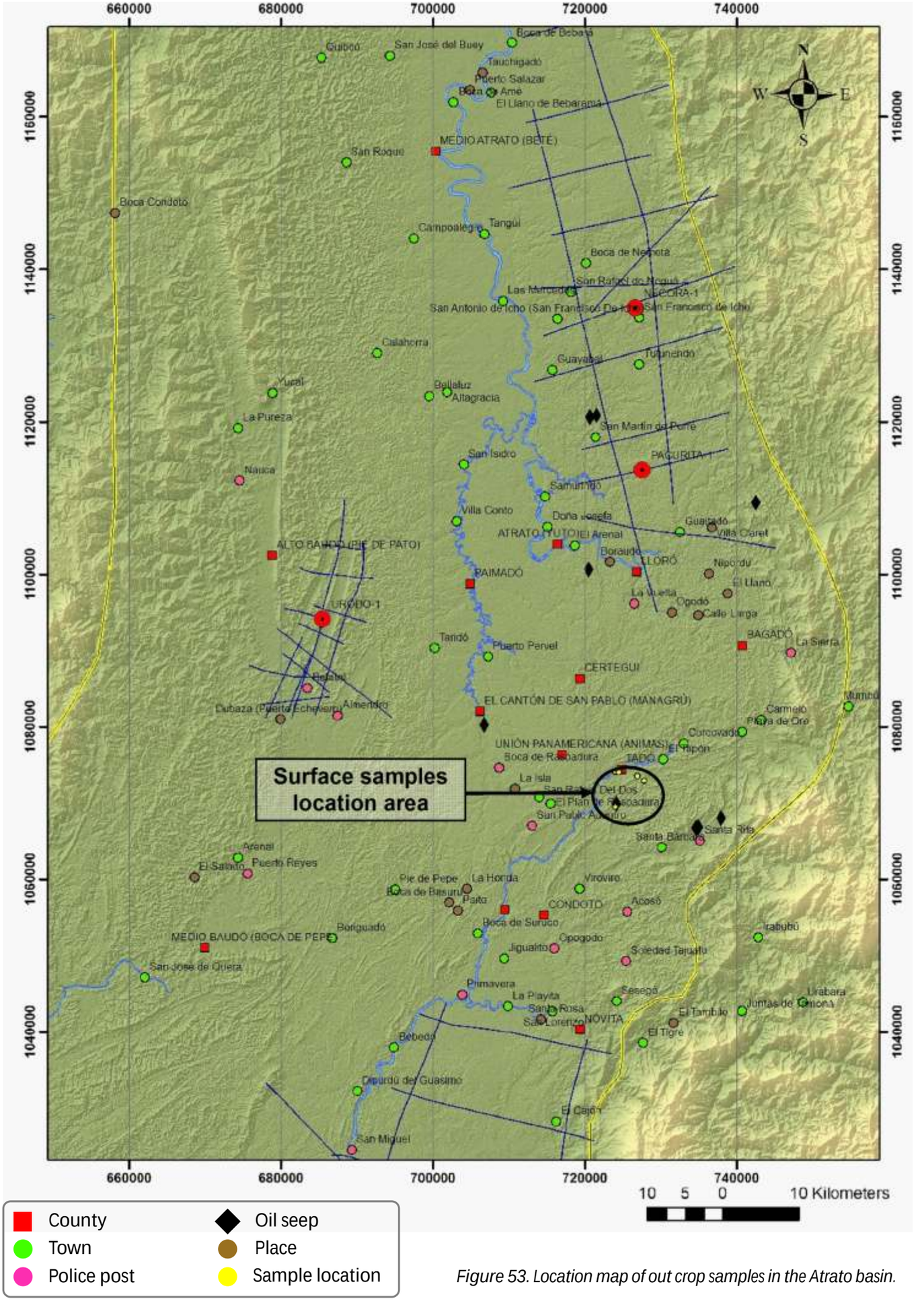

Figure 53. Location map of out crop samples in the Atrato basin.

6.3.5. Kerogen Type

According to Robertson Research (1988), within Buchadó-1, 59% inertinite, 40% vitrinite, 1% sapropelite, and kerogen type III was identified by means of organic petrographic analysis. It is evident that kerogen type III, with gas-generating characteristics, is not the precursor of the oil reported in the basin.

6.3.6. Generating Potential

According to the scant information assessed, generating potential is poor, but it is impossible to define the true generating potential of the basin's potential source rocks until they are geochemically characterized, and until it has been defined whether or not they function as part of an effective oil-generating system.

6.3.7. Oil-Rock Correlation

It would be necessary to initiate a field campaign designed to map and sample the Salaquí and Clavo Formations (hypothetical generating rocks). Such a program would permit geochemical characterization of these units, and correlate them to hydrocarbons reported for Buchadó-1 and the oil seeps found in the region.

6.3.8. Hydrocarbon Generation and Expulsion Simulation

Hydrocarbon generation and expulsion processes for Clavo Formation were modeled using PetroMod 1D software.

In order to simulate a point (Atrato Pseudo-well) where the rocks would have reached sufficient depths, a point was chosen on the projection of seismic line QA-1982-20. This point was adjusted to the basement maps produced in the present study *(Figs. 54 and 55)*.

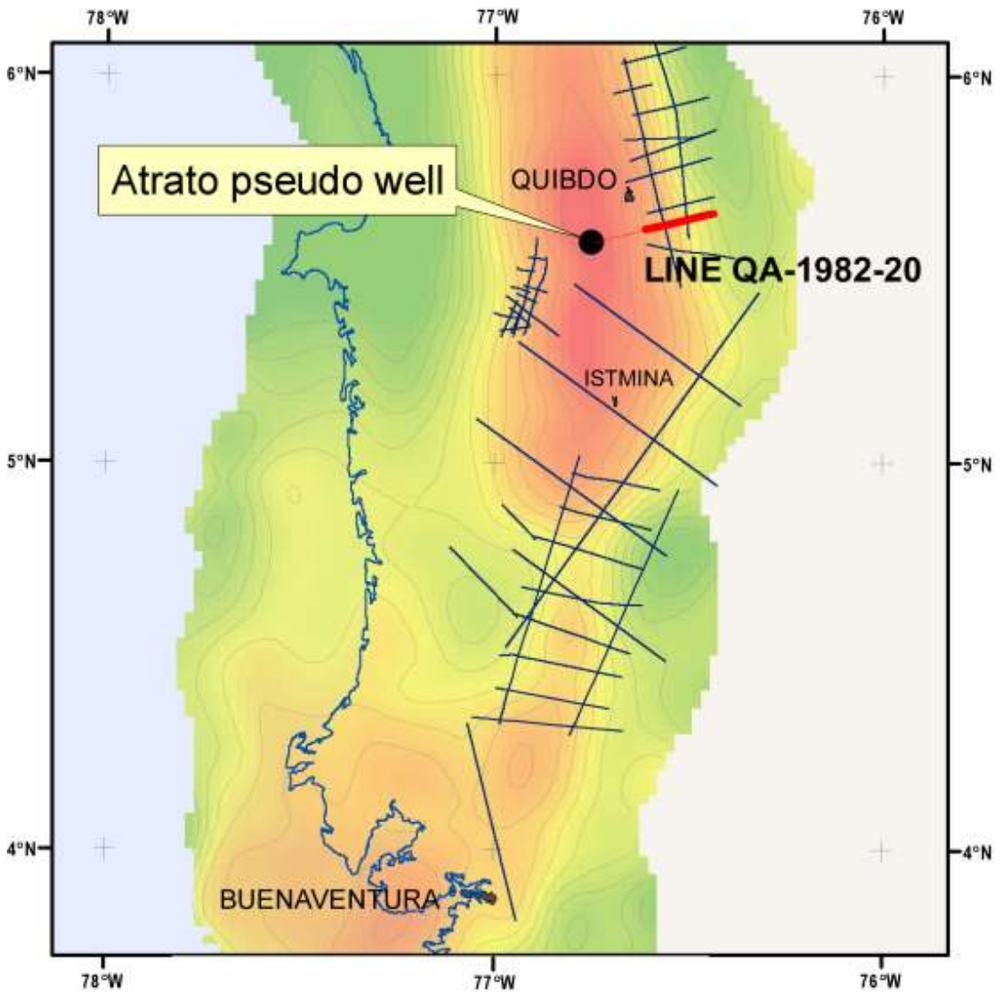

Figure 54. Location of selected seismic line QA-1982-20.

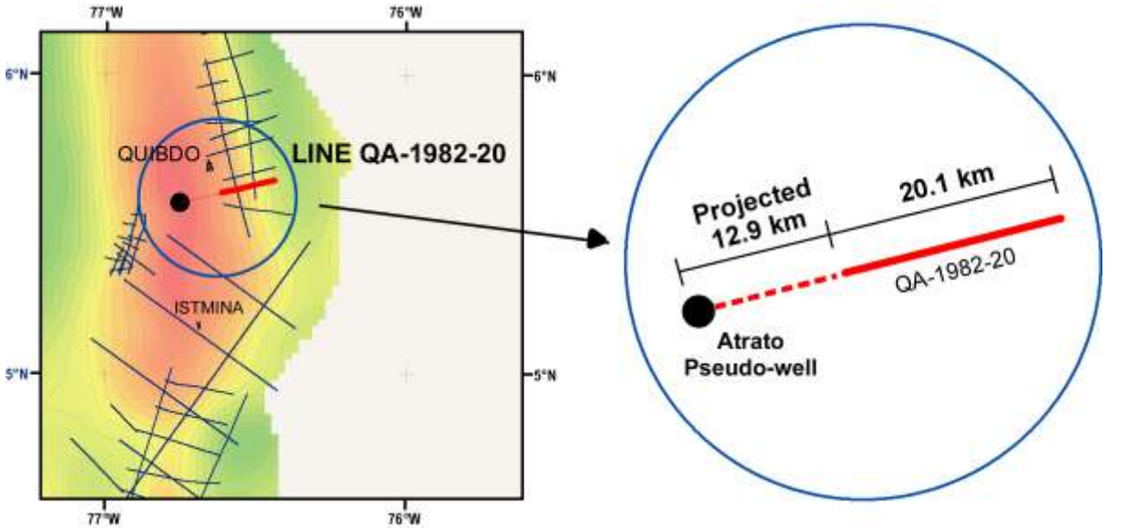

Figure 55. Location of Atrato Pseudo-well projected toward the center of the basin.

The interpretation of each stratigraphic unit's top with respect to the pseudo-well is presented in *Fig. 56*

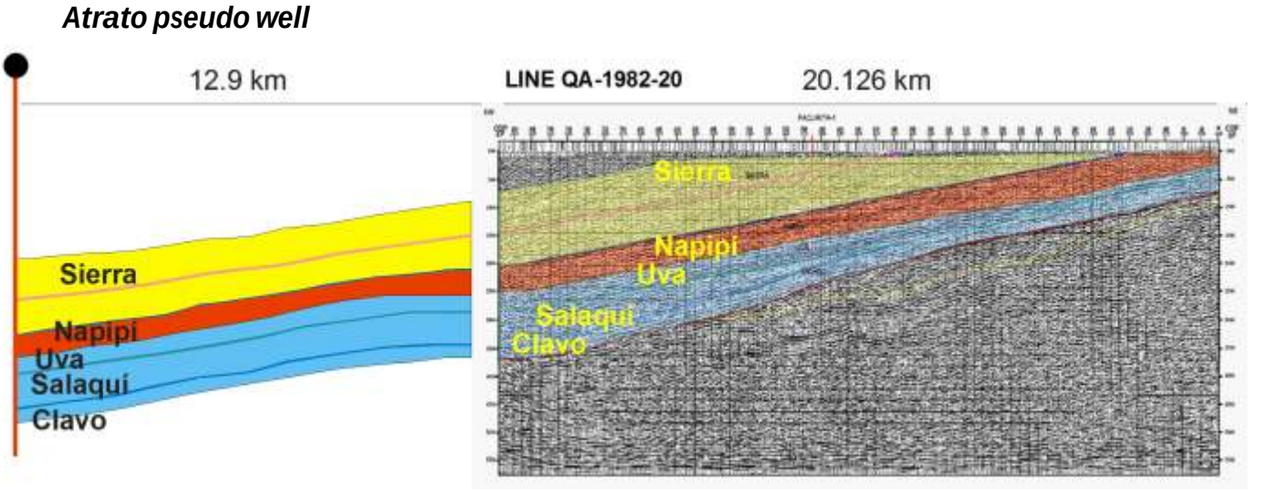

Figure 56. Seismic line QA-1982-20 interpreted along a southwesterly projection.

6.3.8.1. Thermal Model

The lack of maturity data makes it difficult to interpret the basin's definitive thermal history. In the present study, a conservative scenario using a constant heat flow history characteristic of Cenozoic basins was applied. Current heat flow was interpreted based upon the zone's BHT data *(Fig. 57)*.

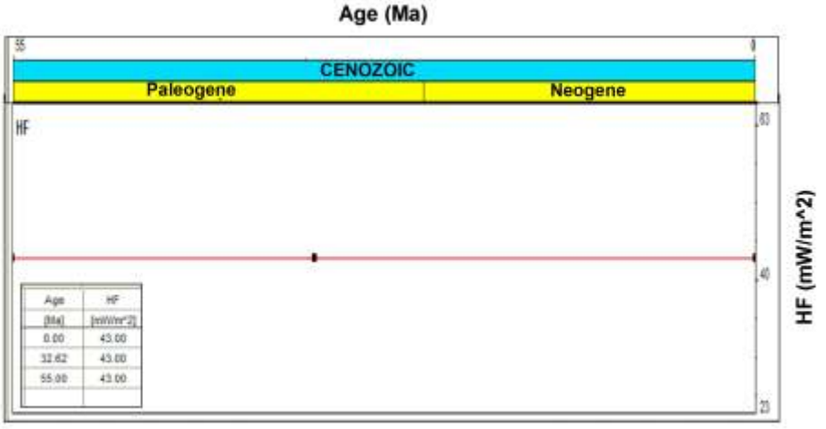

Figure 57. Atrato basin heat flow history.

BHT data from Buchadó-1 were used to generate the present geothermal gradient and to calibrate the pseudo-well obtained *(Fig. 58)*.

BUCHADÓ-1

Gradient: 1.0651 °F/100 ft

Depth feet	BHT (ºF)	T corr (°F)
0	86	94.6
12400	205	225.5
15550	232	255.2

Depth.feet	T corr (°F)	Depth. Meters	T corr (°C)
0	94.91	0	34.95
2000	115.70	610	46.50
4000	136.49	1219	58.05
6000	157.29	1829	69.61
8000	178.08	2438	81.16
10000	198.87	3048	92.71
12000	219.66	3658	104.26
14000	240.45	4267	115.81
16000	261.25	4877	127.36

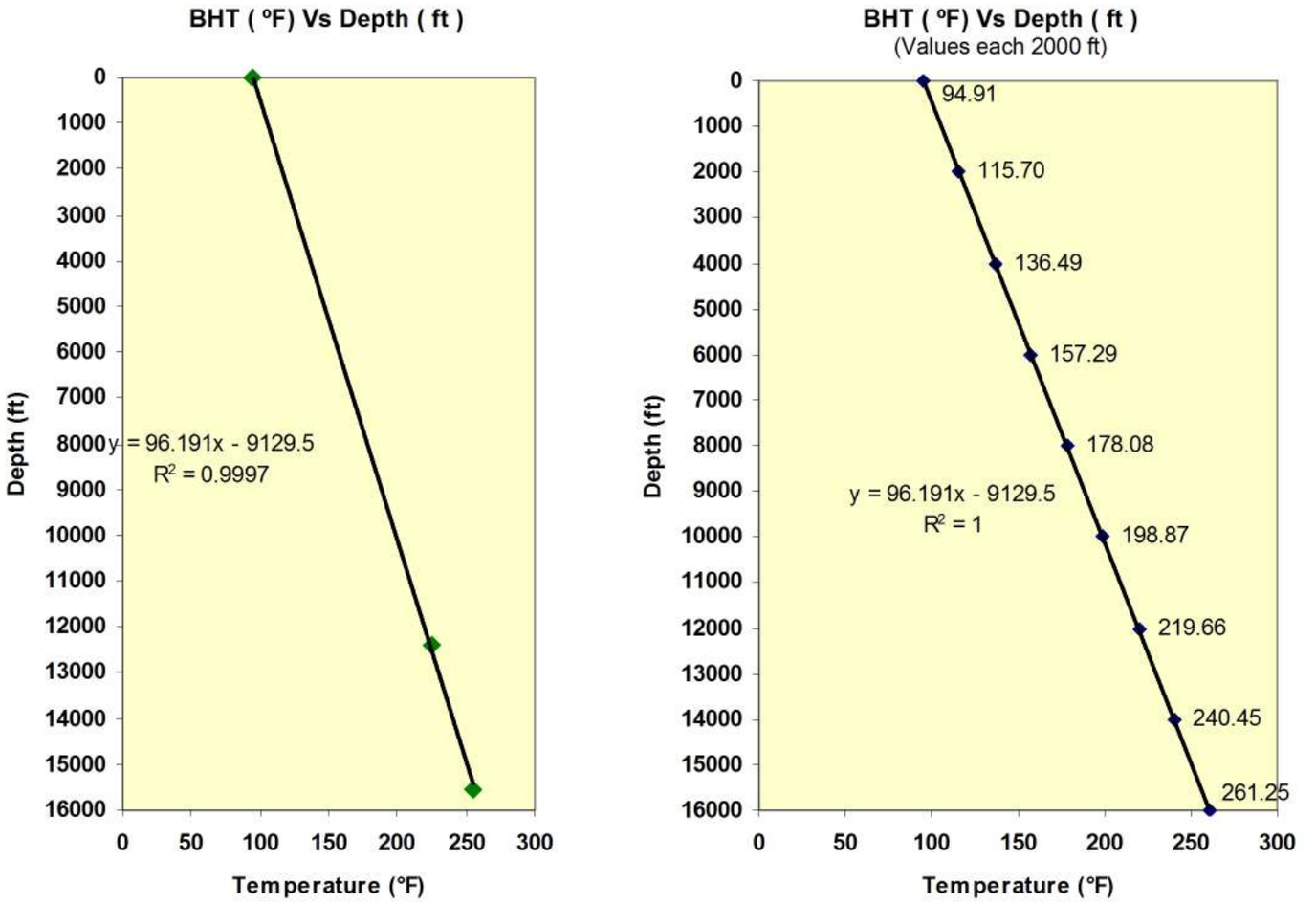

Figure 58. BHT data and thermal gradient calculation.

This model provides graphs of A) expected temperatures in the calibrated sequence, using the current calculated thermal gradient, B) thermal maturity behavior curve in the sequence, C) paleotemperatures of Clavo Formation generating interval, and D) maturity behavior over time *(Fig. 59)*.

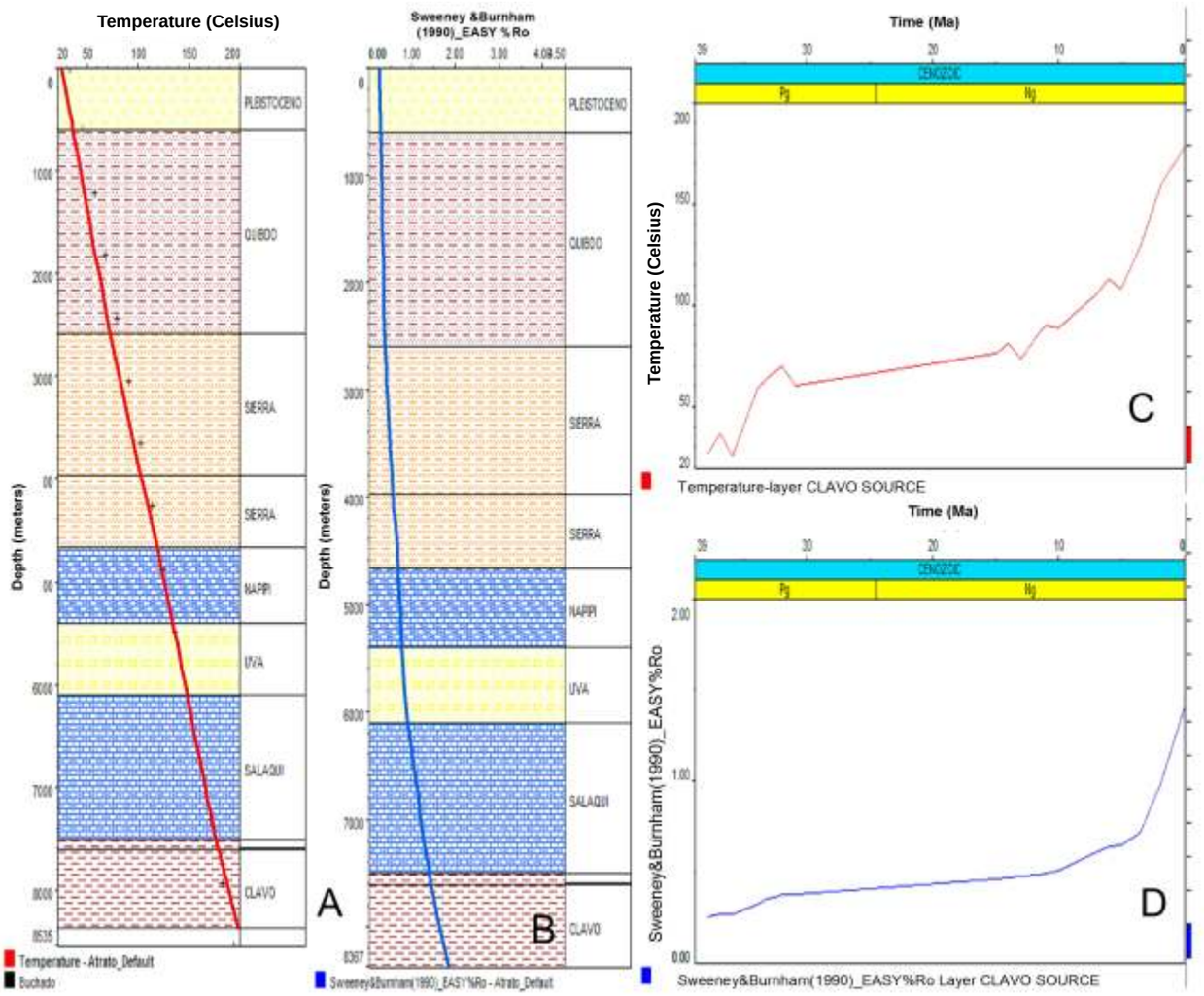

Figure 59. Calibration, temperature, and maturity vs. time curves

6.3.8.2. Geochemical Model

Geochemical modeling indicates that the hydrocarbon seeps are definite evidence of past or current hydrocarbon generation processes, despite the fact that generating rocks are still to be identified and characterized. However, based on lithological characteristics and sedimentary environment, it can be speculated that the upper section of El Clavo Formation could exhibit source rock characteristics that can be correlated to the reported oil seeps *(Fig. 60)*.

Input | Boundary Assig

	1	13	14	15
		TOC	Kinetics	HI
	Name			
		[wt%]		[mg HC/g TOC]
1	Sediment Surface			
2	PLEISTOCENE	0.00	none	0.00
3	QUIBDÓ	0.00	none	0.00
4	SIERRA	0.00	none	0.00
5	SIERRA ERODED	0.00	none	0.00
6	SIERRA	0.00	none	0.00
7	NAPIPÍ ERODED	0.00	none	0.00
8	NAPIPÍ	0.00	none	0.00
9	UVA ERODED	0.00	none	0.00
10	UVA	0.00	none	0.00
11	SALAQUÍ ERODED	0.00	none	0.00
12	SALAQUÍ	0.00	none	0.00
13	CLAVO ERODED	0.00	none	0.00
14	CLAVO SOURCE	4.00	Behar_et_al(1997)_T2-S(MontSh)-CS	450.00
15	CLAVO	0.00	none	0.00

Figure 60. Geochemical model input data

6.3.8.3. Generation and Expulsion Model

Hydrocarbon generation and expulsion processes for the Clavo source interval were modeled by using PetroMod 1D software. Input data for the sedimentary sequence and lithostratigraphic units, including erosion and sedimentation times, were taken from the Atrato chronostratigraphic column (Chapter 3). Input data for the thickness of each of the formations were obtained from the interpreted seismic lines *(see Chapter 4 and Fig. 61)*

Input | Boundary Assignment | Output

	1	2	3	4	5	6	7	8	9	10
				Present	Eroded	Deposition Age		Erosion Age		
	Name	Top	Base	Thickness	Thickness	from	to	from	to	Lithology
		[feet]	[feet]	[feet]	[feet]	[Ma]	[Ma]	[Ma]	[Ma]	
1	Sediment Surface			0.00						
2	PLEISTOCENE	0.00	2000.01	2000.01		1.80	0.00			SANDcongl
3	QUIBDÓ	2000.01	8500.00	6499.99		3.50	1.80			SHALE&SAND
4	SIERRA	8500.00	13000.01	4500.01		5.00	3.50			SILT&SHALE
5	SIERRA ERODED	13000.01	13000.01	0.00	1500.01	7.00	6.00	6.00	5.00	SILT&SHALE
6	SIERRA	13000.01	15300.01	2300.00		10.00	7.00			SILT&SHALE
7	NAPIPÍ ERODED	15300.01	15300.01	0.00	699.99	11.50	11.00	11.00	10.00	LIMEshaly
8	NAPIPÍ	15300.01	17700.01	2400.00		13.00	11.50			LIMEshaly
9	UVA ERODED	17700.01	17700.01	0.00	1500.01	15.00	14.00	14.00	13.00	SANDcalc.
10	UVA	17700.01	20000.01	2300.00		32.00	15.00			SANDcalc.
11	SALAQUÍ ERODED	20000.01	20000.01	0.00	1800.01	34.00	32.00	32.00	31.00	LIMEmarly
12	SALAQUÍ	20000.01	24600.02	4600.01		36.00	34.00			LIMEmarly
13	CLAVO ERODED	24600.02	24600.02	0.00	999.99	38.00	37.00	37.00	36.00	SHALEcarb
14	CLAVO SOURCE	24600.02	24950.02	350.00		39.00	38.00			SHALE
15	CLAVO	24950.02	27450.02	2500.00		55.00	39.00			SHALE
16		27450.02								

Figure 61. Input data for the geological model

According to the model, the temperature curve and calibration points match very well, and the thermal maturity (Ro) values expected at the base of Clavo Formation stand at around 1.70%, as indicated in the burial history graph (*Fig. 62)*

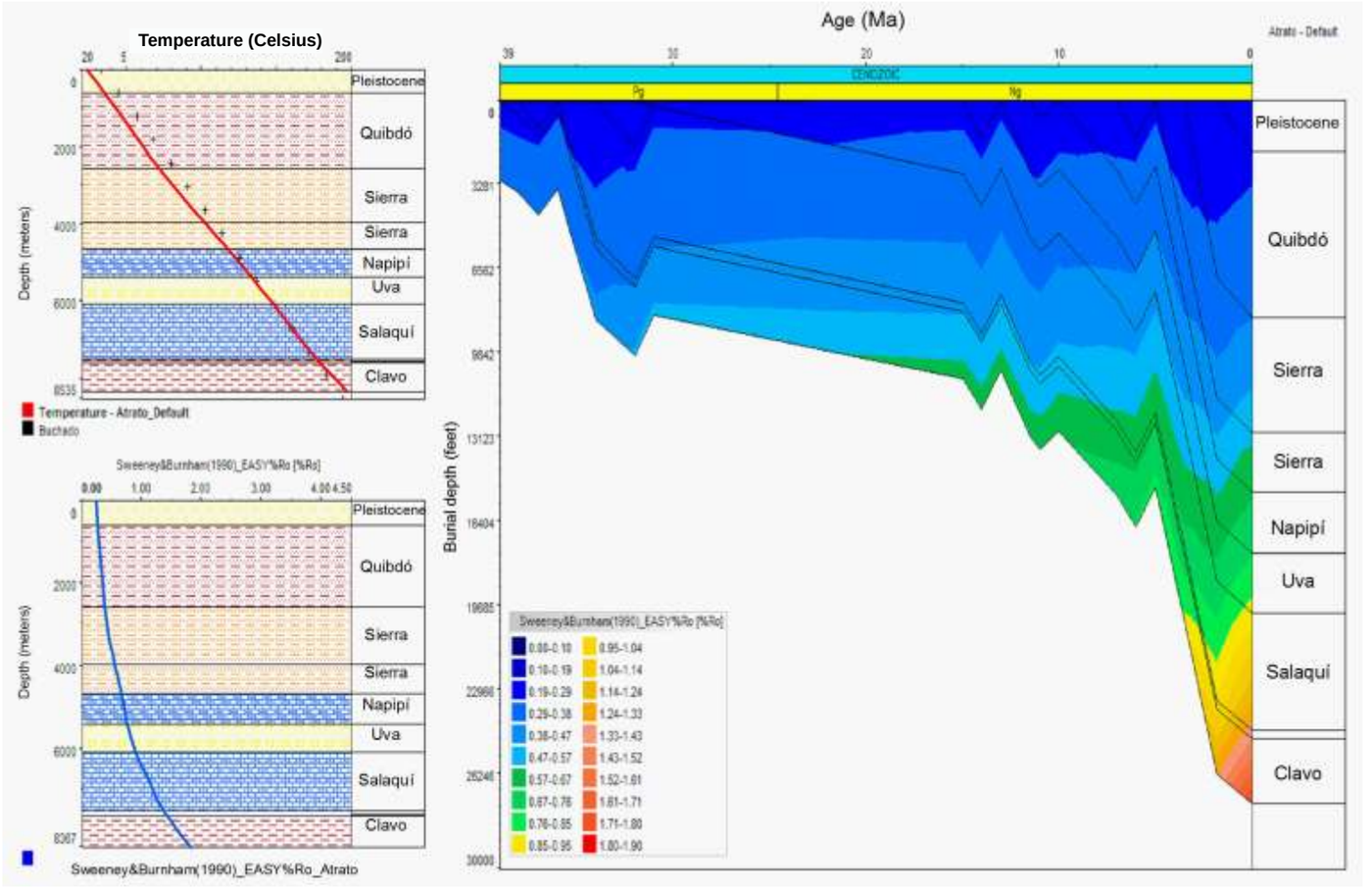

Figure 62. Burial history of Atrato Basin vs. thermal maturity

Modeling results indicate that the Clavo Formation's generating interval attained 100% transformation. Hydrocarbon expulsion time for the Clavo generating interval initiated in the Lower Miocene (about 20 Ma), with important expulsion peaks between the Miocene and the Upper Pliocene (8-3 Ma), contemporary with Sierra Formation sedimentation *(Fig. 63)*.

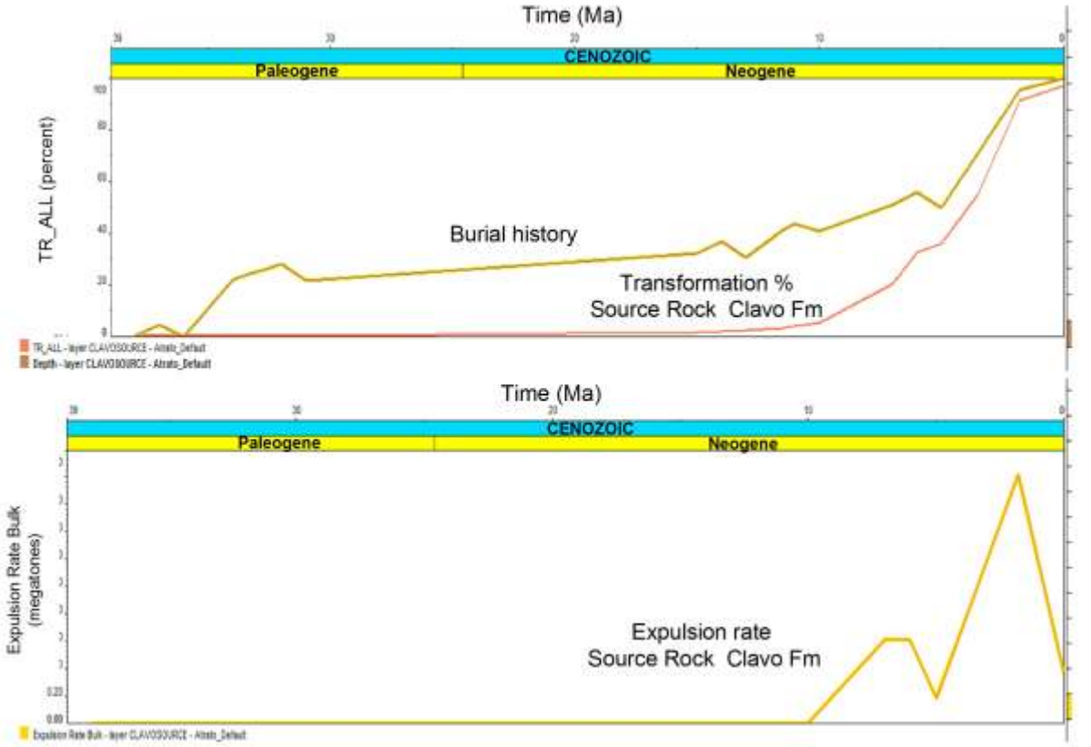

Figure 63. Transformation percentage and main generation peaks.

6.4. San Juan Basin

6.4.1. Geochemical Characterization

Source rock characterization was undertaken based upon 57 out crop samples collected south of the Municipality of Tadó, within stratigraphic sections exposed along the Aguas Claras, La Cuelga, Profundó, and San Bernabe creeks, as well as along the Mongarrá River (Mera and Piragua, 2000; Fig. 64).

Of the 57 samples collected to define the generating potential and maturity of the sequence, 21 samples were from the upper Iró Formation, 16 from the middle Iró Formation and 20 from the lower Iró Formation. Samples also underwent pyrolysis and total organic carbon (TOC) analysis.

6.4.1.1. Parameters

Source rock assessment and characterization were made through analysis of quantity, quality, and maturity parameters with respect to contained organic matter *(see Tables 8, 9, and 10.)*

	Organic Matter		
Petroleum Potential	TOC (wt.%)	Rock – Eval S^{1a}	Pyrolisis S^{2b}
Poor	0 – 0.5	0 – 0.5	0 – 2.5
Fair	0.5 – 1	0.5 – 1	2.5 – 5
Good	1 – 2	1 – 2	5 – 10
Very Good	2 – 4	2 – 4	10 – 20
Excellent	> 4	> 4	> 20

Table 8. Geochemical parameters describing oil-producing potential (quantity) of immature rock.

Kerogen Type	HI (mg HC/g) TOC	S2 / S3
I	> 600	> 15
II	300 – 600	10 – 15
II/III[b]	200 – 300	5 – 10
III	50 – 200	1 -5
IV	< 50	< 1

Table 9. Geochemical Parameters describing kerogen type (quality).

		Maturation		Generation	
Stage of Thermal Maturity for Oil		Ro (%)	Tmax (°C)	Bitumen / TOC[b]	Pic [S1 / (S1+S2)]
Immature		0.2 – 0.6	< 435	1.5 – 2.6	< 0.10
Mature	Early	0.6 – 0.65	435 - 445	0.05 – 0.10	0.10 – 0.15
	Peak	0.65 -0.9	445 – 450	0.15 – 0.25	0.25 – 0.40
	Late	0.9 – 1.35	450 – 470	-	> 0.40
Postmature		> 1.35	> 470	-	-

Table 10. Geochemical parameters describing thermal maturity level.

6.4.2. Thermal Maturity

Maturity level for the whole section (upper, middle, and lower Iró) shows an average Tmax of 435º C, characterizing it as immature but very close to entering the oil-generating window *(Fig. 64)*.

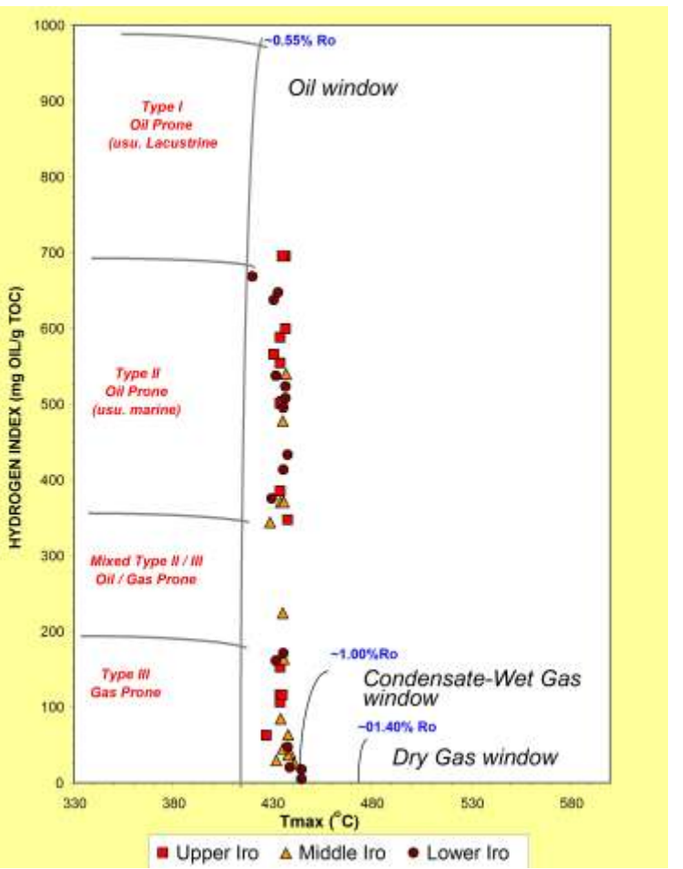

Figure 64. Tmax vs. Hydrogen Index Diagram.

6.4.3. Organic Content

The upper Iró shows TOC values between 0.12% and 23.95%, with a 7.55% average, placing it in an excellent range. The Middle-Medium Iró shows a 2.12% average TOC, which places it in a good range.The lower Iró shows 4.77% average, also placing it in an excellent range. It must be highlighted here that, in terms of organic matter content, at least four intervals are identified with excellent generating potential *(Fig. 65).*

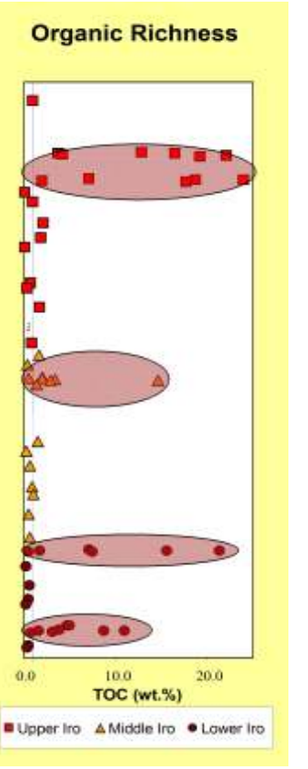

Figure 65. Organic content geochemical profile

6.4.4. Kerogen Type

Hydrogen Index (HI) average content for the Upper Iró is 405 mg HC/gr COT, showing type II kerogen predominance; HI average content for Middle Iró is 201 mg HC/gr COT, showing type III kerogen predominance, and HI average content for Lower Iró is 332,33 mg HC/gr COT, showing type II kerogen predominance. *(Fig. 66)*

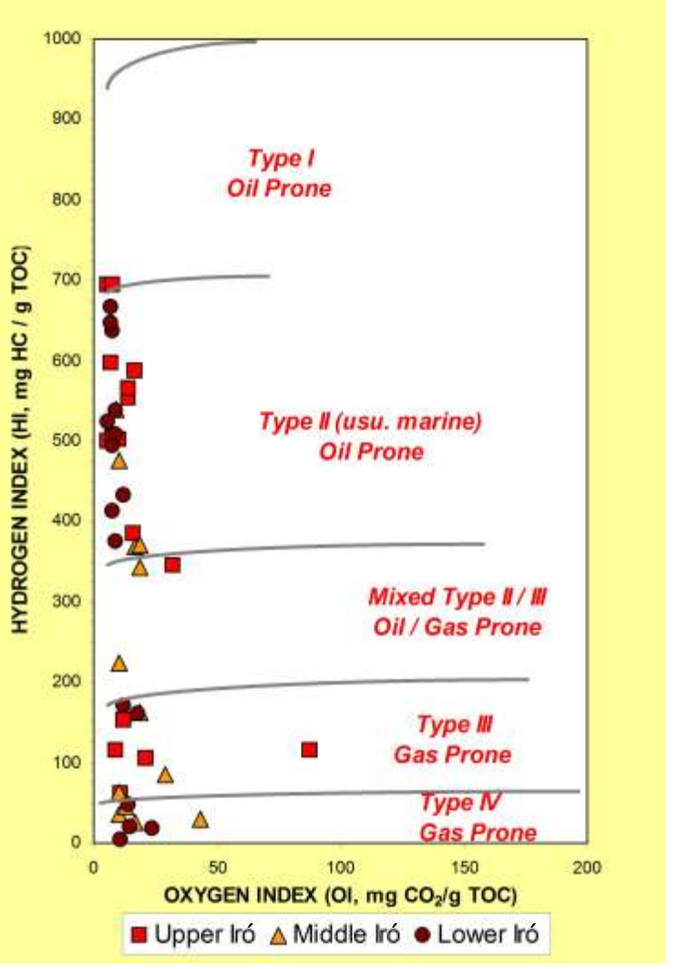

Figure 66. Van Krevelen Diagram

6.4.5. Generating Potential

The Upper Iró shows 38.99 mg Hc/ rock gr average oil-producing potential (S1+S2), which is considered excellent; the Middle Iró shows 9.35 mg Hc/ rock gr oil-producing potential, a good potential; the Lower Iró records 23.36 mg Hc/ rock gr, also an excellent potential. In general, by relating the genetic potential (S1+S2) to percentage of organic content, the Iró Formation samples (upper, middle, lower) show generating potential ranging from favorable to excellent *(Fig. 67)*.

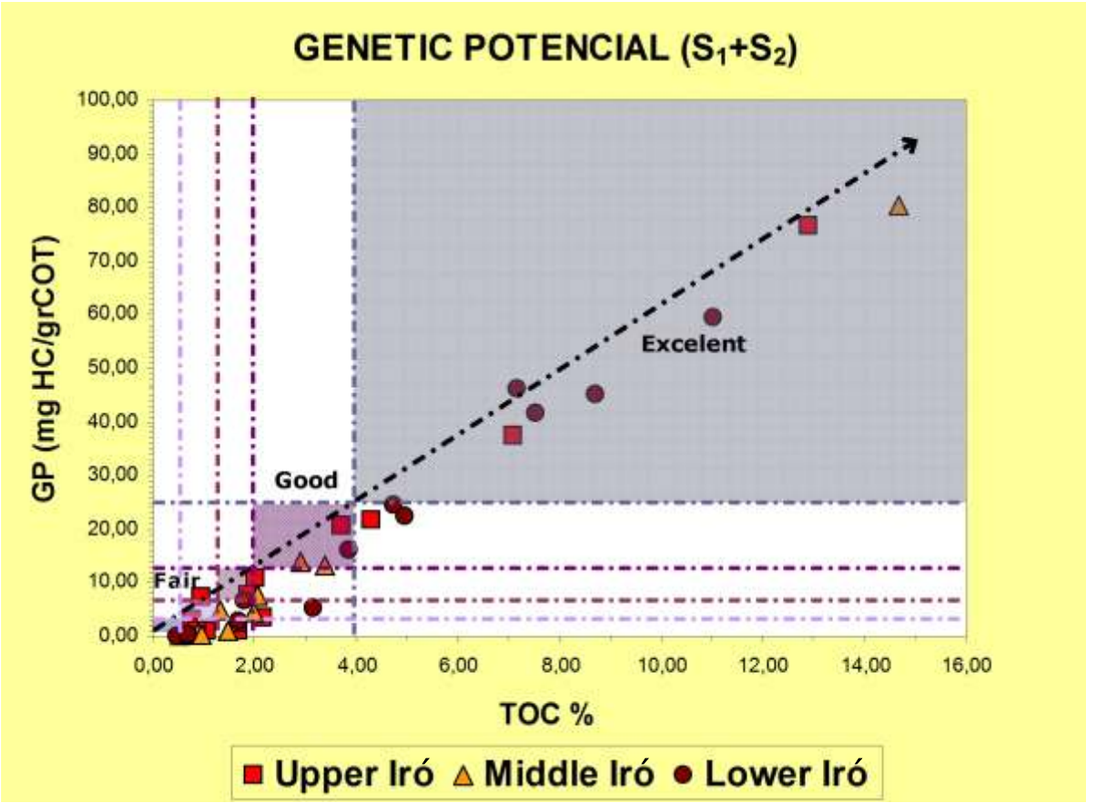

Figure 67. Genetic potential (S1+S2) vs. % TOC

6.4.6. Oil Rock Correlation

Seven rock extracts derived from out crop samples, including two from the Upper Iró, two from Middle Iró, and three from the Lower Iró, were analyzed by means of liquid and gas chromatography, fitted with a mass spectrometer (GC-MS). This work was intended to characterize bitumen and to correlate the results with analysis from four oil seeps found in the region (biomarker analysis). Oil seeps and out crop samples are located to the south of the Municipality of Tadó *(Fig. 68)*.

Crude oil - rock correlation was achieved through the application of biomarker analysis. Some features of the organic molecules used in biomarker analysis are outlined below are:

- They comprise complex organic compounds, made up of C and H and other elements.
- They are found in crude oil, bitumen and rock.
- They show no structural change in comparison to that which living organisms had.
- They include compounds of the pristine-, phitane-, sterane-, triterpane- and porfirine-types.
- They are analyzed using gas chromatography coupled with mass spectrometry.

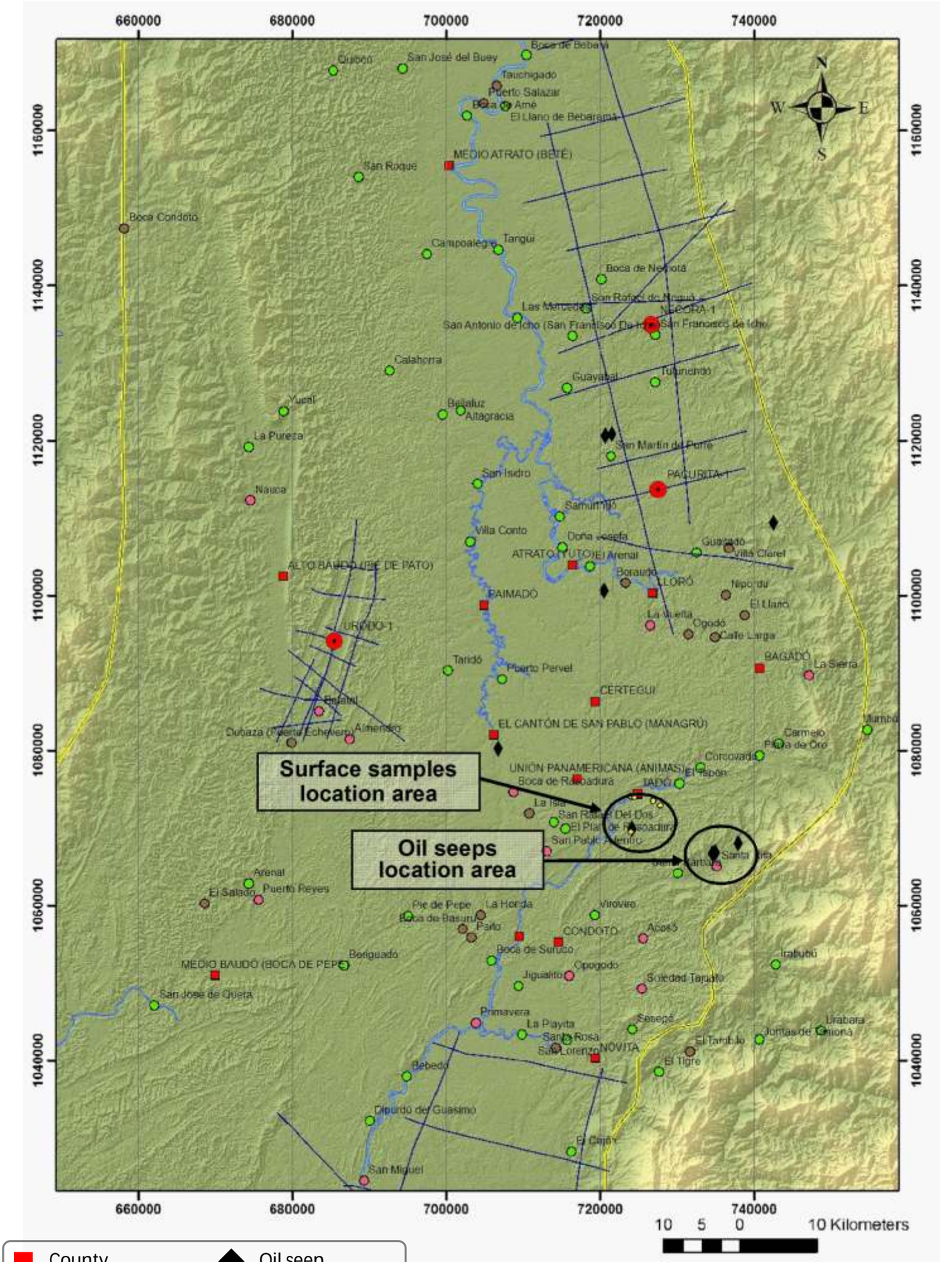

Figure 68. Location of oil seeps and rock samples

6.4.6.1. Biodegradation in Oil Seeps

Oil from seeps was subjected to liquid chromatography in order to quantify saturates, aromatics, and NSO compound contents, which partially reveal the nature of the organic matter in the source rock, including the degree of maturity and the intensity of the post-expulsion alteration processes *(Fig. 69)*.

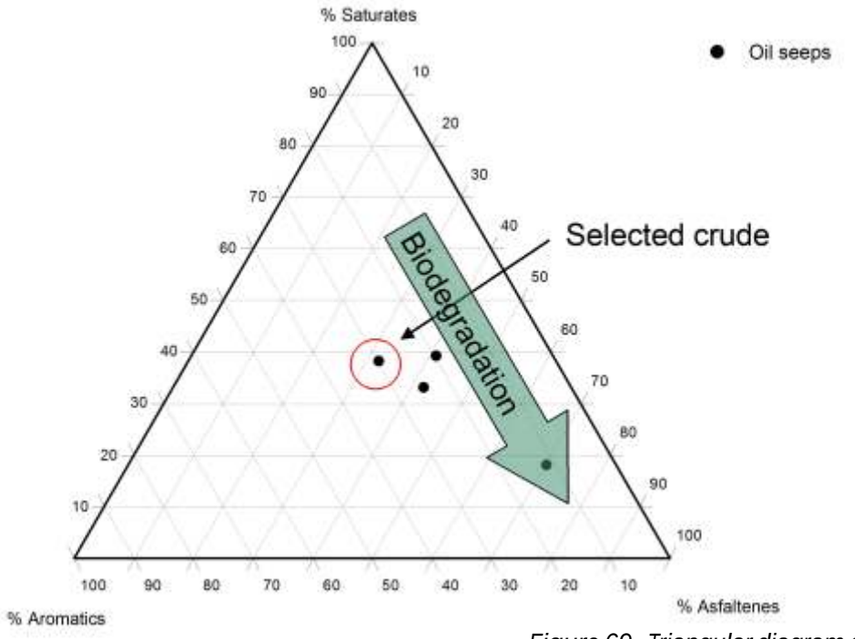

Figure 69. Triangular diagram of crude oil factions

This simple analysis aided in the determination of the least biodegraded crude oil, which in this case corresponds to slightly biodegraded oil found in El Padre creek (ID=QP-I-07). This crude had the lowest value for resins and asphaltane fractions. It's saturates value however was relatively high.

6.4.6.2. Sedimentation Environment

Determining the sedimentary environment of source rocks for the Iró Formation (rock extracts), and the oil seep's source rock, was undertaken on the basis of characteristic biomarkers.

The Disteranes/Steranes ratio increases in siliciclastic or proximal (deltaic) continental marine environments, where the presence of clay increases the steranes content. The Ts/Tm ratio indicates siliciclastic environments and/or a higher degree of thermal evolution.

In the present case, the oil from the selected seep correlated perfectly to the extracts in the ratios <1 Disteranes/Steranes and Ts/Tm <1, suggesting a carbonate-influenced marine sedimentary environment. *(Fig. 70)*

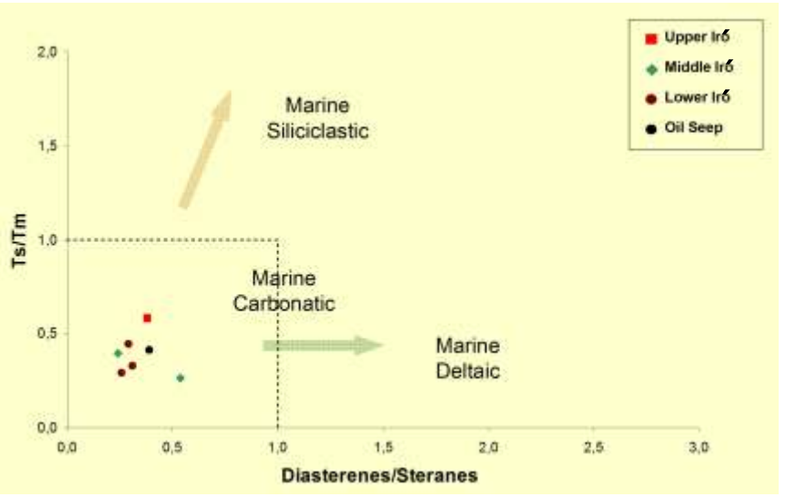

Figure 70. Relations of biomarkers indicating sedimentation environment.

The high level of C29 steranes relates to proximal marine environments, with a large contribution from superior plants, whereas the abundance of C27 steranes are associated with marine environments with a larger contribution from plankton.

Again, studied oil seep and rock extracts show excellent correlation with respect to biomarker ratios, indicating that source rocks were not deposited in proximal environments, but in platform environments, with a regular contribution from plankton *(Fig. 71)*.

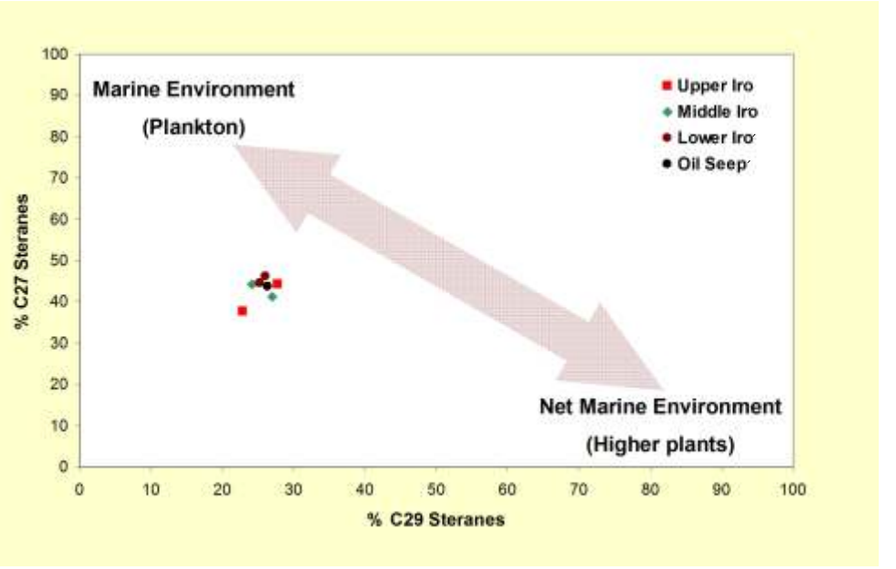

Figure 71. Relations of biomarkers indicating sedimentation environment

6.4.6.3. Oxic vs. Anoxic Conditions

Although high C35/C34 hopane ratios (>1) are characteristic of anoxic hipersaline environments, in the present case the relation of oil seep to rock extracts reveals a <1 ratio, despite good correlation, suggesting that the sedimentary environment was not totally anoxic *(Fig. 72)*

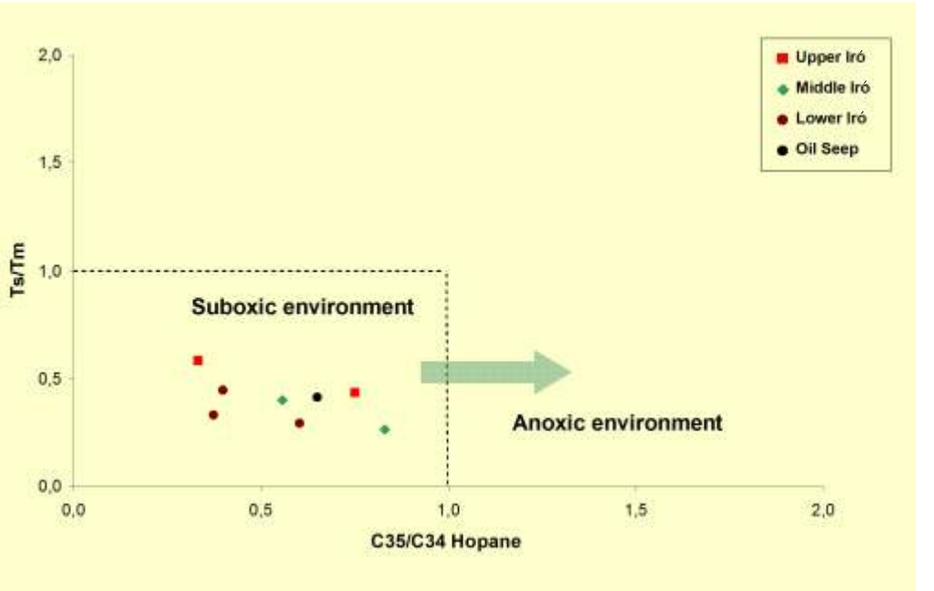

Figure 72. Ratios of anoxia-indicating biomarkers.

High Gamacerane/C30 Hopanes ratios are another major indicator of highly anoxic and salinity conditions in the sedimentary environment. By graphing the C35/C34 hopane ratios, we obtain an excellent tool to determine anoxic conditions.

In the present case, seep samples and outcrop rock extracts fall in an intermediate zone, indicating suboxic sedimentary environments (*Fig. 73)*

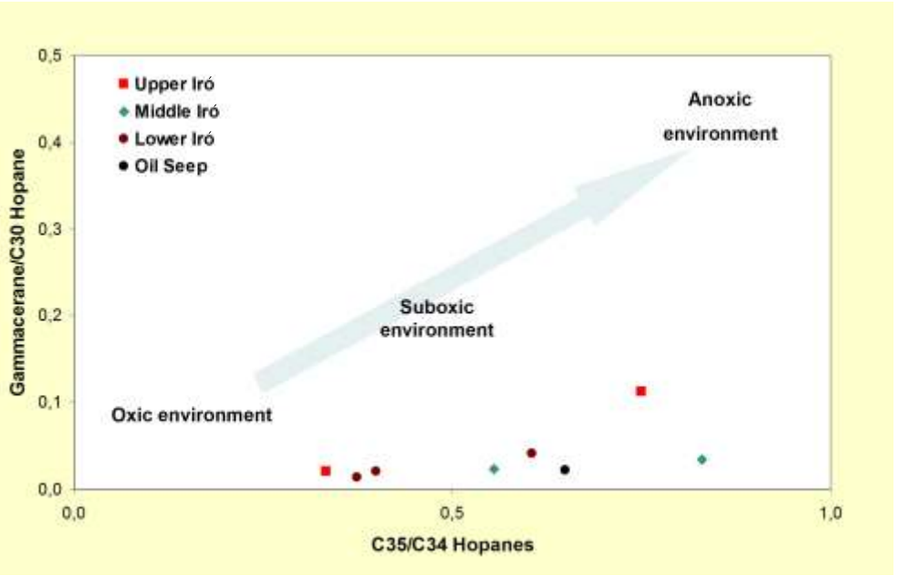

Figure 73. Ratios of anoxia-indicating biomarkers

6.4.7. Hydrocarbon Generation and Expulsion Simulation

Hydrocarbon generation and expulsion processes for the Iró Formation were modeled using PetroMod 1D software. In order to simulate a location (San Juan Pseudo-well) where rocks had reached sufficient depths, a point was selected on a deeper interpreted seismic line, adjusted to the basement map built for this project (*Fig. 74*).

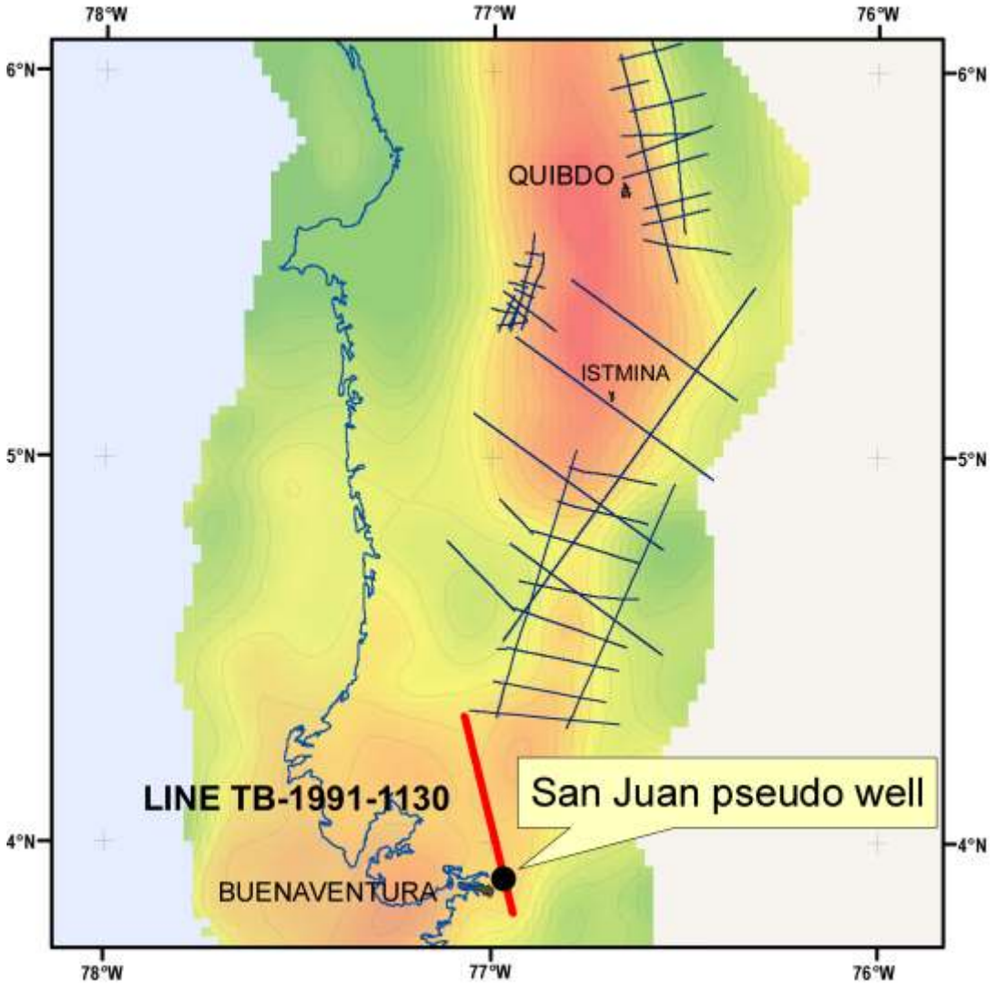

Figure 74. Location of San Juan Pseudowell

The seismic line chosen for location of the pseudo-well, and interpretation of each stratigraphic unit's limits was TB-91-1130 *(Fig. 75)*

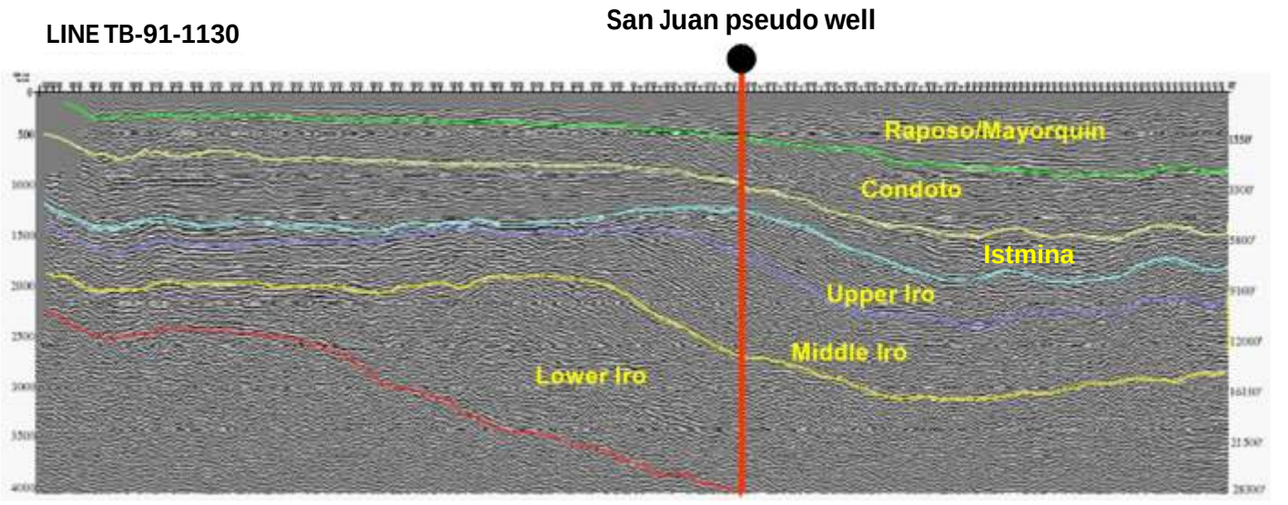

Figure 75. Interpreted seismic line TB-91-1130

6.4.7.1 Thermal Model.

The lack of maturity data makes it difficult to interpret the basin's thermal history. In the present study, a conservative scenario using a constant heat flow history characteristic of Cenozoic basins was applied. Current heat flow was interpreted based upon the zone's BHT data *(Fig.76)*.

Figure 76. Heat flow history

BHT data used to generate the current geothermal gradient and calibrate the model corresponded to the Urodó-1 well *(Fig. 77)*.

URODÓ-1
Gradient: 1.0067 °F/100 ft

Depth feet	BHT (°F)	T corr (°F)
0	86	94.6
14100	223	245.3
14700	225	247.5
15000	235	258.5

Depth.feet	T corr (°F)	Depth. Meters	T corr (°C)
0	94.34	0.00	34.63
2000	115.73	609.61	46.52
4000	137.13	1219.21	58.41
6000	158.52	1828.82	70.29
8000	179.92	2438.43	82.18
10000	201.31	3048.04	94.06
12000	222.71	3657.64	105.95
14000	244.10	4267.25	117.83
16000	265.50	4876.86	129.72

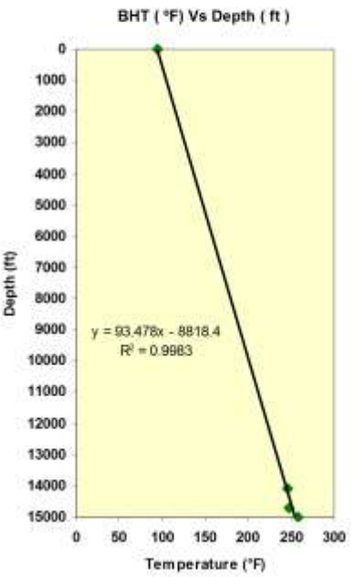

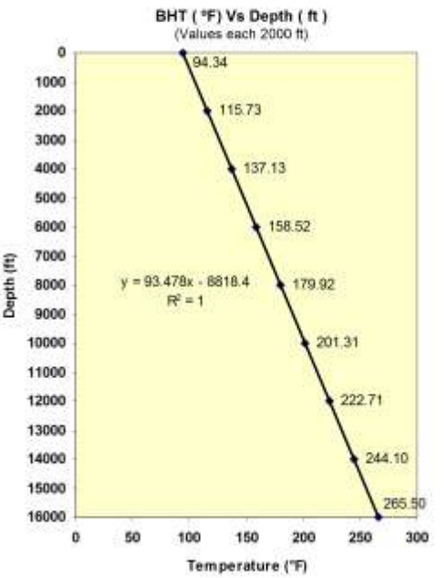

Figure 77. BHT data and thermal gradient calculation.

This model provides graphs of expected temperature levels; A) in the sequence using the current calculated thermal gradient, B) thermal maturity behavior curve in the sequence, C) generating interval, D) paleotemperatures and, E) maturity behavior over time *(Fig. 78)*.

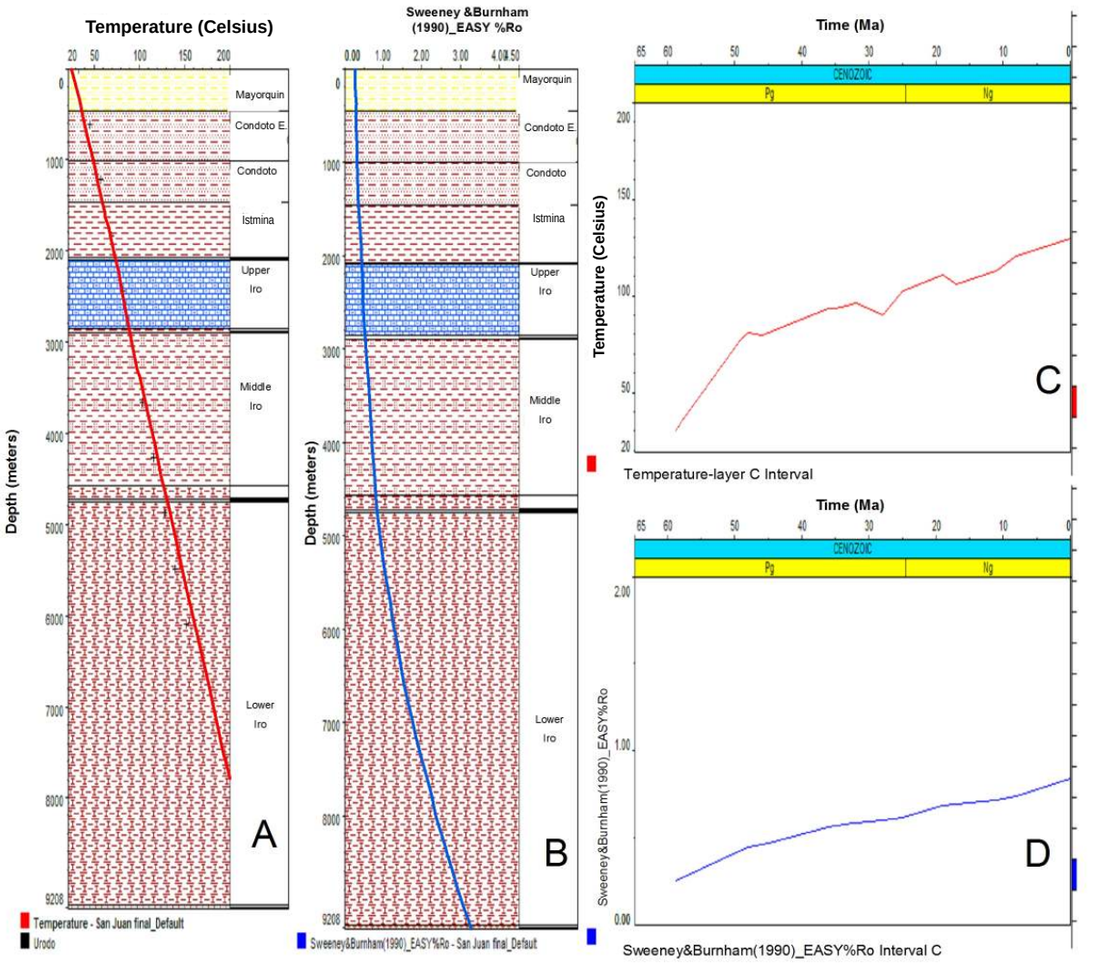

Figure 78. Calibration, temperature and maturity along time curves.

6.4.7.2 Geochemical Model

Given geochemical data indicating that the Iró Formation's generating intervals show excellent generating potential, and additionally correlate well with the oil seep samples, we conclude that these geochemical characteristics provide valid input data for the proposed model *(Fig. 79)*.

1	13	14	15
	TOC	Kinetics	HI
Name			
	[wt%]		[mg HC/g TOC]
Sediment Surface			
Mayorquin	0.00	none	0.00
Condoto Eroded	0.00	none	0.00
Condoto	0.00	none	0.00
Istmina Eroded	0.00	none	0.00
Istmina	0.00	none	0.00
Int A Eroded	0.00	none	0.00
Int A	13.00	Behar_et_al(1997)_T2-S(MontSh)-CS	550.00
Iró Upper	0.00	none	0.00
Int B	4.80	Behar_et_al(1997)_T2-S(MontSh)-CS	420.00
Iró Medio Eroded	0.00	none	0.00
Iró Medio	0.00	none	0.00
Iró Lower A	0.00	none	0.00
Intervalo C	5.50	Behar_et_al(1997)_T2-S(MontSh)-CS	450.00
Iró Lower B	0.00	none	0.00
Basement	0.00	none	0.00

Figure 79. Geochemical model input data

6.4.7.3. Generation and Expulsion Model

Hydrocarbon generation and expulsion processes for the Iró Formation were modeled with PetroMod 1D software. Input data for the sedimentary sequences, lithostratigraphic units, erosion, and sedimentation time data, were taken from the chronostratigraphic column studied for this project. Input data for the thickness of each formation were taken from seismic lines interpreted in this project *(Fig. 80)*.

Input | Boundary Assignment | Output

	1	2	3	4	5	6	7	8	9	10
				Present	Eroded	Deposition Age		Erosion Age		
	Name	Top	Base	Thickness	Thickness	from	to	from	to	Lithology
		[feet]	[feet]	[feet]	[feet]	[Ma]	[Ma]	[Ma]	[Ma]	
1	Mayorquin			0.00						
2	Condoto Eroded	0.00	1500.01	1500.01		8.00	0.00			SAND&SHALE
3	Condoto	1500.01	1500.01	0.00	1800.01	11.00	8.00			SHALE&SAND
4	Istmina Eroded	1500.01	3000.02	1500.01		17.00	11.00			SHALE&SAND
5	Istmina	3000.02	3000.02	0.00	999.99	25.00	19.00	19.00	17.00	SHALE
6	Int A Eroded	3000.02	5000.03	2000.01		28.00	25.00			SHALE
7	Int A	5000.03	5000.03	0.00	849.99	35.00	32.00	32.00	28.00	SHALE
8	Iró Upper	5000.03	5070.04	70.01		36.00	35.00			SHALE
9	Int B	5070.04	7570.04	2500.00		45.00	36.00			LIMEsandy
10	Iró Medio Eroded	7570.04	7690.05	120.01		46.00	45.00			SHALE
11	Iró Medio	7690.05	7690.05	0.00	400.00	49.00	48.00	48.00	46.00	SHALEsand
12	Iró Lower A	7690.05	13190.05	5500.00		58.00	49.00			SHALEsand
13	Intervalo C	13190.05	13690.04	499.99		59.00	58.00			SHALEcalc
14	Iró Lower B	13690.04	13810.05	120.01		59.50	59.00			SHALE
15	Basement	13810.05	28310.04	14499.99		65.00	59.50			SHALEcalc
16	Basamento	28310.04	28410.04	100.00		66.00	65.00			BASEMENT
17		28410.04								

Figure 80. Geologic model input data

According to the model, temperature curve and calibration points match well, as do the expected thermal maturity data at the base of lower Iró Formation, which would stand at Ro = 3.5%, as indicated in the burial history graph *(Fig. 81)*.

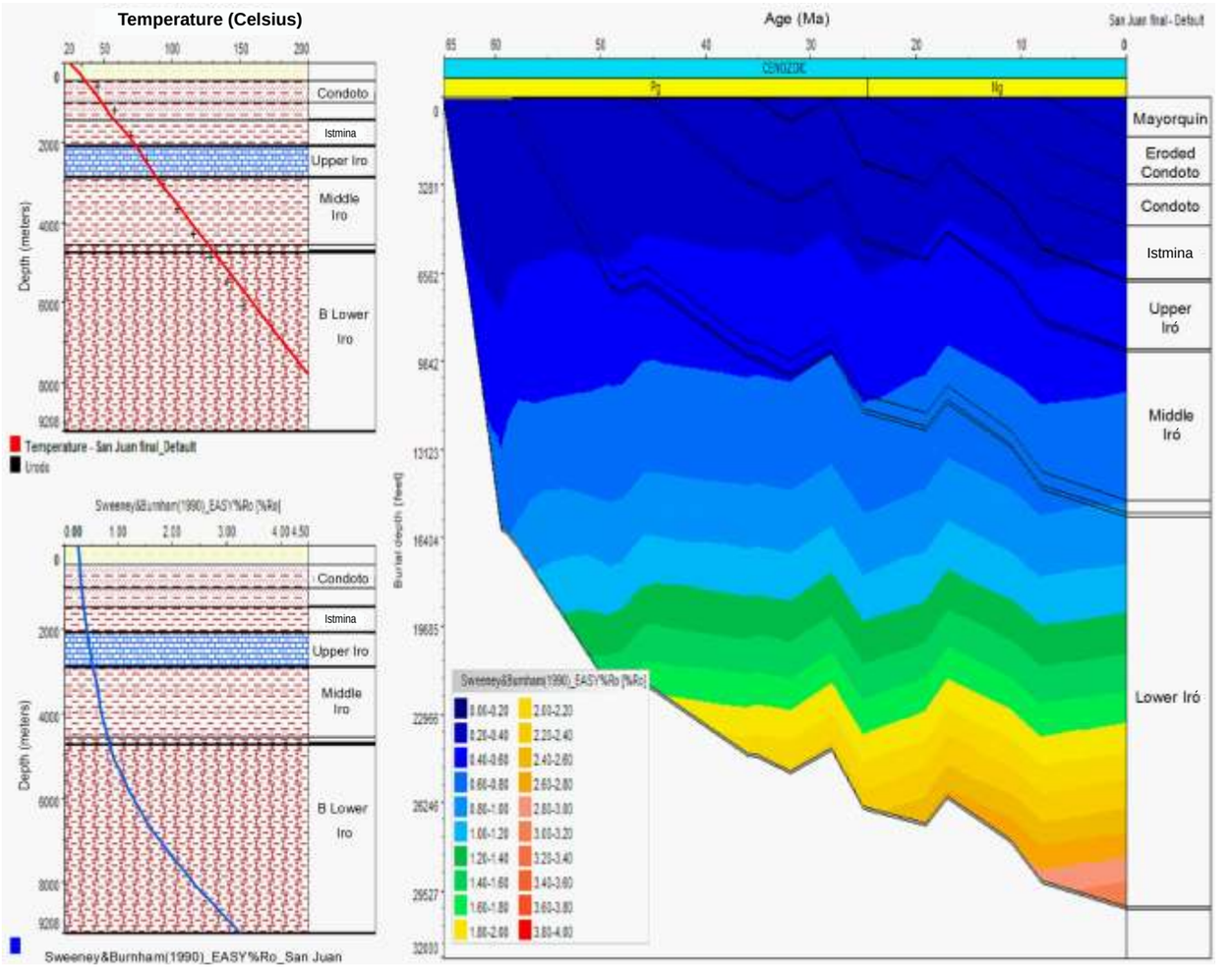

Figure 81. Burial history vs. thermal maturity

Modeling results show that the generating interval C located within the Iró Formation, reached approximately 80% transformation, whereas interval B reached about 5% transformation, and interval A generated no hydrocarbon. Hydrocarbon expulsion time for interval C starts in the Lower Eocene (~43 Ma) with an important expulsion peak in the Lower Miocene (~20 Ma) contemporary with Istmina Formation sedimentation *(Fig. 82).*

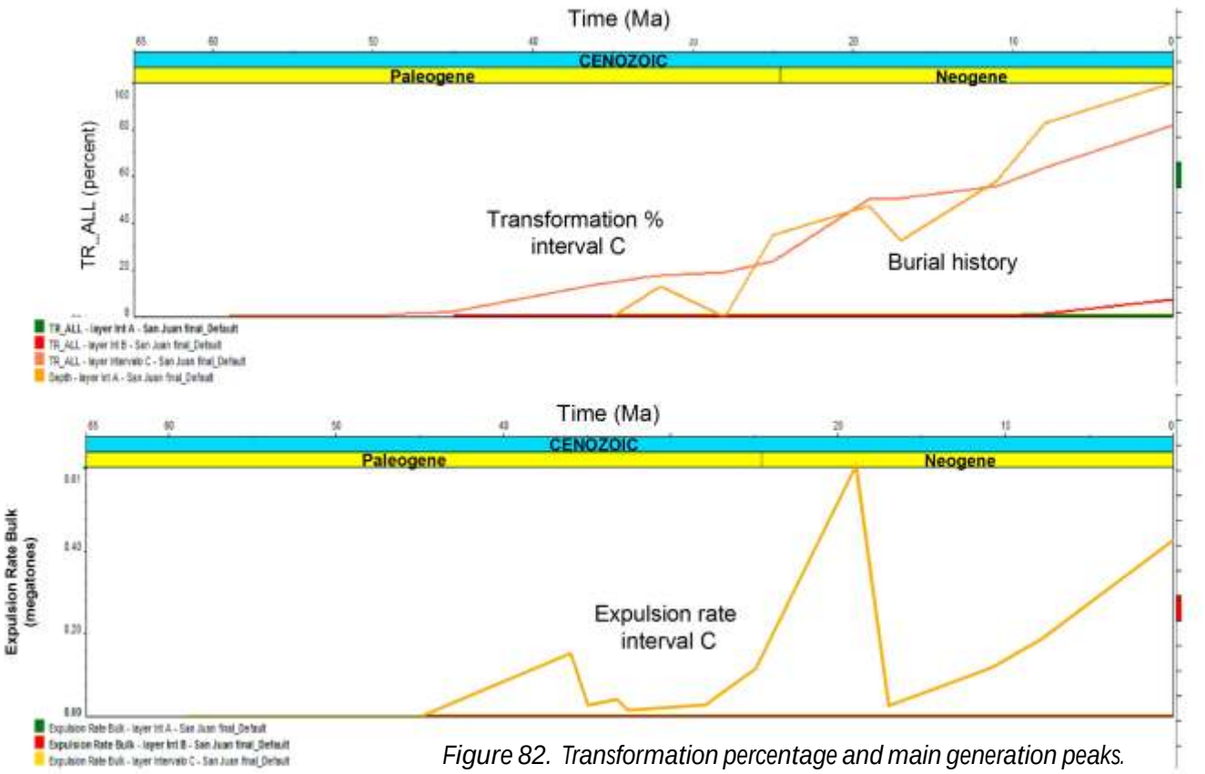

Figure 82. Transformation percentage and main generation peaks.

6.5. Conclusions

6.5.1 Atrato Basin

- Oil and gas samples reported from Buchadó-1 well, and the presence of oil seeps, provide evidence of hydrocarbon generation in the basin, which must ultimately correspond to some sedimentary facies (source interval), with good hydrocarbon generation characteristics. This interval remains to be pinpointed and geochemically characterized.
- According to the hypothetical expulsion and generation model proposed, any interval with good generation characteristics located below 11,000 feet would have expulsed hydrocarbon.
- The Clavo Formation source interval initiated generation in the Middle Eocene and attained 100% transformation.
- The main generation peaks for this source interval would be concentrated between the Upper Miocene and Pliocene.

6.5.2. San Juan Basin

- The geochemical characteristics determined in this study indicate that some of the Iró Formation intervals show very high organic content and excellent generating potential. In comparison, Iró Formation organic contents and generating potential are higher than those of the source formations of the Middle Magdalena and Upper Magdalena Basins.
- The extracts and less biodegraded crude from the oil seeps show good geochemical parameter correlation, suggesting that more mature facies of the Iró formation might be genetically related to hydrocarbon showings.

- Interpretation of biomarkers suggests that Iró Formation-facies sedimentation took place in a carbonate-influenced suboxic marine platform environment.
- According to the model, source rocks would reach the oil generation window at approximately 12,000 feet
- Interval C, at the top of lower Iró Formation, is the only interval to expulse hydrocarbon. Largest volumes appear in the upper Eocene, Lower Miocene, and Pliocene.
- Any source interval located beneath Interval C of the lower Iró Formation would have 100% transformation, and expulsion would be earlier.
- Transformation rates for Interval C are approximately 80%

7. PETROLEUM GEOLOGY
(Summary)

7. PETROLEUM GEOLOGY (Summary)

7.1. General Statement

The available seismic information permits visualization and definition of stratigraphic and structural characteristics as a whole, which in turn enables the inference of structural and stratigraphic traps suitable for hydrocarbon accumulation.

Major structures found in both the Atrato and San Juan Basins merit the undertaking of formal exploration campaigns.

The strategic location of the Atrato and San Juan Basins along the Pacific margin and their vicinity to the port of Buenaventura are valuable elements with respect to their future potential as productive basins.

In terms of identified traps, several deserve mention:

7.2. Traps

7.2.1. Atrato Basin

- Structural traps associated with anticlines formed during inverse faulting along the western flank of the basin.
- Structural traps associated to mud diapirism on the western flank of the basin.
- Stratigraphic traps within the Salaquí and Uva Formations, especially related to formational pinch-out along the eastern margin of the basin.

7.2.2. San Juan Basin

- Combined structural and stratigraphic traps associated with progradation observed in the southern portion of the basin.
- Stratigraphic traps associated with stacked calcareous lenses, which where exposed exhibit excellent secondary porosity, and thus good potential to host hydrocarbons.
- Anticlines associated with reverse faulting along the margins of the basin.

7.3. Source Rock

The presence of hydrocarbon source rocks in the San Juan and Atrato basins is inferred on the basis of the geochemical characterization of the Iró Formation, specifically in the Istmina-Condoto highland sector. According to the data, this unit presents immature intervals with good to excellent generation potential. These intervals present high organic matter contents and the predominance of Type II kerogen, with very high hydrogen contents. If the organic facies present in these units still exist at deeper basinal levels, such source rock characteristics would be highly attractive with respect to hydrocarbon exploration. Furthermore, it is possible that additional generative intervals can be found in poorly studied units such as the Salaquí Formation.

7.4. Generation and Migration

On the basis of the results obtained in the hydrocarbon generation modeling (1D), it may be inferred that the lower part of the Iró Formation in the San Juan basin, and its chronostratigraphic equivalent the Clavo Formation in the Atrato basin, were affected by important hydrocarbon generation and expulsion processes during the late Miocene to Miocene. The volumes of hydrocarbons which could potentially be expulsed by these units would generate good potential in terms of resources to be discovered.

7.5. Timing

The presence of pre-late Miocene tectonic events and the possibility of the formation of stratigraphic traps in the San Juan and Atrato basins generate a low risk synchronism scenario for possible trapping in pre-late Miocene units. (see figure 83 and 84)

7.6. Potential resources to be discovered

On the basis of geological and geochemical modeling, mass balance calculations were completed for both basins. According to the results, resource expectations on the order of 600 MBPE (P50) for the San Juan basin and of 850 MBPE (P50) for the Atrato basin are observed.

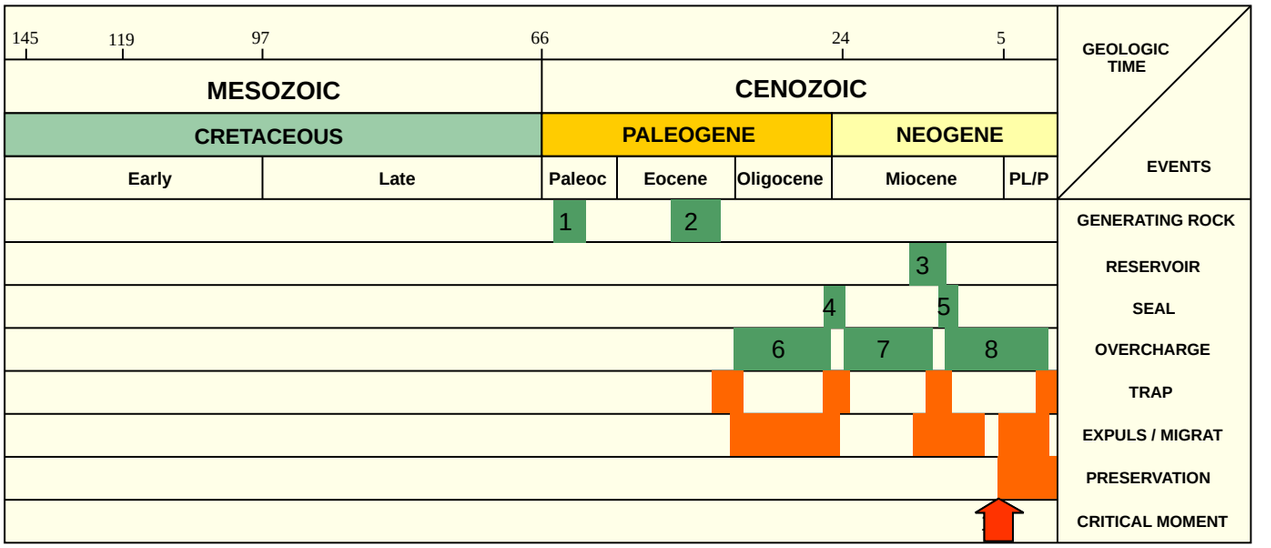

1, 2: Iró Formation
3: Condoto Formation
4, 5: Istmina Fm. , Upper Condoto Fm.
6, 7, 8: Sierra, Istmina, La Mojarra, Condoto, Munguidó, Atrato Fms.

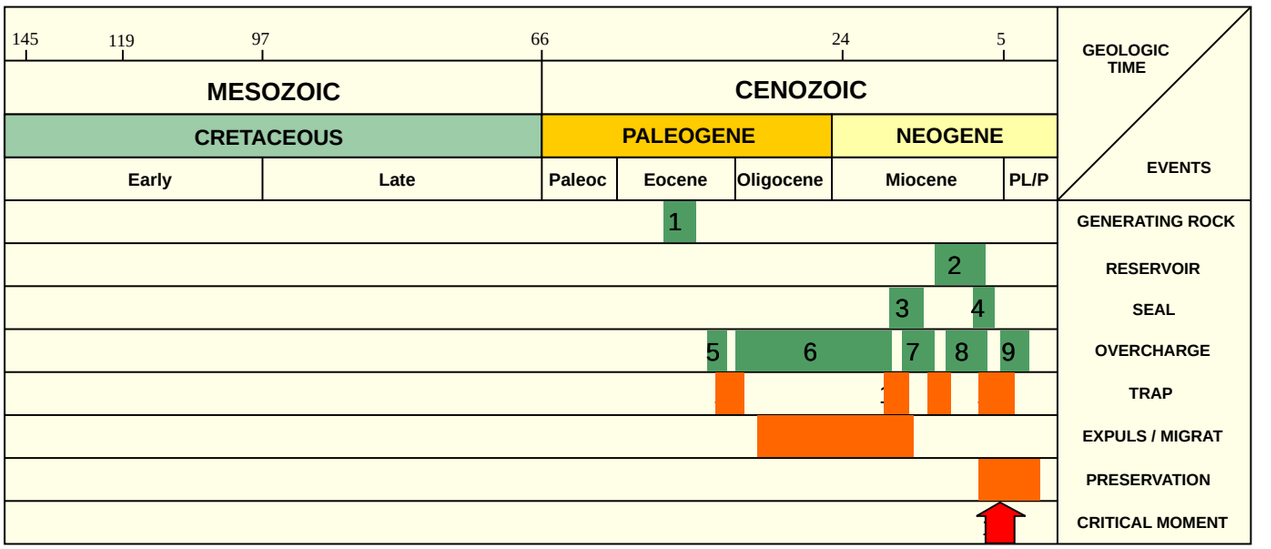

1: Clavo Formation
2: Sierra Formation
3, 4: Napipí Fm., Upper Sierra Fm.
5, 6, 7, 8, 9: Clavo, Salaquí, Uva, Napípí, Sierra, Quibdó Fms.

Figures 83 and 84. summarize the sequence of events for the San Juan and Atrato basins respectively.

PANAMA
PACIFIC OCEAN
Punta Ardita
Bahía de Humboldt
Punta Cabo Marzo
Punta La Tortuguera
Bahía de Cupica
Punta Nabugá
Bahía Solano
Ensenada de Utría
GOLFO DE TRIBUGÁ
Ensenada Coquí
Punta Arusí
Cabo Corrientes
Playa Nueva
Bahía Baudó
Boca Usuraga
Ensenada Docampadó
Boca Hijuá
Boca Orpúa
Boca Cacagual
Playa El Choncho
Bahía de Buenaventura
BUENAVENTURA
SISTEMA DE FALLAS GARRAPATAS
Qui
Uv
Qall
Siu
Si
Sa
Ma
Pen
Peu
Co
Rp
Br
Is
My
Ci
QTT
BETULIA
CONCORDIA
SALGAR
HISPANIA
BETANIA
MISTRATÓ
PUEBLO RICO
LA CELIA
BALBOA
EL AGUILA
EL CAIRO
ARGELIA
VERSALLES
EL DOVIO
BOLÍVAR
N
0
25
50
km

REFERENCES

Published works

REFERENCES

Published works

- Amaefule J., Altunbay M. et al. Enhanced Reservoir Description: Using Core and Log Data to Identify Hydraulic (Flow) Units and Predict Permeability in Uncored Intervals/Wells. Society of Petroleum Engineers. SPE 26436. October 1993.
- ANH (2007) Barrero. D. , Pardo. A., Vargas C.A., Martínez J.F., 2007 Colombian Sedimentary Basins: Nomenclature, Boundaries and Petroleum Geology. A New Proposal. ANH
- Aspden, J.A., McCourt, W. J. and Brook, M., 1987. Geometrical control of subduction-related magmatism: the Mesozoic and Cenozoic plutonic history of Western Colombia. Journal of the Geological Society, London. 144, 893-905.
- Arias, O., Camacho, J., Erazo, A., Gabela, V., Jones, D., Manderson, N., Rodríguez, D., Vargas, J. Compañía Petrolera Latina Inc., 1988. Chocó Pacific basin evaluation western Colombia. Bogotá. 38 p.
- Barlow, C. A., 1981. Radar geology and tectonic implications of the Chocó Basin, Colombia, South America: Arkansas University, M.Sc. thesis. p. 102.
- Berggren, W. A., D.V. Kent, C.C. Swisher, and M. Aubry., 1995. A revised Cenozoic geochronology and chronostratigraphy, pp. 129-212, IN Berggren, W. A., D.V. Kent, C.C., Swisher, M. Aubry, and J. Hardenbol (eds), Geochronology, Time Scales and Global Stratigraphic Correlation. SEPM Special Publication No. 54.
- Billich, A. Frohlich, C. and Mann, P. 2001. Global seismicity characteristics of subduction to strike slip transitions. In: Journal of Geophysical Research, 106:B9. pp 19443-19452.
- Bilotti, F., Shaw, J., Brennan, P., 2000. Quantitative structural analysis with stereoscopic remote sensing imagery. AAPG Bulletin. 84(6): 727-740.
- Bolli, H.M., Saunders, J.B., and Perch Nielsen, K. (Eds.), 1985. Plankton stratigraphy: Cambridge (Cambridge Univ. Press). p. 1032.
- Bolli, H., M., Beckmann, J., P., and Saunders, J. B., 1994. Benthic foraminiferal biostratigraphy of the south Caribbean region. NY: Cambridge University press. p. 408.
- Bond, C.E., et al., What do you think this is?"Conceptual uncertainty" in geoscience Interpretation. GSA Today: v. 17, no. 11.
- Bouman, Q.C., 1965. Geological reconnaissance in the central Chocó. Bogota. 26 p.
- Buzar Consultores Limitada. Empresa Colombiana de Petróleos ECOPETROL, 1993. Mapas de "plays" exploratorios Cuencas del Patia, Valle del Cauca y Chocó Pacífico. Bogota. 24 p.
- Bhaskara R. D. y Rameshu B. N., 1991, A Fortran-77 Program for Three-Dimensional Analysis of Gravity Anomalies with Variable Density Contrast, Computers and Geosciences 17, 655-667
- Carmen Island, Gulf of California: implications for oblique-rifting tectonics. Sedimentary Geology 144(2001):97-123.
- Carson Helicopters. 2006, Programa Adquisición, procesamiento e interpretación de datos aeromagnetogravimétricos en el litoral pacífico de Colombia, informe técnico de la ANH.
- Cediel, F., F. Etayo, and C. Cáceres, 1994, Facies Distribution and Tectonic Setting through the Phanerozoic of Colombia: INGEOMINAS, ed., Geotec Ltd., Bogota (17time-slices/maps in scale 1:2,000.000).
- Cediel, F., D. Barrero, and C. Cáceres, 1998, Seismic Atlas of Colombia: Seismic expression of structural styles in the basins of Colombia: Robertson Research International, UK, ed., Geotec Ltd., Bogota, v. 1 to 6.
- Cediel, F., and C. Cáceres, 2000, Geological Map of Colombia, Third Edition: Geotec Ltd., Bogotá´, digital format with legend and tectonostratigraphic chart.
- Cediel, F., Shaw R.P., and C. Cáceres, 2003, Tectonic assembly of the Northern Andean Block, in C. Bartolini, R. T. Buffer, and J, Blickwede, eds., The Circum-Gulf of Mexico and the Caribbean: Hydrocarbon habitats, basin formation, and plate tectonics: AAPG Memoir 79, p.815-848.
- Continental de Colombia & Oil Gulf Company. 1974. Opogadó-1 Well. Summary Information. p. 1.
- Coates, A. G., Laurel S. Collins, Marie-Pierre Aubry, William A. Berggren, 2004. The Geology of the Darien, Panama, and the late Miocene-Pliocene collision of the Panama arc with northwestern South America. GSA. Bulletin.
- Core Laboratories. Applications of Core Data in Integrated Reservoir Description and Exploitation. 1990.
- Core Laboratorios. Petrobras, 2001. Petrobras Internacional subcuencas San Juan Pacífico surface sample. Bogota. 16 p.
- Correa Iván D. y Restrepo, Juan D. (eds.) 1992. Geología y Oceanografía del delta del Río San Juan, Litoral Pacífico colombiano. COLCIENCIAS UNIV: EAFIT. Fondo Editorial Universidad EAFIT, Medellín. 221 p.
- Cossio, U., 2003. Geología de las planchas 202 Pilizá, 203 Istmina, 221 Pizarro y 222 Sipí. Departamento del Chocó. Escala 1:100000. Memoria explicativa. Ingeominas Bogotá. p. 71. y anexos.
- Dorsey, R., Umhoefer, P., Ingle, C., Mayer, L., 2001. Late Miocene to Pliocene stratigraphic evolution of northeast Carmen Island, Gulf of California: implications for oblique-rifting tectonics. Sedimentary Geology 144(2001):97-123.
- Dunia Consultores, 2006. Informe de integración e interpretación de la información geológica de campo. Contrato 078 2005 Dunia-Agencia Nacional de Hidrocarburos-ANH. Bogotá. 101 p.
- Dunia Consultores, 2006. Informe de integración e interpretación de la información geológica de campo. Contrato 078 2005 Dunia-Agencia Nacional de Hidrocarburos-ANH. Anexos 9, 10 y 11. Bogotá. 101 p.

REFERENCES

Published works

- Duque-Caro, H., 1989. El Arco de Dabeiba: Nuevas aportaciones al conocimiento del Noroccidente de la Cordillera Occidental. Memorias del V Congreso Colombiano de Geología, tomo 1:108-126, Bucaramanga.
- Duque-Caro, H., 1989. Neogene stratigraphy, paleoceanography and paleobiogeography in Northwest South America and the evolution of the Panamá Seaway.
- Duque-Caro, H. 1990. The Chocó Block in the northwestern corner of South America: Structural tectonostratigraphy and paleogeographycal implications. Journal of South American Earth Sciences. 3 (19): 71-84
- Duque-Caro, H., 1991. Contributions to the geology of the Pacific and Caribbean coastal areas of northwestern Colombia and South America: Princeton University, PhD. thesis. p. 132.
- Earth Satellite Corporation, 1999. Geology of the pacific coast of Colombia.
- Empresa Colombiana de Petróleos, ECOPETROL and Asamera Inc., 1982. Final Field Report A Gravity Meter Survey On The Chocó-Río Atrato Prospect. By: GEOPHYSICAL SERVICE INCORPORATED Party 1536A Colombia. 10 p.
- Empresa Colombiana de Petróleos, ECOPETROL and Asamera Inc., 1982. Interpretation of gravity survey Chocó - Río Atrato. TRB Dundas and Associates Límited. 12 p
- Empresa Colombiana de Petróleos, ECOPETROL and Asamera Inc., 1982. Gravimetría área Chocó-Río Atrato Project.
- Empresa Colombiana de Petróleos, ECOPETROL, 1990. Contrato de asociación Istmina. Bogota. 27 p.
- Escobar, J. Empresa Colombiana de Petróleos, ECOPETROL, 1993. Análisis de los play maps y evaluación de riesgo cuencas: Guajira, Los Cayos; San Juan Atrato, Tumaco, Patia y Valle del Cauca. Bogota. 71 p.
- Escobar, J., 2002. Exploration Opportunities San Juan Basin (onshore portion). Trabajo realizado para ECOPETROL y Petrobras. Bogotá. 56 p.
- Escobar, J., 2002. Central Pacific project (offshore-onshore portion). Trabajo realizado para ECOPETROL y Petrobras. Bogota. 21 p.
- Estrada, J.J., 1995. Paleomagnetism and accretion events in the Northern Andes. PhD. thesis. State University of New York. Binghamton. 172 p.
- Fertl Walter H. Log-Derived Evaluation of Shaly Clastic Reservoirs. Society of Petroleum Engineers (SPE) from Journal of Petroleum Technology, v.39, no. 2 (1987), p. 175-194.
- Figueroa, Y., Nuñez, A., 1990. Cartografía geológica de un área en las cabeceras del Río San Juan (Chocó). Trabajo de grado. Universidad Nacional de Colombia, Bogotá. 61 p.
- Fischborn, J., Carrillo, V., 1983. Informe geológico, área de Contrato de Asociación de Asamera Inc. Cuenca Chocó Atrato. Bloque Quibdó. EPIS; Informe No. 997. p. 41
- Fischborn, J., Carrillo, V. Empresa Colombiana de Petróleos, ECOPETROL y Asamera Inc., 1983. Informe geológico Cuenca Atrato-Chocó. 16 p. más anexos.
- Fischborn, J. Empresa Colombiana de Petróleos, ECOPETROL y Asamera Inc., 1982. Chocó Atrato basin. Bogota. 71 p.
- Fischborn, H., Parra, C., Parra, M. Moreno, J. Empresa Colombiana de Petróleos, ECOPETROL y Asamera Inc., 1982. Geologic map Chocó Area, Escala 1:100.000.
- Fischborn, J., Carrillo, V., 1983. Informe geológico, área de contrato de asociación de Asamera Inc. Cuenca Chocó Atrato. Bloque Quibdó. EPIS; Informe No. 997. p. 41
- Galvis, G., 1980. Un arco de islas terciario en el occidente colombiano. Geología Colombiana. 11, 7-43.
- Gansser, A., Poborski, S., Bächlin, R., Swolfs, H., Haanstra, U., 1945. Informes geológicos del área Chocó Pacífico. 75 p.
- García, D., Hernández, C., Niño, C., Escobar, J., Escalante, C. Piedecuesta. Empresa Colombiana de Petróleos ECOPETROL, 2001. Evaluación y modelamiento geoquímico de la Formación Iró Subcuenca San Juan (Chocó). 208 p.
- Geophysical Service Incorporated. Empresa Colombiana de Petróleos, ECOPETROL, 1982. San Juan 1981-1982 prospección sísmica, informe de operación de campo grupo 1536. Bogota. 51 p.
- Geoterrex Ltd. Empresa Colombiana de Petróleos ECOPETROL, 1979. Resolution airborne survey in the Atrato-Sinu Área and Cauca Valley (Colombia). Canadá. 87 p.
- Geosource Exploration Company. Empresa Colombiana de Petróleos ECOPETROL, 1982. Reporte geofísico de procesamiento San Juan-Chocó-Colombia. Bogotá. 17 p.
- Gradstein, F.M., Ogg, J.G., and Smith, A.G., Agterberg, F.P., Bleeker, W., Cooper, R.A., Davydov, V., Gibbard, P., Hinnov, L.A., House, M.R., Lourens, L., Luterbacher, H.P., McArthur, J., Melchin, M.J., Robb, L.J., Shergold, J., Villeneuve, M., Wardlaw, B.R., Ali, J., Brinkhuis, H., Hilgen, F.J., Hooker, J., Howarth, R.J., Knoll, A.H., Laskar, J., Monechi, S., Plumb, K.A., Powell, J., Raffi, I., Röhl, U., Sadler, P., Sanfilippo, A., Schmitz, B., Shackleton, N.J., Shields, G.A., Strauss, H., Van Dam, J., van Kolfschoten, T., Veizer, J., and Wilson, D., 2004. A Geologic Time Scale 2004. Cambridge University Press, 589 pages.
- Graterol V. and Gumert, W., 1998, 3-D gravity inversion with variable datum, The Leading Edge, 1769-1772
- Graterol, V., 2006. Mapa de anomalías de Bouguer (p= 2.30 Grs/cc). Agencia Nacional de Hidrocarburos. Escala 1:1.000.000.
- Graterol, V., 2006. Mapa de Intensidad Magnética. Total reducida al polo (IMTRP). Agencia Nacional de Hidrocarburos. Escala 1:1.000.000.
- Gutscher, M.A., Malavieille, J., Lallemand, S. Collot, Y., 1998. Tectonic segmentation of North Andean margin: impact of the Carnegie Ridge collision. Earth and Planetary Letters. 168, 255-270.
- Haffer, J., 1967. On the geology of the Urabá and Northern Chocó regions, NW Colombia. Colombian Petroleum Company, COLPET. Gr-351. 106 p. Bogotá.
- Haffer, J., 1967. Geologic compilation map Northwestern Colombia. Colombian Petroleum Company, Escala 1:500.000.
- Haffer, J., 1965. Río Uva-traverse. Colombian Petroleum Company, Ecala 1:50.000.
- Hallam, A., 1981. Facies interpretation and the stratigraphic record. San Francisco: W. H. Freeman and Company. p. 291.
- Hardy Nicolas C., 1991, A marine geophysical study of the pacific margins of Colombia and southeast Panamá. Thesis of Doctor of Philisophy. School of Earth sciences, University of Birmingham.
- Hinze W.,2003, Bouguer reduction density, why 2.67 ?. Geophysics vol. 68, n 5, p.1559.1560.

REFERENCES

Published works

- Ibaraki, M., 1997. Closing of the Central American Seaway and Neogene coastal upwelling along the Pacific coast of South America. Tectonophysics. 281, 99-104
- IGAC-INGEOMINAS, 2006. Investigación integral del andén Pacífico colombiano. Tomo 1, Geología. Bogotá. p. 152.
- Ingeominas, 2005, Mapa Geológico del Andén Pacífico Colombiano, escala. 1:100.000
- Irving, E. La evolución estructural de los Andes más septentrionales de Colombia. Boletín Geológico. 1971.
- Karl, F., Richardson,A., 1989. Atrato river valley, Gulf of Urabá, Colombia, phase 1: photogeology survey. USA. 24 p.
- Kjar, P. Empresa Colombiana de Petróleos Asamera Inc., 1982. Chocó-Río Atrato Project, shot point location map. Escala 1:100.000.
- Kellogg, J.N., and Vega, V., 1995. Tectonic development of Panamá, Costa Rica, and the Colombian Andes: Constraint from global positioning system geodetic studies and gravity. Geological Society of America, Special paper. 295, 75-90.
- Kroonenberg. S.B., Bakker, G.M. and Van der Wiel, A.M., 1990. Late Cenozoic uplift and paleogeography of the Colombian Andes: constraints on the development of high-Andean biota. 69, 279-290.
- Lack, M. Empresa Colombiana de Petróleos Asamera Inc., 1983. Río Atrato/Quibdó proyectos. Escala 1:100.000. Chocó, Colombia.
- Lüschen, E. 1986. Gravity and height changes in the ocean-continent transition zone in western Colombia. Tectonophysics. 130:141-157.
- McCourt, W.J., Aspden, J.A. and Brook, M. 1984. New geological and geochronological data from the Colombian Andes: continental growth by multiple accretion. Journal of the Geological Society, London. 141, 831-845.
- McClay, K. (1997): Structural interpretation in sedimentary basins. Royal Holloway University of London.
- Mesa, A. Empresa Colombiana de Petróleos ECOPETROL, 2000. Potencial generador del Pacífico Colombiano-Cuenca San Juan, estudio petrológico de las formaciones del Cretáceo Superior al Mioceno Inferior. Piedecuesta. 53 p.
- Mera, R., Piragua, A., 2000. Correlación de las rocas del intervalo Paleoceno-Oligoceno, Subcuenca de San Juan, Chocó. Trabajo de grado. Universidad Nacional de Colombia, Bogotá. 93 p.
- Mera, R. Piragua, A. Petrobras, 2001. Sección estratigráfica de la quebrada Suruco, análisis estructural de fracturas. Área del río San Juan, Chocó. Bogotá. 83 p.
- Minera Utah de Colombia Ltda, 1980. Geological map of the Atrato-San Juan Basins and Surrounding Areas. Escala 1:500.000
- Mitra, S. & Namson, J. (1991): Balanced Cross Sections in Hydrocarbons exploration and production, an AAPG short course.
- Mountney, N. and Westbrook, G., 1997. Quantitative analysis of Miocene to Recent forearc basin evolution along the Colombian convergent margin. Basin Research. 9, 177-196
- Muñoz, R., Salinas, R., James, M., Bergmann, H., Tistl, M., 1989. Mineralizaciones primarias del grupo del platino y oro en la cuenca de los ríos Condoto e Iró, Chocó, Colombia. BGR - Ingeominas, Informe técnico, Medellín.
- Muñoz, F., Cogollo, M. Piedecuesta. Empresa Colombiana de Petróleos ECOPETROL, 2000. Potencial generador del Pacífico Colombiano-Cuenca San Juan, biocronología y paleoambientes. 150 p.
- Muñoz, F., Cogollo, M. 2000. Potencial generador del pacífico colombiano-Cuenca del San Juan. Biocronología y paleoambientes. Instituto Colombiano del Petróleo. Piedecuesta. p.150.
- Murray, J., 1991. Ecology and palaeoecology of benthic foraminifera. NY: Pearson Education. p. 397.
- Novoa, E. Suppe, J. & Shaw, J. (2000): Inclined shear restorations of growth folds. AAPG Bulletin, V. 84, No. 6, p 787804.
- Nygren, W.E., 1950. Bolivar geosyncline of northwestern South America. Bulletin of the American Association of Petroleum Geologists. 34 (10), 1998-2005.
- Ojeda, H., Calife, P. Petrobras, 1987. Avaliação do potencial petrolífero, Bacia de San Juan-Tumaco. Río de Janeiro. 59p.
- Oldenburg D., 1974, The inversion and interpretation of gravity anomalies, Geophysics, vol 39, n4, 526-536.
- Parker, R.L., 1972, The rapid calculation of potential anomalies: Geophysical Journal of the Royal Astronomical Society, v.42:315-334.
- Parker R.L., 1973, The rapid calculation of potential anomalies, Geophysics J.J. Astr. Soc., vol 31, 447-455.
- Pennington, W., 1981. Subduction of the Eastern Panamá Basin and Seismotectonics of Northwestern South America. Journal of Geophysical Research. 86, 10753-10770.
- Peña, J. Repsol Exploración Colombia S.A., 1996. Informe técnico anual 1995, Contrato de Asociación Chocó central. Bogota. 9 p.
- Peña, J. Repsol Exploración Colombia S.A., 1995. Informe técnico anual 1994, Contrato de Asociación Chocó central. Bogotá. 10 p.
- Pérez, G.1980. Evolución geológica de la cuenca Pacifica (geosinclinal de Bolívar), sector noroccidental de Suramérica. Boletín de Geología. 14 (21), 25-44.
- Petrobras, Ecopetrol, 2002. Regional Evaluation and petroleum potential of the offshore portion of central Pacific block. Brazil. 30p.
- Petters V. and Sarmiento, S., 1956. Oligocene and Lower Miocene biostratigraphy of the Carmen-Zambrano área, Colombia. Micropaleontology, 2(1):7-35.
- Porta de J., La Formación del Istmo de Panamá. Su incidencia en Colombia. Revista Academia Colombiana de Ciencias. 27(103), 191-216.
- Repsol Exploración Colombia S.A., 1996. Informe final geología y geofísica, Contrato de Asociación Chocó central. Bogotá. 15 p.
- Repsol Exploración Colombia S.A., sin fecha. Levantamiento sísmico terrestre, Chocó central. SISMOCOL S.A. Bogotá. 106
- Restrepo, J.J., Toussaint, J.F. 1988. Terrenes and continental accretion in the Colombian Andes. Episodes. 11 (3), 189-193
- Restrepo, Juan D., Kjerfve, B.; Correa, Iván D. y González, Juan L.; 2002. Morphodynamics of a high discharge tropical delta, San Juan river, pacific coast of Colombia. Marine Geology 192; 355-381.
- Richmond Petroleum Company. 1954. Buchadó-1. Final report. Bogotá. p. 50.
- Robertson Research. 1985. Opogadó-1. Stratigraphic summary. Project No. 856-M-992-B. Enclosure 14.3.
- Robertson Research. 1985. Buchadó-1. Stratigraphic summary. Project No. 856-M-992-B. Enclosure 14.4.
- Robertson Research. 1988. The biostratigraphic, paleoenvironments and petroleum geochemistry of the Buchadó-1, Tambora-1 and Sandí-1 wells, Pacific coastal region of Colombia. Report No. 3792/lb for Ecopetrol. Bogotá. p. 104.

REFERENCES

Published works

- Rojas, O., 1967. Geological traverses in the Chocó regions. Northwestern, Colombia. EPIS; ISN 434, Informe No. 810. p. 43 más apéndice.
- Rojas, O. Colombian Petroleum Company, 1967. Geological traverses in the Chocó region (northwestern Colombia). Bogotá. 137 p.
- Ruiz, J., Tosdal, R. M., Restrepo, P. A., Murillo-Muñeton, G., 1999. Pb isotope evidence for Colombia-southern Mexico connections in the Proterozoic. In Ramos, V. A., and Keppie, J.D., eds., Laurentia-Gondwana Connections before Pangea: Boulder, Colorado, Geological Society of America Special Paper 336.
- Schmidt-Thomé, M., Feldhaus, L., Salazar, G., Muñoz, R., 1992. Explicación del mapa geológico, escala 1:250.000, del flanco Oeste de la cordillera occidental entre los Ríos Andágueda y Murindó, Departamentos Antioquia y Chocó, República de Colombia.
- Suárez, M. Empresa Colombiana de Petróleos ECOPETROL, 1990. Columna estratigráfica generalizada de la cuenca del San Juan. Escala 1:25.000.
- Suárez, M. Empresa Colombiana de Petróleos ECOPETROL, 1990. Mapa geológico compilado de la Cuenca del San Juan, Escala 1:500.000. Bogotá.
- Suppe, J. Connors, C. & Zhang, Y. (2004): Shear fault bend folding, in K. R. McClay, ed., Thrust tectonics and hydrocarbon systems: AAPG Memoir 82, p 303323.
- Taborda, B. Empresa Colombiana de Petróleos ECOPETROL, 1961. Cuencas sedimentarias de Colombia. Bogotá. 29 p.
- Texas Petroleum Company, 1989. Informe geológico área de asociación Istmina. Bogotá. 29 p.
- Texas Petroleum Company, 1988. Pacific Coast of Colombia and SW Panamá Geologic Map, Oligocene Limestone Isolith. Bogota. Escala 1:500.000
- Texas Petroleum Company, 1989. Informe geológico área de asociación Istmina. EPIS; ISN: 1290, Informe No. 2352.
- Vargas, J. Compañía Petrolera Latina Inc., 1988. Chocó Pacific basin Geologic Section S-N Atrato Sub-basin and San Juan-Tumaco Sub-basin. File I-A-11.
- Vargas, C., 2007, Seismic structure of South-Central Andes of Colombia by tomographic Inversion (in press).
- Wokittel, R. Ingeominas, 1958. Geología Económica del Chocó. Bogotá. 66 p.
- Worthington P. The Evolution of Shaly Sand Concepts in Reservoir Evaluation. Society of Professional Well Log Analysis from The Log Analyst, v.26, no. 1 (1985), p. 23-40.

Punta Ardita
Bahia de Humboldt
Punta Cabo Marzo
Punta La Tortuguera
Bahia de Cupica
Punta Nabugá
Bahia Solano
Ensenada de Utria
GOLFO DE TRIBUGÁ
Ensenada Coquí
Punta Arusi
Cabo Corrientes
PACIFIC OCEAN
Playa Nueva
Bahia Baudo
Boca Usuragá
Ensenada Docampado
Boca Hijua
Boca Orpúa
Boca Cacagual
Playa El Choncho
N
25
50
km
SISTEMA DE FALLAS GARRAPATAS
Qui
Uv
Qall
Sa
Siu
Si
Sil
Ma
Pen
Peu
Co
Rp
Br
Is
QTt
My
Ci
CONCORDIA
SALGAR
EL CARMEN DE ATRATO
BETANIA
MISTRATO
PUEBLO RICO
SANTUARIO
LA CELIA
BALBOA
ANSERMANUEVO
ARGELIA
EL CAIRO
CARTAGO
VERSALLES
TORO
OBANDO
EL DOVIO
BOLIVAR
SAN JUAN
NOVITA
SAN JOSE DEL PALMAR

PART TWO

***Tumaco Basin**: Cenozoic Fore-Arc Basin*

PANAMA
PACIFIC OCEAN
Punta Ardita
Bahía de Humboldt
Punta Cabo Marzo
Punta La Tortuguera
Bahía de Cupica
Punta Nabugá
Bahía Solano
Ensenada de Utría
GOLFO DE TRIBUGÁ
Ensenada Coquí
Punta Arusí
Cabo Corrientes
Playa Nueva
Bahía Baudó
Boca Usuragá
Ensenada Docampadó
Boca Hijuá
Boca Orpúa
Boca Cacagual
Playa El Choncho
Bahía de Buenaventura
BUENAVENTURA
SISTEMA DE FALLAS GARRAPATAS
Qui
Uv
Qall
Siu
Sil
Sa
Ma
Pen
Peu
Co
Rp
Br
Is
QTT
My
Ci
N
0
25
50
km

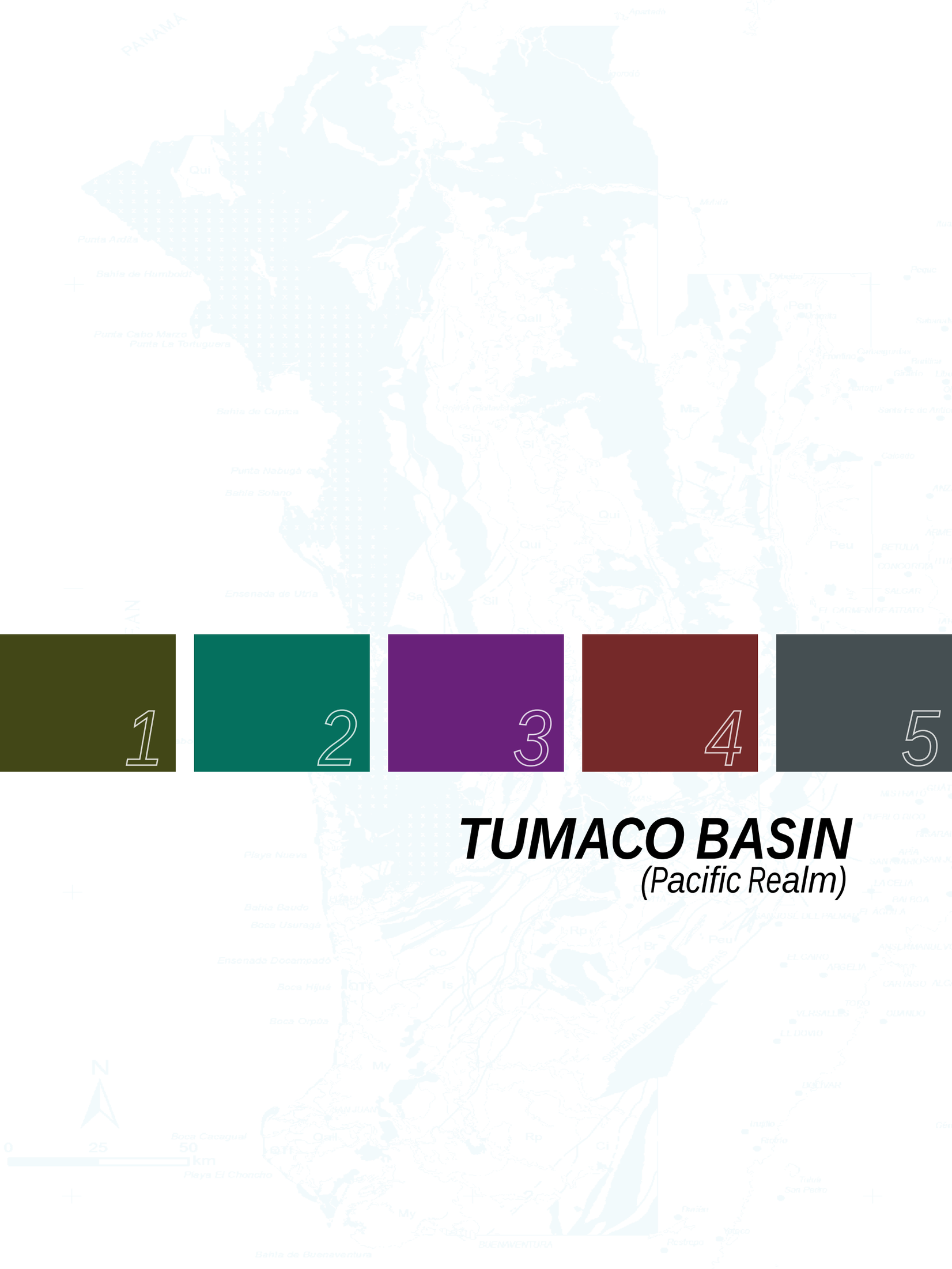
1
2
3
4
5
TUMACO BASIN
(Pacific Realm)
N
0
25
50
km

CONTENTS

LIST OF ILLUSTRATIONS

LIST OF ILLUSTRATIONS

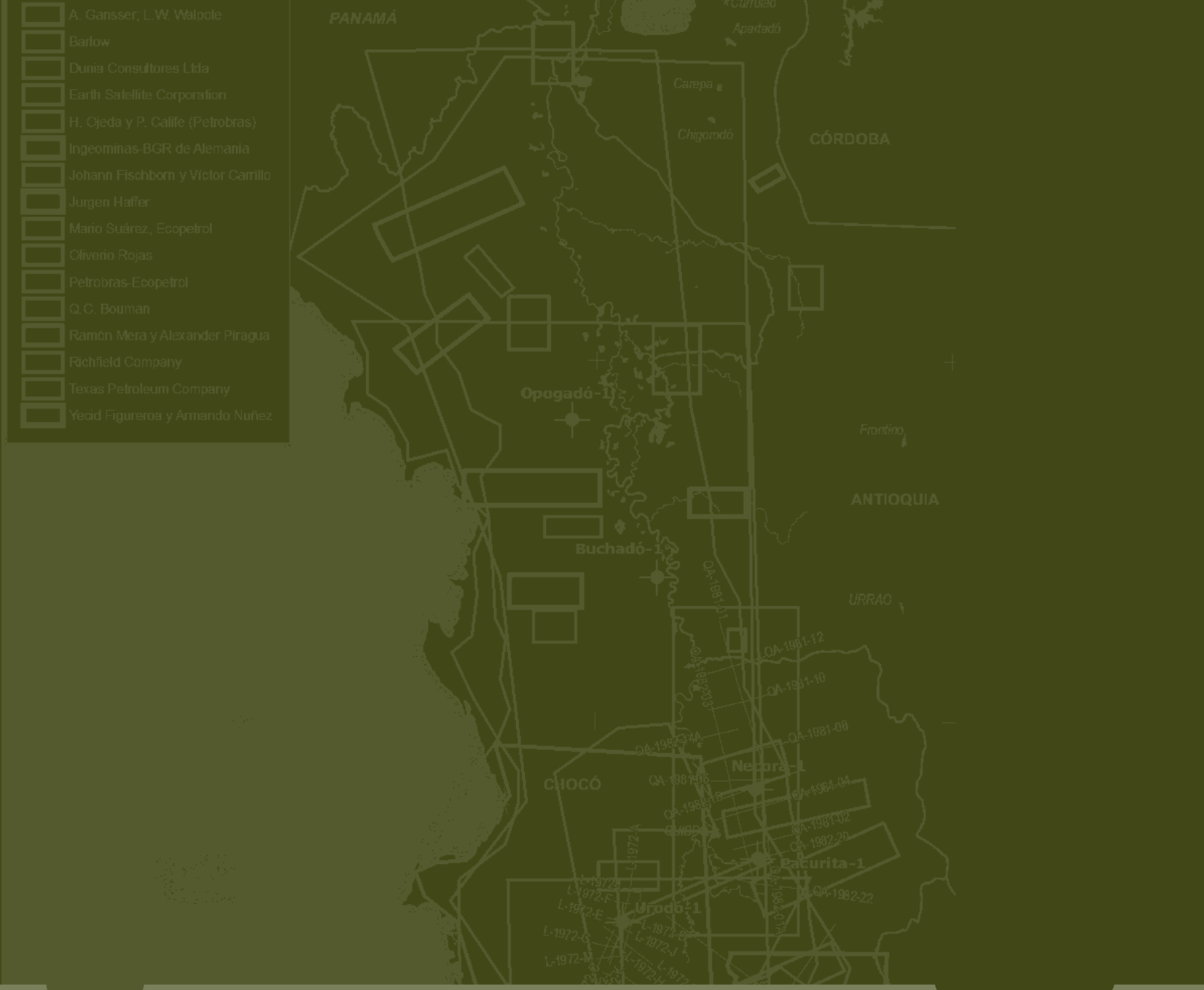

1. INTRODUCTION

1. INTRODUCTION

The geological information of the Tumaco Basin - onshore and offshore - is scarce. Nevertheless, the work aimed at compiling and integrating information carried out during this study produced a modern, regional geological picture and depicts economic possibilities in terms of hydrocarbon resources.

The Tumaco basin is a forearc basin, which contains a pre-Miocene mega-sequence and three post-Lower Miocene sequences, deposited in shelf to bathyal environments. The basin basement is made up of Cretaceous meta-sedimentary and volcanic rocks.

The information provided by five (5) wells drilled in the Tumaco Basin made it possible to understand the principal biostratigraphic units and provide a general stratigraphic framework for the basin.

The presence of oil seeps and hydrocarbon shows indicates that the source rock could have achieved the thermal maturity necessary to produce oil and gas. In order to evaluate any petroliferous system, the available geochemical information was reinterpreted and a preliminary modeling of hydrocarbon generation and expulsion is proposed.

Exploration History

The Tumaco basin has been studied by different authors (e.g. Bueno and Govea, 1974; Bueno, 1989, Suarez, 1990; Galindo and Torres, 1995; EarthSath, 1999) as part of the analysis of the hydrocarbon potential of the coastal Pacific basin. The work carried out by Suarez (1990) includes a summary of the Colombian Pacific province, as well as an extensive bibliography that mentions all the main seismic, gravimetric, and aeromagnetometric studies, the drilled wells and their results, and regional geological studies.

The most significant aeromagnetometric and seismic reflection studies of Tumaco – San Juan basin were carried out during two periods: 1973 y 1982, in which 3500 km and 6500 km of seismic lines were acquired, respectively. Drilling was carried out in 1967 (two wells in the offshore area: Sandi-1 and Tambora-1), and in 1956, 1980 and 1981 in the onshore area: Changui-1, Remolino Grande-1 and Majagua-1.

The above-mentioned studies highlighted the fact that the Tumaco basin features the necessary elements for favorable hydrocarbon exploration, given that three of the five explored wells have shown the presence of hydrocarbons. Such is the case of the Majagua-1 well, which produced good gas samples in fine-grained sandstone and Oligocene-Miocene siltstones. The Chagui-1 well reported good hydrocarbon samples in the Miocene siltstones.

In 1992, ECOPETROL carried out the Tumaco-90 seismic project which recorded 290.88 km, distributed in five lines onshore: NT-90-1100, NT-90-1820, NT-90-2870, NT-90-6230 and NT-90-1200. On the basis of the seismic data interpreted, a preliminary age model was proposed assigning ages from the Eocene to the most recent times to the sediments found in the area. One of the recommendations arising from the acquisition was to carry out a complete study of the information in order to evaluate the hydrocarbons potential in the Chaguí-1, Remolino Grande -1 and Majagua-1 wells. In the offshore region, the Tambora-1 well shows signs of gas and tar in the Lower Tertiary clastic rocks.

In the year 2000, the cruiser SISTEUR acquired marine multichannel seismic reflection data and wide-angle seismic data using an Ocean Bottom Seismometer along the North Ecuador-South Colombia (NESC) margin. In 2001, the cruiser Salieri acquired wide-angle seismic data and multibeam bathymetric data in order to explore the crust and the structure of the ocean bottom in the same region (Flueh et al., 2001). In 2005, the cruiser Amadeus collected 55000 km2 of bathymetric and geophysical data, sedimentary core, rock dredging and heat flow data (Collot et al., 2005).

The most recent studies in the offshore area (Mountney y Westbrook, 1997; Collot et al., 2004; Marcaillou et al.; Collot et al., 2008; López, E., et al., 2008) include studies of the tectonic and thermal regime of the NESC margin, the tectonic evolution and sedimentary development of so called Tumaco–Borbón and Manglares basins during the Cenozoic and the interpretation of the subduction process currently under way in this continental margin.

A Base Map was compiled (Figure 1), showing the main field studies, the seismic programs shot to date, and five exploratory wells that have been drilled: Chaguí-1 (1955) ,Sandi-1 (offshore) (1967): Tambora- 1 (offshore 1967),Remolino Grande-1 (1980), and Majagua-1 (1981) (see Figure 1).

The Chaguí-1 well was drilled on an anticline produced by diapirism and declared dry at the moment of completion. The well presents oil shows at the 1890'-2060', 5930'-5950' and 6190 to 6760 intervals, and gas samples from 4230' to 12.107'. An overpressured area was reported between 6100´ and 7130´. The information on Chaguí-1 is deficient, since it lacks biostratigraphy and velocity records. However, it can be compared with to Majagua-1.

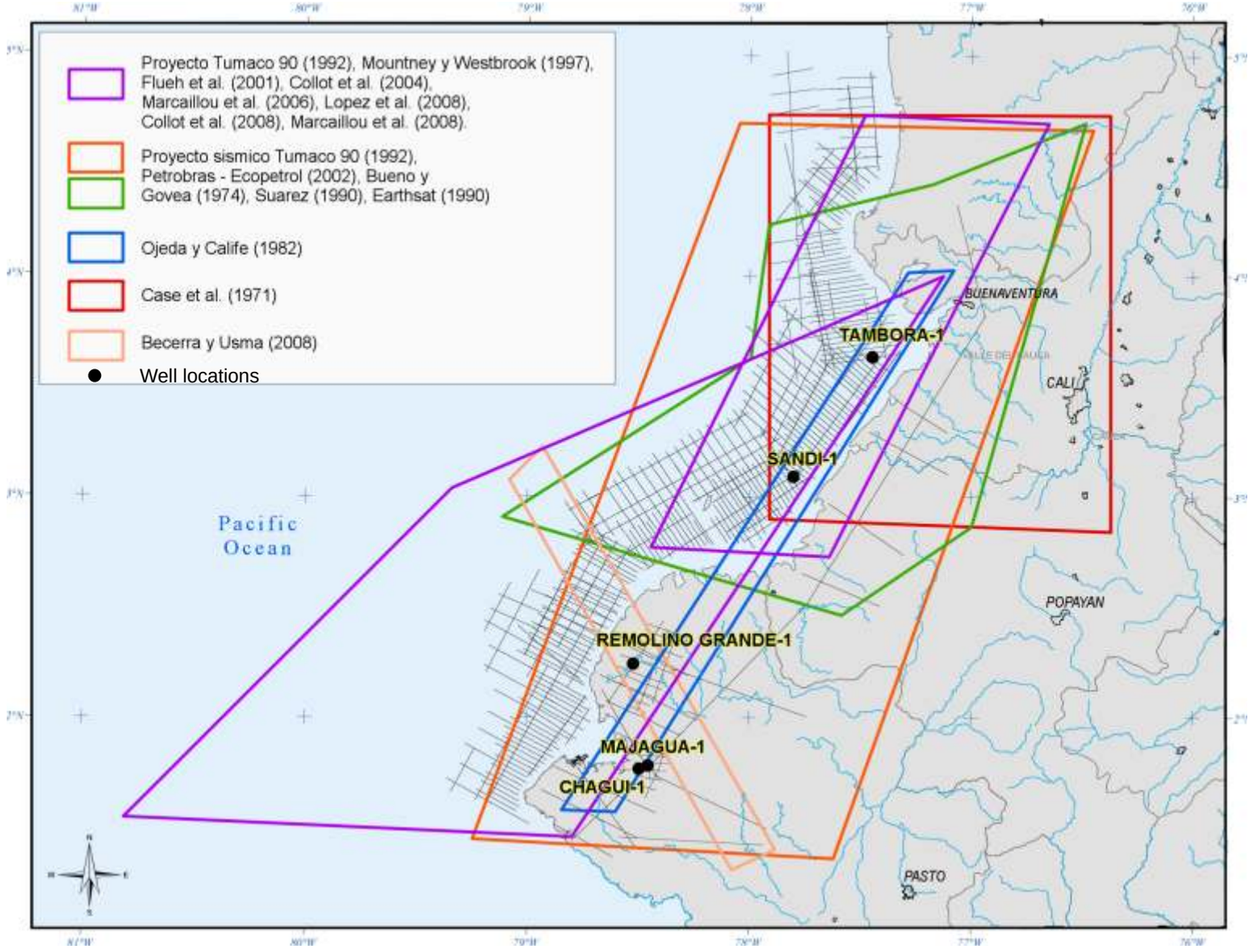

Figure 1. *Based map of studies carried out in the Tumaco basin*

The Sandi-1 well reached a final total depth of 12.161'. There were no hydrocarbon shows and the conclusion drawn was that it had been located on the axis of a diapir whose penetration started at 5.000' and never got out of it.

The Tambora-I well reached 11.365' and penetrated a potent sequence of thick sandstone and conglomerates, starting at 8.500'. Later studies (Ojeda y Calife 1.987) affirm that the well was possibly located above a diapiric structure which was not penetrated.

The Remolino Grande-1 well was drilled in a basement high, with average quality seismic information (CDI, ECP). The well drilled through a section located between the Cretaceous basement and the Middle Miocene. It contains biostratigraphic information, information regarding deposition environments velocity records, geochemistry, wall samples, and a good range of electrical logs. Some of the wall samples showed liquid hydrocarbons.

The last of the wells drilled in the basin was Majagua-1, located on the axis of a highly developed syncline zone, for which reason, in spite of having drilled down to 14.287' it only reached sediments dated as Lower Miocene, without reaching deeper stratigraphic objectives.

PACIFIC OCEAN
Punta Ardita
Bahía de Humboldt
Punta Cabo Marzo
Punta La Tortuguera
Bahía de Cupica
Punta Nabugá
Bahía Solano
Ensenada de Utría
GOLFO DE TRIBUGÁ
Ensenada Coquí
Punta Arusí
Cabo Corrientes
Playa Nueva
Bahía Baudó
Boca Usuragá
Ensenada Docampado
Boca Hijua
Boca Orpúa
Boca Cacagual
Playa El Choncho
N
25
50
km
Qui
Uv
Qall
Siu
Si
Sil
Sa
Ma
Pen
Peu
Co
Rp
Is
My
Br
Ci
QTt
SISTEMA DE FALLAS GARRAPATAS
Dabeiba
Uramita
Frontino
Cañasgordas
Abriaquí
Caicedo
BETULIA
CONCORDIA
SALGAR
EL CARMEN DE ATRATO
HISPANIA
BETANIA
MISTRATÓ
PUEBLO RICO
SANTUARIO
LA CELIA
BALBOA
SAN JOSÉ DEL PALMAR
EL CAIRO
ARGELIA
CARTAGO
TORO
VERSALLES
OBANDO
EL DOVIO
BOLÍVAR
SAN JUAN
NÓVITA
Tuluá
San Pedro

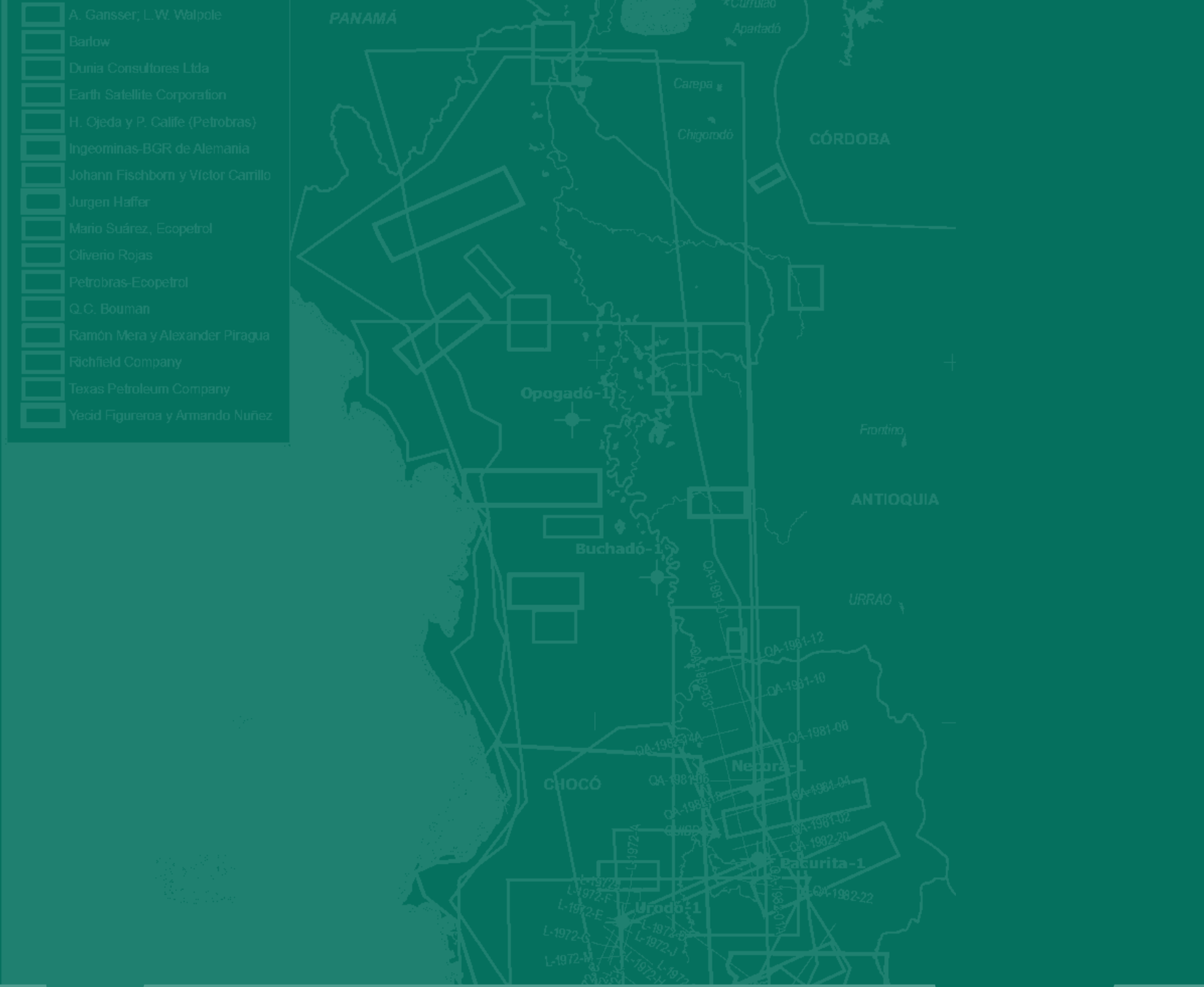
A. Gansser; L.W. Walpole
Barlow
Dunia Consultores Ltda
Earth Satellite Corporation
H. Ojeda y P. Calife (Petrobras)
Ingeominas-BGR de Alemania
Johann Fischborn y Víctor Carrillo
Jurgen Haffer
Mario Suárez, Ecopetrol
Oliverio Rojas
Petrobras-Ecopetrol
Q.C. Bouman
Ramón Mera y Alexander Piragua
Richfield Company
Texas Petroleum Company
Yecid Figueroa y Armando Nuñez
PANAMÁ
Apartadó
Carepa
Chigorodó
CÓRDOBA
Opogadó-1
Frontino
ANTIOQUIA
Buchadó-1
URRAO
CHOCÓ
Necocli-1
Pacurita-1
Urodó-1
BUENAVENTURA
Tuluá
Buga
Tambora-1
VALLE DEL CAUCA
Yumbo
Palmira

2. GEOLOGY

2. GEOLOGY

Regional Overview

The onshore sector of the Tumaco basin is bounded by the Garrapatas fault system to the North; the Western cordillera to the East; the border with Ecuador to the South; and the Pacific Ocean to the West. The offshore Tumaco basin borders on the onshore basin to the East, the Garrapatas fault system to the North, the border with Ecuador to the South, and with the Colombia-Ecuador trench to the West (See Figure 2). Various authors (e.g. Bueno Salazar and Govea (1974), Bueno Salazar (1989), Cediel et al. (2003), Baldock and Longo (1982), Evans and Whittaker (1982), Jaillard et al. (1995, 2000)) have indicated that, from the stratigraphic perspective, there is a close correlation between this basin and the Borbón basin in Ecuador, which extends to the Jama-Quininde fault. Escovar and others (1992) propose the existence of a forearc megabasin known as the Guayaquil-Buenaventura basin.

At the regional level, the Tumaco basin forms part of the North Ecuador-South Colombia (NESC) physiographic region. The basement of this margin is made up of ocean plateau and island arc accreted terrains on the Colombian coast (Ortiz, 1979; Marriner and Millward, 1984; Kerr et al., 1996b), the Ecuadorian coast (Feininger and Bristow, 1980; Hall and Calle, 1982; Lebrat et al., 1987; Daly, 1989), and in the westernmost portion of the Manglares basin (McGeary and Ben-Avraham, 1986; Kerr et al., 1996a; Cediel et al., 2003).

In Colombia, these accreted terrains are known as the Dagua Formation, dominated by basaltic rocks with an affinity to the ocean plateau defined through geochemical and isotopic studies (Kerr et al., 1996b; Ortiz, 1979). This formation has been correlated to the so-called Piñón Formation in Ecuador (Feininger y Bristow, 1980; Baldock y Longo, 1982). Toward the offshore area, the Gorgona Terrain has been defined, where Gorgona Island outcrops (Echevarria and Aitken, 1986; Révillon et al., 2000), extending from the northern part of the Garrapatas Fault, underneath the Manglares basin (Cediel et al., 2003; Kerr, 2005). This terrain is made up of a peridotitic-gabroic complex, massive basalt flows, and Late Cretaceous komatiites (Echevarria, 1980; Kerr et al., 1996b). (See Figure 3)

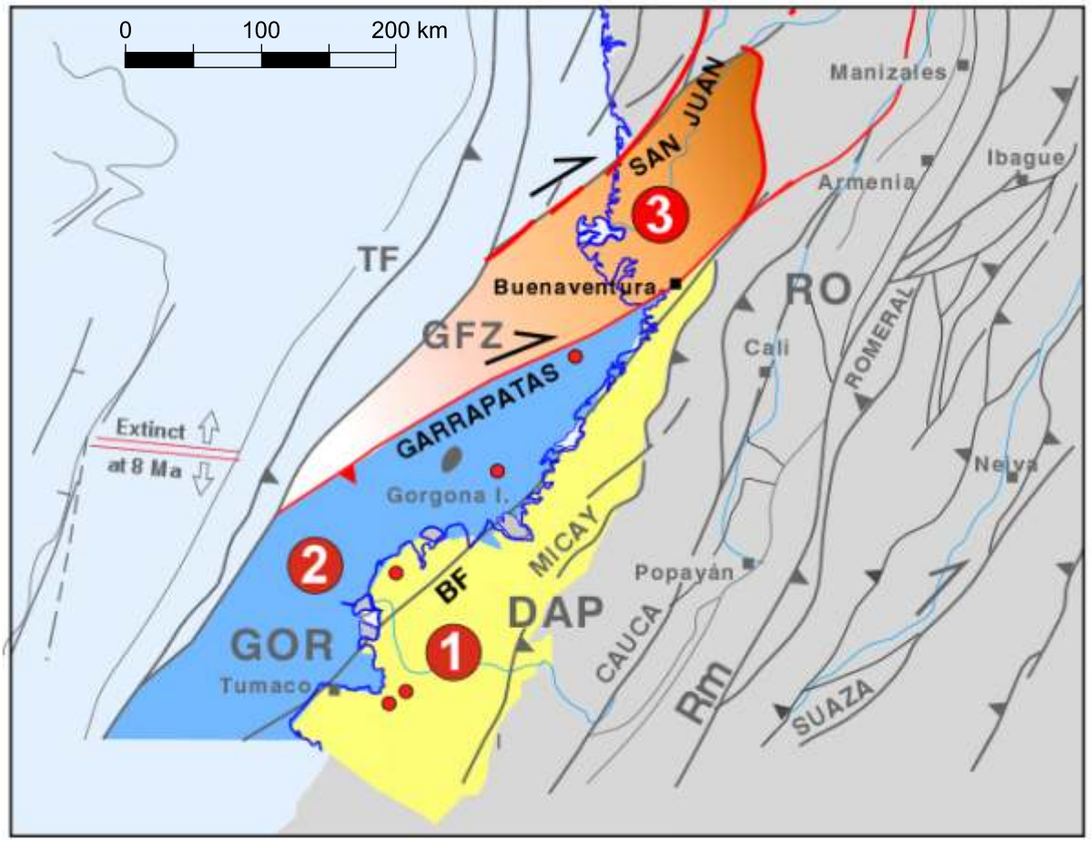

Figure 2. *Location of the Tumaco (onshore and offshore) basin.*

Modified after Cediel, et al, 2003.

Any difference between the origin and the structural relation among the Gorgona, Dagua and Piñón oceanic terrains has not been established and continues to be a topic of debate. The geochemical affinities and the radiometric ages suggest that the coastal region Ecuador and Colombia have distinct basement blocks of different origin and that they possibly do not belong to a singular magmatic province, previously identified as the Colombian–Caribbean Oceanic Plateau (CCOP) (Juteau et al., 1977; Reynaud et al., 1999). At the morphostructural level, Cediel et al. (2003) have grouped the Dagua and Piñón formations in the terrain bearing the same name. Small Paleocene-Miocene age metaluminous plutons with calco-alkaline features whose composition varies from tonalites to granodiorites, intrude in the Dagua-Piñon terrain. Based on seismic interpretation, the same authors suggest that the Gorgona terrain is an isolated terrain, separated from the Dagua-Piñón terrain by the Buenaventura fault (Figure 2).

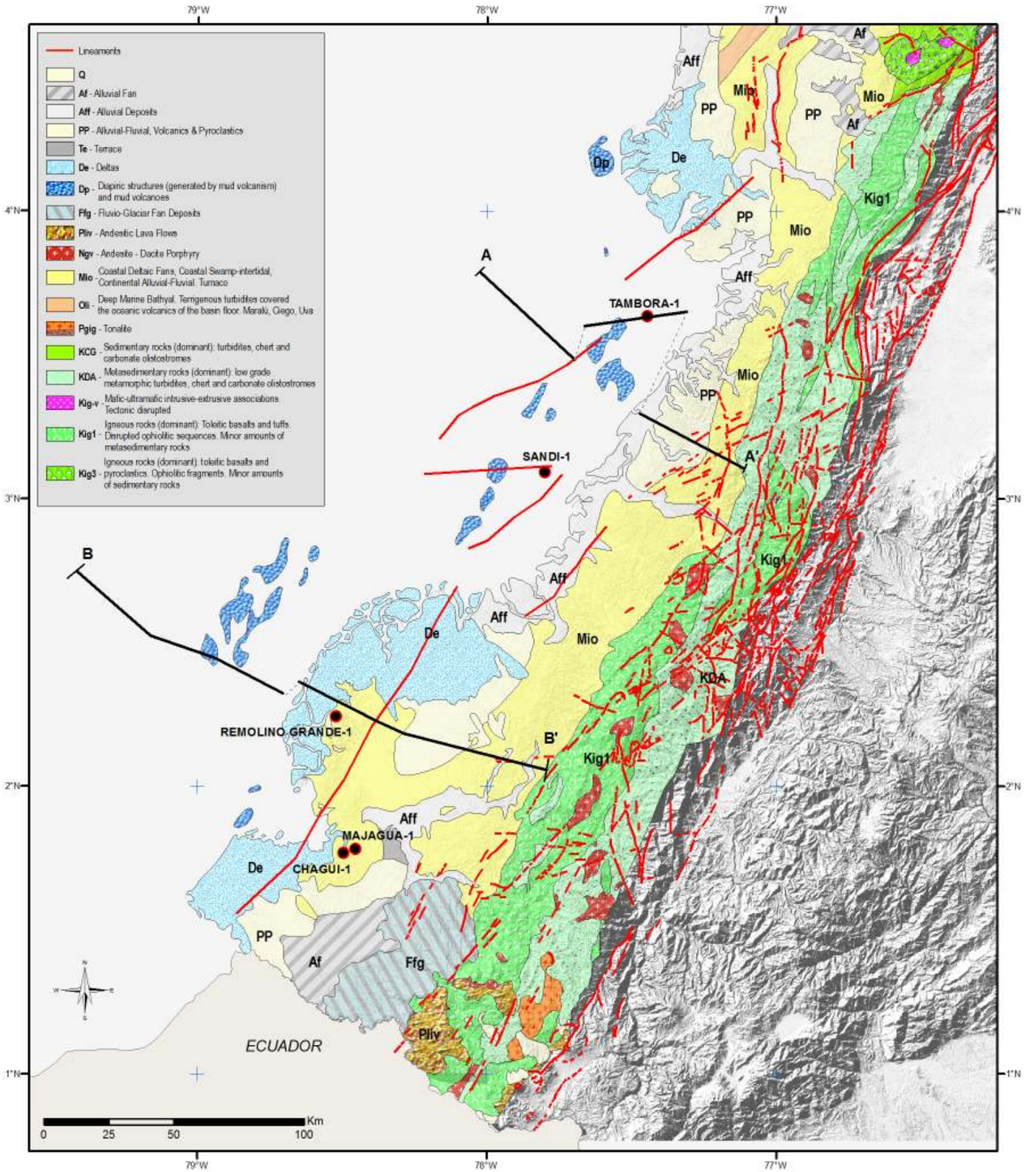

Figure 3. Geological Map. (Modified after Cediel et al., 2000)

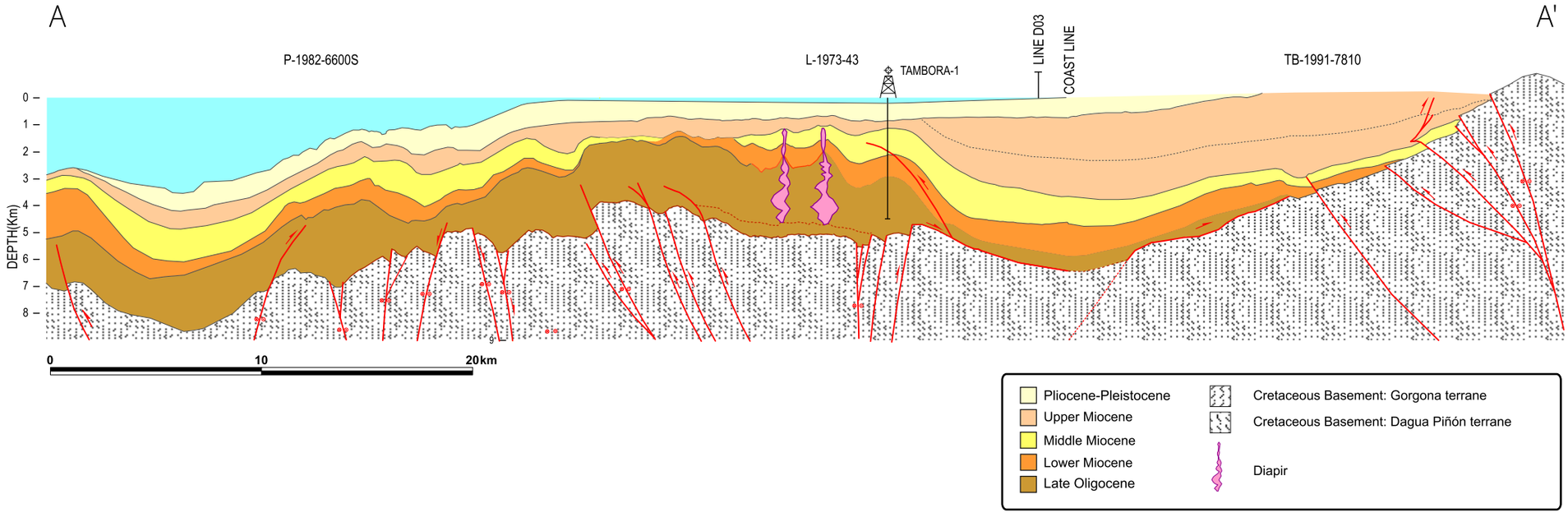

Figure 4a. Schematic section of the Tumaco basin. Cross-section A-A', near the Tambora-1 well. This section represents the structural geometry of the northern sector of Tumaco basin in the vicinity of the Tambora-1 well (3° 30' N). Reflectors were interpreted for the sub-Oligocene, sub-Lower-Miocene, sub-Upper-Miocene, and sub-Pliocene. Two depocenter and two basement highs were recognized as the major features. It can be inferred that the sedimentary deposit exceeds 6 Km in thickness in the eastern depocenter under the coast line (section TB-1991-7810). All of the units are deposited with onlap onto the basement (section TB-1991-7810), and some disappear locally over structural highs. In this section, at least two structural domains controlled by the Cretaceous can be identified from West to East: (1) a strike-slip faulting domain (section P-1982-6600S), and (2) a compressive domain with tectonic inversion (sections L-1973-58 and section TB-1991-7810).

Schematic geological sections A-A' and B-B' of the Tumaco basin (Figure 4a and 4b) are located in the geological map.

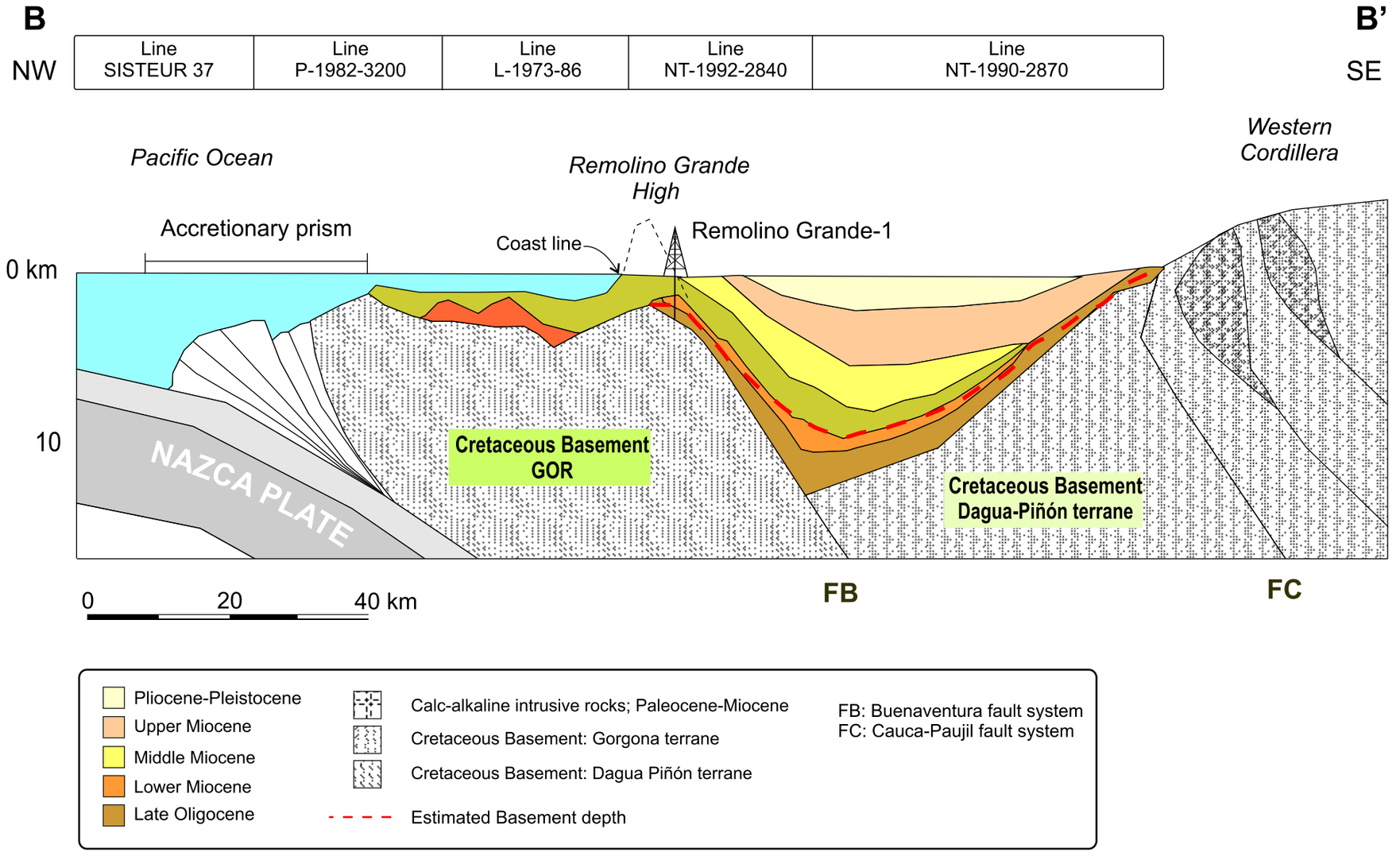

Figure 4b. Schematic section of the Tumaco basin. Cross-section B-B' near the Remolino Grande-1 well. Seismic, gravimetric, and magnetometric interpretation made it possible to clearly identify the Remolino Grande paleo-high, which divides the Tumaco basin into two sectors with different structural styles: 1) an internal sector located mostly onshore, which features inverse faulting of low intensity, little deformation, and is asymmetric, with gentle slopes and onlap type deposition on the crystalline basement that outcrops on the western flank of the Western Cordillera, known as the Dagua-Piñón terrain (Cediel et al., 2003). To the West, the basin slopes are steep and clearly delimited by the topography of the Gorgona terrain basement (e.g. Estrada, 1999: Cediel et al., 2003); 2), an external sector of the basin, totally located offshore, with a structural style characterized by high-angle extensional faults with eastward vergence. The discontinuous red line corresponds to the basement estimated by the 2D basement inversion model according to Bouguer gravimetric profiles, which indicate a maximum depth of approximately 9 km for the basin.

Stratigraphy

The study presents the results of the compilation, revision, and evaluation of the stratigraphic information provided by ANH, and by Duque Caro y Cia. Ltda. Files related to the Majagua-1, Remolino Grande-1, Sandi-1, and Tambora-1 wells were used to establish the stratigraphic correlation among these four wells; because the information on the Chagüí well was insufficient and outdated, it was not possible to integrate it with that of the other wells. Figure 5 is a comparative chart of the stratigraphic nomenclature of the Tumaco basin.

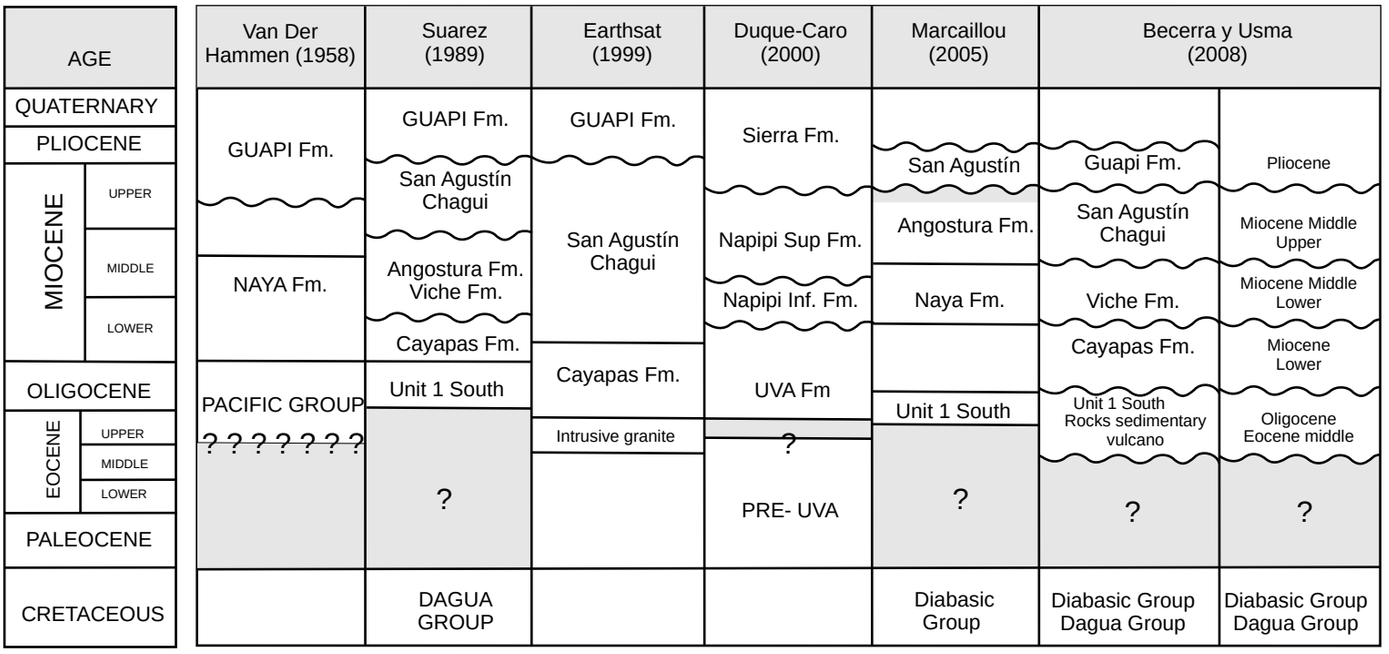

Figure 5. Stratigraphic chart of the Tumaco basin. Comparative chart of the different suggested nomenclatures (modified after Becerra and Usma, 2008).

Five regional unconformities, associated with tectonic events of the northwestern corner of South America (cf. Duque-Caro, 1990), have been used to evaluate the stratigraphic sequences dealt with in this report: (1), Lower Oligocene, prior to the planktonic zone P.21, (2) Late Oligocene, prior to the Lower Miocene, planktonic zone N.5-6, (3) Early Miocene, before planktonic zone N.7, (4) Middle Miocene, before Upper Middle Miocene planktonic zone N.14-N.16, and (5) Upper Miocene, prior to the interval of zones N.17 to N.19 of Upper Miocene to Early Miocene age. These unconformities have usually been recognized by changes in the faunal composition, which, in turn, coincide with paleo-environmental and lithological changes.

Majagua-1 Well

The Majagua-1 well is characterized by five microfacies: (1) (Bolivina bicostata-Buliminella curta, 0'-1720') of Late Miocene to Pliocene age, (2) (Bolivina dispar-Nonion goudkoffi, 1720'-2820') of Late Miocene age, (3) (Concavella gyroidinaformis-Uvigerinella obesa, 2820'-8200') of Upper Middle Miocene to Late Miocene age, (4) (Uvigerina adiposa-Cibicidoides floridanus, 8200'-10500') of Middle Miocene age, and (5), (Globigerínidos-Radiolarios,10.500'-14.287') of Early Miocene to basal Middle Miocene age. The recovery of foraminifera is very good and well-preserved between 520' and 3950', poor to abundant and badly preserved between 3950' and 8200', and abundant and badly preserved between 8200' and 14280' (deepest interval) (See Figure 6).

The environmental interpretation indicates a deepening cycle that culminates in the well top with (1) external platform environment (520'-4720').

On the basis of the information compiled from previous studies of the Pacific and Caribbean coastal margins of Colombia (Duque-Caro, 1979, 1984 y 1990ab), the limits of the microfacies appear to be unconformities and coincide with (1) the Early Miocene, (2) the Middle Miocene (3) the Upper-Middle Miocene, and (4) the Upper Miocene. These stratigraphic interruptions correspond to major hiatuses registered in the oceans (Keller y Barron, 1983) and to regional unconformities produced by tectonic and erosive events that are observable in the surface stratigraphy.

Remolino Grande-1 Well

The stratigraphic information provided is similar to that of the Majagua-1 well with respect to electric logs; it is the well with the greatest amount of processed data by different fossil groups such as foraminifera, nanoplankton and palynology (lower portion of the well). Radiometric dating showed Upper Cretaceous in a volcanic-sedimentary sequence below 5400 feet, until the well's total depth (9082 feet) making this the best documented well of the Oligocene to Miocene interval in the Colombian South Pacific (See Figure 7).

The stratigraphy of the Remolino Grande-1 well is characterized by four microfacies: (1) microfacies (Uvigerina subperegrina, 608'-2000'), of Upper Middle Miocene age, (2) microfacies (Uvigerina gallowayi (2000'-3521') of Lower Middle Miocene Age, (3) microfacies (Radiolarios-Arenáceos, 3521'-5640') of Oligocene to Early Miocene age, and (4) microfacies (Radiolaria, 5640'-9082', T.D.)

The environmental interpretation indicates a deepening cycle that begins with (1) an outer shelf domain (608-2000'), (2) an upper slope environment (2000'-3521'), (3) a lower slope environment (bathyal, 3521'-5640'), and (4) a deep environment (5640'-9082') associated with a sedimentary volcanic sequence.

According to previous studies of the Pacific and Caribbean coastal regions of Colombia (Duque-Caro, 1979, 1984 y 1990, 1991), the microstratigraphic limits recognized in this well also appear to be unconformities and coincide with (1) the Upper Oligocene in the upper portion of planktonic zone N.4, (2) the Early Miocene, and (3) the Middle Miocene in the upper portion. It was not possible to recognize physically the Upper Miocene unconformity. These stratigraphic interruptions correspond to major hiatuses registered in the oceans (Keller y Barron, 1983) and to regional unconformities produced by tectonic and erosive events that are observable in the surface stratigraphy.

Sandi-1 Well

The stratigraphic column of Sandi-1 well is characterized by five microfacies and a short level in the lower portion: (1) (Bolivina-Uvigerina, 0'-1500') of Late Miocene to Pliocene age, (2) (Uvigerina-Valvulineria, 1500'-3257') of Late Miocene age, (3) (Radiolaria, 3257'-7000') of Middle Miocene Age, (4) (Radiolaria-Arenaceous, 7000'-9750') of basal Middle Miocene age, (5) (Siphogenerina transversa, 9750'-12.000') of Upper Early Miocene age, and (6) the Acarinina-Radiolaria level (12.000'-12.161') of Middle Eocene age, which could correspond to an olistostromic block (See Figure 8).

The recovery of foraminifera was good and well-preserved between 830' and 2500', poor, relatively abundant, badly preserved, and sterile between 2750' and 9500', and abundant to poor and badly preserved between 9750' and 12161', T.D.

The environmental interpretation indicates a deepening cycle of: (1) an outer shelf environment (830'-1500'), (2) an upper slope environment (1500'-3257'), (3) an upper slope environment (3257'-7000') with the influence of turbidites, and (4) general and middle slope environments (7000'-12160') in the lower portion of the well.

The microstratigraphic limits appear to be unconformities and coincide with (1) the Early Miocene-basal Middle Miocene, (2) the Middle Miocene, and (3) the Upper Miocene. These stratigraphic interruptions correspond to major hiatuses registered in the oceans (Keller and Barron, 1983) and to regional unconformities produced by tectonic and erosive events that are observable in the surface stratigraphy. (cf. Duque-Caro, 1990a).

This well showed an occurrence of Middle Eocene microfauna at the bottom of the sequence, which, given its age, was correlated with the Suruco unit in the Manglares or Tumaco basin (Marcaillou and Collot, 2008, Figure 3) and has been interpreted as a possible olistostromic phenomenon.

Tambora-1 Well

Four microfacies and a sterile interval were recognized at the Tambora-1 well: (1) (Bulimina-Buliminella, 370'-750') of Late Miocene to a younger age, (2) (Radiolaria 750'-1250') of Upper Middle Miocene to Late Miocene age, (3) (Arenaceous Foraminifera-Radiolaria, 1250'-3250') of Middle Miocene age, (4) (Globorotalia-Globigerinoides, 3250'-7500') of Middle Miocene age, and (5) a Sterile Interval (7500'-11220' and T.D.) which comprises a mainly clastic sequence that apparently belongs to the Early Miocene-Middle Miocene interval (See Figure 9).

The environmental interpretation indicates a shallowing interval above 750' and a deep interval below (Slope), and an unknown sequence below 7500'.

Just as in the case of the previous wells, Majagua-1, Remolino Grande-1 and Sandi-1, and on the basis of the knowledge contributed by previous studies of the Pacific and Caribbean coastal regions of Colombia (Duque-Caro, 1979, 1984 and 1990ab, 1991), the microstratigraphic limits recognized in this well are also unconformities and coincide with (1) the Middle Miocene, and (2) the Upper Miocene. These stratigraphic gaps correspond to major hiatuses registered in the oceans (Keller and Barron, 1983) and to regional unconformities produced by tectonic and erosive events.

MICROSTRATIGRAPHIC SYNTHESIS OF MAJAGUA-1 WELL

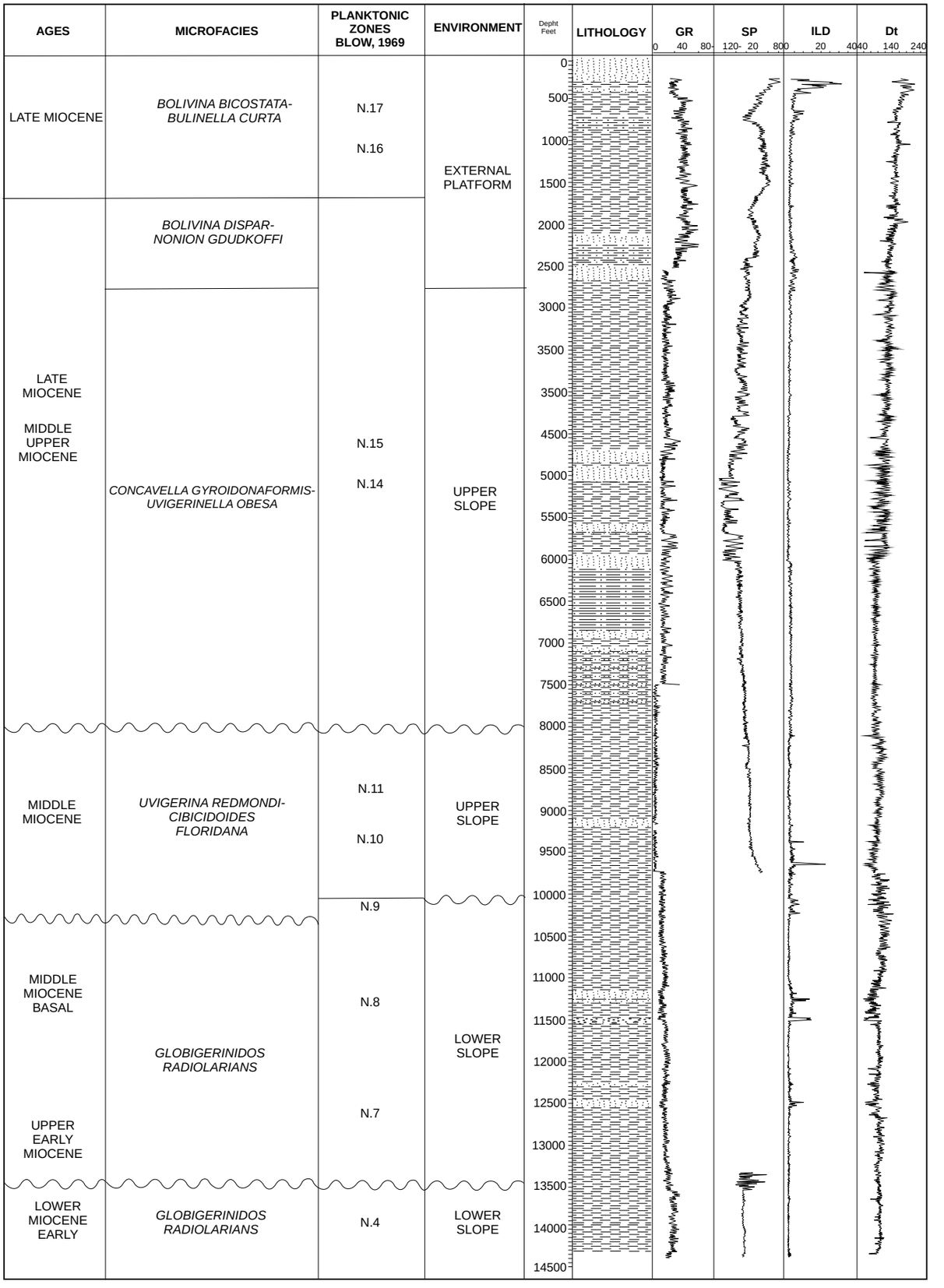

Figure 6. Majagua-1 Well log

MICROSTRATIGRAPHIC SYNTHESIS OF REMOLINO GRANDE-1 WELL

AGES	MICROFACIES	PLANKTONIC ZONES BLOW, 1969	ENVIRONMENT
POST LATE MIOCENE	NO SAMPLE	POST N.14	NO SAMPLE
LATE MIOCENE	*UVIGERINA SUBPEREGRINA*	N.14	EXTERNAL PLATFORM
MIDDLE MIOCENE	*UVIGERINA GALLOWAYI*	N.10-N.9	UPPER SLOPE
EARLY LOWER MIOCENE	*ARENACEOUS RADIOLARIANS*	N.6-N.4	UPPER SLOPE
LATE OLIGOCENE		P.21	
LATE CRETACEOUS	*RADIOLARIANS*	LATE CRETACEOUS	UPPER SLOPE

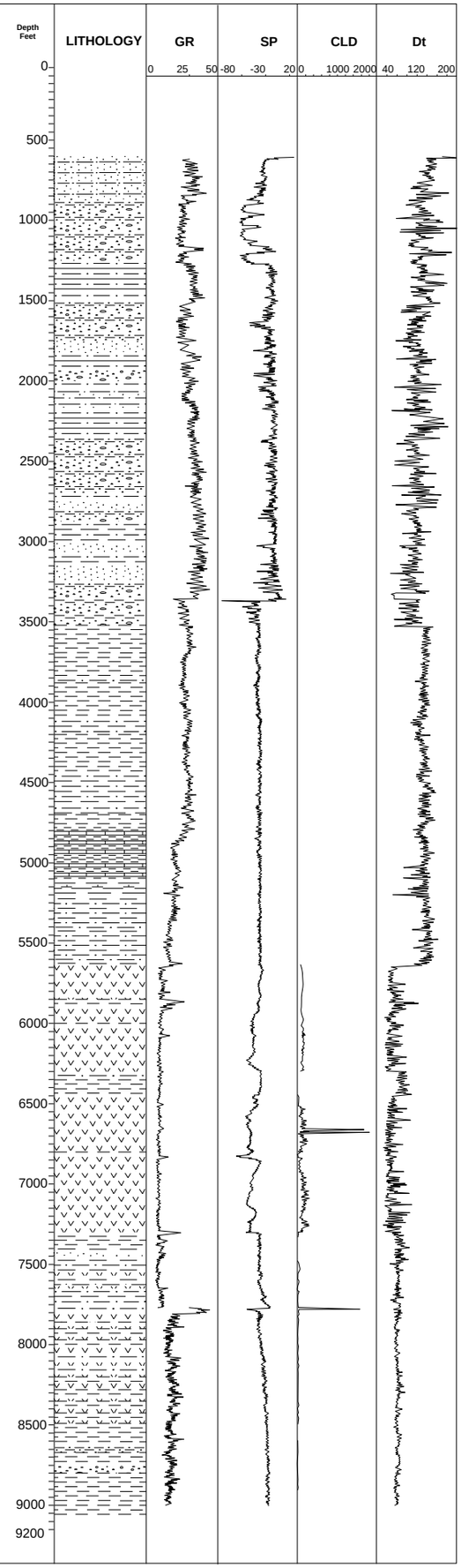

Figure 7. Remolino Grande-1 Well Log

MICROSTRATIGRAPHIC SYNTHESIS OF SANDI-1 WELL

AGES	MICROFACIES	PLANKTONIC ZONES BLOW, 1969	ENVIRONMENT
POST LATE MIOCENE	NO SAMPLE	NO SAMPLE	NO SAMPLE
LATE MIOCENE	*BOLIVINA-UVIGERINA*	N.17	EXTERNAL PLATFORM
LATE MIOCENE MIDDLE UPPER MIOCENE	*UVIGERINA VALVULINERIA*	N.16 N.14	UPPER SLOPE
MIDDLE MIOCENE	*RADIOLARIANS*	N.10- N.9	UPPER SLOPE
MIDDLE MIOCENE BASAL	*ARENACEOUS RADIOLARIANS*	N.9?	UPPER SLOPE
LATE CRETACEOUS	*TRANSVERSE SIPHOGENERINA*	N.7	
MIDDLE EOCENE	*ACARININA RADIOLARIANS*	P.12 - P.14	LOWER MIDDLE SLOPE

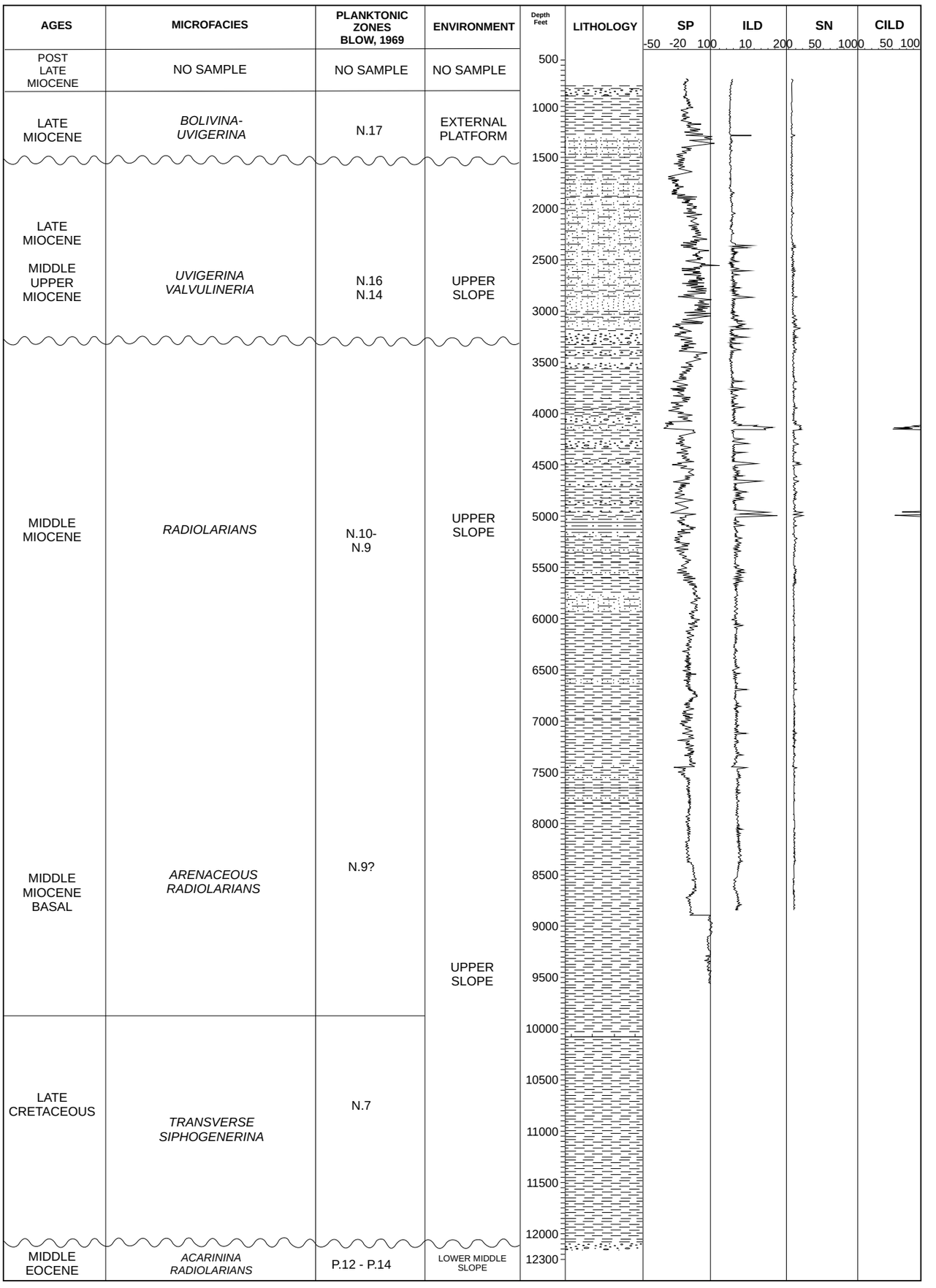

Figure 8. Sandi-1 Well Log

MICROSTRATIGRAPHIC SYNTHESIS OF TAMBORA-1 WELL

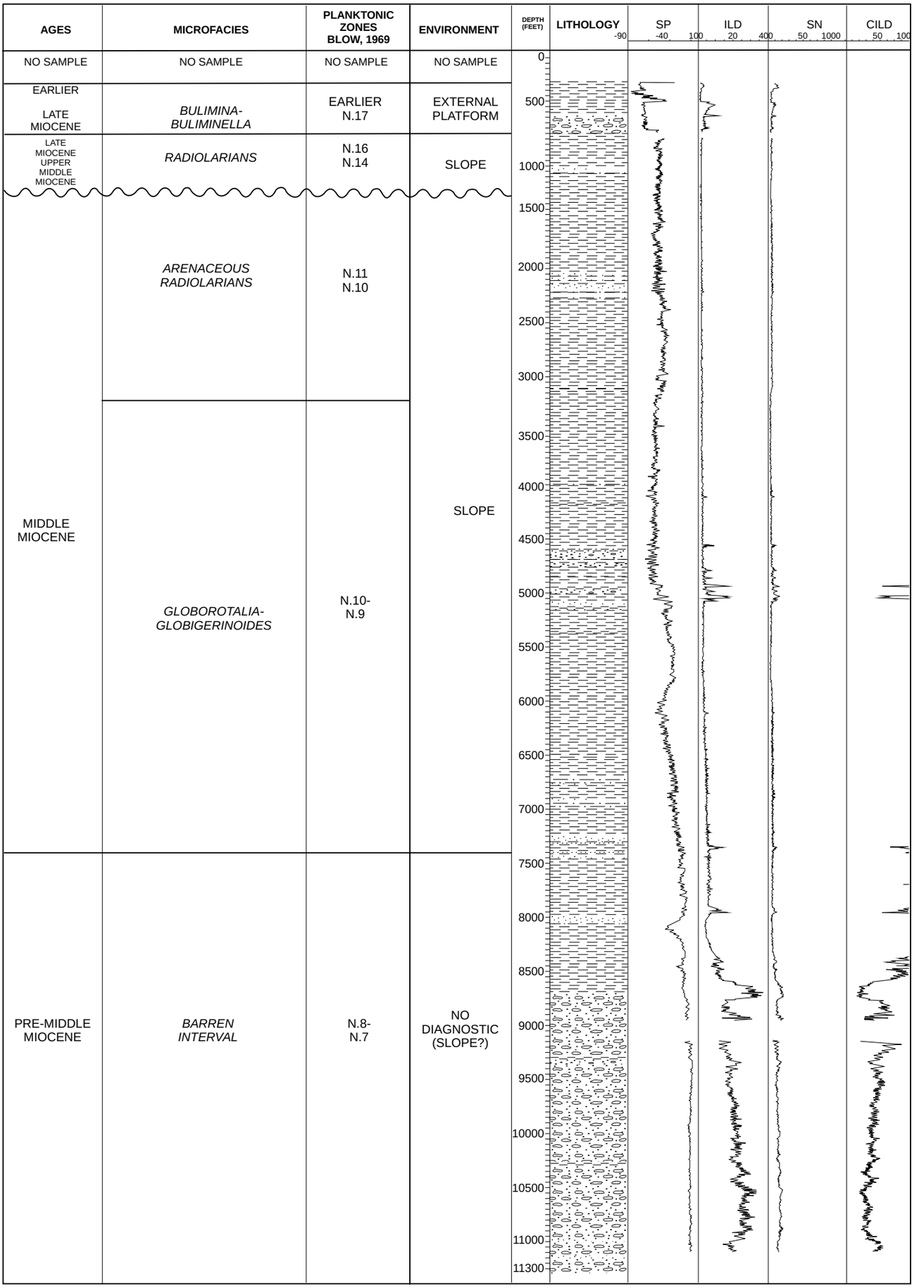

Figure 9. Tambora-1 Well Log

Stratigraphic Summary

Microstratigraphy. The microstratigraphy recognized in the four wells analyzed comprises various microfacies: Oligocene to Early Miocene; the Middle Miocene microfacies; the Upper Middle to Late Miocene microfacies, and the Late Miocene to younger microfacies.

Unconformities. The limits of the stratigraphic units appear to be unconformities and coincide with major interruptions: (1) during the Upper Oligocene in the lower portion of planktonic zone P.21, (2) during the Early Miocene, (3) during the Middle Miocene, (4) during the Upper Middle Miocene, and (5) during the Upper Miocene. These correspond to major hiatuses registered in the oceans and to regional unconformities produced by tectonic and erosive events that are observable in the surface stratigraphy.

Environment. The environmental succession indicates: (a) a deep sequence (slope) of Oligocene to Upper Middle Miocene age, and (b) a younger sequence (slope to shelf) of Upper Middle Miocene to Upper Miocene age and younger sequences.
In the evaluation of the environmental interpretation, which was previously summarized, it is necessary to take into account the following aspects:

- The information given by the studied well samples represents only a partial knowledge of the basin; thus the extrapolation of these interpretations may lead to generalizations and errors.

- Paleoenvironmental interpretations obtained from microfauna, particularly the planktonic one (foram and radiolaria in the lower sections of the Majagua and Remolino Grande wells), are associated to the lower portion of a slope, taking into account their abundance and poor representation of benthonic fauna. However, being possible this evaluation, it is not conclusive for a slope-outer shelf section when it lacks enough support of benthonic fauna.

- In general, slope and outer platform environments are affected by water volume dynamics (bottom, intermediate or surface), which are rich in oxygen and carry plankton and planktonic microfauna. For this reason they prevent the preservation of organic matter and generate physical and chemical interactions with streams coming from the continent.

- The stratigraphic record of the studied wells lacks enough information to confirm or refute the occurrence of reworked fauna.

Well Stratigraphic Correlation

As a result, and for purposes of a coherent correlation of the four wells under study, four time units or events were selected, units limited by hiatuses and erosion surfaces, to characterize the Late Oligocene to Early Pliocene interval, which is the predominant interval in the stratigraphy of the Colombian Pacific Realm. These events, listed from the youngest to the oldest are: (1) Late Miocene to Early Pliocene (2) Upper Middle Miocene to Late Miocene, (3) Middle Miocene, and (4) Late Oligocene to basal Middle Miocene.

Structural Geology

The structural characterization of a sedimentary basin includes the determination of its geometry and thickness, as well as of the structures that affect the basement and allows a better understanding of its evolution. This chapter contains a description of the Tumaco basin in terms of aero-gravimetric, aero-magnetometric and seismic images.

Gravimetry

The aerogravimetric and aeromagnetometric data was provided by the Agencia Nacional de Hidrocarburos (ANH). The data was collected by Carson Helicopters in 2006 and it covers the Tumaco basin and a part of the San Juan basin, as shown in Figure 10. The campaign was carried out at an altitude of 1280 m and a flight grid of 7.5 km x 10 km. The files were received in ASCII format with Magna flat coordinates.

Total magnetic intensity (TMI) values, the Bouguer gravimetric anomaly (BGA) (p=2.67 gr/cm3), and the Free Air anomaly were used to generate the total magnetic intensity maps, the reduction to the magnetic pole, the Bouguer anomalies, and the Free Air gravimetric anomalies.

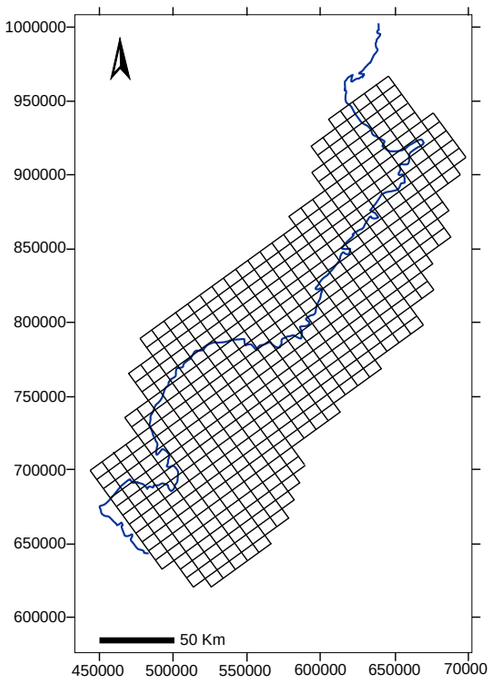

Figure 10. Location of the data grid used for the geophysical modeling.

Bouguer Anomaly Map (BGA) (p=2.67 gr/cm3)

The Bouguer anomaly map was generated using the minimum curvature interpolation method (Figure 11). Given the reference density value (p=2.67 gr/cm3), this map is more adequate for understanding the onshore Bouguer anomaly; in the case of the offshore area, the Free Air anomaly map, included below, was used.

The interpretation of the Bouguer anomaly map was supplemented with gravimetric profiles to which an inverse modeling was applied in order to obtain the gravimetric basement profile that adjusts best to the observed values. The inverse profiling modeling was carried out using a program developed by ICP (Research Group for Reduction of Exploratory Risk). This program is based on the determination of the Fourier transform for a set of data (x,z) according to the equation proposed by Parker (1973) and improved by Oldenburg (1974) in order to make it more iterative. This equation calculates the shape of a body on the basis of its anomaly. The program builds the relief function that best adjusts to the Bouguer anomaly profile, prior determination of certain parameters such as density contrast, separation of input data, and topographic inversion level (z0). Figure 12 shows the gravimetric basement modeling for two profiles in the basin. These profiles were used to generate the two schematic sections.

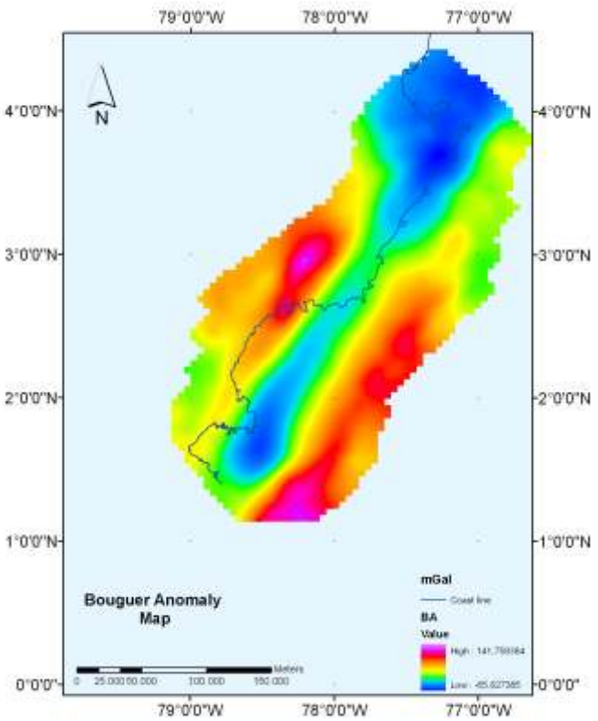

Figure 11. Bouguer anomaly map for the Tumaco basin.

Gravimetric Profile
Southern Tumaco Basin

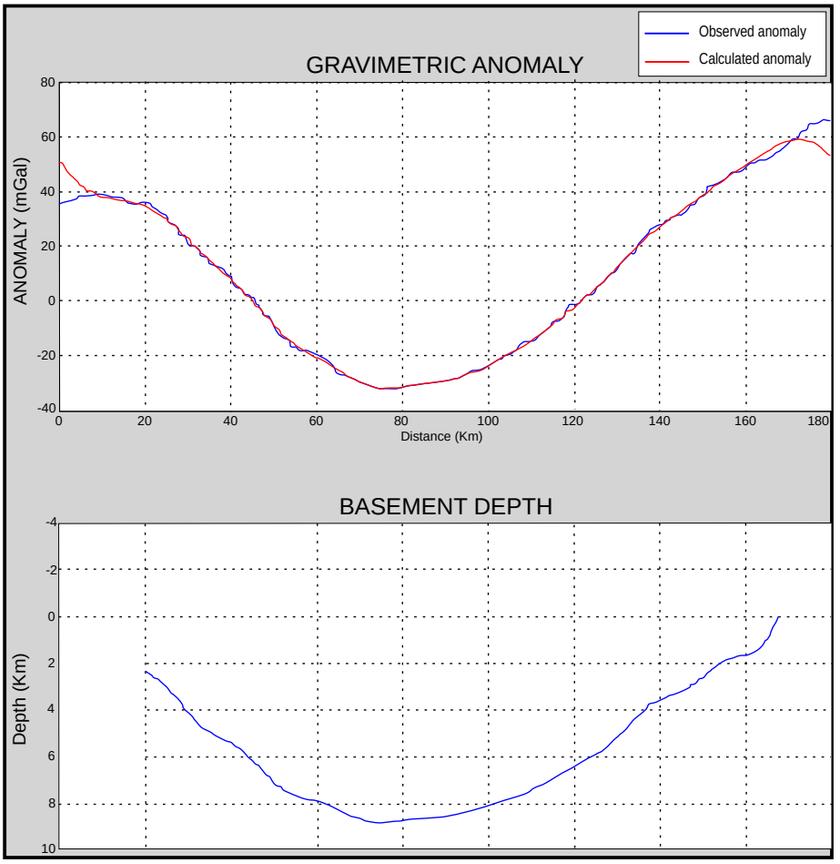

Gravimetric Profile
Northern Tumaco Basin

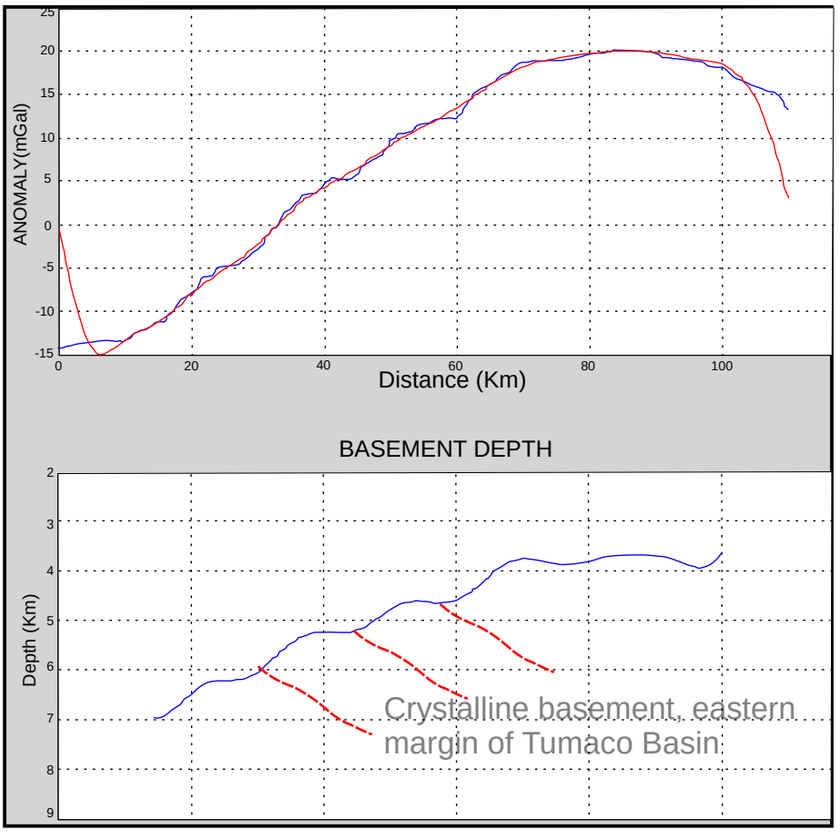

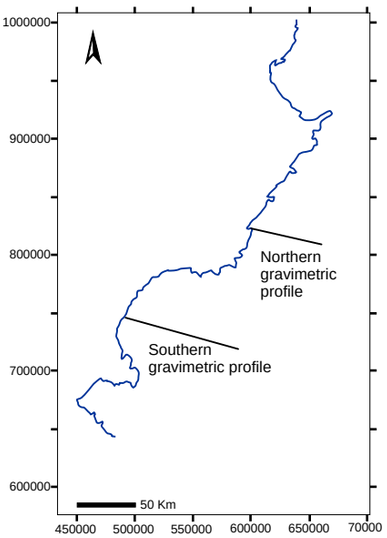

Figure 12. 2D model of basement inversion based on Bouguer gravimetric profiles.

Free Air Gravimetric Anomaly Map

The Free Air anomaly map was obtained in a way similar to that of the Bouguer anomaly map, using the minimum curvature method as the interpolation algorithm. This map, shown in Figure 13 is used for the interpretation of the offshore variation of the gravitational field.

Magnetometry

The total magnetic intensity map (TMI, Fig.14) and the Reduction to the Magnetic Pole Map (Fig. 15) were developed on the basis of aeromagnetometric data (acquired by ANH 2005), and it is being used to generate magnetometric profiles in order to analyze the magnetic basement structures. Likewise, estimates of the basement depth are being made in order to compare it with the gravimetric results. Once both the gravimetric and magnetometric profiles are obtained, along with the gravimetric basement map, they will be integrated with all of the structural, geochemical, stratigraphic, and surface geology information, in order to build a model of the tectonic evolution of the basin.

Magnetometric Derivatives Maps

In order to highlight the magnetic susceptibility contrast areas, which will be used to identify discontinuities in the magnetometric basement, horizontal magnetometric derivatives maps were generated in different directions, NS, EW, N45E, and N45W. These, together with the above-mentioned maps, were used to draw the basement faults shown on the N45W magnetometric derivative map (Figure 16).

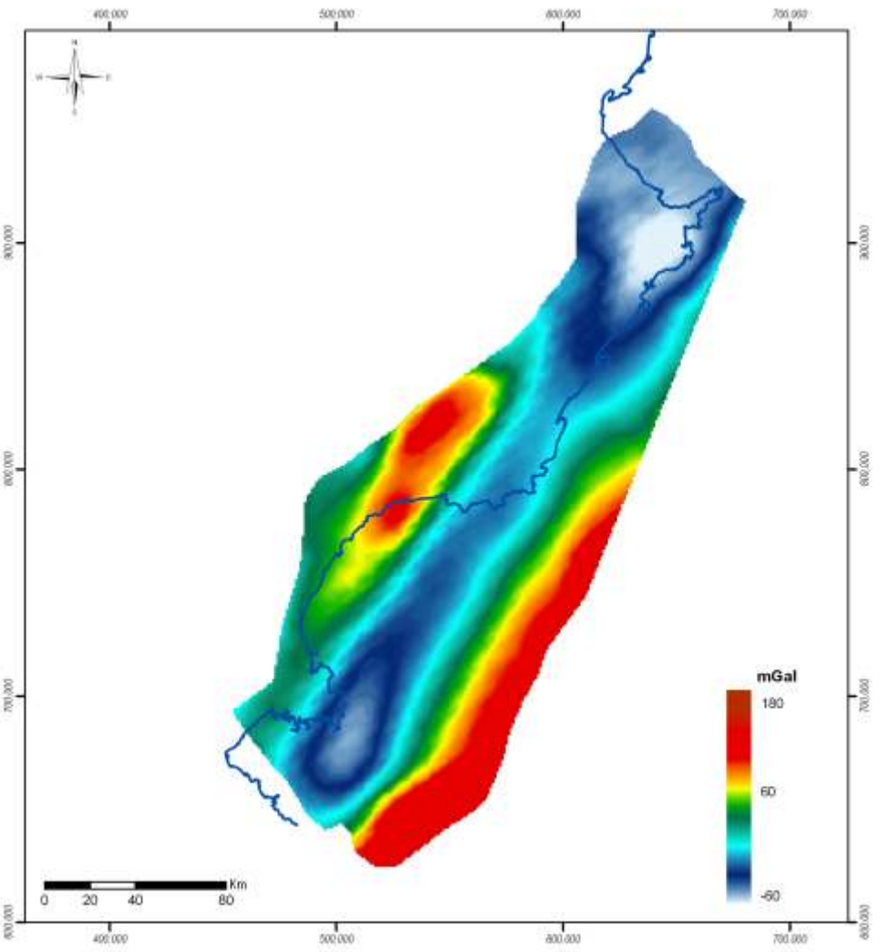

Figure 13. Free Air Gravimetric Anomalies Map.

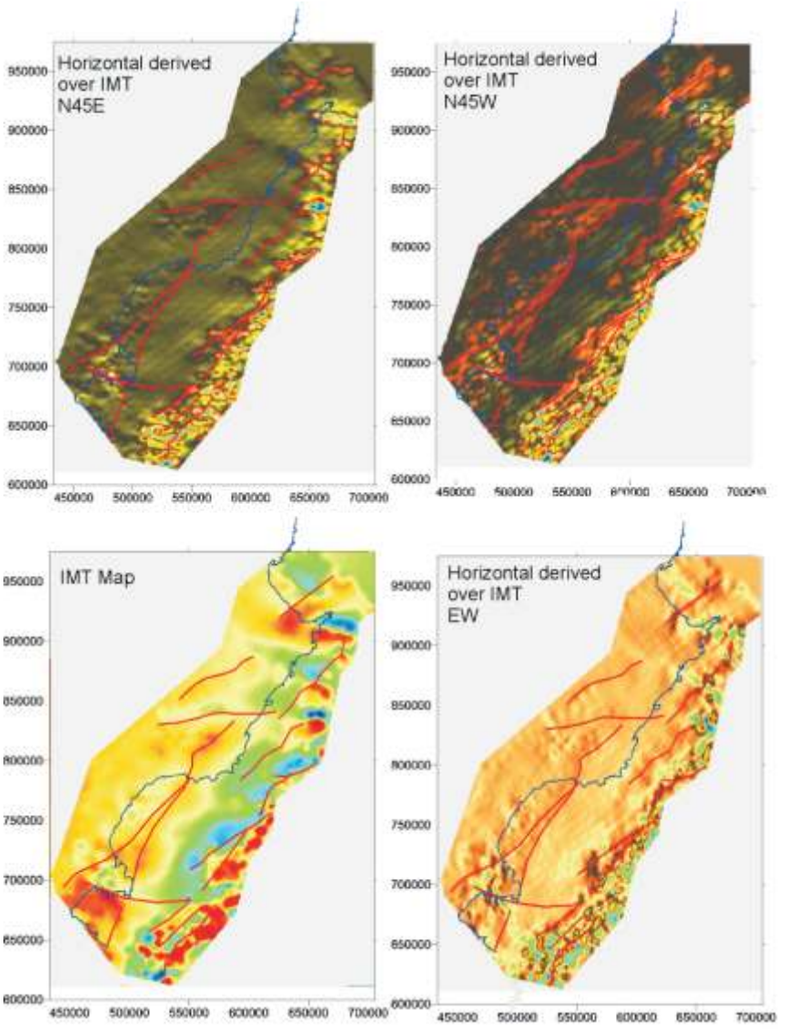

Figure 14. Total Magnetic Intensity Map.

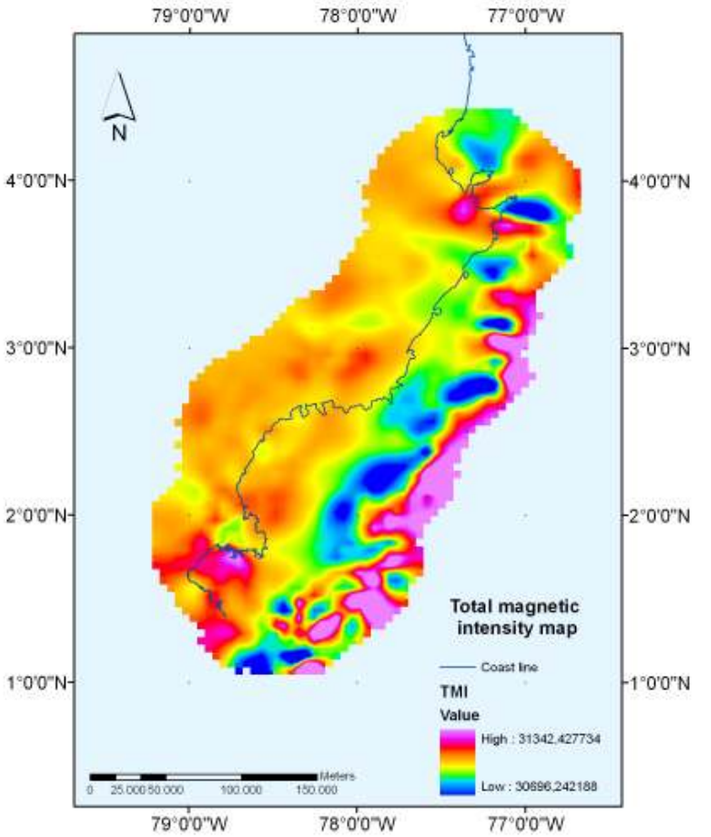

Figure 15. Total magnetic intensity map of Tumaco basin.

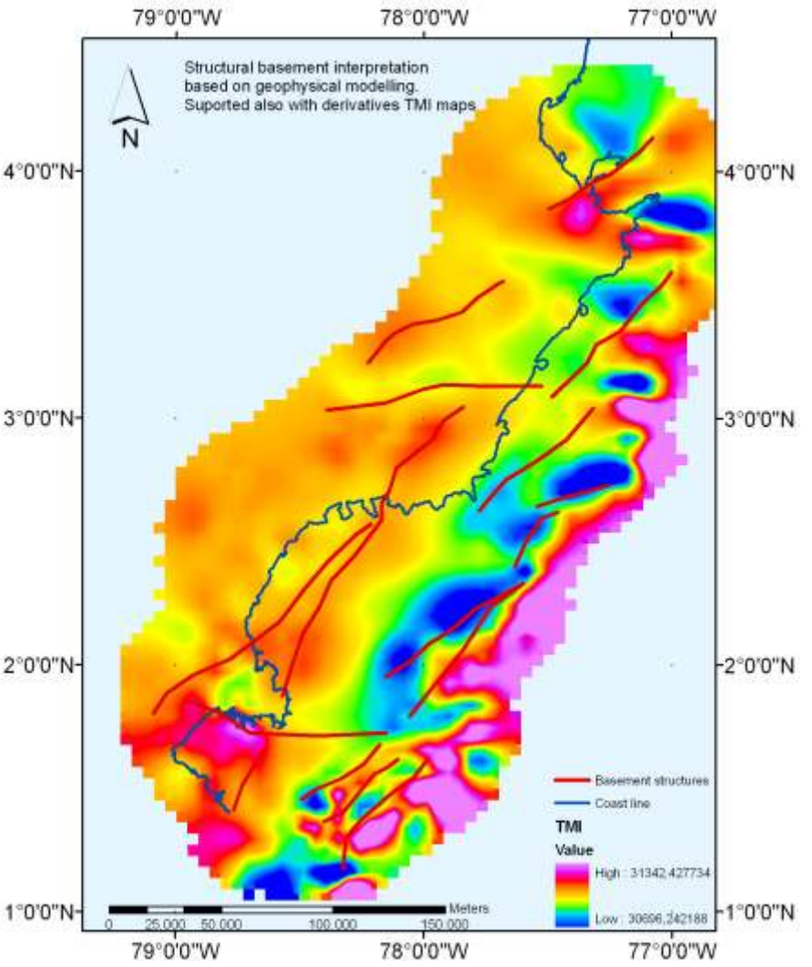

Figure 16. Magnetometric derivative map.

Seismic Interpretation

Figure 17 summarizes the available seismic programs, the interpreted lines and the location of the wells in the Tumaco basin.

The Offshore Sections

SEISMIC SECTION L-1973-43 (TAMBORA-1 WELL)

In the Tambora-1 well, the reflectors correspond to the Neogene and Paleogene sequences. Lower reflectors were interpreted as corresponding to the top of the Cretaceous basement. The seismic section shows a mainly compressive (transpressive?) system. Folds due to fault propagation associated with high-angle faulting in the basement were also interpreted in this section. Additionally, mud diapirism (2) and a negative flower structure were interpreted in the Cretaceous basement (Figure 18).

SEISMIC SECTION L-1973-58 (SANDI-1 WELL)

In the Sandi-1 well, the reflectors correspond to Neogene rocks. Lower reflectors were interpreted as corresponding to the base of the Miocene. Although reflectors corresponding to the top of the Cretaceous basement were also interpreted, the position of the latter is somewhat less reliable than in the previous section. The folds are of the low-angle fault propagation type and detachment folds (Figure 19).

SEISMIC SECTION L-1973-D03

This section contains the complete sequence starting from the Cretaceous basement. The most outstanding feature of this section is a horst in the Cretaceous basement, with a greater subsidence in the southern section. In the northern section, a positive flower structure was interpreted in the Cretaceous basement (Figure 20).

The three seismic sections that were interpreted are good representatives of the compressional component (sections 43 and 58) and the extensional component (section D03) of a transcurrent system (strike-slip).

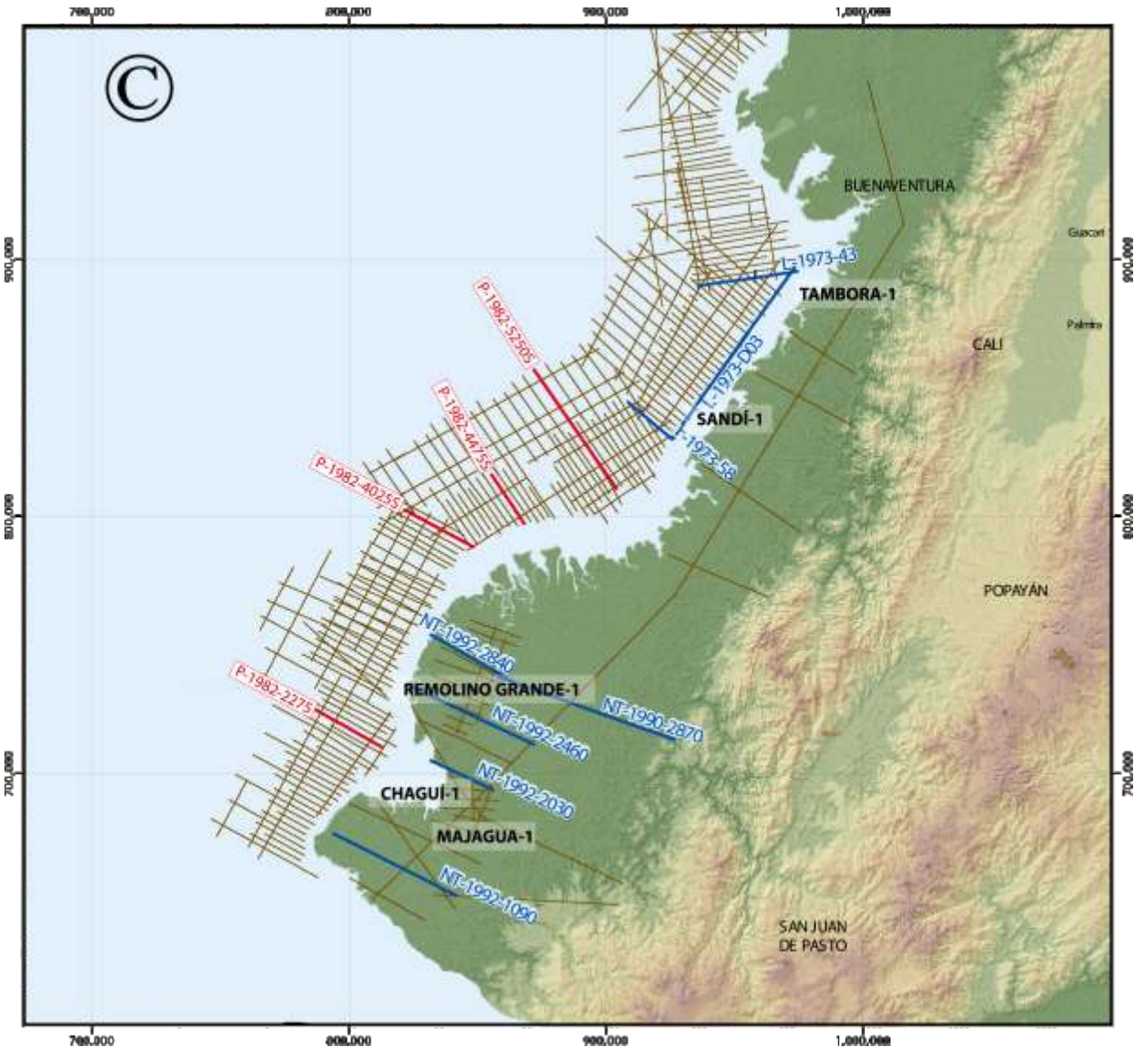

Figure 17. Map showing the location of seismic lines and wells.

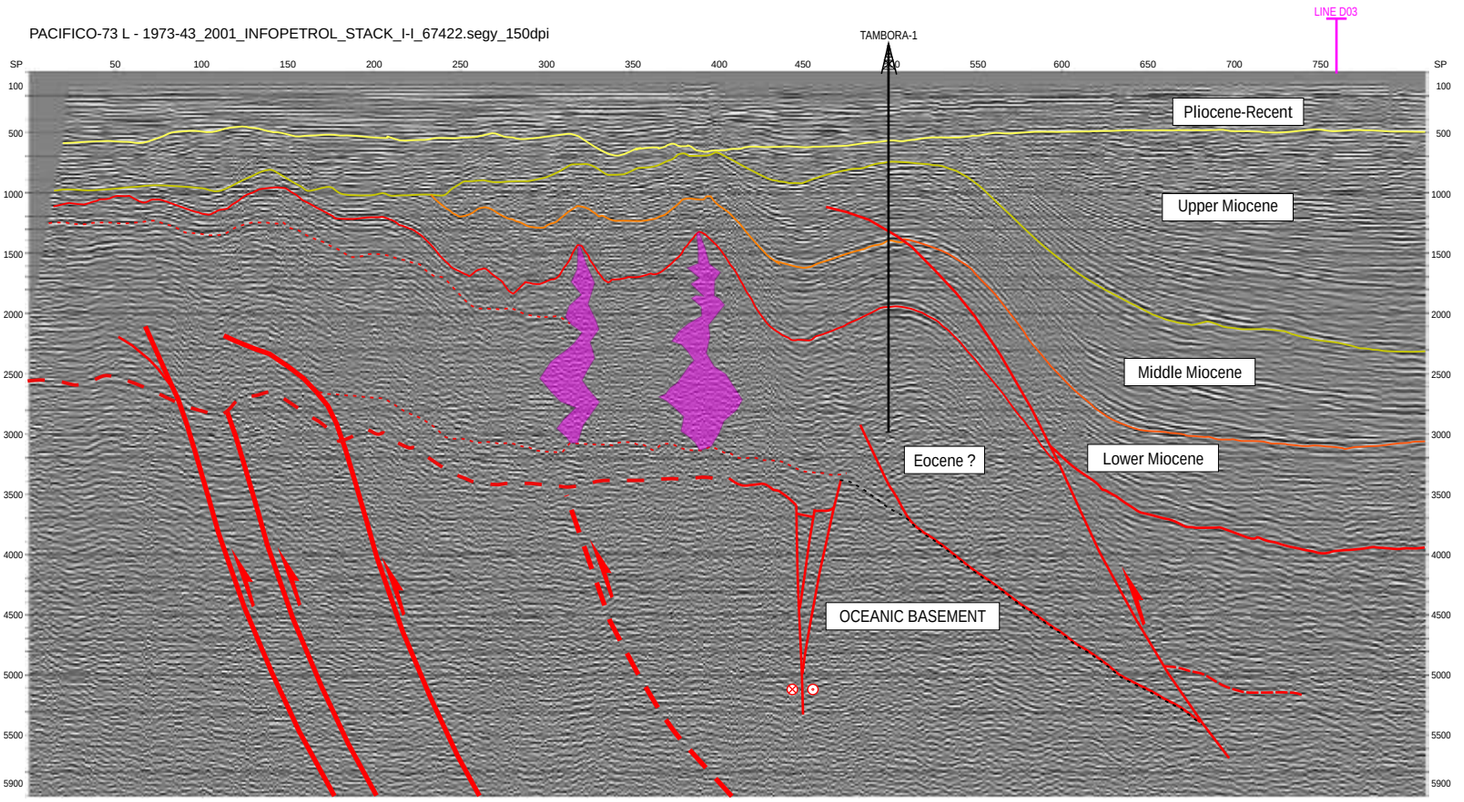

Figure 18. Interpretation of seismic section L-1973-43 (Tambora-1 well)

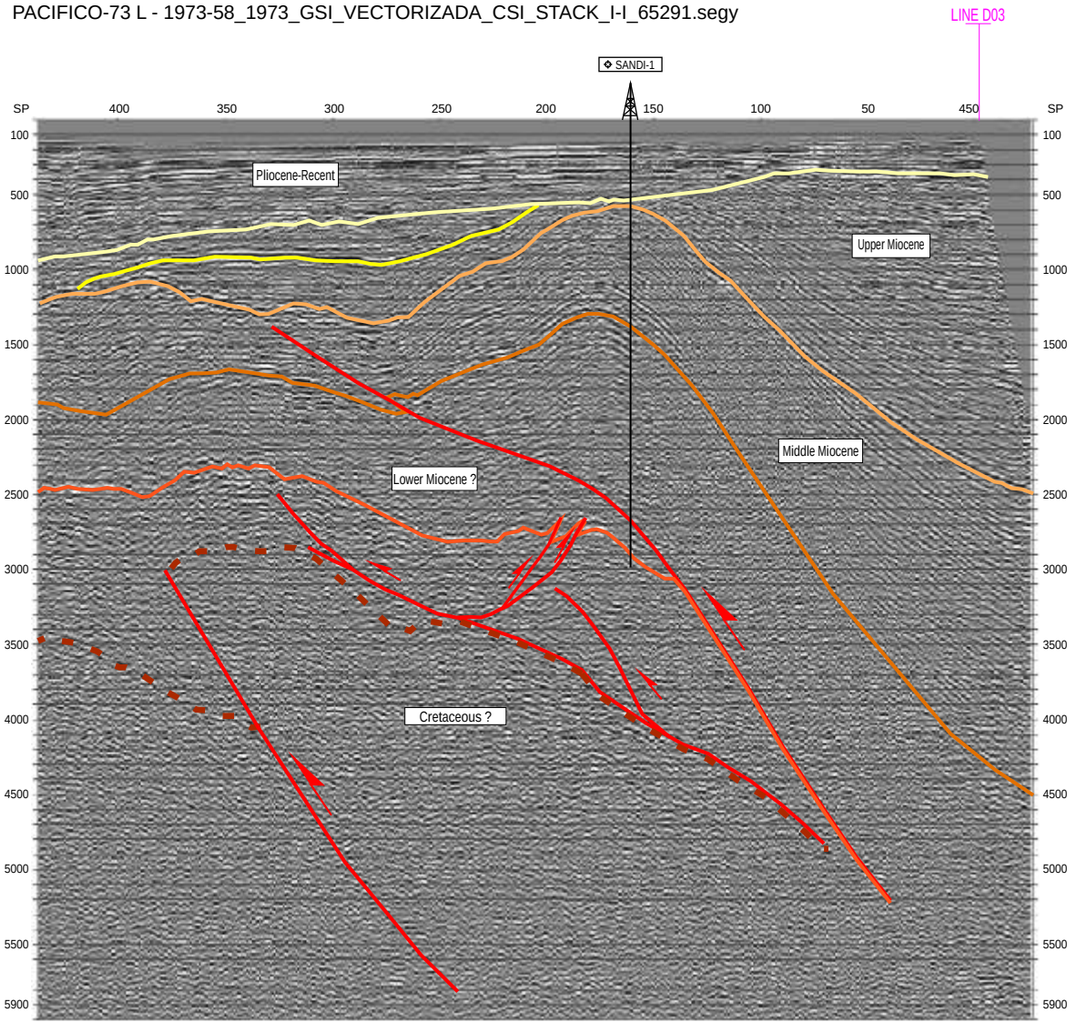

Figure 19. Interpretation of seismic section L-1973-58 (TSandi-1 well)

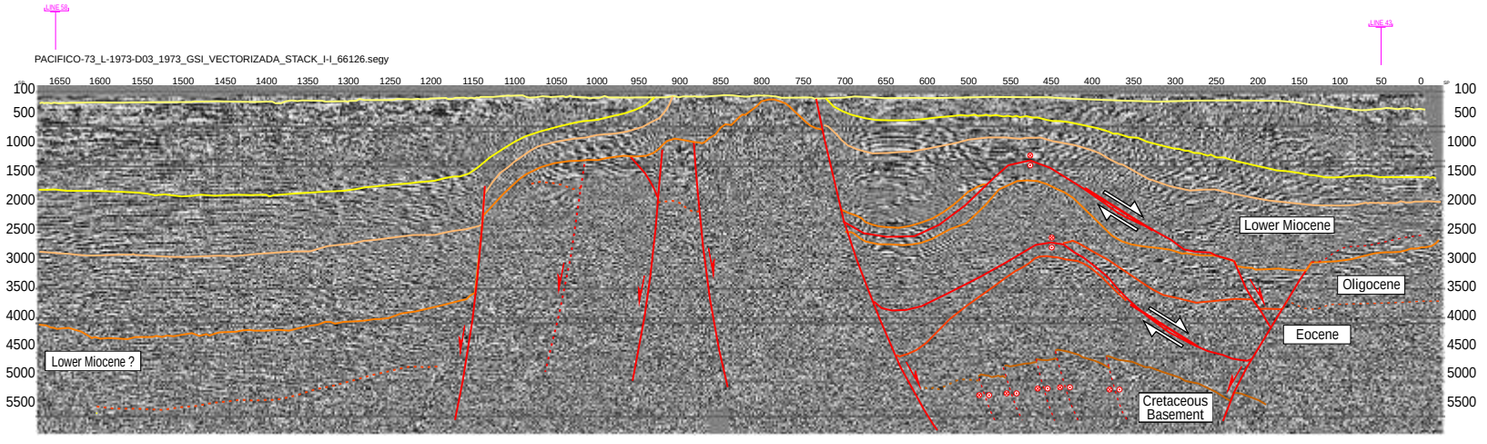

Figure 20. Interpretation of seismic section L-1973-D03

SEISMIC SECTION P-1982-5250S

In this seismic section grabens and horst were interpreted and they represent two transtensive episodes: (1) a pre-Miocene and (2) another Pliocene to recent episode. Due to the poor quality of the section, the interpretation below the sub-Pliocene unconformity is highly speculative (Figure 21).

SEISMIC SECTION P-1982-4475S

In this section a horst was interpreted; it represents (1) a transtensional episode from early Miocene to medium-Miocene and (2) a local tectonic inversion episode during late Miocene (Figure 22).

SEISMIC SECTION P-1982-4025S

In this section three anticlines were interpreted; they are associated with antithetic thrusts to a main surface with eastern vergence. The interpreted structures represent (1) an extension episode during lower Miocene and (2) a Pliocene tectonic inversion (Figure 23).

SEISMIC SECTION P-1982-2275S

In this seismic section a superposition of at least three tectonic episodes was interpreted: (1) an extension episode during Oligocene; (2) local tectonic inversion, which occurred from lower Miocene to medium Miocene; (3) an incipient transtension after late Miocene. (Figure 24).

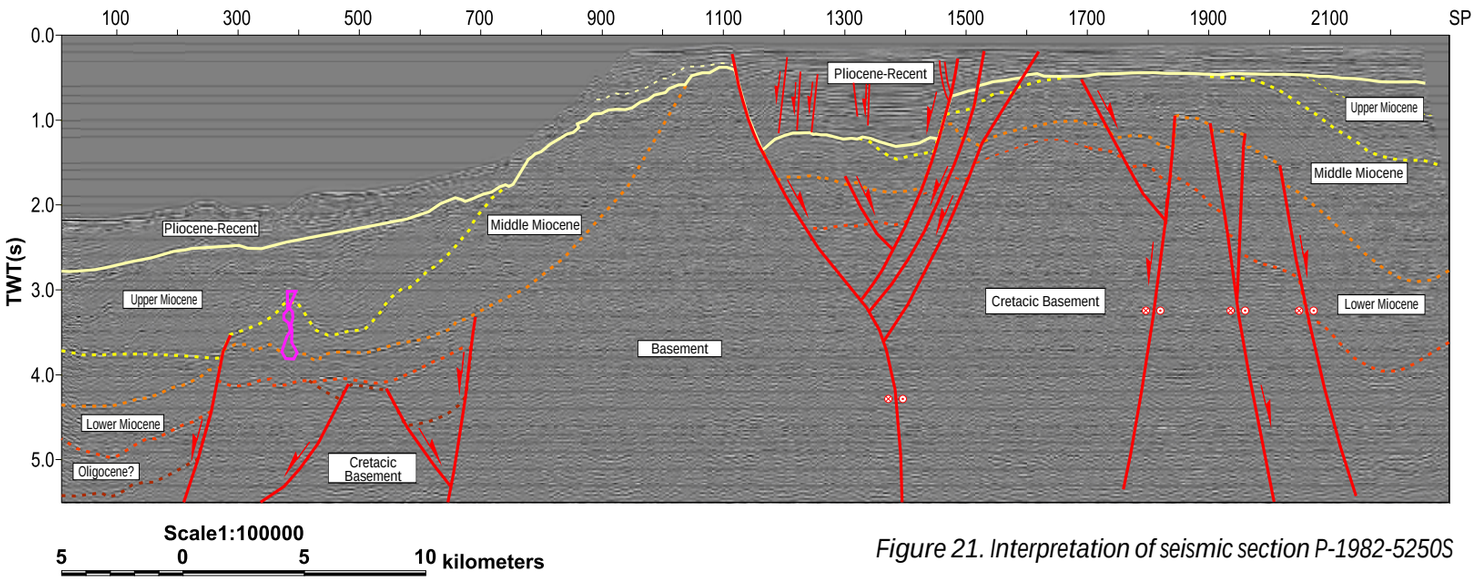

Figure 21. Interpretation of seismic section P-1982-5250S

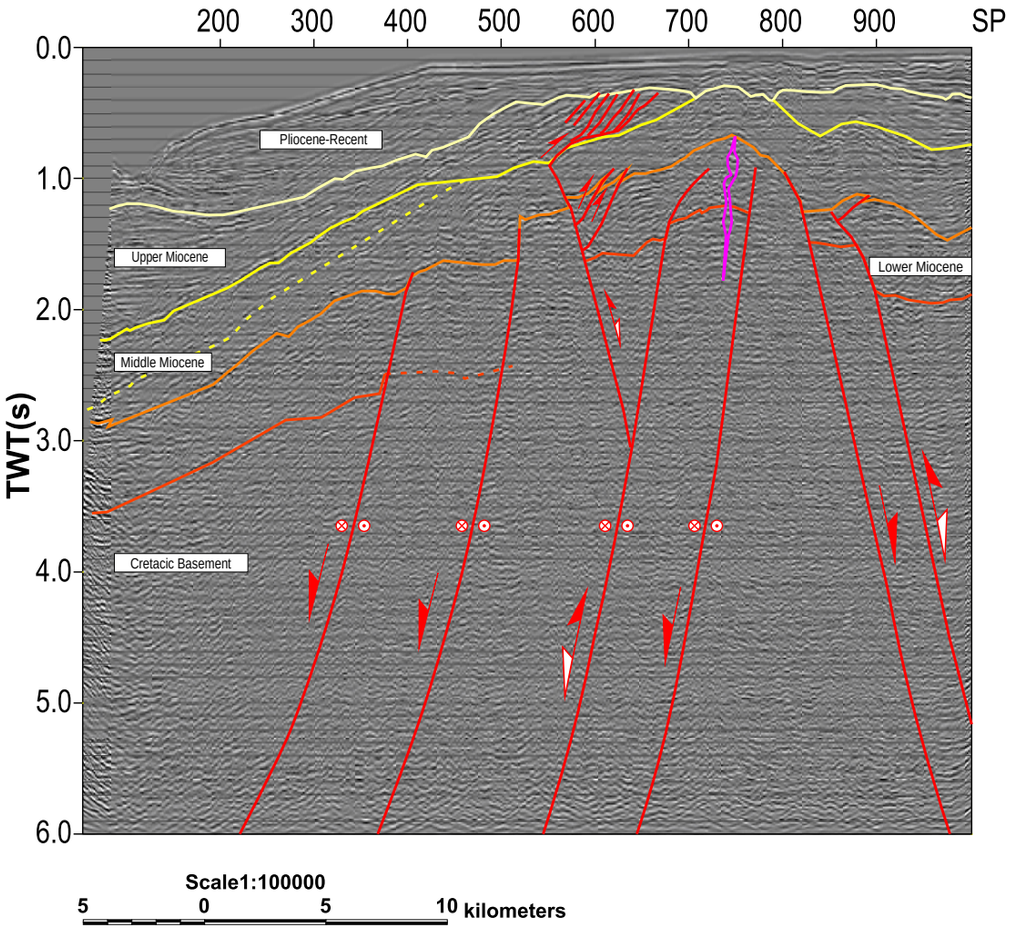

Figure 22. *Interpretation of seismic section P-1982-4475S*

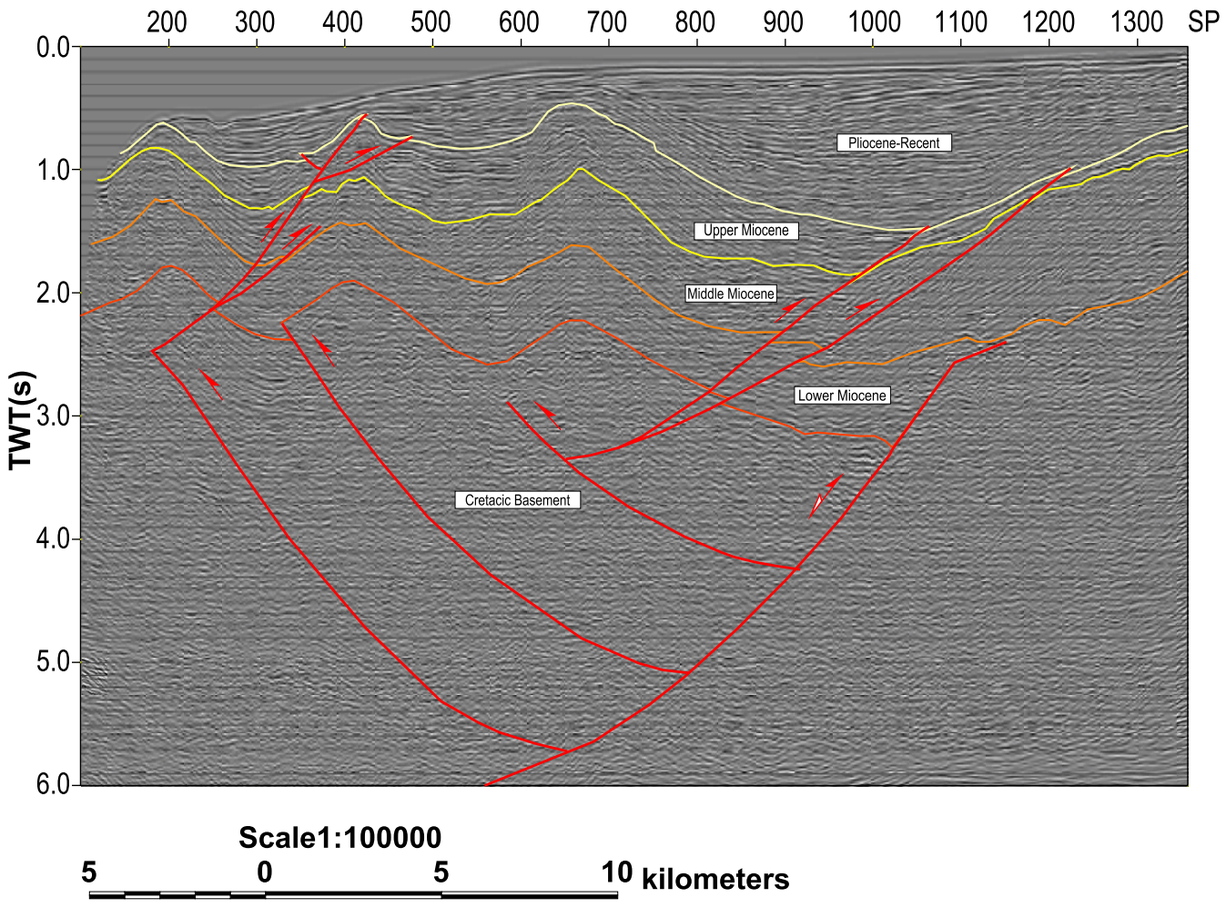

Figure 23. Interpretation of seismic section P-1982-4025S

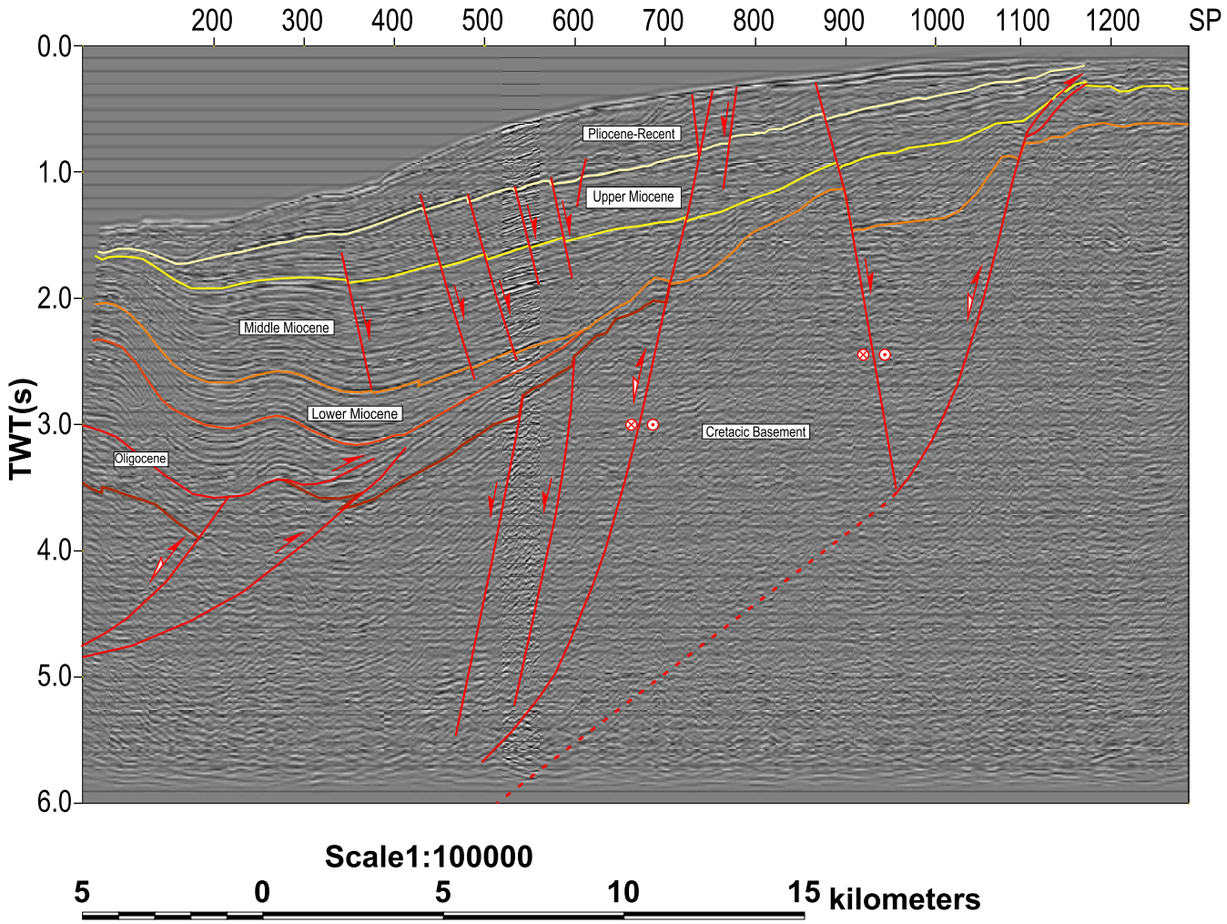

Figure 24. Interpretation of seismic section P-1982-2275S

The Onshore Eastern Sections (After the Seismic Atlas of Colombia)

These sections show a sedimentary sequence, ranging form Oligocene to Pliocene, overlying the Cretaceous basement. All of the sections of the onshore sector (south) illustrate a distensive regime that is coetaneous with the sub-Pliocene sequence.

SEISMIC SECTIONS NT-1992-2840 AND NT-1990-2870
These two sections close to the Remolino Grande-1 well show the symmetric geometry of the basin, between two basement highs. In section NT-1990-2870 it is possible to observe onlaps on the basement (Oligocene to Lower Pliocene), pinchouts (Upper Miocene), and a deltaic sequence (Upper Pliocene) in a quiescent structural regime in which subsidence phenomena predominate, subtly deformed by rollover folds associated with normal faulting (Figure 25 and 26).

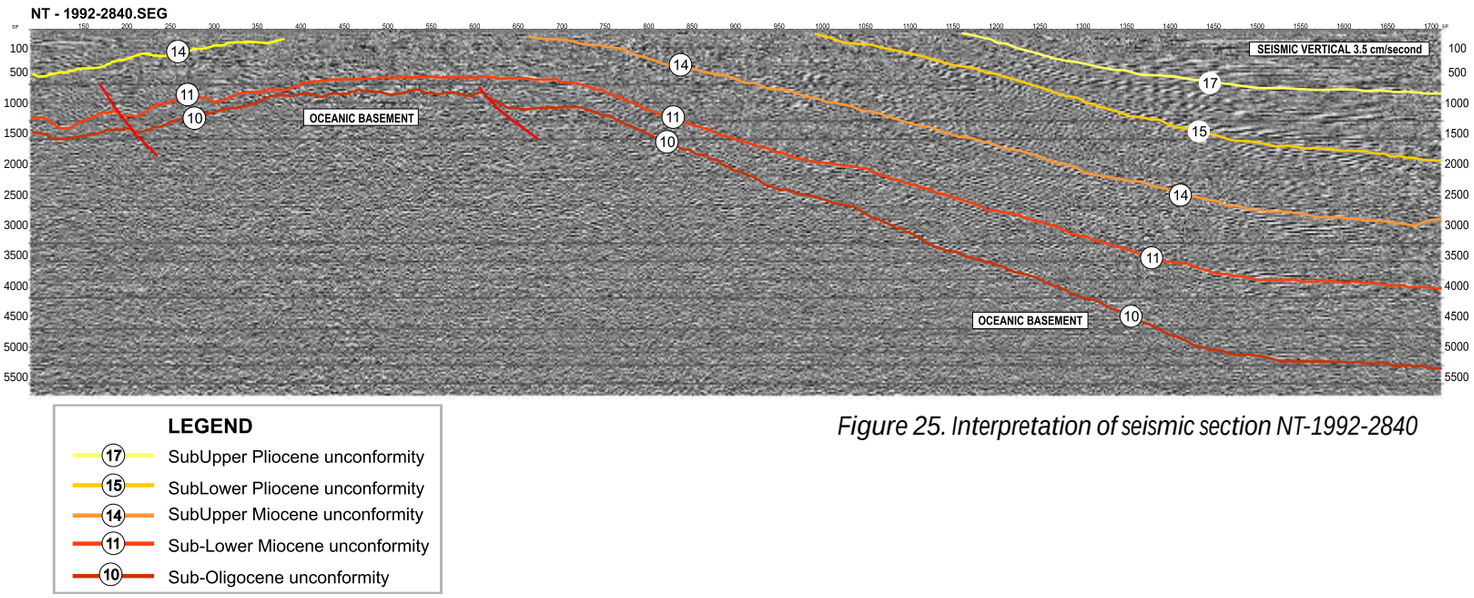

Figure 25. Interpretation of seismic section NT-1992-2840

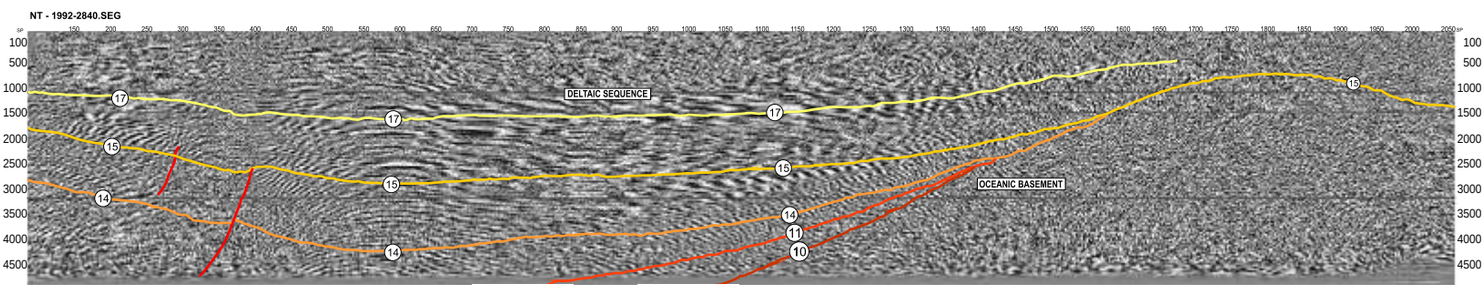

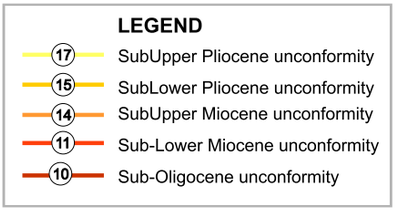

Figure 26. *Interpretation of seismic section NT-1990-2870*

SEISMIC SECTION NT-1992-2460

This section, which is consistent with the previous ones, features a basement high to the West. The normal faulting indicates extension during the Lower Miocene and the Pliocene (Figure 27).

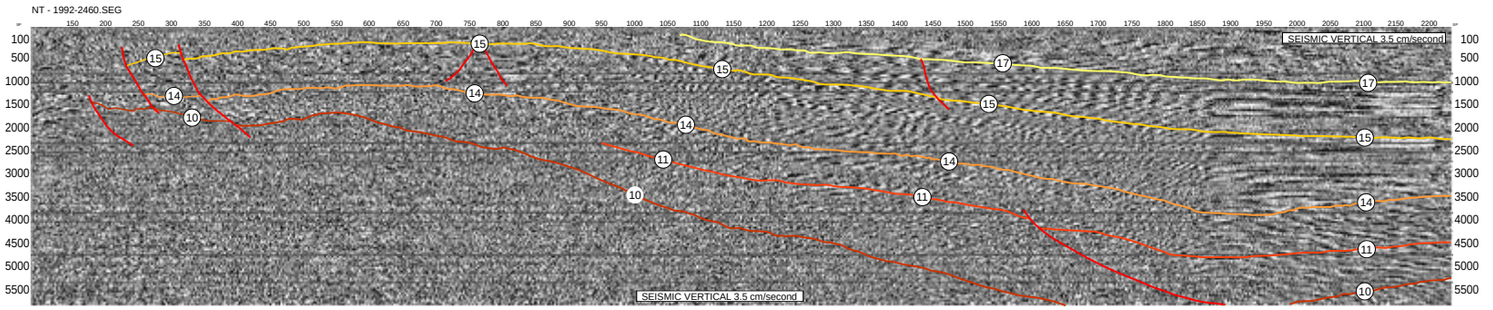

LEGEND

- 17 SubUpper Pliocene unconformity
- 15 SubLower Pliocene unconformity
- 14 SubUpper Miocene unconformity
- 11 Sub-Lower Miocene unconformity
- 10 Sub-Oligocene unconformity

Figure 27. Interpretation of seismic section NT-1992-2460

SEISMIC SECTION NT-1992-2030

In this section, a fold associated with mud diapirism or, possibly, a local tectonic reactivation in the basement (?) was interpreted. (Figure 28).

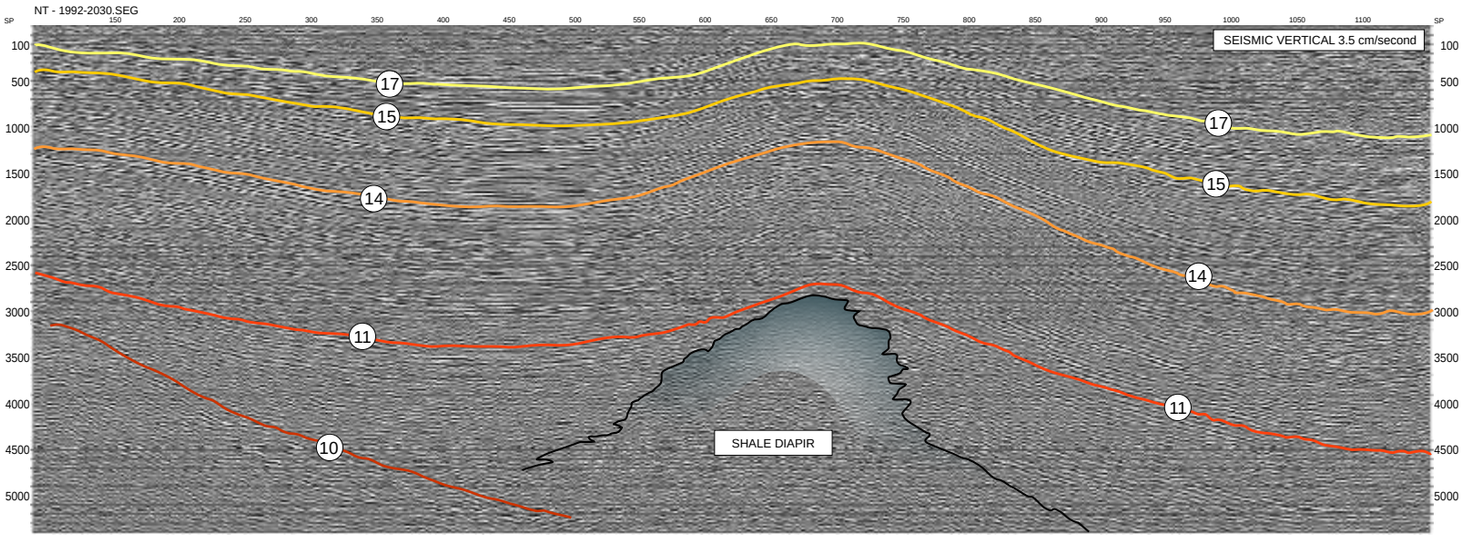

LEGEND

- 17 SubUpper Pliocene unconformity
- 15 SubLower Pliocene unconformity
- 14 SubUpper Miocene unconformity
- 11 Sub-Lower Miocene unconformity
- 10 Sub-Oligocene unconformity

Figure 28. Interpretation of seismic section NT-1992-2030

SEISMIC SECTION NT-1992-1090

This section illustrates a notoriously distensive regime with horst structures in the basement. Additionally, the existence of mud diapirism is postulated (Figure 29)

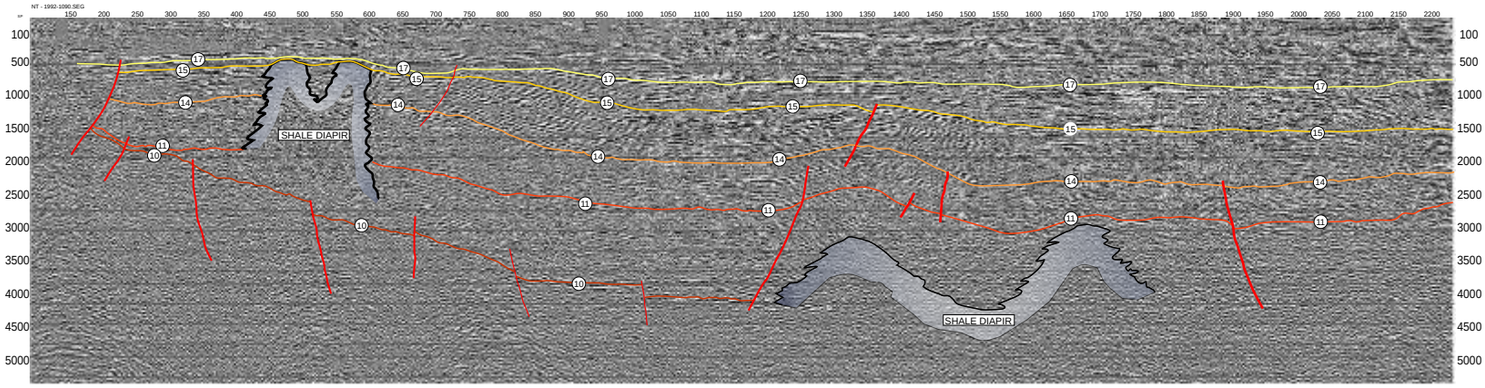

LEGEND

- 17 SubUpper Pliocene unconformity
- 15 SubLower Pliocene unconformity
- 14 SubUpper Miocene unconformity
- 11 Sub-Lower Miocene unconformity
- 10 Sub-Oligocene unconformity

Figure 29. Interpretation of seismic section NT-1992-1090

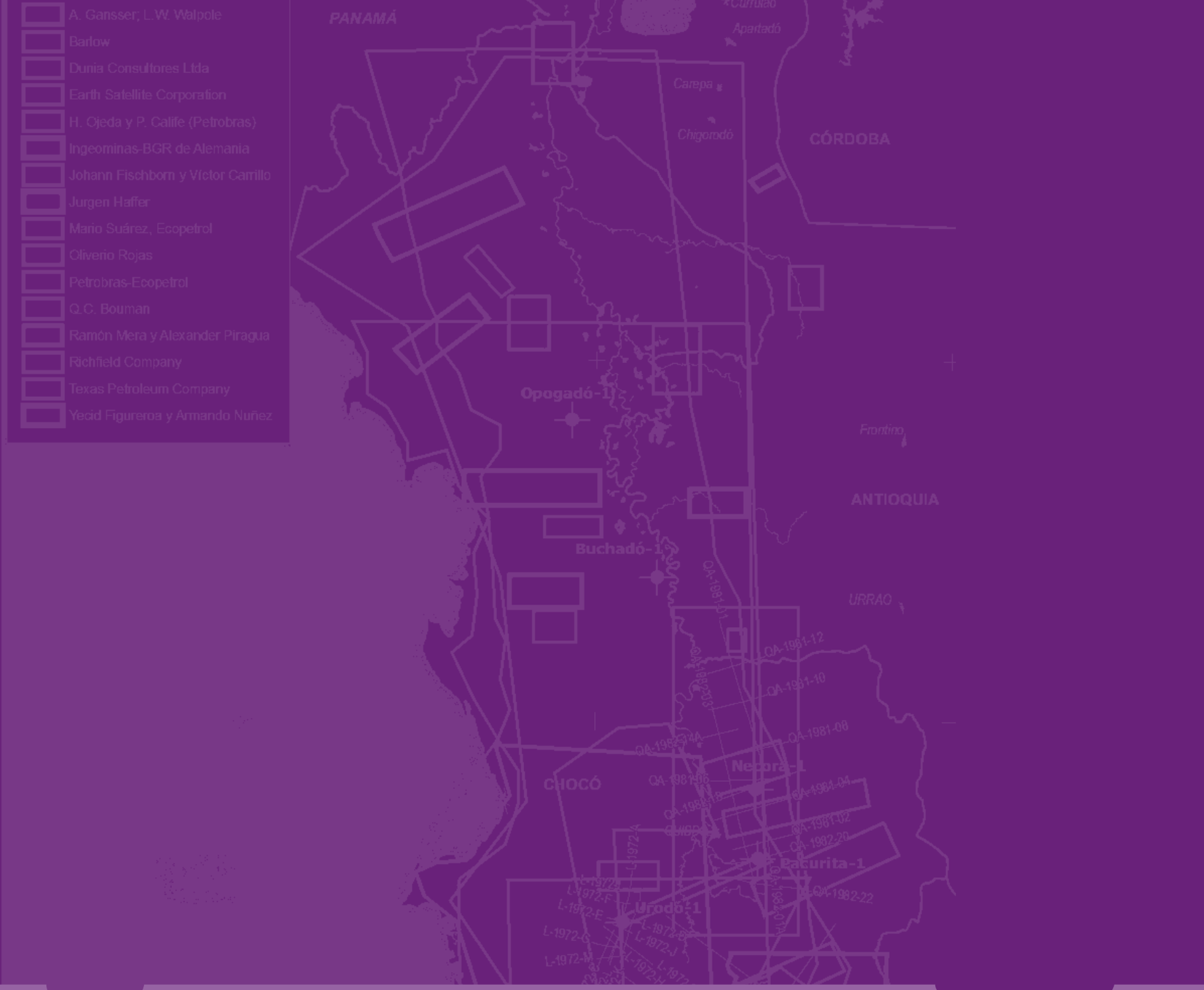

3. TECTONIC EVOLUTION OF THE TUMACO BASIN

3. TECTONIC EVOLUTION OF THE TUMACO BASIN

Regional Framework

In the western flank of the Western Cordillera a SW-NE fault pattern constitutes the eastern border of the Tumaco basin. In the Western Cordillera outcrops well-differentiated crystalline bodies; on the western border of the basin appears a magnetometric signal that is different from that of the crystalline bodies in the Cordillera.

The western margin of the Tumaco basin is delimited by a crystalline basement high (Alto de Remolino Grande) and a fault system that significantly affects the basement. This fault, which has a NS-NE bearing, crosses the Patía river delta and extends north across the sea, bordering Gorgona Island. This fault forms a border between two bodies that feature very different patterns of magnetic susceptibility, thus suggesting a division between crystalline rocks of diverse origin. This high deepens toward the West, giving way to the development of the western Tumaco basin.

The Tumaco basin is an elongated and asymmetric basin with an approximate bearing of N30E. The western margin of the basin features a steeper slope than the eastern flank. The basin becomes deeper to the southwest. Its main depocenter is found in the Tumaco Bay, to the east (on-shore), where it reaches depths close to 9 km. On the east, it is bordered by crystalline bodies that outcrop on the Western flank of the Western Cordillera. To the North of the basin, a group of sub-vertical faults give the crystalline basement a "step-down" pattern, as can be observed in Figure 4a, North profile (A-A'). The maps also show a crystalline basement high, which reaches 2 km depth and serves as a division between the depocenter of the onshore basin and the offshore basin. This high could correspond to the so-called Remolino Grande High, described by several authors.

The maps show not only that the Tumaco onshore basin becomes deeper toward the South and is slightly narrower to the North, but also that the structural style present in the basement changes. To the South it is less structured, while to the North, a group of sub-vertical faults characterizes the structural picture

In the Bouguer Anomaly Map, the basin is defined by its very low anomaly values, and in the Total Magnetic Intensity Map it shows relatively homogeneous features in its central part. Toward the flanks of the basin, the TMI values become more irregular due to the existence of faults and to the contact with bodies with a higher magnetic susceptibility.

Basin Development

A digital elevation model with a resolution of 30 meters, radar images, and the INGEOMINAS geological map (2007) were used to generate the structural surface map in scale of 1:500.000. The subsurface control of these structures was carried out on the basis of the interpretation of the gravimetry and magnetometry (see Figures 10-16).

The tectonic model of the Tumaco basin is supported by two schematic geoseismic sections (Figures 4a and 4b): 1) Section a-a´, located to the South, which includes the data from the Remolino Grande well, and 2) Section b-b´, located to the North, close to Gorgona island. This analysis included the interpretation of onshore and offshore seismic lines, the gravimetric basement inversion model (Figure 12).

The seismic, gravimetric, and magnetometric interpretation made it possible to clearly identify the Remolino Grande paleo-high, which separates the Tumaco basin into two sectors with different structural styles: 1) the onshore sector, which features inverse faulting and minor deformation; it is asymmetric, with gentle slopes and onlap type deposition on the crystalline basement that outcrops on the western flank of the Western Cordillera, known as the Dagua-Piñón terrain (Cediel et al., 2003). To the west, the basin slopes are steep and clearly delimited by the topography of the Gorgona terrain basement (e.g. Estrada, 1999: Cediel et al., 2003); 2). In the offshore sector of the basin the structural style is one of high-angle extensional faults with eastward vergence. To the north of this basin, it appears complex folding and faulting which could be indicative of the Garrapatas fault shear zone.

To summarize, the main tectonic events that contributed to the formation of the Tumaco basin are:

1. Late Paleocene-Early Eocene event (59–49 M.a.): the Dagua-Piñón terrain was accreted against the pre-existing Romeral terrain of oceanic affinity (Cediel et al., 2003).

2. Middle Eocene (45 M.a.) to Late Eocene (~37–40 M.a,) event: collision of the Gorgona terrain with the Dagua–Piñon terrain (Kerr et al., 2002; Kerr and Tarney, 2005); according to Franco and Abbot (1999), this collision ended with a jump toward the west of the trench.

3. From the end of the Eocene to the Pliocene, small metaluminous plutons with calc-alkaline characteristics related to a Chile-type arc magmatism intrude into the Dagua-Piñon terrain (Cediel et al., 2003). It is during this period that the development of the forearc-type Tumaco basin begins.

4. Oligocene – Pliocene event. The discontinuous uplift of the Western Cordillera during this subduction cycle generated at least four periods of erosion and deposition: 1) Oligocene-Miocene Event; 2) Middle Miocene– Upper Miocene Event; 3) Upper Miocene- Pliocene Event; 4) Guapi Event. These events gave origin to the thick sequences of sediments (~ 9 km) that have been deposited on the Dagua-Piñón and Gorgona terrains, forming the Tumaco onshore and offshore basin, which can be correlated to the Manglares basin in Ecuador.

PACIFIC OCEAN
Punta Ardita
Bahía de Humboldt
Punta Cabo Marzo
Punta La Tortuguera
Bahía de Cupica
Punta Nabugá
Bahía Solano
Ensenada de Utría
GOLFO DE TRIBUGÁ
Ensenada Coquí
Punta Arusí
Cabo Corrientes
Playa Nueva
Bahía Baudó
Boca Usuragá
Ensenada Docampado
Boca Hijua
Boca Orpúa
Boca Cacagual
Playa El Choncho
Qui
Uv
Qall
Sa
Pen
Ma
Siu
Si
Sil
Peu
Co
Rp
Br
Is
QTt
My
Ci
SAN JUAN
SISTEMA DE FALLAS GARRAPATAS
Mutatá
Dabeiba
Cañasgordas
BETULIA
CONCORDIA
SALGAR
EL CARMEN DE ATRATO
HISPANIA
BETANIA
MISTRATÓ
PUEBLO RICO
SANTUARIO
LA CELIA
BALBOA
SAN JOSÉ DEL PALMAR
EL ÁGUILA
ANSERMANUEVO
EL CAIRO
ARGELIA
CARTAGO
TORO
VERSALLES
OBANDO
EL DOVIO
BOLÍVAR
Tuluá
San Pedro
N
25
50
km

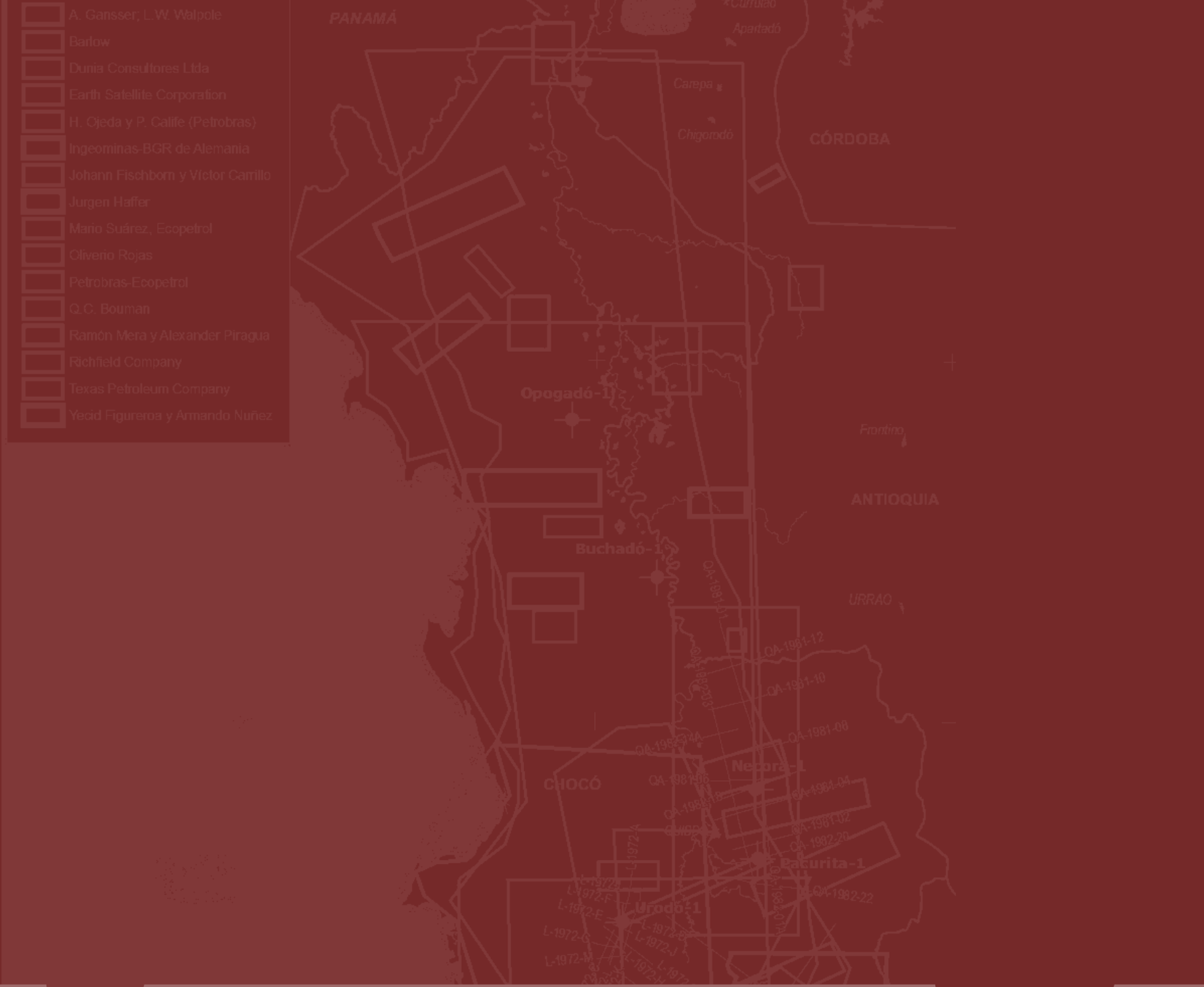

4. PETROLEUM GEOLOGY

4. PETROLEUM GEOLOGY

Geochemistry

The characterization of the source rock was carried out on the basis of 115 rock samples collected at the Sandi-1, Majagua-1 and Tambora-1 wells, in order to define the generating potential and the level of maturity.

Sixteen samples from the Sandi-1 well, 93 samples from the Majagua-1 well, and 5 samples from the Tambora-1 well were analyzed; the interpretation corresponds to results of the pyrolysis and total organic carbon (TOC) analyses.

Taking into account that the precise location of the analized samples in the stratigraphic column of each well is not known, laboratory results cannot be generalized for the entire stratigraphic sequence. However if in the evaluation of the laboratory results the possibility is considered that currents existed which brought continental organic matter and increased the environment energy and brought oxygen, it would be possible to explain the predominance of kerogen II and III as consequence of the degradation of type II organic matter (of predominantly marine origin).

Geochemical Characterization of the Rocks

The geochemical characterization was carried out for samples collected at the Majagua-1, Sandi-1, and Tambora-1 wells. Graphs were drawn differentiating each one of the formations by series in order to observe changes in the geochemical characteristics throughout the sequence.

Thermal Maturity

The level of maturity of the samples evaluated in the three wells is immature overall, with the exception of a few samples from the Sandi-1 and Majagua-1 wells, which can be located at the beginning of the oil generating window. Figure 30.

Types of Kerogen

The type of kerogen evaluated in the three wells is generally of type III/IV, of predominantly continental origin with a potential for gas generation; however, some of the samples collected at the Majagua-1 well correspond to a mixed type II/III kerogen, with generating potential for oil and gas. Figure 31.

Generating Potential

The sequence analyzed in the three wells features a potential that varies from poor to average, but some of the samples collected at the Majagua-1 well show excellent organic content, with values ranging from 2 to 16 %. Figure 32.

Production Index

The maturity vs. production index graph defines the following aspects:

- The sample belonging to the Tambora -1 well shows contamination due to hydrocarbons not generated in situ.
- A high percentage of the samples from the Sandi-1 well are located in the early expulsion zone for liquid hydrocarbons. In spite of the fact that a high percentage of the samples from the Majagua-1 well are located in the early expulsion zone for liquid hydrocarbon, the conversion-expulsion level is low. Figure 33.

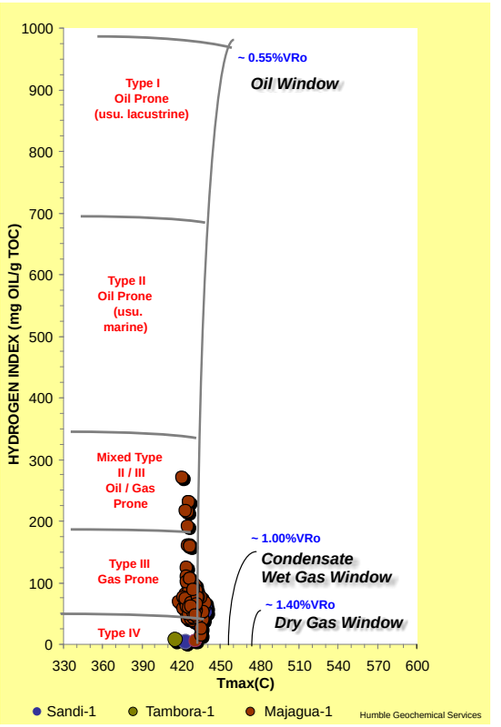

Figure 30. Tmax Diagram vs. Hydrogen Index

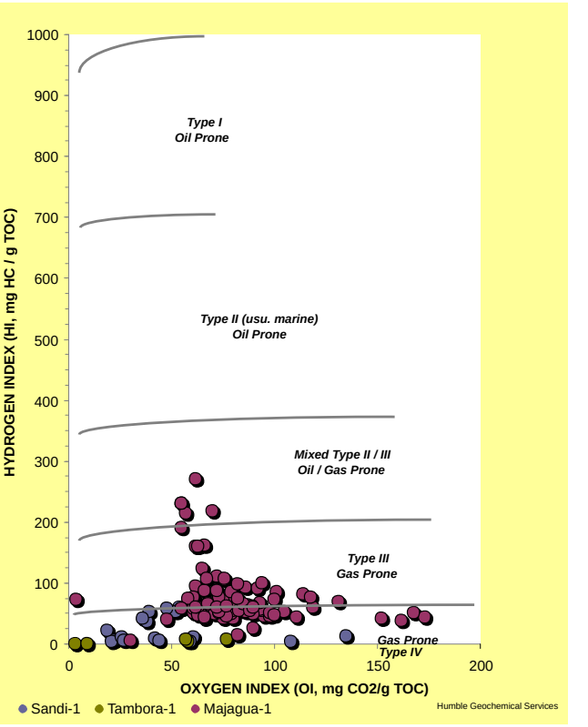

Figure 31. Van Krevelen Diagram

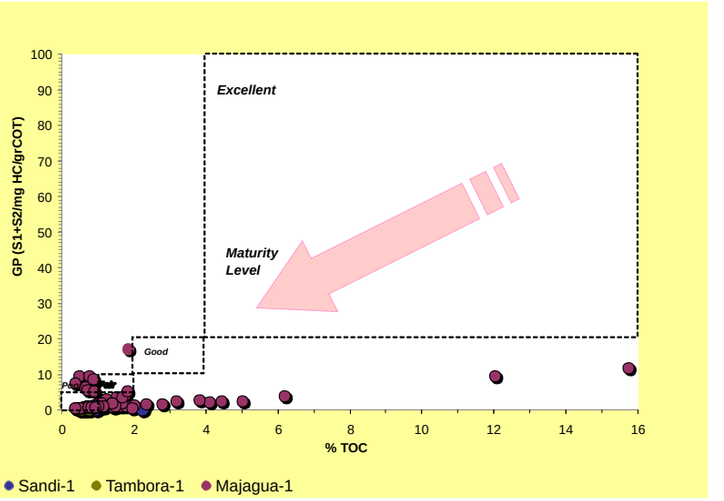

Figure 32. Genetic Potencial vs. TOC

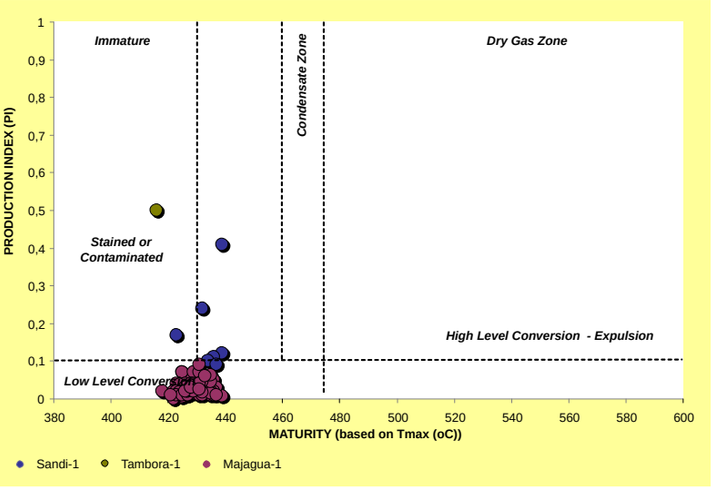

Figure 33. Production Index vs. Maturity Diagram

Organic Petrography

In order to corroborate the maturity and kerogen type data previously analyzed through pyrolysis, a study is carried out of the data obtained from the organic petrography (vitrinite reflectance analysis % Ro and visual determination of the kerogen type).

In total, 87 samples were analyzed for organic petrography, of which 41 belong to the Majagua-1 well, 23 to the Remolino Grande-1 well, 14 to the Sandi-1 well, and 9 to the Tambora-1 well.

Thermal Maturity

The vitrinite reflectance percentage data confirm the level of maturity obtained through pyrolysis. Most of the section in the four wells is immature, except a few samples from the Sandi-1 well, which are within the oil window and the samples from the Tambora-1 well that make it into the gas window. It is important to mention that the data with high % Ro values in the Tambora-1 well appear to be anomalous and do not calibrate with the typical maturity curve for the deepest part of the basin, as can be seen in the chapter on modeling. Figure 34.

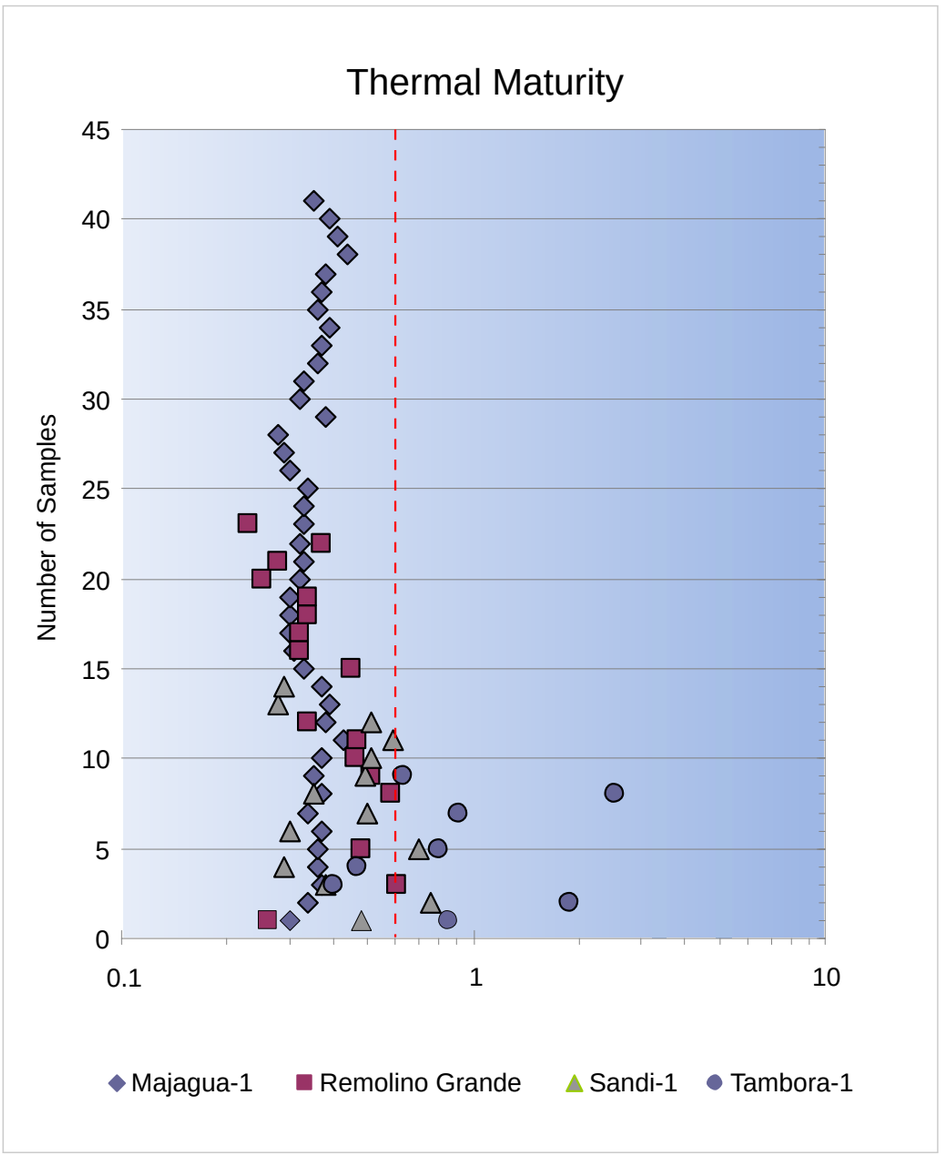

Figure 34. Thermal Maturity Profile (%Ro)

Type of Kerogen

The samples taken form the Majagua-1 well confirm a variable kerogen ranging from type II, to mixed II/III, to III, while the samples obtained in the Tambora-1 and Sandi-1 wells correspond to type III/IV kerogen with a generating potential for gas. Figure 35.

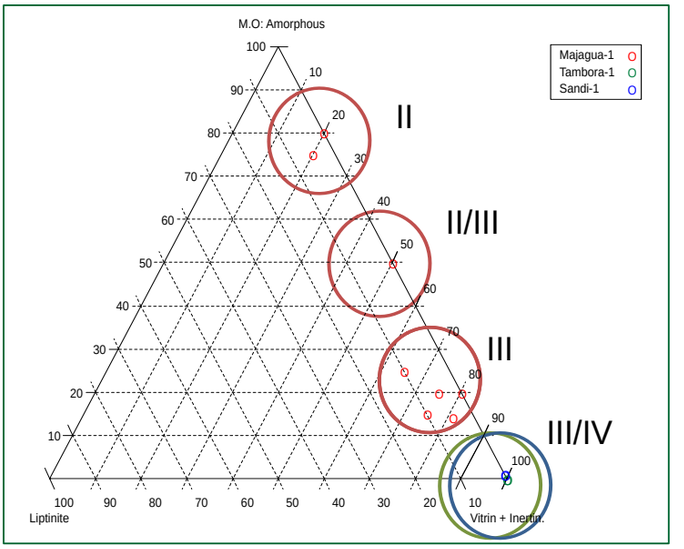

Figure 35. Ternary Diagram showing the predominan type of maceral

Hydrocarbon Charge Model

In order to define a model in terms of hydrocarbon expulsion and migration time, some simulations were carried out using the PetroMod 1D software in two pseudo-wells located along seismic lines NT-1990-2870 and NT-1992-2840 (Figure 36). The geochemical model used for the Oligocene source rock intervals was drawn from the geochemical characterization carried out for this project. The calibration of the thermal model used the vitrinite reflectance information.

The pseudo-wells that were selected are located on line NT-1990-2870 at a point where the probable source rocks reach a significant depth in the basin, and on line NT-1992-2840, near the Remolino Grande-1 well (Figures 37).

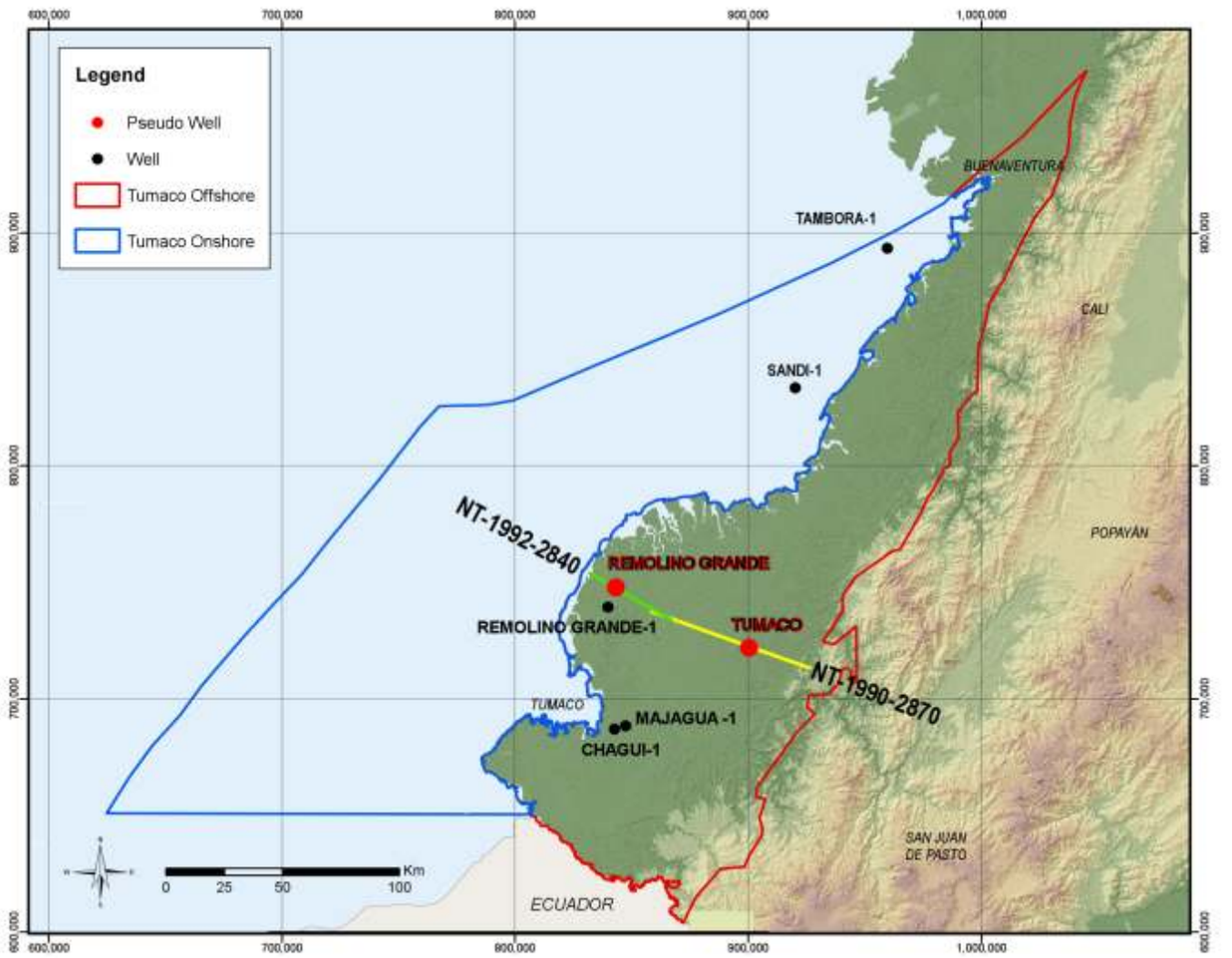

Figure 36. Location of the selected pseudo-wells

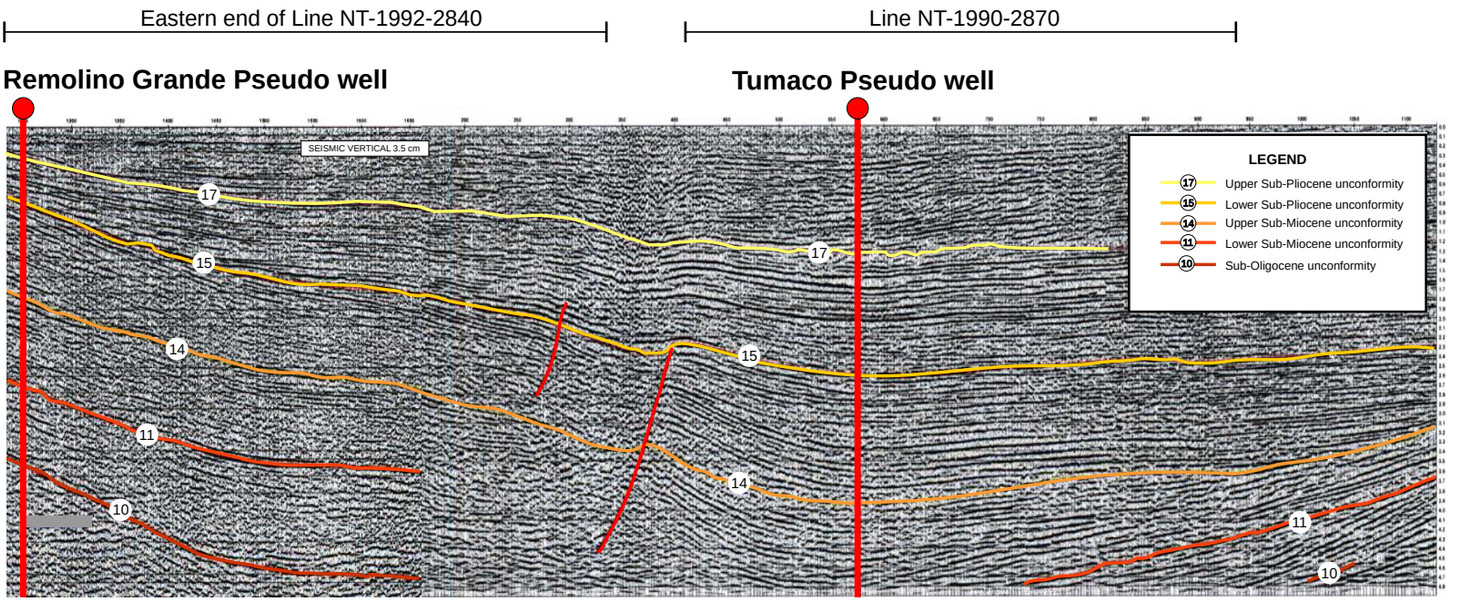

Figure 37. Location of the selected pseudo-wells on the seismic lines

The Tumaco Pseudo-well

The pseudo-well known as Tumaco is located in the central part of a syncline in which the generating formations reached a greater burial depth (Figure 38).

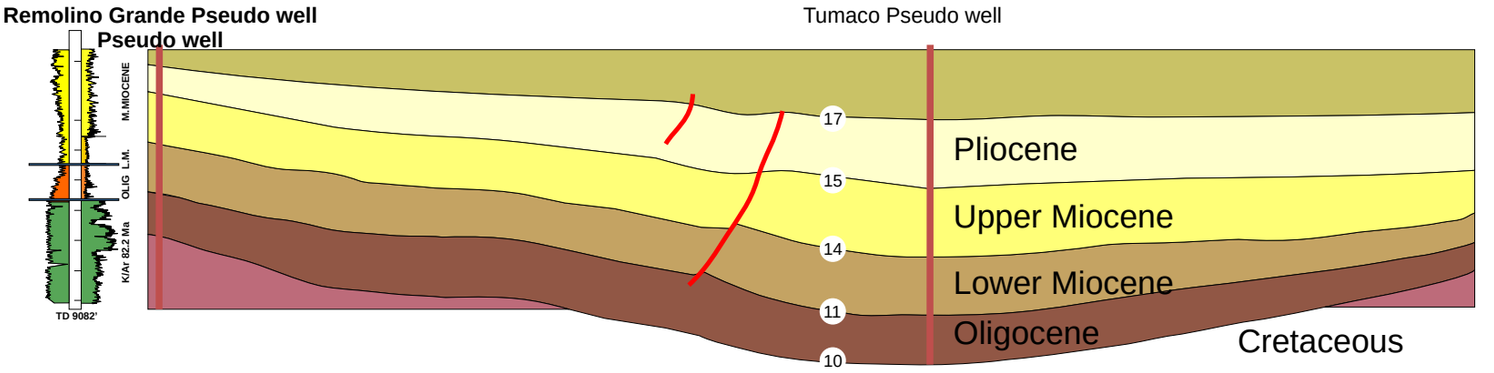

Figure 38. Digital section showing the location of the Tumaco pseudo-well.

Geological Model

The geological model is supported by regional information. In this case, an interpreted seismic section was used, from which the data regarding all the thicknesses of the stratigraphic units were drawn, carrying out the conversion from time to depth by means of the interpolation of the following time vs. depth diagram (Figure 39). The different lithologies were taken from the published stratigraphic units and the eroded thicknesses were established according to differences in thickness among the same units in the sector.

For the sake of coherence with the seismic interpretation, names of formations were not used for this model, but rather thicknesses, differentiated by ages (Figure 40).

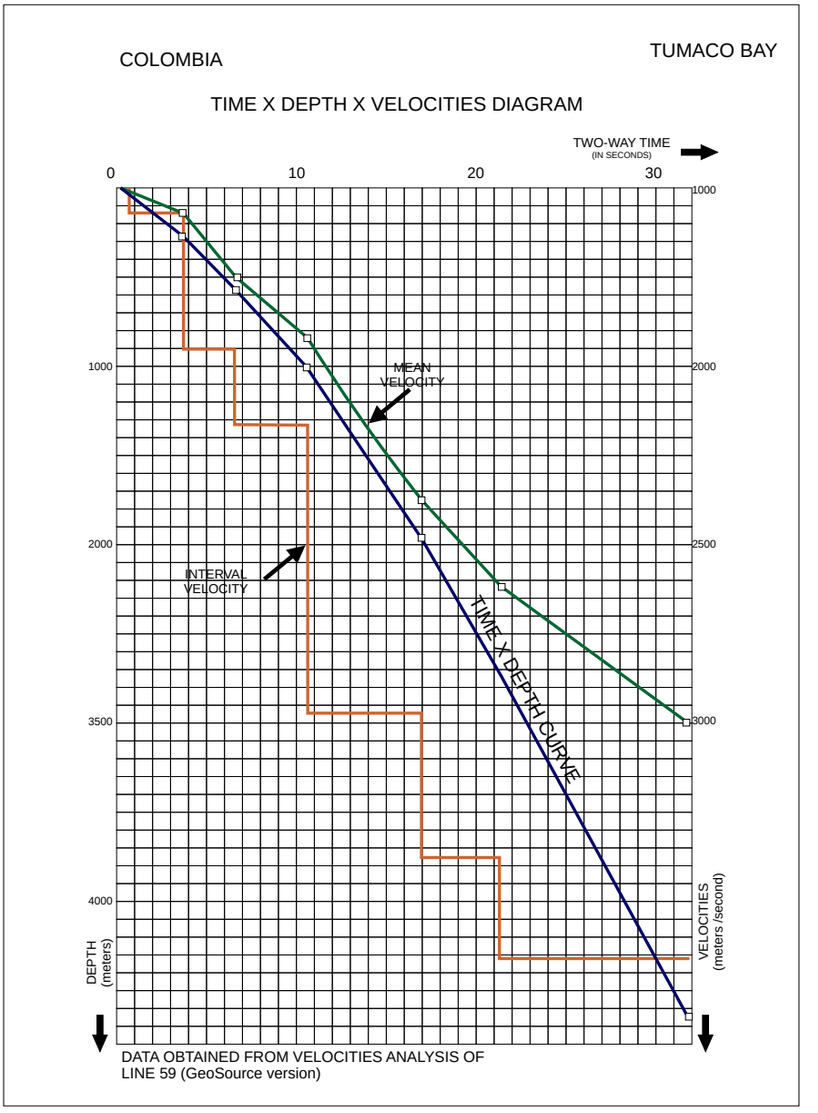

Figure 39. Time vs. depth diagram. Taken from Ojeda and Calife (1987).

				Present	Eroded	Deposition Age		Erosion Age	
	NAME	Top	Base	Thickness	Thickness	From	To	From	To
		Feet	Feet	Feet	Feet	(My)	(My)	(My)	(My)
1	Sediment Surface			0.00					
2	Pleistocene-Holocene	0.00	656.00	656.00		1.00	0.00		
3	Pliocene-eroded	656.00	656.00	0.00	999.99	3.00	2.50	2.50	1.00
4	Pliocene	656.00	1967.99	1311.99		5.50	3.00		
5	Upper Miocene Eroded	1967.99	1967.99	0.00	499.99	8.00	7.00	7.00	5.50
6	Upper Miocene	1967.99	7053.00	5085.01		15.00	8.00		
7	Lower Miocene eroded	7053.00	7053.00	0.00		17.00	16.00	16.00	15.00
8	Lower Miocene	7053.00	12138.99	5085.99		23.00	17.00		
9	Oligocene Eroded	12138.99	12138.99	0.00	499.99	26.50	25.00	25.00	23.00
10	Oligocene Generator	12138.99	17715.99	5577.00		33.50	26.50		
11	Oligocene	17715.99	17915.99	200.00		34.00	33.50		
12	Paleocene Eocene Eroded	17915.99	17915.99	0.00	15000.01	65.00	40.00	40.00	34.00
13	Basement	17915.99	18415.98	499.99		80.00	65.00		
14		18415.98							

Figure 40. Input data for the geological model

Thermal Model

A constant heat flow (43 mw/m2) history was used. The actual heat flow was calculated using the Mackenzie model, calibrated according to regional thermal maturity information. The geothermal gradient data was taken from Ojeda and Calife in the Petrobras report (1987, Figures 41 and 42).

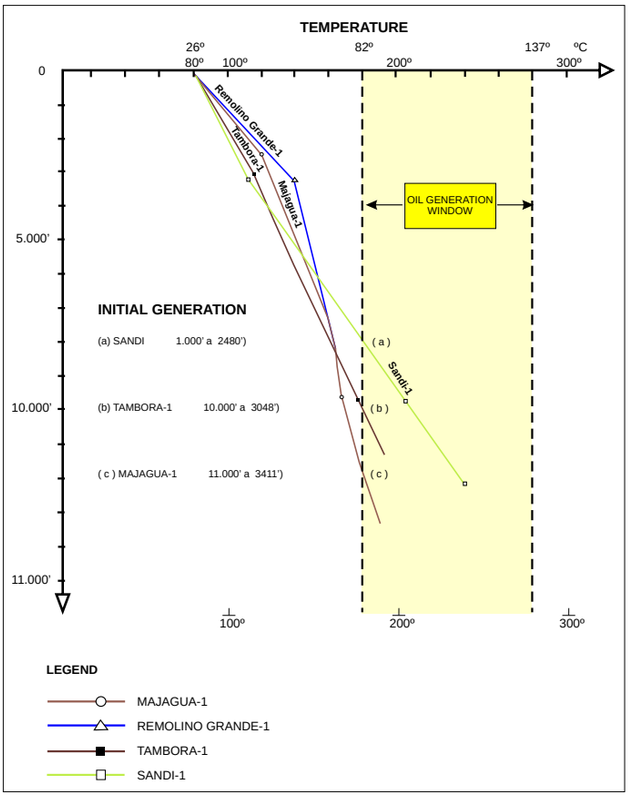

Figure 41. Temperature date used. Taked from Ojeda and Calife, 1987.

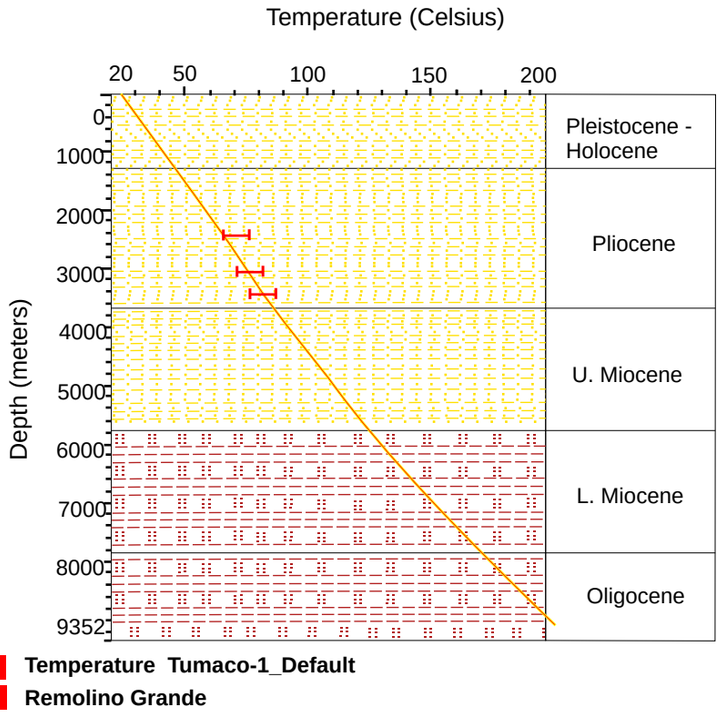

Figure 42. Calibration of temperature in the Tumaco model.

Geochemical Model

The geochemical model was developed on the basis of the geochemical characterization developed during this project. An Oligocene interval was taken as the probable source rock (Figure 43).

		TOC	Kinetics	H
	NAME			
		Wt%		(mg HC/g TOC)
1	Sediment Surface	0.00		0.00
2	Pleistocene-Holocene	0.00	None	0.00
3	Pliocene - eroded	0.00	None	0.00
4	Pliocene	0.00	None	0.00
5	U. Miocene - eroded	0.00	None	0.00
6	U. Miocene	0.00	None	0.00
7	L. Miocene - eroded	0.00	None	0.00
8	L. Miocene	0.00	None	0.00
9	Oligocene - Eroded	0.00	None	0.00
10	Oligocene	0.00	None	0.00
11	Oligocene Generator	0.00	Tissot et al (1988 T-3)	150.00
12	Paleocene Eocene Eroded	0.00	None	0.00
13	Basement	0.00	None	0.00

Figure 43. Input data for the geochemical model

Calibration

The calibration of maturity within the model was carried out with vitrinite reflectance data obtained from the analyzed wells (Figures 44 and 45).

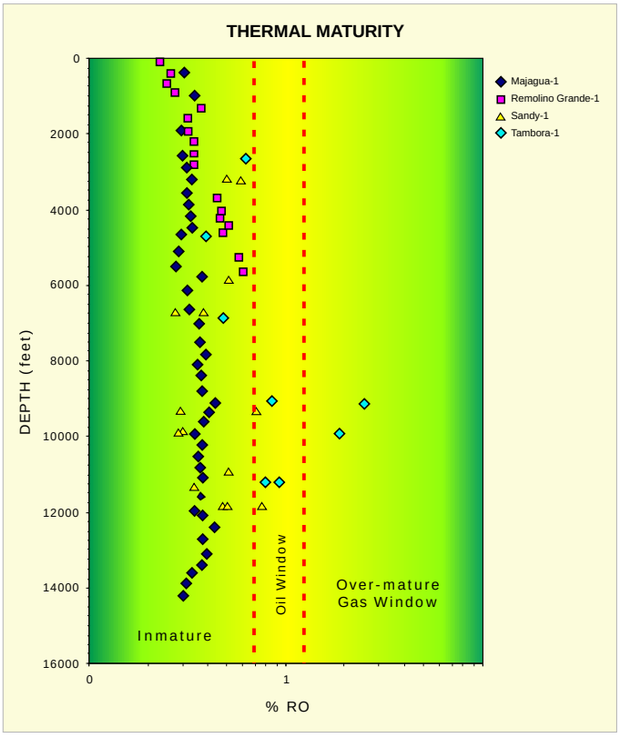

Figure 44. Geochemical profile of % Ro

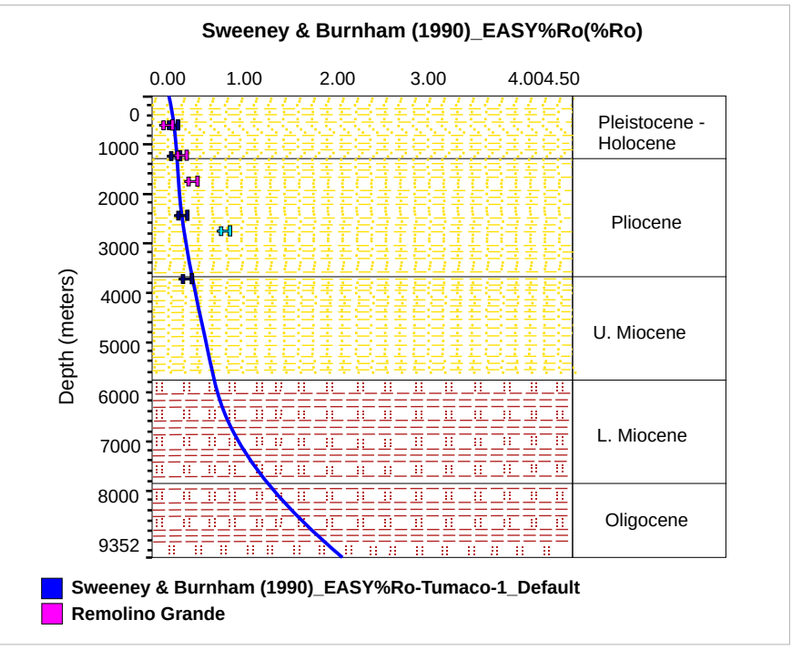

Figure 45. Calibration of maturity in the model

Results

The interval located in the lower part of the Oligocene reaches a transformation rate of 65% until today; the process began 15 million years ago (Figures 46 and 47).

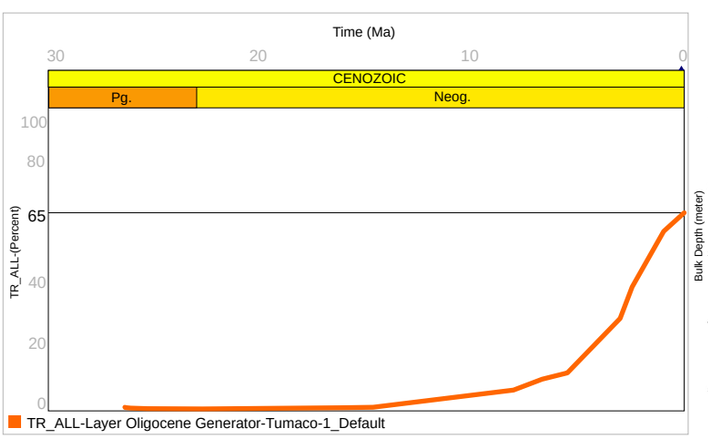

Figure 46. Transformation rate

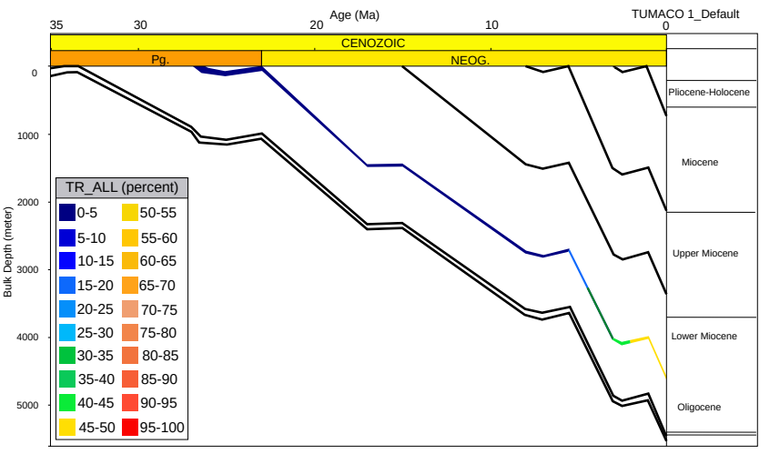

Figure 47. Burial history vs. Transformation rate

The generation rate shows a very significant episode over time: a pulse with a maximum expulsion 3 million years ago (Figure 48).

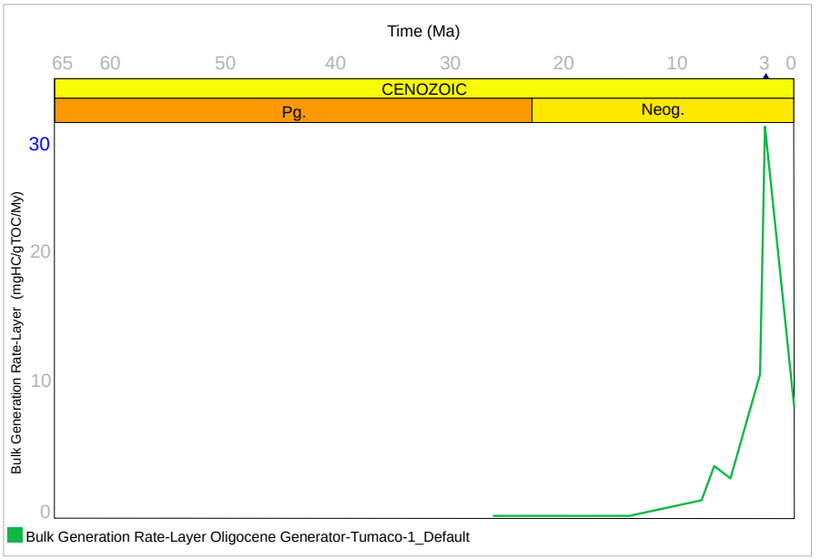

Figure 48. Expulsion rate

The maximum temperatures reached at this point are around 165-180 degrees Celsius (Figure 49).

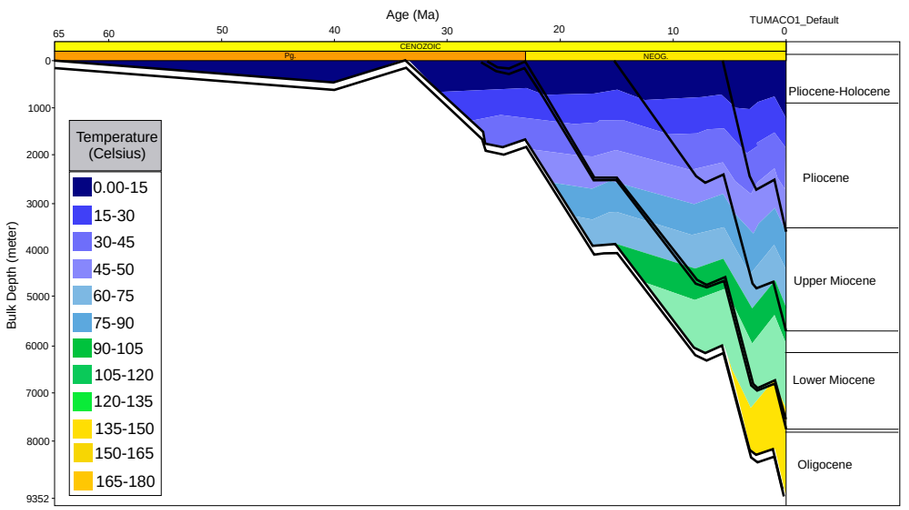

Figure 49. Burial history vs. temperature graph

Remolino Grande Pseudo-Well

The pseudo-well known as Remolino Grande is located on the western part of a syncline in which the generating formations did not reach the maximum possible depth (Figures 50).

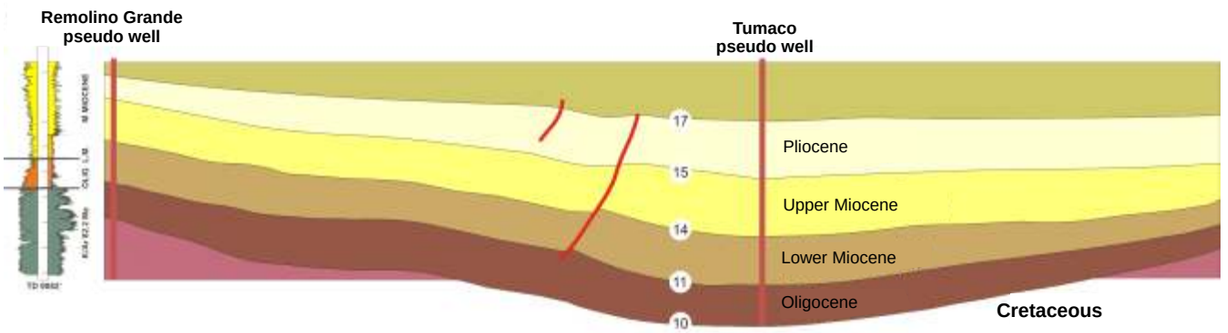

Figure 50. Digital section showing the location of the Remolino Grande pseudo-well

The geological model is supported by regional information. In this case, an interpreted seismic section was used, from which the data regarding the thicknesses of the stratigraphic units was drawn, carrying out the conversion from time to depth by means of the interpolation of the following time vs. depth graph (Figure 51).

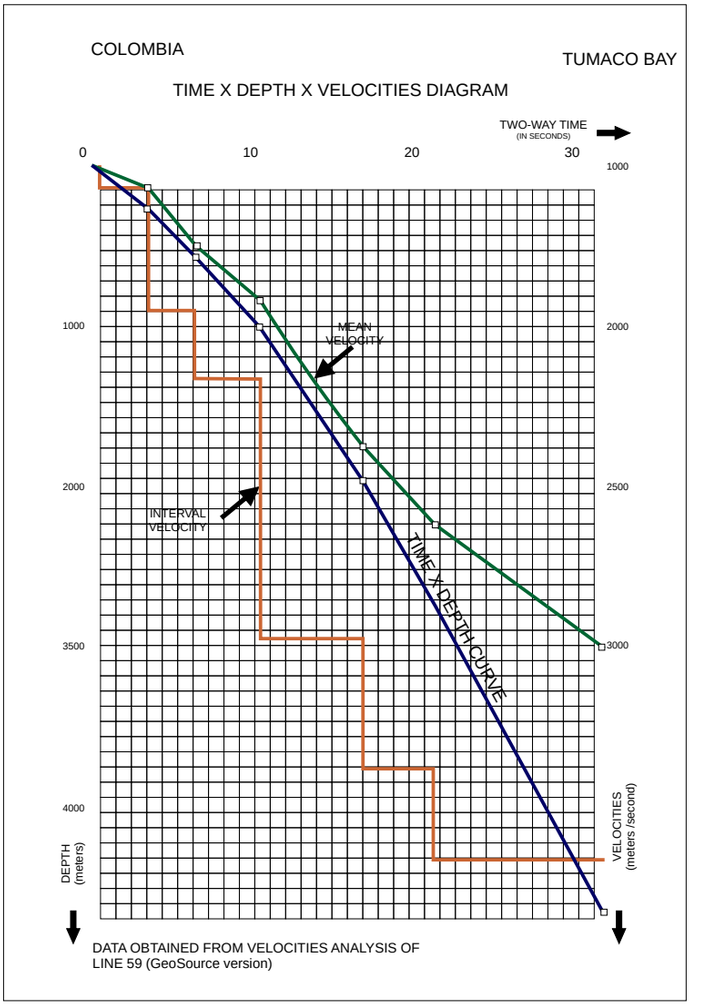

Figure 51. Time vs. depth diagram. Taken from Ojeda and Calife, 1987

The different lithologies were taken from the published stratigraphic units and the eroded thicknesses were established according to differences in thickness among the same units in the sector.

For the sake of coherence with the seismic interpretation, names of formations were not used for this model, but rather thicknesses, differentiated by ages (Figure 52).

				Present	Eroded	Deposition Age		Erosion Age	
	NAME	Top	Base	Thickness	Thickness	From	To	From	To
		Feet	Feet	Feet	Feet	(My)	(My)	(My	(My)
1	Sediment Surface			0.00					
2	Pleistocene-Holocene	0.00	4161.01	4161.01		1.00	0.00		
3	Pliocene-eroded	4161.01	4161.01	0.00	499.99	3.00	2.50	2.50	1.00
4	Pliocene	4161.01	11898.02	7737.01		5.50	3.00		
5	Upper Miocene Eroded	11898.02	11898.02	0.00	499.99	8.00	7.00	7.00	5.50
6	Upper Miocene	11898.02	18688.03	6790.01		15.00	8.00		
7	Lower Miocene eroded	18688.03	18688.03	0.00		17.00	16.00	16.00	15.00
8	Lower Miocene	18688.03	25478.04	6790.01		23.00	17.00		
9	Oligocene Eroded	25478.04	25478.04	0.00	499.99	26.50	25.00	25.00	23.00
10	Oligocene Generator	25478.04	25678.04	200.00		27.00	26.50		
11	Oligocene	25678.04	30178.05	4500.01		33.50	26.50		
12	Paleocene Eocene Eroded	30178.05	30178.05	0.00	15000.01	65.00	40.00	40.00	34.00
13	Basement	30178.05	30678.04	499.99		80.00	65.00		
14		30678.04							

Figure 52. Input data for the geological model

Thermal Model

A constant heat flow (43 mw/m2) history was used. The actual heat flow was calculated, using the Mackenzie model, calibrated according to regional thermal maturity information. The geothermal gradient data was taken from a Petrobras report (See Ojeda and Calife, 1987), (Figures 53 and 54).

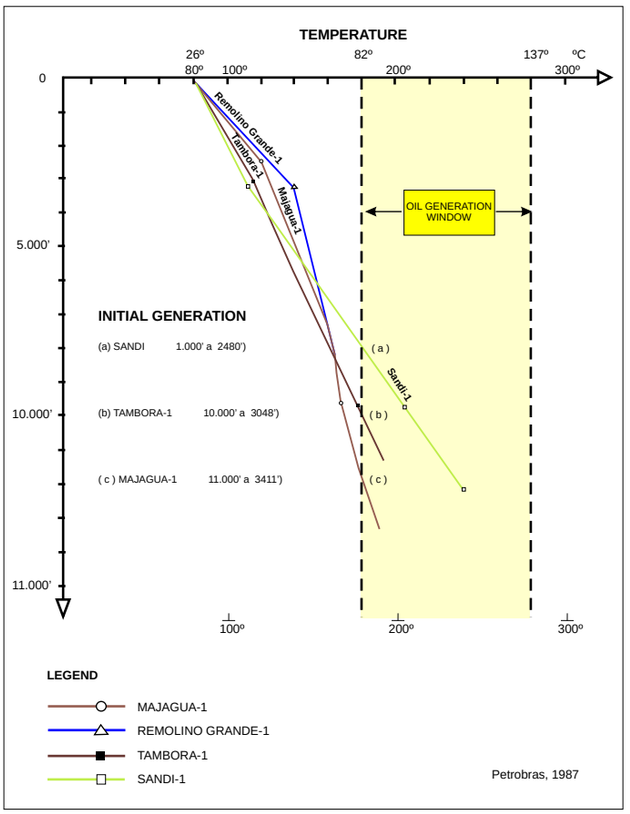

Figure 53. Temperature date used. Taken from Ojeda and Calife, 1987

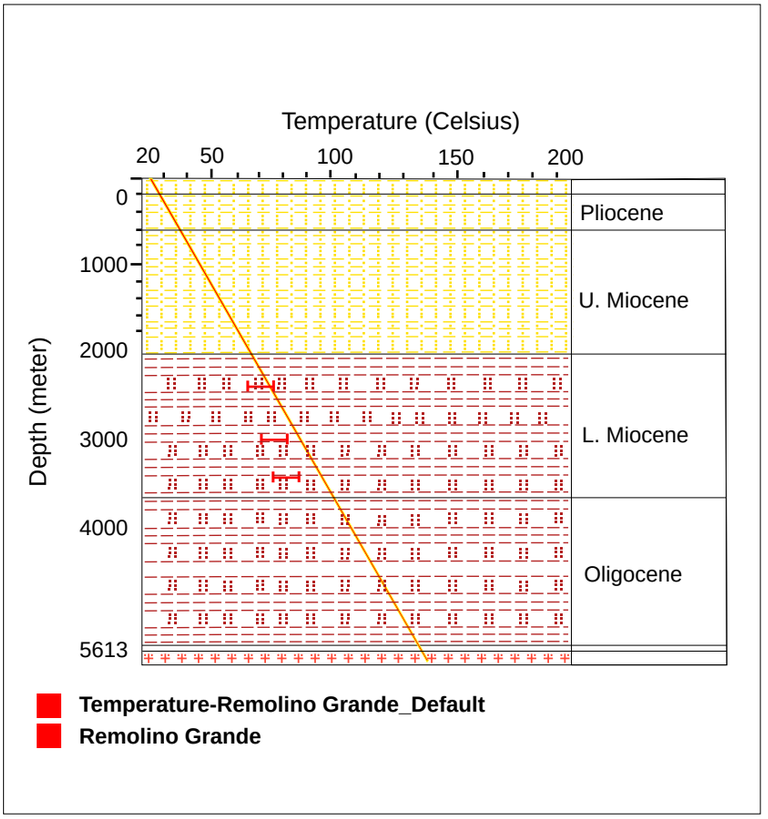

Figure 54. Calibration of temperature in the Remolino Grande model

Geochemical Model

The geochemical model was developed on the basis of the geochemical characterization developed during this project. An Oligocene interval was taken as the probable source rock (Figure 55).

		TOC	Kinetics	H
	NAME			
		Wt%		(mg HC/g TOC)
1	Sediment Surface	0.00		0.00
2	Pleistocene-Holocene	0.00	None	0.00
3	Pliocene - eroded	0.00	None	0.00
4	Pliocene	0.00	None	0.00
5	U. Miocene - eroded	0.00	None	0.00
6	U. Miocene	0.00	None	0.00
7	L. Miocene - eroded	0.00	None	0.00
8	L. Miocene	0.00	None	0.00
9	Oligocene - Eroded	0.00	None	0.00
10	Oligocene	0.00	None	0.00
11	Oligocene Generator	0.00	Tissot et al (1988 T-3)	150.00
12	Paleocene Eocene Eroded	0.00	None	0.00
13	Basement	0.00	None	0.00

Figure 55. Input data for the geochemical model

Calibration

The calibration of maturity within the model was carried out with vitrinite reflectance data obtained from the analyzed wells (Figures 56 and 57).

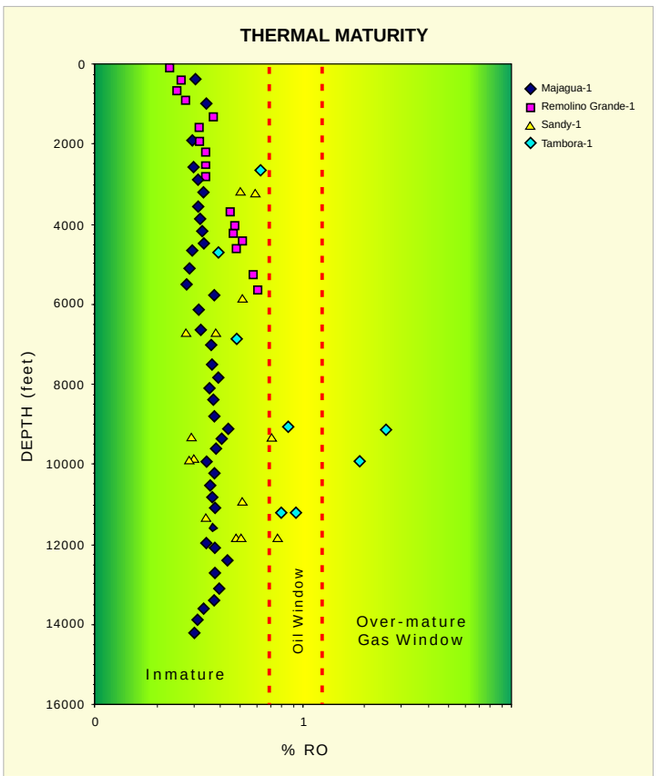

Figure 56. Geochemical profile of % Ro

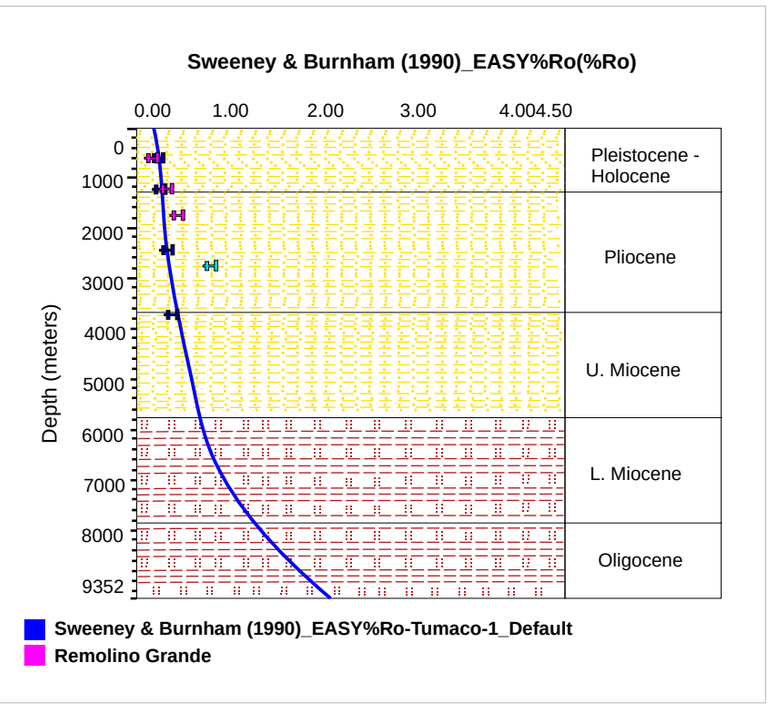

Figure 57. Calibration of maturity within the model

Results

The interval located in the Oligocene reaches a transformation rate of 12% until today; the process began 15 million years ago (Figures 58 and 59).

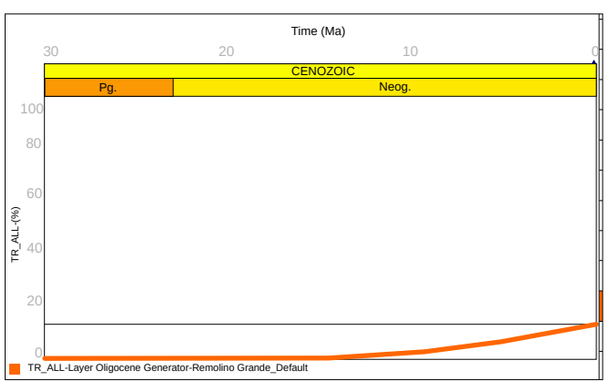

Figure 58. Transformation rate

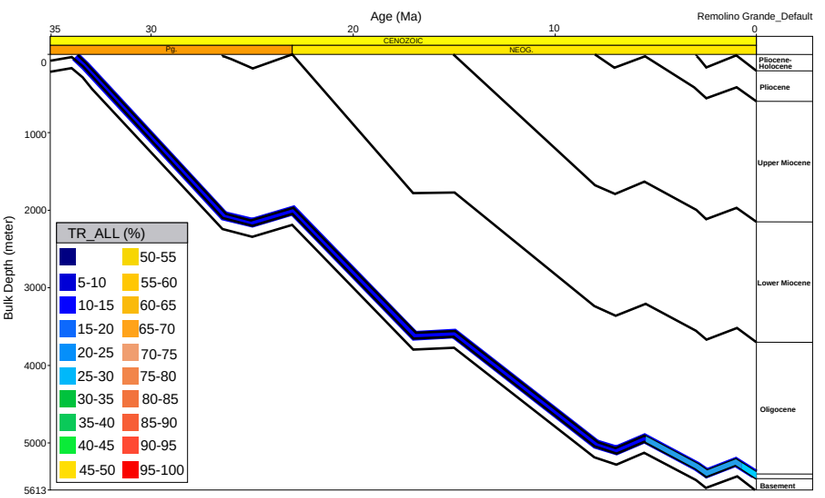

Figure 59. Burial history vs. Transformation rate

The generation rate shows two very significant episodes over time: a pulse with a maximum expulsion 7 million years ago, and another one, 3 million years ago. Figure 60.

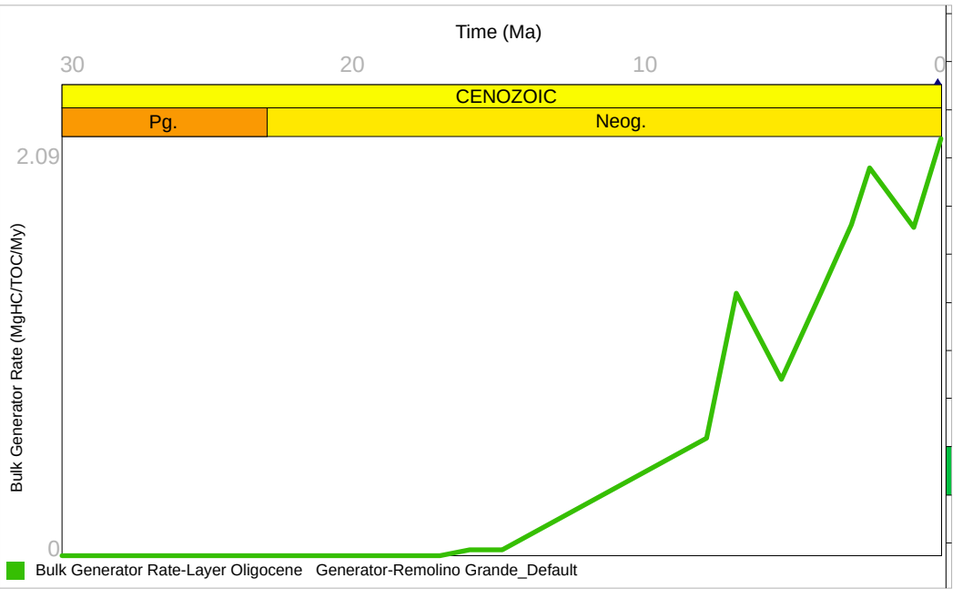

Figure 60. Expulsion rate

The maximum temperatures reached at this point are around 105-110 degrees Celsius (Figure 61).

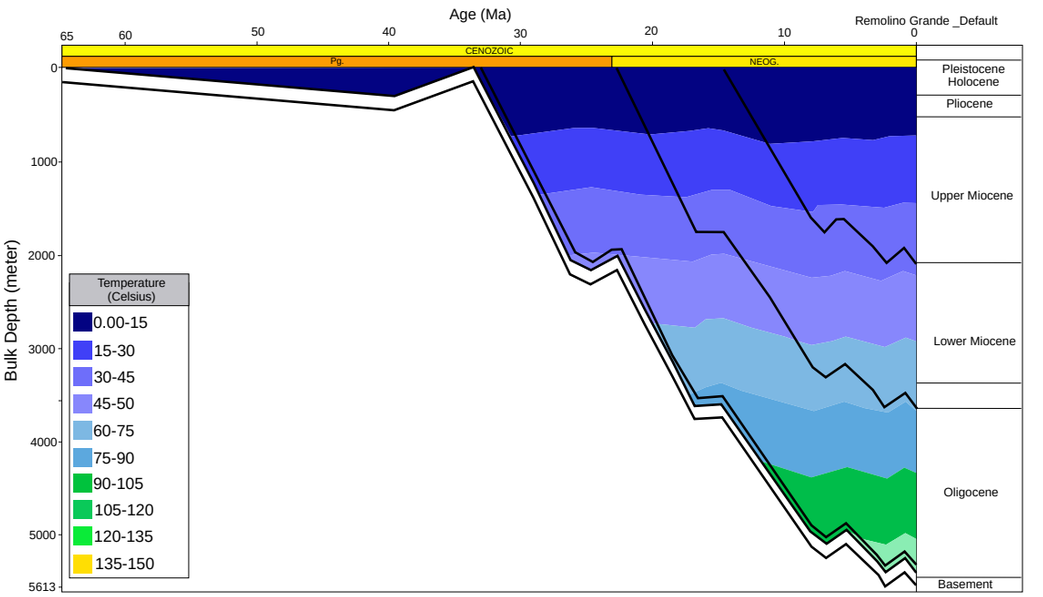

Figure 61. Burial history vs. temperature graph

Probable Generation Zones in the Basin

According to the 1D modeling carried out, intervals with geochemical characteristics equivalent to those evaluated in this study and reaching depths greater than 20,000 feet fall into the oil generation window. On the basis of this premise and taking the gravimetric basement map (Bouguer anomalies) as reference, it is possible to identify two important generation zones in the basin, shown in green below (Figure 62).

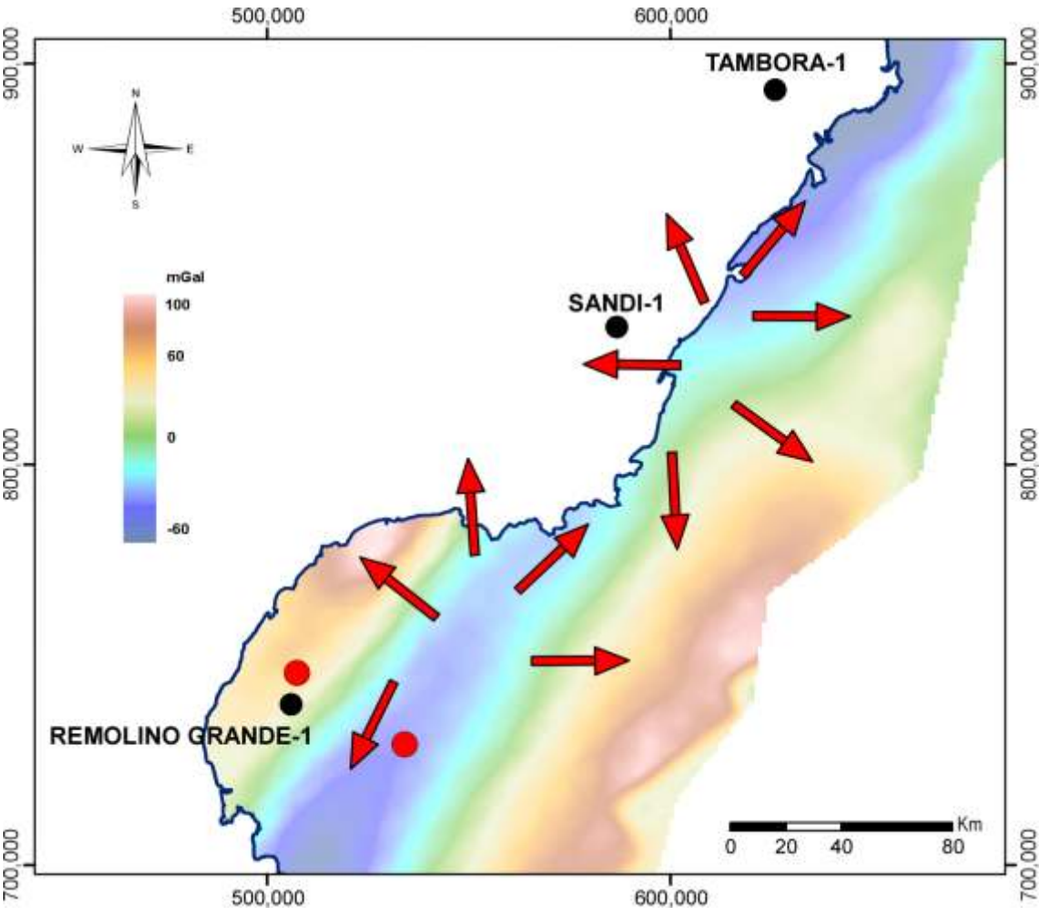

Figure 62. Probable generation zones in the basin.

PACIFIC OCEAN
Punta Ardita
Bahía de Humboldt
Punta Cabo Marzo
Punta La Tortuguera
Bahía de Cupica
Punta Nabugá
Bahía Solano
Ensenada de Utría
GOLFO DE TRIBUGÁ
Ensenada Coquí
Punta Arusí
Cabo Corrientes
Playa Nueva
Bahía Baudó
Boca Usuragá
Ensenada Docampadó
Boca Hijua
Boca Orpúa
Boca Cacagual
Playa El Choncho
Mutatá
Bojayá (Bellavista)
Dabeiba
Uramita
Frontino
Cañasgordas
Abriaquí
Caicedo
BETULIA
CONCORDIA
SALGAR
EL CARMEN DE ATRATO
HISPANIA
BETANIA
MISTRATÓ
PUEBLO RICO
APÍA
SANTUARIO
LA CELIA
BALBOA
EL ÁGUILA
SAN JOSÉ DEL PALMAR
NÓVITA
ANSERMANUEVO
EL CAIRO
ARGELIA
CARTAGO
TORO
VERSALLES
OBANDO
EL DOVIO
BOLÍVAR
Trujillo
Riofrío
Tuluá
San Pedro
SAN JUAN
SISTEMA DE FALLAS GARRAPATAS
Qui
Uv
Qall
Sa
Pen
Ma
Siu
Si
Peu
Sil
Co
Rp
Br
Is
QTt
My
Ci
N
25
50
km

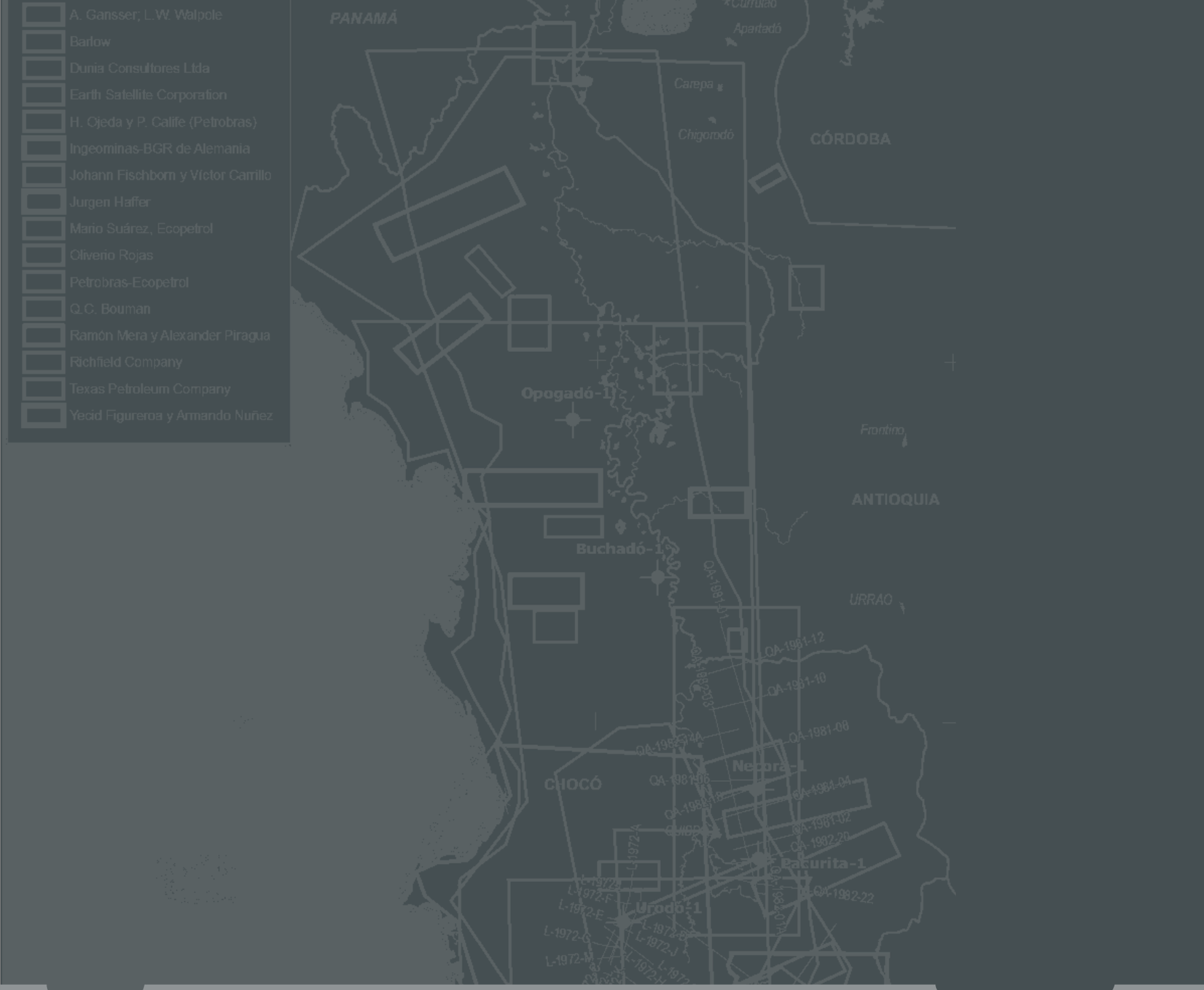

5. CONCLUSIONS

5. CONCLUSIONS

The basement of the Tumaco basin is made up of the Dagua-Piñón terrain to the East, and the Gorgona terrain to the West, both of oceanic affinity. These Cretaceous age terrains were accreted onto the continent in the Late Paleocene and the Late Eocene, respectively.

The Tumaco basin is a forearc basin that contains a sedimentary mega-sequence of pre-Miocene age and three sequences of post-Lower Miocene age. Basement paleo-highs (such as the Remolino Grande paleo-high) divide the basin into two sectors with different tectonic styles: (1) to the East, a sub-basin located mainly onshore, under a probably transpressive domain, and (2) to the West, a sub-basin located totally offshore, under a mainly compressive regime.

Taking into account the scarce geological information and the lack of updated stratigraphic information for the Tumaco basin (and in general for the Colombian Pacific basins), this study proposes four time-units or events, limited by hiatuses or erosion surfaces. From the oldest to the most recent, these events are: (1) Late Oligocene to basal Middle Miocene, (2) Middle Miocene, (3) Upper Middle Miocene to Late Miocene, and (4) Late Miocene to Early Pliocene.

On the basis of the scarce lithological knowledge, it can be said very generally that shale predominates toward the base of the sequences, and that minor packages of conglomerates and sandstone appear only in the upper segments.

The geochemical study indicated that the sequence drilled in the different wells is immature overall, with the exception of a few samples located at the beginning of an oil generation window. The data obtained from organic petrography shows that the pre-Miocene sequence is immature, except for some samples located at the beginning of the oil generation window. The results of the analysis of organic petrography indicate that the predominant type of kerogen in the sequence is type III, although some samples show a mixed type II/III, while other samples are located in the area of kerogen type II, which generates mainly oil.

Although the generating potential ranges from poor to average, some samples exhibit an excellent organic content. Additionally, an interval with a high potential for the generation of liquid and gaseous hydrocarbons in deep zones of the basin has been identified in the Majagua-1 well. According to the data obtained in the production index, there is evidence of slight contamination and an adequate conversion-expulsion level in the samples taken from Sandi-1 well.

The transformation rate is quite high at the point known as Tumaco. If the geochemical facies characterized here are preserved in this deep part of the basin, the generation of liquid hydrocarbons can be expected. The most important expulsion times occurred 7 and 3 million years ago.

The main tectonic events that were operative in the formation of the Tumaco basin are:

1. Late Paleocene – Early Eocene (59–49 M.a.): accretion of the Dagua-Piñón terrain against the pre-existing Romeral terrain of oceanic affinity (Cediel et al., 2003).
2. Middle Eocene (45 M.a.) to Late Eocene (~37–40 M.a,): collision of the Gorgona terrain with the Dagua–Piñon terrain (Kerr et al., 2002; Kerr and Tarney, 2005); according to Franco and Abbot (1999), this collision ended with the transfer of the subduction zone toward the West.
3. End of the Eocene – Pliocene: small metaluminous plutons with calc-alkaline characteristics related to Chile-type arc magmatism intrude into the Dagua-Piñon terrain (Cediel et al., 2003). It is during this period that the development of the forearc-type Tumaco basin begins.
4. Oligocene – Pliocene: the discontinuous rise of the Western Cordillera during this subduction cycle generated at least four periods of erosion and deposition: 1) Oligocene-Miocene; 2) Middle Miocene– Upper Miocene; 3) Upper Miocene-Pliocenet; 4) Quaternary. These events gave origin to the thick sequences of sediments (~ 9 km) that have been deposited on the Dagua-Piñón and Gorgona terrains from their accretions to the paleo-margin, forming the two sectors of the Tumaco basin, that is, the internal sector and the external sector, separated by basement highs.

BIBLIOGRAPHIC

references

BIBLIOGRAPHIC
references

- Baldock, J.W. and Longo, R., 1982. Geology of Ecuador (Explanation of the 1:1,000,000 geological map). Direccion general de Geologia y Minas, Ministerio de Recursos Naturales y energeticos, Quito.
- Berggren, W. A., Kent, D. V., Swisher, I. I. I., CC, and Aubry, M.-P., 1995, A revised Cenozoic geochronology and chronostratigraphy: Society of Economic Paleontologists and Mineralogists, Special Publication, v. 54, p. 129-212.
- Becerra, I., y Usma, V. 2008. Modelamiento geologico-geofisico a la altura de 3N desde el graben de Yaquina hasta el craton de la Guyana, Trabajo dirigido de grado, Universidad de Caldas, sin publicar, p.
- Blow, W.A., I969. Late middle Eocene to Recent Planktonic Foraminiferal Biostratigraphy. In P. Bronnimann and H.H. Renz (Editors): Proc. First Inter. Conf. Planktonic Microfossils, Geneva, I967, 1, pp. I99421.
- Bueno Salazar, R., Govea, C., 1974. Potential for exploration and development of Hydrocarbons in Atrato Valley and Pacific Coastal and Shelf Basins of Colombia. Am. Assoc. Pet. Geol. Bull. 25, 318–327.
- Bueno, R., and Govea, C., 1976, Potential for exploration and development of hydrocarbons in the Atrato valley and Pacific coastal and shelf basins of Colombia, in Halbouty, M. T., Maher, J. C., and Lian, H. M., eds., Circum-Pacific Energy and Mineral Resources: Amer. Assoc. Petrol. Geol. Mem. 25: Tulsa, Amer. Assoc. Petrol. Geol., p. 318-327.
- Bueno Salazar, R., 1989. Hydrocarbon exploration and potential of the Pacific coastal basin of Colombia. In: Ericksen, G.E., Canas Pinochet, M.T., Reinemund, J.A. (Eds.), Geology of the Andes and its relation to hydrocarbon and mineral resources. Circum-Pacific Council for Energy and Mineral Resources Earth Sciences Series, Houston, Texas, pp. 335–343.
- Carson Helicopters.,2006, Programa Adquisición, procesamiento e interpretación de datos aeromagnetogravimetricos en el litoral pacífico de Colombia, informe técnico de la ANH.
- Case, J. E., Moore W. R., Durán L. G., López R., 1971. Junction of the Andean and Panamanian chains in northern Colombia. Transactions of the Caribbean. Geological Conference, Memorias - Conferencia Geológica del Caribe, 5: 11-13.
- Cediel, F. and Cáceres, C., 2000. Geological map of Colombia, Scale 1:1,000,000, (3rd. ed.). Geotec Ltd Ed., Bogotá, Colombia.
- Cediel, F., Shaw, P., Caceres, C., 2003. Tectonic assembly of the Northern Andean Block. In: Bartoloni, C., Buffler, R.T., Blickwede, J. (Eds.), The circum-Gulf of Mexico and the Carribean: Hydrocarbon habitats, basin formation and plate tectonics. AAPG Memoirs, pp. 815–848.
- Collot Jean-Yves,Marcaillou Boris, Sage Franc¸oise, Michaud Franc¸ois, Agudelo William, Charvis Philippe, Graindorge David, Gutscher Marc-Andre´and Spence George, 2004. Are rupture zone limits of great subduction earthquakes controlled by upper plate structures? Evidence from multichannel seismic reflection data acquired across the northern Ecuador– southwest Colombia margin. JOURNAL OF GEOPHYSICAL RESEARCH, VOL. 109, B11103, doi:10.1029/2004JB003060, 14 p.
- Collot, J.-Y., S. Migeon, G. Spence, Y. Legonidec, B. Marcaillou, J.-L. Schneider, F. Michaud, A. Alvarado, J.-F. Lebrun, M. Sosson, and A. Pazmiño, 2005. Seafloor margin map helps in understanding subduction earthquakes, EOS Transactions, American Geophysical Union, 86 (46), 464-466.
- Daly, M., 1989. Correlations between Nazca/Farallon plate kinematics and forearc basin evolution in Ecuador. Tectonics 8 (4), 769–790.
- Deniaud, Y., 2000. Enregistrement sédimentaire et structural de l'évolution géodynamique des Andes Equatoriennes au cours du Néogène: étude de bassins d'avantarc et bilan de masse. Phd Thesis, Université Joseph Fourier, Grenoble, 157 pp.
- Duque-Caro, H., 1975, Los foraminíferos planctónicos y el terciario de Colombia: Revista Española de Micropaleontología, v. 7, p. 403-427.
- Duque-Caro, H., 1979, Major structural elements and evolution of northwestern Colombia: American Association of Petroleum Geologists, Memoir, v. 29, p. 329-351.
- Duque-Caro, H., 1984, Structural style, diapirism and accretionary episodes of the Sinu-San Jacinto terrane, southwestern Caribbean borderland: Geological Society of America Memoir, v. 162, p. 303-316.
- Duque-Caro, H., 1989, Benthic Cenozoic foraminifera from Ecuador: Taxonomy and distribution of smaller benthic foraminifera from coastal Ecuador (Late Oligoceno-Late Pliocene). 1988, By J.E. Whittaker. British Museum of Natural History: Journal of South American Earth Sciences, Review. v. 2, p. 401.
- Duque-Caro, H., 1990a, Neogene stratigraphy, paleoceanography and paleobiogeography in northwest South America and the evolution of the Panama seaway: Palaeogeography, Palaeoclimatology, Palaeoecology, v. 77, p. 203-234.
- Duque-Caro, H., 1990b, The Choco block in the northwestern corner of South America: structural, tectonostratigraphic and paleogeographic implications: Journal of South American Earth Sciences, v. 3, p. 71-84.
- Duque-Caro, H., 1991, Contributions to the geology of the Pacific and Caribbean Coastal Areas of Northwestern Colombia and South America [Ph.D. Dissertation]: Princeton University, Princeton, 132 p.
- Duque-Caro, H., 2005, Microstratigraphic Changes: A Methodology to Identify Stratigraphic Packages and Geologic Events. Geologic Problems Solving with Microfossils: Abstract Volume with Program, March 6-11, 2005. Rice University, Houston, Texas, USA, Pg. 64.
- Earth Satellite Corporation, 1999. Geology of the Pacific coast of Colombia. P. 30
- Echevarria, L.M., 1980. Tertiary or mesozoic komatiites from Gorgona Island, Colombia: field relation and geochemistry. Contrib. Mineral. Petrol. 73, 253–266.
- Echevarria, L.M., Aitken, B.G., 1986. Pyroclastic rocks: another manifestation of ultramafic volcanism on Gorgona Island, Colombia. Contrib. Mineral. Petrol. 92, 428–436.
- Escovar, R., Gomez, L.A., Ramirez, J.R., 1992. Interpretacion de la Sismica Tumaco 90 y evaluacion preliminar del area, Empresa Colombiana de Petroleos (ECOPETROL), Santafe de Bogota. 58 pp.
- Estrada, J.J., 1995. Paleomagnetism and Accretion events in the Northern Andes. PhD. Thesis Graduate School of the State University of New York at Binghamton, p. 154.
- Evans, C.D.R., Whittaker, J.E., 1982. The geology of the western part of the Borbón Basin, Northwest Ecuador. In: Leggett, J.K. (Ed.), Trench–forearc geology. Geological Society of London Special Publication, pp. 191–198.
- Feininger, T., Bristow, C.R., 1980. Cretaceous and Paleogene geologic history of Coastal Ecuador. Geol. Rundsch. 69, 849–874.
- Flueh, E.R., J. Bialas, P. Charvis, and Salieri scientific party, 2001. Cruise report SO159 SALIERI, in Report 101, pp. 256, Geomar Research center, Kiel, Germany.
- Hall, M.L., Calle, J., 1982. Geochronological control for the main tectonic–magmatic events of Ecuador. Earth Sci. Rev. 18, 215–239.
- Galindo, V., y Torres, M.E., 1995, Mapa Geológico Compilado de la Cuenca de Tumaco, Ecopetrol – Geología Sistematizada Ltda.

- Hinze W.,2003, Bouguer reduction density,why 2.67?, Geophysics vol. 68, n 5, p.1559.1560.
- Ingeominas, 2005, Mapa Geológico del Andén Pacífico Colombiano, Escala 1:100.000.
- Jaillard, E., et al., 1995. Basin development in an accretionary, oceanic-floored fore-arc setting: southern coastal Ecuador during late Cretaceous–late Eocene time. In: Tankard, A.J., Suárez, R., Welsink, H.J. (Eds.), Petroleum basins of South America, pp. 615–631.
- Jaillard, E., Benítez, S., Mascle, G.H., 1997. Les déformations paléogènes de la zone d'avant-arc sud-equatorienne en relation avec l'évolution géodynamique. Bull. Soc. Géol. Fr. 168 (4), 403–412.
- Jaillard, E., et al., 2000. Tectonic evolution of the Andes of Ecuador, Peru, Bolivia and northernmost Chile. In: Cordani, U.G., Milani, E.J., Thomaz Filho, A., Campos, D.A. (Eds.), Tectonic evolution of South America, pp. 481–559.
- Keller, G., and Barron, J. A., 1983, Paleoceanographic implications of Miocene deep-sea hiatuses: Geological Society of America Bulletin, v. 94, p. 590-613.
- Kerr, A.C., et al., 1996a. The petrogenesis of Gorgona komatiites, picrites and basalts: new field, petrographic and geochemical constraints. Lithos 37, 245–260.
- Kerr, A.C., et al., 1996b. The geochemistry and tectonic setting of Late Cretaceous Carribbean and Colombian volcanism. J. South Am. Earth Sci. 9, 111–120.
- Kerr, A.C., Aspden, J.A., Tarney, J., Pilatasig, L.F., 2002. The nature and provenance of accreted oceanic terranes in western Ecuador: geochemical and tectonic constraints. J. Geol. Soc. London 159, 577–594.
- Kerr, A.C., 2005. La isla de Gorgona, Colombia: a petrological enigma? Lithos 84, 77–101.
- Lebrat, M., Mégard, F., Dupuy, C., Dostal, J., 1987. Geochemistry and tectonics setting of pre-collision Cretaceous and Paleogene volcanics rocks of Ecuador. Geol. Soc. Amer. Bull. 99, 569–578.
- López, E., Collot J-Y, and Sosson, M., 2008. Sedimentary constraints on the tectonic evolution of the paired Tumaco–Borbón and Manglares forearc basins (southern Colombia - northern Ecuador) during the Late Cenozoic. 7th International Symposium on Andean Geodynamics (ISAG 2008, Nice), Extended Abstracts: 292-294.
- Marcaillou, B., and Collot, J.-Y., 2008, Chronostratigraphy and tectonic deformation of the North Ecuadorian-South Colombian offshore Manglares forearc basin: Marine Geology, v. 255, p. 30-44.
- Marcaillou, B., Spence George, Collot Jean-Yves and Wang Kelin, 2006. Thermal regime from bottom simulating reflectors along the north Ecuador–south Colombia margin: Relation to margin segmentation and great subduction earthquakes. Journal of Geophysical Research. VOL. 111, B12407, doi:10.1029/2005JB004239. P.16.
- Millward, D.; Marriner G. F. & Saunders A. D., 1984. Cretaceous tholeiitic volcanic rocks from the Western Cordillera of Colombia. J. geof. Soc. London. Vol. 141. 847-860.
- McGeary, S., Ben-Avraham, Z., 1986. The accretion of Gorgona Island, Colombia: multichannel seismic evidence. In: Howell, D.G. (Ed.), Tectonostratigraphic terranes of the circum-pacific Region. Circum-Pacific council for Energy and Mineral Resources, Earth Sciences Series, pp. 543–554.
- Mountney Nigel P. and Westbrook Graham K., 1997. Quantitative analysis of Miocene to Recent forearc basin evolution along the Colombian convergent margin. Basin Research 9. 177–196.
- Oldenburg D.,1974, The inversion and interpretation of gravity anomalies, Geophysics, vol 39, n4, 526-536.
- Ojeda, H. y Calife, P., 1987. Evaluacion del potencial petrolífero de la cuenca de Tumaco. Petrobras. 81. P.
- Ortiz, F., 1979. Petroquimica del volcanismo basico de la Cordillera Occidental (informe preliminar). Bol. Cienc. Tierra - Universidad Nacional de Colombia, Medellin 4, 29–44.
- Parker R.L., 1973, The rapid calculation of potential anomalies, Geophysics J.J. Astr.Soc.,vol 31, 447-455.
- Petters, V. and Sarmiento, R., I956. Early Oligocene and Miocene biostratigraphy of the Carmen Zambrano areas, Colombia: Micropaleontology, v.2, pp. 735. New York.
- Petrobras, Ecopetrol, 2002. Regional evaluation and petroleum potential of the offshore portion of central Pacific block. Brazil. 30p.
- Révillon, S., Arndt, N.T., Chauvel, C., Hallot, E., 2000. Geochemical study of ultramafic volcanic and plutonic rocks from Gorgona Island, Colombia: the plumbing system of an oceanic plateau. J. Petrol. 41, 1127–1153.
- Reynaud, C., Jaillard, E., Lapierre, H., Mamberti, M., Mascle, G.H., 1999. Oceanic plateau and island arcs of southwestern Ecuador: their place in the geodynamic evolution of northwestern South America. Tectonophysics 307, 235–254.
- Robertson Research. 1985. Opogadó-1. Stratigraphic summary. Project No. 856-M-992-B. Enclosure 14.3.
- Robertson Research. 1985. Buchadó-1. Stratigraphic summary. Project No. 856-M-992-B. Enclosure 14.4.
- Robertson Research. 1988. The biostratigraphic, paleoenvironments and petroleum geochemistry of the Buchadó-1, Tambora-1 and Sandí-1 wells, Pacific coastal region of Colombia. Report No. 3792/Ib for Ecopetrol. Bogotá. p. 104.
- Suárez Rodríguez, M.,1990. Estado actual del conocimiento geológico de la Provincia del Pacífico. Empresa Colombiana de Petroleos, Instituto Colombiano del Petroleo, 54 pp.

PACIFIC OCEAN
Punta Ardita
Bahía de Humboldt
Punta Cabo Marzo
Punta La Tortuguera
Bahía de Cupica
Punta Nabugá
Bahía Solano
Ensenada de Utría
GOLFO DE TRIBUGÁ
Ensenada Coquí
Punta Arusí
Cabo Corrientes
Playa Nueva
Bahía Baudó
Boca Usuragá
Ensenada Docampado
Boca Hijua
Boca Orpúa
Boca Cacaguai
Playa El Choncho
N
25
50
km
Qui
Uv
Qall
Sa
Pen
Ma
Siu
Si
Peu
Sil
Co
Rp
Br
Is
My
Ci
QTf
Mutatá
Dabeiba
Uramita
Frontino
Cañasgordas
Abriaquí
Caicedo
BETULIA
CONCORDIA
SALGAR
EL CARMEN DE ATRATO
HISPANIA
BETANIA
MISTRATÓ
PUEBLO RICO
APÍA
SANTUARIO
LA CELIA
BALBOA
EL ÁGUILA
SAN JOSÉ DEL PALMAR
ANSERMANUEVO
EL CAIRO
ARGELIA
CARTAGO
TORO
VERSALLES
OBANDO
EL DOVIO
BOLÍVAR
SAN JUAN
Tuluá
San Pedro
SISTEMA DE FALLAS GARRAPATAS